OPEN WATER EVAPORATION MEASUREMENT USING MICROMETEOROLOGICAL METHODS

MJ Savage, JM Pasi, L Myeni and AD Clulow

WATER RESEARCH COMMISSION

TT 729/17

OPEN WATER EVAPORATION MEASUREMENT USING MICROMETEOROLOGICAL METHODS

Report to the
Water Research Commission

MJ Savage, JM Pasi, L Myeni and AD Clulow

Soil-Plant-Atmosphere Continuum Research Unit
Agrometeorology Discipline
School of Agricultural, Earth and Environmental Sciences
University of KwaZulu-Natal

WRC Report No. TT 729/17

August 2017

Obtainable from

Water Research Commission
Private Bag X03
Gezina, 0031

orders@wrc.org.za or download from www.wrc.org.za

The publication of this report emanates from a project entitled *Open water evaporation measurement using micrometeorological methods* (WRC Project No. K5/2355)

DISCLAIMER

This report has been reviewed by the Water Research Commission (WRC) and approved for publication. Approval does not signify that the contents necessarily reflect the views and policies of the WRC, nor does mention of trade names or commercial products constitute endorsement or recommendation for use.

ISBN 978-1-4312-0913-2
Printed in the Republic of South Africa

EXECUTIVE SUMMARY

Background and motivation

Evaporation from open water surfaces is a neglected research area in water resources management in South Africa in spite of South Africa's known high evaporative demand. Our previous research efforts on evaporation have been almost exclusively concerned with evaporation from vegetation (Savage et al., 1997, 2004; Savage 2009, 2010). Comparatively, very little research attention has been devoted to the modelling or measurement of open water evaporation, in spite of its general importance and its importance in relation to climate change.

Evaporation from bare soil, vegetation-covered land surfaces and open water surfaces is one of the main components of the hydrologic cycle. Estimates of the total amount and the rate of evaporation from open water surfaces are required in water resources management for many purposes: management of irrigation of agricultural lands, management of wetlands, catchment water balance studies, design of storage reservoirs, and municipal and industrial water supply (Brutsaert, 1982; Marsh and Bigras, 1988; Finch, 2001). Studies of open water evaporation from fresh water systems to date have been predominantly carried out on reservoirs and larger lakes. There have been relatively few investigations on smaller reservoirs and ponds (Rosenberry et al., 2007; Mengistu and Savage, 2010a).

Open water evaporation (*LE*) may be estimated using many different hydrometeorological methods and approaches, including:

1. Symon's tank/class-A pan measurements;
2. Modelling approaches based on the Penman-Monteith method (for example, Allen et al., 1998, 2006) and Jensen and Allen (n.d.). The method relies on means of solar irradiance, air temperature, relative humidity and wind speed from measurements of net radiation, soil heat flux and two profile measurements of air temperature and water vapour pressure;
3. The Bowen ratio energy balance (BREB) method (Everson, 2001; Savage et al., 2009 for montane grassland);
4. The sensible heat flux measurement approach using, for example, surface renewal (SR) (see Paw U et al., 1995; Snyder et al. 1996; Castellví et al. 2002, 2008), or scintillometer methods (Savage 2009, Savage et al. 2010) or temperature variance (TV), from which *LE* is calculated using measurements of the water-stored heat flux (Mengistu and Savage, 2010a);
5. Eddy covariance (EC) which enables direct measures of sensible heat flux *H* and latent energy flux, the latter also referred to as *LE* (Savage 2009);
6. Remote sensing methods for determining *H* and *LE* (Kalma et al., 2008);

7. The Monin-Obukhov similarity theory (MOST) method (Savage, 2010a);
8. The bulk transfer method given by Sene et al. (1991).

Reasons for the research

The above-mentioned methods have been used extensively for estimating evaporation from vegetated surfaces. There have, however, been very few attempts at applying these methods to estimating open water evaporation.

Most of the methods listed involve the estimation of evaporation through the application of an energy balance equation for the water surface from which evaporation is calculated. These methods suffer from the weakness that the difficult term of the energy balance, *viz.* the water-stored heat flux, needs to be estimated or measured. The first method involves measurement of pan evaporation from which evaporation is estimated using a pan to dam factor. The full eddy covariance method allows determination of *LE* directly. Remote sensing methods are becoming more popular but the methodology still needs calibration and validation with ground truth data and are unlikely to yield daily evaporation. In the case of the MOST method, it is proposed that four measurements, including remote-sensed open water measurements, be used to calculate evaporation independent of the assumption of the energy balance.

Value of the proposed research

The goal of this research was to improve the following hydrometeorological methods and improve the estimation of open water evaporation:

(a) daily estimation of open water evaporation based on automatic weather station measurements and defined protocols for the calculation of *LE* (based on the Penman-Monteith method);
(b) estimates of sub-daily evaporation by surface renewal and/or temperature variance;
(c) developing and testing of a four-measurement inexpensive method, based on MOST, for estimating sub-daily evaporation independent of the energy balance. See for example, Businger and Yaglom (1971).

Sound and documented procedures for estimating open water evaporation would have significant value in terms of weather and climate modelling, and, in particular, applying climate change modelling.

Products

(a) A spreadsheet-based model (Penman-Monteith based) methodology for calculating open water evaporation at daily and possibly hourly time scales from measurements of solar irradiance, air temperature, relative humidity and wind speed - or in the case of the daily time scale, reduced data sets for which solar irradiance measurements, for example, are not available (Abraha and Savage, 2008);

(b) Methodology for the estimation of open water evaporation, in real-time, using SR (Savage 2010a, b);

(c) Methodology for estimating evaporation using a relatively inexpensive four-measurement method that requires further investigation.

Knowledge contribution impacts

1. Potentially, the proposed research on improving the procedures and protocols for open water evaporation estimation would make a significant contribution to science and society. The hydrometeorological modelling approach would enable investigation of climate change impacts on open water evaporation, given the availability of a long-term dataset.
2. To date, there have been no attempts to obtain near real-time estimates of evaporation using surface renewal. The proposed research would therefore contribute knowledge by extending the initial surface renewal efforts of Savage et al. (2004), Mengistu and Savage (2010a, b) and Savage (2010), and the web-based agro-environmental data and information system used by Savage et al. (2014).
3. It was anticipated that there would be further knowledge contributions, relevant to this research endeavour, in the form of published papers.

The research would assist with sustainable development solutions in relation to further knowledge of open water evaporation. This would inform policy and decision making in respect of the assessment through a modelling approach of evaporation from open water bodies. The research experience would also supply South African skills and capacity in the neglected research area of hydrometeorology.

Improved open water evaporation estimates would provide water managers with a very useful tool. Furthermore, this research should further enhance the standing of South African science within the international community.

Improved evaporation estimates would mean improved predictions of future water useand the effect on the environment, and improved mitigation measures, which might lessen the impact on the economy of South Africa.

Improved open water evaporation estimation for South Africa would mean improved predictions as to the future impacts of limited water and climate change on the environment, and improved mitigation measures, which will directly impact the environment. This research would have immediate application that would assist scientists, water resource planners and managers and other stakeholders to make timely and informed decisions related to the management of water resources.

Structure of the report

The report consists of seven chapters – an introductory chapter (Chapter 1), a literature review chapter (Chapter 2), four research chapters (Chapters 3 to 6) and a conclusions and recommendations chapter (Chapter 7).

Summary of the research results

A Penman-Monteith model (DPMETHS), that uses land-based meteorological data, was used to estimate daily open water evaporation from the Midmar Dam in KwaZulu-Natal, South Africa. The DPMETHS model estimates, accumulated annually, exceeded 1300 mm during El Niño years. The maximum annual evaporation for the 1963 to 2014 period exceeded 1400 mm with a minimum of 975 mm. Statistically, there has been no significant change in annual evaporation for the 1963 to 2014 period. Agreement between Symon's pan (annual) open water evaporation (available for 1976 to 2006) and DPMETHS model estimates was poor for the period 1976 to 1993 with the Symon's pan significantly underestimating compared to the DPMETHS estimates. For the period 1994 to 2006, there was greater agreement. In a field above-water study at Midmar Dam, in spite of the reasonable MOST versus eddy covariance comparisons, more than 30% of the eddy covariance evaporation measurement data collected was discarded as a result of application of the data quality assurance protocols. It was therefore not possible to use the eddy covariance method to obtain continuous 30-min measurements of evaporation.

Unlike vegetated surfaces, for which there is stomatal control of evaporation during the daytime and virtually no evaporation at night due to stomatal closure, open water surfaces are not constrained. MOST evaporation measurements demonstrated that 44% of daily total evaporation occurs at night and 56% during the daytime. The MOST measurements demonstrated the significant wind control influence on the evaporation estimates. Surprisingly, too, maximum wind speeds generally occurred at night with the nighttime wind run comprising 42% of the total wind run. Over land, vegetation would offer more resistance to wind so wind effects on evaporation would be reduced, compared to open water surfaces. Evaporation was the greatest component of the energy balance by far, representing about 75% of the net irradiance, 12.8% for water-stored heat flux and 12.1% for sensible heat flux. This study has demonstrated the importance of above-water weather data collection for evaporation estimation. Future research should focus on collecting data above open water for an extended period of time that includes a full summer season, in winter and summer rainfall areas and small and large dams.

Synopsis

Evaporation is an important component of the water balance. Evaporation from open water surfaces is a neglected research area in water resources management in South Africa in spite of South Africa's known high evaporative demand. Our previous research on evaporation, based on WRC funding, have been almost exclusively focused on evaporation from vegetation (Savage et al., 1997, 2004; Savage 2009, 2010). Comparatively, very little research attention has been devoted to the hydrometeorological modelling or measurement of open water evaporation, in spite of its general importance and its importance in relation to climate change.

Investigating the impacts of global warming on open water evaporation requires measurements and a model for open water evaporation.

Many methods have been used to measure evaporation for soil and vegetated systems. However, there is a severe lack of measurements and methodology for measurements of open water evaporation.

At the beginning of the research work, three methods had been used previously for the estimation of open water evaporation in South Africa, namely Symon's tank method, eddy covariance (EC) and surface renewal (SR), the latter two based on the work for a two-week period by Mengistu and Savage (2010a). Traditionally, daily open water evaporation is estimated using a Symon's pan daily measurement and a pan-to-dam multiplicative factor.

It was therefore decided to use a whole range of methods: Symon's pan, EC, SR, the Monin-Obukhov similarity theory (MOST) method, (modified) Bowen ratio (BR), TV and a daily Penman-Monteith equilibrium temperature Hargreaves-Samani (DPMETHS) model, that requires land-based meteorological measurements, that was implemented in a spreadsheet. All of these methods, apart from Symon's pan and DPMETHS methods, allow half-hourly estimations of open water evaporation.

While measurements for Midmar Dam in the KwaZulu-Natal Midlands were for the period February 2016 to February 2017, measurements reported on were for the period 14th February to 25th May 2016.

The objectives of the study were to investigate the use of a variety of measurement methods for the estimation of daily and sub-daily open water evaporation. Furthermore, the DPMETHS daily evaporation model was used to estimate daily evaporation for the history of Midmar Dam (1963 to 2014).

The DPMETHS model estimates, accumulated annually, exceeded 1300 mm during El Niño years. The maximum annual evaporation for the 1963 to 2014 period exceeded 1400 mm with a minimum of 975 mm. Annually, evaporation rates peaked at 8 mm day^{-1} during the summer months, decreasing to less than 1 mm day^{-1} in winter. Average evaporation rates ranged between 1 in winter and 5 mm day^{-1} in summer. The average evaporation rate for the period 1963 to 2014 is 3.3 mm day^{-1}. Statistically, there has been no significant change in annual evaporation for the 1963 to 2014 period.

The agreement between Symon's pan (annual) open water evaporation, available for the period 1976 to 2006, and the DPMETHS model estimates was poor for the period 1976 and 1993 with the Symon's pan method significantly underestimating compared to the DPMETHS estimates. For the period 1994 to 2006, the agreement was improved.

The sub-daily evaporation methods are divided into two main categories: methods that rely on the energy balance equation for the open water surface and those that do not. Sub-daily measurements were collected in a field study above Midmar Dam.

The SR, (modified) BR and TV methods, dependent on the energy balance for estimating evaporation, allow for sub-daily measurements of the sensible heat flux term of the energy balance. It was subsequently established that sensible heat flux is the smallest component of the energy balance. If the net irradiance and the water-stored heat flux S are measured, then evaporation can be estimated as a residual of the energy balance. However, unlike the measurement of soil heat flux, for which the soil is stationary, water is not stationary and water movement around the temperature sensors used for the measurement of S results in considerable variation. Due to the small magnitude of the sensible heat flux for open water and the variable nature of S, the SR, TV and BR methods were not pursued further as methods for estimating open water evaporation.

The EC and MOST methods received close attention as they do not require measurements of S. The EC method is expensive and relies on high frequency measurements of vertical wind speed, air temperature and atmospheric humidity. For the first time in South Africa, the EC fluxes of sensible heat and evaporation were determined in near real-time without the need for post-calculations. The MOST method is relatively inexpensive, relying only on routine measurements of air temperature, surface water temperature (using an infrared thermometer), atmospheric humidity and wind speed. The MOST method requires iterative calculations which were implemented in a spreadsheet.

The MOST method is dependent on the roughness length z_o (mm), the height above the water surface at which the horizontal wind speed is 0 m s^{-1}. Two approaches were used for determining z_o. A fixed value of 0.2 mm was obtained as a “best” value by comparing MOST and EC measurements of sensible heat flux for z_o varying between 0.00001 and 5 mm. The value of z_o = 0.2 mm agreed with that used by Blanc (1983). Alternatively, various expressions found in the literature were used for estimating z_o. Temporal comparisons between the EC and MOST measurements of evaporation showed much improved agreement when z_o = 0.2 mm was used in the MOST iterative calculations compared to use of the various expressions for z_o. However, the EC measurements were much more variable than the MOST measurements. Recommended (standard) quality assurance data protocols were applied to the EC measurements. The choice of EC quality assurance grades was a compromise between the amount of data loss and data quality when compared to the MOST measurements. Following data quality control of the EC data, there was reasonable to good comparisons between EC and the MOST evaporation estimates. More than 30 % of the EC evaporation measurement data were discarded as a result of application of the quality assurance protocols. It was therefore not possible to use the EC method to obtain continuous 30-min measurements of evaporation.

The MOST estimates of evaporation demonstrated that even on near-cloudless days, evaporation can be lower than for cloudy but windier days. Unlike vegetated surfaces, for which there is stomatal control of evaporation during the daytime and virtually no evaporation at night due to stomatal closure, open water surfaces are not constrained. MOST measurements for the 100-day measurement period (14^{th} February to 26^{th} May 2016) demonstrated that 44 % of daily total evaporation occurs at night with 56 % during the daytime. The MOST measurements demonstrated the wind control influence on the evaporation estimates. Surprisingly too, maximum wind speeds generally occurred at night with the nighttime wind run comprising 42 % of the total wind run over the measurement period. Over land, vegetation would offer more resistance to wind so wind effects on evaporation would be reduced, compared to open water surfaces.

Evaporation was the greatest component of the energy balance by far, representing about 75 % of the net irradiance, 12.8 % for water-stored heat flux and 12.1 % for sensible heat flux. Evaporation was 86 % of the available energy flux, with sensible heat flux 14 %, representing a long-term average BR of 0.16. Vegetated surfaces would usually have much higher BR values.

Comparisons between the DPMETHS and MOST cumulative evaporation totals showed that the DPMETHS estimates were, over the period of 100 days, 9 % lower than the MOST estimates. MOST estimates of evaporation have the significant advantage of being independent on the available energy flux compared to the DPMETHS method.

MOST estimates of evaporation increase with increasing surface water temperature and these estimates are also dependent on wind speed, air temperature and atmospheric stability. Other controls for open water evaporation include increased atmospheric water vapour pressure which reduces evaporation. LANDSAT data showed that the greatest water temperatures occur along the shoreline with increases in water depth away from the shoreline resulting in decreased surface water temperatures away from the shoreline. It can be hypothesised therefore that shallower dams could have increased evaporation compared to deeper dams. Furthermore, dams in cooler areas could have reduced evaporation compared to those in warmer climates.

Extent to which contract objectives have been met

All contract objectives have been met, including a number of additional objectives. Valuable open water evaporation data (above-water) for a period of in excess of four months have been collected and a daily model for evaporation developed and tested using historical data and the collected open water data. The research showed that the daily model to be within 9.2 % of MOST estimates of evaporation. Two methods, based on the research conducted, are recommended for further use: the MOST method and the spreadsheet model, the latter if automatic weather station data are available. The MOST method would require above-water measurements. This should be a focus for the future.

Future research

Automatic weather stations are now common in South Africa. At present, however, there is not a single above-water automatic weather station. This study has demonstrated the importance of above-water weather data collection for evaporation estimation. Future research should focus on collecting data above open water for an extended period of time that includes a full summer season. A more permanent water station would greatly assist in future testing and refining of the MOST method and collection of evaporation data using the eddy covariance method. This research would require the infrastructural and facilities support of water boards and government departments.

While the MOST measurement method is robust, the results of the study are for a summer rainfall area on one dam. Ideally, the study needs to be repeated in other areas, using a tethered system well away from the shoreline, for large and small, deep and shallow dams, in different climates, including both winter and summer rainfall areas.

In terms of technology transfer, workshops on the important techniques used in this project are recommended including the following topics:

- While the surface renewal method was eventually not favoured for open water evaporation, it is a method that forms the basis of a number of vegetation-based WRC research projects but using methods that are nearly a decade out of date. Researchers need to be updated on the SR methods used in this study;
- The online EC method is also new and researchers need to be made aware of this capability and the capability of offline post-calculations;
- Water managers need to be made aware of the outcomes of this research project through a one-day workshop conducted in Pretoria. In particular, they need to be made aware of the problems associated with the use of the Symon's pan for estimating open water evaporation;
- The suggestion that there should be follow-up studies for large vs small dams, winter rainfall and summer rainfall dams, and dams located in cool compared to warmer climates should be pursued.

CAPACITY BUILDING

Four postgraduate students have been registered against the project:

- Ms PM Mogane, BSc Hons Hydrology, completed: Evaluation of the global data assimilation system-based reference evaporation in southern Africa.
- Mr ANB Lubanyana, BSc Hons Hydrology, completed: The current State of El Niño in Pietermaritburg.
  Mr L Myeni, MSc Agrometeorology, submitted for examination: The radiation balance of Midmar Dam in KwaZulu-Natal, South Africa,
- Mr JM Pasi, PhD Agrometeorology in progress: Open water energy balance of Midmar Dam in KwaZulu-Natal, South Africa.
- S Mojola, A Ndlanzi, KN Ndlazi and N Zulu, four AMET212 (second-year) students, completed a project on adverse weather with a focus on drought, using the Midmar Dam water level data and Cedara weather station data compiled during the course of the WRC project.
- Ms P Meth, a second-year student, spent the July 2016 vacation working on Midmar data. She investigated use of RClimDex software for analysing climate data for climate change.

CONFERENCE PRESENTATIONS

A paper on the research conducted was presented at the 18th SANCIAHS Symposium, Durban, South Africa in September 2016: Monin-Obukhov Similarity Method for Open Water Evaporation
Authors: MJ Savage, JM Pasi, L Myeni, AD Clulow.

An invited (plenary) paper was presented at the 32nd Annual Conference of the South African Society for Atmospheric Sciences, Cape Town, South Africa in November 2016: Open Water Evaporation – Quo Vadis?
Author: MJ Savage.

ACKNOWLEDGEMENTS

This report is an output of WRC Project K5/2355, entitled "OPEN WATER EVAPORATION MEASUREMENT USING MICROMETEOROLOGICAL METHODS". This project was funded and managed by the Water Research Commission. The project was co-funded by the National Research Foundation and the University of KwaZulu-Natal (UKZN).

The contribution of each project team member was invaluable to the project, and we would like to acknowledge:

- Agricultural Research Council, South African Weather Service and Department of Water and Sanitation for supplying water depth data, Symon's pan data and daily weather data;
- Department of Water and Sanitation for use of facilities at Midmar;
- Mr Vivek Naiken and Mr Nicholas Mbangiwa of UKZN for their involvement in aspects of the project;
- Ms Meryl A Savage for her support and minutes of the meetings.

The members of the project steering committee contributed greatly to the research process by guiding and supporting the project team. Apart from the authors, the steering committee comprised the following members:

Mr W Nomquphu	Water Research Commission (Chairman)
Professor JG Annandale	University of Pretoria
Professor CS Everson	South African Earth Observation Network (SAEON)
Dr MG Mengistu	South African Weather Service (formerly UKZN)
Dr NA Rivers-Moore	Research Associate, UKZN
Professor RE Schulze	UKZN
Mr V Singh	Department of Water and Sanitation
Mr CD Tylcoat	Department of Water and Sanitation

STATEMENT ABOUT ARCHIVING OF MATERIAL

Raw data will be stored on two hard drives and on Dropbox. The processed data, in the form of Excel spreadsheets, will be made available to SAEON. The raw data will be made available on request.

Isaiah 55:10 (KJV) For as the rain cometh down, and the snow from heaven, and returneth not thither, but watereth the earth, and maketh it bring forth and bud, that it may give seed to the sower, and bread to the eater:

TABLE OF CONTENTS

LIST OF TABLES

LIST OF FIGURES

LIST OF ABBREVIATIONS

AWS	Automatic weather station
BR	Bowen ratio
BREB	Bowen ratio energy balance
DPMETHS	Daily Penman, Monteith, Equilibrium Temperature Hargreaves-Samani
EC	Eddy covariance
LAS	Large aperture scintillometer
MOST	Monin-Obukhov similarity theory
SLS	Surface layer scintillometer
SOI	Southern Oscillation Index
SR	Surface renewal
TV	Temperature variance
UKZN	University of KwaZulu-Natal

CHAPTER 1: INTRODUCTION

1.1 Rationale for the research (nature and scope)

Evaporation from open water surfaces is a neglected research area in water resources management in South Africa in spite of South Africa's known high evaporative demand. Our previous research efforts on evaporation have been almost exclusively based on evaporation from vegetation (Savage et al., 1997, 2004; Savage, 2009, 2010). Comparatively, very little research attention has been devoted to the modelling or measurement of open water evaporation.

Evaporation from bare soil, from vegetation-covered land surfaces and from open water surfaces is one of the main components of the hydrologic cycle. Estimates of the total amount, over daily, weekly, monthly and annual periods, and the rate of evaporation from open water surfaces is required in water resources management for many purposes: management ofirrigation of agricultural lands, management of wetlands, catchment water balance studies, design of storage reservoirs, and municipal and industrial water supply (Brutsaert, 1982; Marsh and Bigras, 1988; Finch, 2001). However, studies of open water evaporation from fresh water systems have been predominantly carried out on reservoirs and larger lakes. There have been relatively few investigations for smaller reservoirs and ponds (Rosenberry et al., 2007; Mengistu and Savage, 2010a).

Open water evaporation (*LE*) may be estimated using many different hydrometeorological methods/approaches including:

1. Symon's tank/class-A pan measurements;
2. A modelling approach based on the Penman/Penman-Monteith (PM) method, relying on means of solar irradiance, air temperature, relative humidity and wind speed from measurements of net radiation, soil heat flux and two profile measurements of air temperature and water vapour pressure. Studies using this approach include Allen et al. (1998, 2006) and Jensen and Allen (n.d.);
3. Bowen ratio energy balance (BREB) method (Everson, 2001; Savage et al., 2009, for montane grassland);
4. A sensible heat flux measurement approach using, for example, surface renewal (SR) (see Paw U et al., 1995; Snyder et al., 1996; Castellví et al., 2002, 2008), or scintillometer methods (Savage, 2009; Savage et al., 2010) or temperature variance (TV), from which *LE* is calculated using measurements of the water-stored heat flux (Mengistu and Savage, 2010a);

5. Eddy covariance (EC) which enables direct measures of sensible heat flux *H* and latent energy flux, the latter also referred to as *LE* (Savage, 2009);
6. Remote sensing methods for determining *H* and *LE* (Kalma et al., 2008);
7. Monin-Obukhov similarity theory (MOST) method that has been used almost exclusively for vegetated and bare-soil surfaces (Savage, 2010a);
8. Bulk transfer method given by Sene et al. (1991).

For further information, see Penman (1948), Edinger et al. (1968), Keijman and Koopmans (1973) and de Bruin (1982).

1.2 Reasons for the research

The above-mentioned methods have been used extensively for estimating evaporation for vegetated surfaces. There have, however, been very few attempts at applying these methods for estimating open water evaporation.

Some of the methods involve the estimation of evaporation through the application of an energy balance equation from which evaporation is calculated. Eddy covariance does not use this approach since the full EC method allows determination of *LE* directly. Remote sensing is becoming more popular but the methodology still needs calibration, and validation with ground truth data. In the case of the MOST method, it is proposed that three instruments, including remote-sensed open water measurements, be used to calculate evaporation independent of the assumption of the energy balance.

1.3 Value of proposed research

The goal of this research was the following improved hydrometeorological methods and/or improvements in estimating open water evaporation:

(a) Daily and hourly estimates of open water evaporation based on measurements and defined protocols for the calculation of *LE*;
(b) Daily and sub-daily open water evaporation models;
(c) Real-time estimates of hourly evaporation by surface renewal and temperature variance;
(d) Developing and testing of a two-instrument inexpensive method for estimating evaporation using MOST. See, for example, Businger and Yaglom (1971).

Sound and documented procedures for estimating open water evaporation have significant value in terms of weather and climate modelling, and, in particular, applying climate change modelling.

1.4 Envisaged products

(a) A spreadsheet-based (Penman-Monteith based) model methodology for calculating open water evaporation at daily, and possibly hourly, time scales from measurements of solar irradiance, air temperature, relative humidity and wind speed – or in the case of the daily time scale, reduced data sets for which solar irradiance measurements, for example, are not available (Abraha and Savage, 2008);

(b) A methodology for estimating open water evaporation, in real-time, using SR (Savage 2010a, b);

(c) A methodology for estimating evaporation using a relatively inexpensive three-instrument method that requires investigation.

1.5 Knowledge contribution impacts

1. The proposed research had the potential to improve the procedures and protocols for estimating open water evaporation which would make a significant contribution to science and society. The hydrometeorological modelling approach would allow an investigation of climate change impacts on open water evaporation given the availability of a long-term dataset.
2. To date, there have been no attempts to obtain near real-time estimates of evaporation using SR. The proposed research would therefore contribute knowledge by extending the initial SR efforts of Savage et al. (2004), Mengistu and Savage (2010a, b) and Savage (2010) and the web-based agro-environmental data and information system used by Savage et al. (2014).
3. It was anticipated that there could be unexpected knowledge contributions, relevant to this research endeavour, during the course of the research.

The research would assist in sustainable development solutions in relation to further knowledge of open water evaporation. This would in turn inform policy and decision making in respect of the assessment, through a modelling approach, of evaporation from open water bodies. The research experience would also supply South African skill and capacity in a neglected area of research.

Improved open water evaporation estimates would provide water managers with a very useful tool. Furthermore, this research, if successful would further enhance the standing of South African science within the international community.

Improved evaporation estimates would mean improved predictions of future water use and the effect on the environment, and improved mitigation measures, which might lessen the impact on the economy of South Africa.

Improved open water evaporation estimation for South Africa would mean improved predictions of future impacts of limited water as well as climate change impacts on the environment, and improved mitigation measures, which would directly impact on the environment. This research would have immediate application that would assist scientists, water resource planners and managers and other stakeholders to make timely and informed decisions related to the management of water resources.

Table 1.1 List of deliverables for the open water evaporation study

Deliverables			
No.	**Deliverable title**	**Description**	**Target date**
1	Review of literature	Review of literature for the estimation of open water evaporation	15/05/2014
2	Open water evaporation modelling procedures; MOST procedures; materials and methods for data collection	Theoretical development for the modelling of open water evaporation; Theoretical development for the estimation of sensible and latent heat fluxes using MOST	01/07/2014
3	MOST procedures; materials and methods for data collection; air temperature and water vapour pressure error study; field application of open water procedures	Protocols for determining open water evaporation using the following methods: MOST, eddy covariance, surface renewal, temperature variance; Determination of the impact of error in air temperature and water vapour pressure measurement on the MOST estimates of sensible and latent energy estimates; Collection of data sets for estimating open water evaporation – provision of data	01/07/2015
4	Final report	Final report: Comparison between the open water evaporation models and field estimates of open water evaporation; Determination of energy balance components for open water.	01/07/2016

Table 1.2 Project products

Products		
Title/Name	**Target group**	**Application**
Spreadsheet-based model for open water; conference presentation	Researchers/water managers/irrigation engineers	Daily and/or hourly estimation of open water evaporation
Research paper	Scientific community	Estimation of open water evaporation
Surface renewal procedures (spreadsheet-based) and surface renewal and temperature variance datalogger program; conference presentation	Researchers/water managers/irrigation engineers	Surface renewal and temperature variance estimation of open water evaporation (spreadsheet-based) and programme for real-time estimation of sensible heat flux and open water evaporation
Masters dissertation: Methods for estimating open water evaporation	UKZN, WRC	Protocols and models for estimating open water evaporation
Research paper	Scientific community	Near real-time estimation of open water evaporation

1.6 Research location

Midmar Dam is a shallow, turbulent dam subject to periodic draw-down. The dam, constructed in the 1960s, is situated on the Mgeni (Umgeni) River just 3 km south-west of the town Howick. The dam wall was raised in 2003/4 to have a full supply capacity of 235 Mm^3 (Department of Water Affairs and Forestry, 2007). The dam's primary purpose is for municipal and industrial use. The dam is about 24 km from Pietermaritzburg, in the midlands of KwaZulu-Natal, South Africa (Latitude 29°31'10.68" S Longitude 30° 12' 39.21" E, elevation 985 m) (Fig. 1.2). It currently has a surface area of 1788 ha, compared to 1560 ha in 1981 (Breen, 1983).

The area is characterised by a summer rainy season with warm and humid weather and daytime air temperatures exceeding 30°C. Winters are dry and cold with daytime air temperatures less than 20°C and nights below 0°C. November to January (summer) are the wettest months and the mean annual rainfall is around 1000 mm. Water to land wind flows occur (Fig. 1.2) with prevailing winds from the southeast, east and south. Typically, mean water temperatures (0 to 5 m) vary seasonally between 25°C in January and 10°C in July (Akhurst, 1983). The water depth of Midmar Dam, measured in 1981, varied with the season and position. Before the raising of the dam wall, the maximum depth was 20.7 m with a mean depth of 11.36 m, mean width of 1.97 km (maximum of 3.35 km) and maximum length of 5.75 km (Hemens et al., 1977). Breen (1983) and Heeg (1983) give a maximum depth of 23 m with a mean of 11.4 m.

Fig. 1.1 Diagram showing the location of the Midmar Dam study site

Fig. 1.2 An aerial photograph of Midmar Dam. Hobie Point is the location at which the above-water measurements were conducted.

CHAPTER 2: LITERATURE REVIEW

2.1 Introduction

2.1.1 Historical background

Interest in the evaporation phenomenon began centuries ago, around 610 B.C., when Greek philosophers began to make progress in their attempts to rationally explain the physical world they lived in. This yielded the development of some of the elementary concepts and theories that have shaped our understanding of evaporation even to today. Due to limited knowledge at that time, the Greek philosophers mainly formulated theories by observing natural atmospheric events such as mist, or by using their intuition (Brutsaert, 1982a, b). Their writings show little understanding of the hydrological cycle, with a general acceptance of the notion of the evaporation process being both a cause and a result of wind. In 565 B.C., Hippolytus in his doxology stated that:

"Winds are generated when the finest vapours of the air are separated off and they are put into motion by being assembled together; rains are generated from evaporation that is sent up from the earth towards the sun" (Diels, 1934).

By 530 B.C., interest in understanding evaporation had shifted to its cause. Wind as a cause came under scrutiny as more and more philosophers began to understand the influence the sun has on various natural events (Diels, 1934, cited by Brutsaert, 1982b). As a result, theories were proposed which consolidated the sun as the principle governing entity that drove the transformation of elements. More light was shed when philosophers explained that cloud formation results from water leaving the surface of water bodies as water vapour due to a change in energy within the water body (Diels, 1934; Brutsaert, 1982b).

In his book "Meteorology", Aristotle (384 to 332 B.C.) chronicles an improved theory of dual exhalation developed by Herakleitos (Brutsaert, 1982a). Exhalations refer to the rise of fumes or smoke (Wilson, 2013). Dual exhalation is a two-fold exhalation (emissions) from the earth's surface after heating from the sun. The first was thought of and adapted in the Pre-Socratic tradition and was referred to as "wet" (water vapour) exhalation. The second was considered "dry" exhalation (Wilson, 2013). Aristotle realised that moist exhalation required solar irradiance or other forms of heat. He also opposed earlier theories that suggested a connection between evaporation and wind except that both are exhalations and caused by the sun (Brutsaert, 1982a).

It was only in 287 B.C. that a more correct relationship between wind and evaporation was realised. Theophrastos, Aristotle's successor, reiterated that the sun is the most important agent in evaporation but stated that it is not the only factor (Coutant and Eichenlaub, 1974). His view was that the sun sets winds in motion as well as halting them. However, being Aristotle's student, he contradicted his own views as if to appease those who held Aristotle's views when he stated that his views may not hold true universally, and that exhalation is the cause (of wind) while the sun assists (Coutant and Eichenlaub, 1974).

Aristotle's theory enjoyed universal acceptance until the 16th century when Descartes challenged it with new material. His attempts were aimed at expanding Aristotle's theory by explaining in more detail the dynamics involved when the sun energises water particles (Brutsaert, 1982a). Descartes endeavoured to explain separately evaporation and wind by assuming the existence of small particles. He stated that evaporation resulted when the sun heated the water causing an agitation to the particles which then undergo a phase change. He also defined wind as air in motion but a result of evaporation rather than one of its causes, opposing Aristotle's theory (Brutsaert, 1982a). However, Descartes' views could not be trusted due to a lack of evidence. Most questioned the views because experimentation became an essential part of science.

By the 16th to 17th century it was established that the sun's heat causes evaporation, but confusion still reigned over the influence of wind. One of the earliest evaporation experiments recorded was run by Perrault in the winter of 1669 to 1670. He exposed 3.2 kg of frozen water to cold air. After 18 days, the blocks had shrunk to less than 0.5 kg. With more evaporation tests from various oils, Perrault formulated a theory stating that:
"although Aristotle and all other philosophers gave only one cause for the evaporation of water, namely the heat, I would be able to find two more, one the cold, its contrary, and the other the movement of the particles of air".

The effect of cold air on evaporation had previously been suggested. In the 15th century, writers from Lucretius to Vuilhelmus of Conches chronicled views on the effect of cold air on evaporation in a satisfactory manner (Brutsaert, 1982a). However, Perrault's experimental approach validated the earlier theories, making them more acceptable to scientists (Bellhouse, 2011).

2.1.1.1 Initial measurements and experimentation

By the late 16th to early 17th century, experimentation had become an essential part of science. Experiments varied from weight change during the evaporation of water from small pans under different climatic conditions to experiments done in larger basins with the aim of comparing precipitation and evaporation (Brutsaert, 2013). However, due to limited understanding of the evaporation process, ‘scientists’ could not adequately analyse their findings and thus failed to deal with important questions that existed at the time (Brutsaert, 1982a). Though experimentation presented a way to validate the theories, little progress was achieved due to inability to properly apply and analyse experiments (Biswas, 1969). Despite this, the approach stimulated thought and debates which resulted in various hypotheses and theoretical models to explain the phenomenon of evaporation (Bellhouse, 2011).

Two theories dominated this time period: the particle separation theory and the solution theory of evaporation. The particle separation theory assumed that evaporation involves some form of heat which through some electrostatic effects causes small particles of water to jump towards air particles whose gravity is larger, and thus they adhere to them. Once they become electrical, the particles repel each other as the air moves. Since water vapour is less dense, it therefore rises or evaporates as a result. The wind then carries with it the rising water vapour and also, when the wind is dry, it enhances the separation of the particles because of the large amount of fluid electricity it carries (Desaguliers, 1745). The electrical explanation was never widely accepted thus interest deviated to the solution theory of evaporation (Brutsaert, 1982a).

The solution theory of evaporation was generally widely accepted. It explained that air absorbs the water particles at the water surface upon contact. Particles detach and unite with the air and then follow air movements (Mason, 1966). Furthermore, the theory explained air properties (temperature of the air and degree of saturation) that control rates of evaporation (Brutsaert, 1982a).

Some of the advances in the attempt to understand the process of evaporation shed light on other conditions needed for evaporation to occur. The advances included characterisation of the moisture content of the air as influenced by the strength and direction of the wind, and the evaporative cooling effect which led to the discovery of the latent heat concept (Mason, 1966).

By the 18^{th} century, significant progress had been made. However, some theories still carried discrepancies and required investigation (Brutsaert, 1982a). For instance, up until this point, the theory still stated that evaporation required the presence of air to dissolve water. Work by De Luc in 1787 and 1792 addressed this issue when, after running some experiments, he found that when water evaporates, an expansible fluid is produced (steam). This fluid exerted a constant maximum pressure at a given temperature which increases with temperature. The fluid affects a manometer by pressure and a hygrometer by moisture (Brutsaert, 1982a). These findings were the basis for the formulation of the law of partial pressures in gas mixtures, which

Dalton consolidated with further studies (Rodda,1963). At this point, the force of vapour produced by a hot liquid was found to be dependent only on temperature. This seemed unsatisfactory and thus a need for more quantitative work on the theory was paramount.

2.1.1.2 Foundations of present day theories

Dalton's contribution to science in the 19th century was significant in the development of the evaporation theory. The paper he published in 1802 provided more clarity on gas mixtures, vapour pressure as a function of temperature and the influence of humidity (Brutsaert, 1982a). His work received the most recognition after he documented his findings on the effect of wind on the rate of evaporation. He tabled the rate of evaporation under three different wind categories: in calm air, in the middle of a room with closed doors and windows, in a room with open windows with strong wind outside resulting in a draft and in open air exposed to high winds. Dalton found good agreement between the results which were paralleled in numerous subsequent experiments (Rodda, 1963). Dalton did not include the effect of atmospheric pressure in his theory and that evaporation was not solely dependent on water temperature and wind as he implied (Brutsaert, 1982a). By the mid-19th century, evaporation theory began to follow general developments in fluid mechanics and turbulent flow which in turn led to the development of present day similarity theories for the turbulent transfer of water vapour and other scalars in the lower atmosphere (Ferron and Soderholm, 1990).

Further investigation into evaporation saw the discovery of the latent heat of vaporisation. This came about after research on the influence of the cooling effect of the evaporation process. Evaporation from a moistened bulb of a thermometer lowered its temperature and thus it required heat (Brutsaert, 1967). The nature of the heat was unknown and quantification seemed impossible (Brutsaert, 1982a). However, the discovery of the latent heat of vaporisation by Black, in 1760, provided the solution and paved the way for the identification of the major heat transfer mechanisms – conduction, convection and radiation (Brutsaert, 1982a) with latent energy transfer driven by convection.

Radiation is an important factor affecting evaporation. Its influence on evaporation was also investigated concurrently with evaporation theory. By the mid-19th century, the relationship between evaporation, solar radiation and other heat flux components (sensible and latent fluxes) led to formulation of the energy balance concept which quickly became widely accepted (Brutsaert, 1967). By the end of the 19th century, the groundwork had been laid for the development of energy budget procedures (Bowen, 1926).

2.2 Energy fluxes at the earth's surface

2.2.1 Energy balance

Within the earth's lower atmosphere, energy and mass can be transferred from one point to another. The transfer occurs through heat flow, transport of mass (transport of mass is otherwise known as convection), or by performance of work (Wild et al., 2013). Both the energy and mass fluxes are based on the fundamental conservation principles, namely, conservation of energy and conservation of mass. The general energy balance for a process can be expressed in words as: Accumulation of Energy in System = Input of Energy into System – Output of Energy from (Liou and Kar, 2014). However, due to variations in space and time, changes in the energy balance are evident. Some of the variations result from changes in surface conditions, i.e. land, water, snow, ice and different vegetative covers. The different land covers can affect the amount of energy retained and redistributed within the earth's atmosphere (Prueger and Kustas, 2005).

The *shortened* surface energy balance at the land-air interface is:

$$R_{net} = LE + H + S \tag{2.1}$$

where R_{net} is the net irradiance (W m^{-2}), LE the latent energy flux density (W m^{-2}), H the sensible heat flux density and S the soil (or water-stored) heat flux (W m^{-2}). Net irradiance (R_{net}) is partitioned into LE, H and S and hence LE can be determined as a residual provided H and S are known.

2.2.2 Radiation balance

The net radiation balance is considered as the balance between incoming and outgoing shortwave and infrared radiation under steady atmospheric conditions (Allen et al., 1998). It is expressed as:

$$R_{net} = I_s - rI_s + L_d - L_u \tag{2.2}$$

where R_{net} is the net irradiance, I_s the incoming shortwave irradiance, rI_s the reflected shortwave irradiance and L_d and L_u the incoming and outgoing infrared irradiances. All terms are in W m^{-2}.

Shortwave irradiance results directly from the sun. Most of its energy is within the wavelength range of 0.25 to 2.5 µm. Outside the atmosphere, the solar constant is 1395 W m^{-2}. As the irradiance passes through the earth's atmosphere, a reduction in energy occurs after scattering, absorption and reflection by different types of molecules and colloidal particles (Liu and Jordan, 1960). This can be seen from Fig. 2.1 where only half of the solar irradiance is absorbed by the surface, whilst the other half is lost through reflection and absorption in the atmosphere.

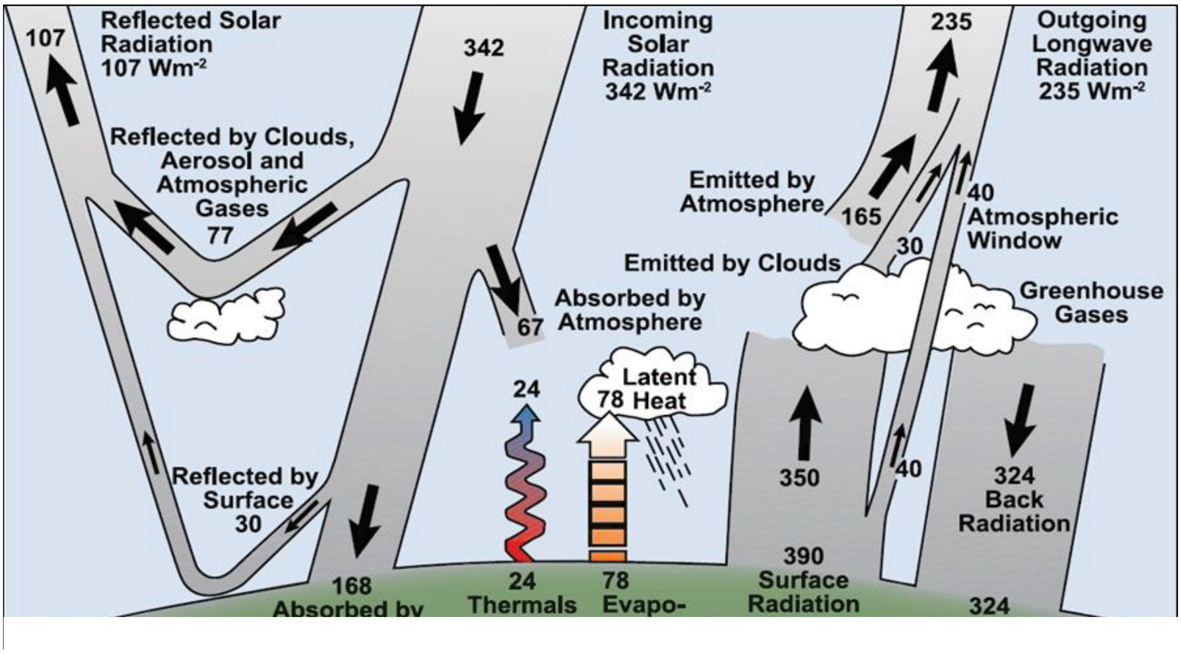

Fig. 2.1 Radiant energy exchange (W m^{-2}) in the atmosphere and at the earth's surface (IPCC, 2013)

Shortwave radiation absorbed by the earth's surface is later emitted as infrared radiation. Infrared radiation is the radiant flux that results from emission from atmospheric gases and the land-water surfaces of the earth (Iqbal, 1983). Infrared radiation is also often referred to as long-wave radiation. These are the third and fourth components of the radiation balance (Eq. 2.2).

From Fig. 2.1, about 10% of the infrared irradiance emitted from the earth's surface (L_u) escapes out of the earth's atmosphere. Clouds and greenhouse gases retain the remainder and re-radiate it back to the earth (L_d). These infrared exchanges contribute to the regulation of the earth's temperature and thus any changes in the fluxes could affect energy transfers within ecosystems on earth.

2.3 Open water evaporation

2.3.1 Introduction

Evaporation from open water, vegetated and bare land surfaces is one of the main components of the hydrologic cycle. An understanding of the amount of open water evaporation and evaporation rates is required for the management of water resources for many different purposes. Examples include the design of reservoirs, water balance studies at the catchment scale, municipal and industrial water supply, irrigation management and wetland management (Brutsaert, 1982b; Finch, 2001). However, the majority of investigations of open water evaporation for fresh water systems have focused on larger lakes and reservoirs with few studies on small reservoirs and ponds (Rosenberry et al., 2007, Mengistu and Savage, 2010a).

Many different methods have been used to estimate open water evaporation, directly or indirectly. The methods used range from relatively simple methods such as the water balance method and floating pan method, to the more complex mass transport approach, potential evaporation approach (Penman, 1948), FAO-56 reference evaporation estimation using the PM method, with some of the methods accounting more accurately for water-stored heat, models based on meteorological data including for example the Priestley-Taylor method, the BREB method and the EC method (Penman, 1948; Bowen, 1926; Swinbank, 1951).

For a small mountain lake, Rosenberry et al. (2007) compared the BREB method with 15 different evaporation methods. The Penman-Monteith method (Monteith, 1965) together with accurate water depth measurements from a pressure-sensitive transducer have been used to estimate evaporation and seepage losses of agricultural water storages (Craig, 2006). Short-term measurements of shallow lake evaporation using the EC and energy balance methods were compared by Stannard and Rosenberry (1991) and Assouline and Mahrer (1993). Assouline et al. (2008) compared evaporation estimates from three water bodies of different sizes and climates. The accuracy and reliability of different methods for estimating open water evaporation is discussed in detail by Craig and Hancock (2004) and McJannet et al. (2008). A combination model which takes into account the heat stored in the water body was introduced by Edinger et al. (1968) and further developed by Keijman and Koopmans (1973) and de Bruin (1982). This model is based on the concept of an equilibrium temperature (for water) for the determination of the energy balance for a well-mixed body of water.

Surface renewal (SR) analysis, based on high frequency measurements of air temperature, for example, is a relatively new, low cost, and simple method for estimating sensible heat flux, latent energy flux, and other scalars (Paw U et al., 1995; Snyder et al., 1996; Spano et al., 1997; Spano et al., 2000; Paw U et al., 2005; Castellví et al., 2006). In South Africa, the SR method for estimation of sensible heat flux has been calibrated and validated for a mixed-community grassland (Savage et al., 2004) and an open water surface (Mengistu and Savage, 2010a) with the method reviewed by Mengistu and Savage (2010b). The SR method has the advantage over other micrometeorological methods since it requires only temporal measurement of the scalar of interest at one point. Zapata and Martınez-Cob (2001) used the SR method to estimate latent energy flux for an endorheic salty lagoon, an aquatic environment characterised by short, sparse vegetation with high proportions of bare soil.

Open water evaporation may be estimated using the shortened energy balance (Eq. 2.1). The effect of advection, both latent energy and sensible heat flux advections, is not accounted for in Eq. 2.1. The SR measurements, for example, may be used to estimate *H* but measurements of R_{net} and *S* are then required to calculate *LE* as a residual using Eq. 2.1. Measurements of *S* are difficult and may fluctuate from positive to negative for each measurement period, mainly due to water turbulence around the temperature sensors, as noted by Tanny et al. (2008) and Mengistu and Savage (2010a). An alternative to using the shortened energy balance is the use of radiometric Bowen ratio (BR) measurements using infrared thermometers for surface water temperature measurements and above-surface air temperature and humidity measurements. Evaporation may then be estimated from the BR and measurements of *H* using EC or SR without relying on stored water flux measurements.

The net irradiance at the surface of the earth is used to evaporate water, heat the air above the soil, heat the soil and vegetation and cause photosynthesis. These terms, excluding stored heat in vegetation, and photosynthesis, constitute the simplified energy balance (Eq. 2.1). The energy associated with photosynthesis is usually small, over a period of less than a day, compared to the other components of the energy balance. When applying the shortened energy balance, photosynthesis is not included. For tall crops with a dense canopy, the heat stored in the canopy and the surrounding air may have to be taken into account. The evaporation of water requires energy to cause a change in the phase of water from the liquid form to water vapour. The symbols used for these forms of energy per unit time interval per unit area and information about each term are as follows:

- R_{net} (W m^{-2}): net irradiance above the water surface. This is measured directly using a net radiometer placed above the surface, typically at 2 to 3 m.
- *S* (W m^{-2}): energy per unit time interval per unit area required to heat water – referred to as stored heat. Generally, *S* is positive during the day and negative at night if the sign convention of Eq. 2.1 is used. This term is estimated using a profile of water temperature sensors.
- *H* (W m^{-2}): energy per unit time interval per unit area required to heat the atmosphere above water – referred to as the sensible heat flux. Generally, *H* is positive during the day and negative during the night. Many methods have been used to estimate *H*.
- *LE* (W m^{-2}): energy per unit time interval per unit area required to evaporate water – referred to as latent energy flux or evaporation.

Generally, LE is positive during the day corresponding to evaporation and negative at night corresponding to condensation. This term may be estimated using the simplified energy balance, assuming that every other term is known, or by aerodynamic methods. Terms ignored in the shortened energy balance include, for example, advection (horizontal transport of energy and water vapour into or out of the area under consideration) and photosynthesis. The term associated with evaporation, LE, could be estimated assuming that there are no other terms of significance in the shortened form of the energy balance, using:

$$LE = R_{net} - H - S \tag{2.3}$$

In words, evaporation (LE) is estimated as the net irradiance (R_{net}) less the sensible heat (H) less the stored heat flux (S). In summary, evaporation may be estimated if R_{net}, H and S are known, assuming that other terms that may contribute are negligible over time periods of less than a day.

2.3.2 Controls on evaporation

Estimation of evaporation from lakes and reservoirs is not a simple matter as there are a number of factors that can affect the rate. The factors are either climatic and physiography of the water body and its surroundings (Granger and Hedstrom, 2010, 2011). Also, evaporation can be enhanced when water is transported by stored heat. The rate of evaporation is, however, fundamentally controlled by the available energy and the ease with which water vapour diffuses into the atmosphere (Finch and Calver, 2008). When the air above the water body is still, the movement of water molecules from the water surface into the air would lead to the saturation of the lowest portion of the air leading to a decline in evaporation. However, turbulence and convection mixes the air near the water surface with the drier air overlying it permitting evaporation to continue. The stronger the wind, the more vigorous and effective the mixing. Also, the greater the difference in temperature between the surface and overlying air, the greater the convective mixing (Granger and Hedstrom, 2010).

2.3.3 Meteorological factors

2.3.3.1 Radiation and wind speed

In the past, radiant energy captured by the water body (net irradiance) was regarded as the dominant control on annual evaporation rates (Finch and Hall, 2001). However, more recent studies have shown otherwise. For instance, Granger and Hedstrom (2011) showed very little relationship between net irradiance and the hourly evaporation for open water. Wind speed showed the strongest relationship with evaporation. This is illustrated in Fig. 2.2.

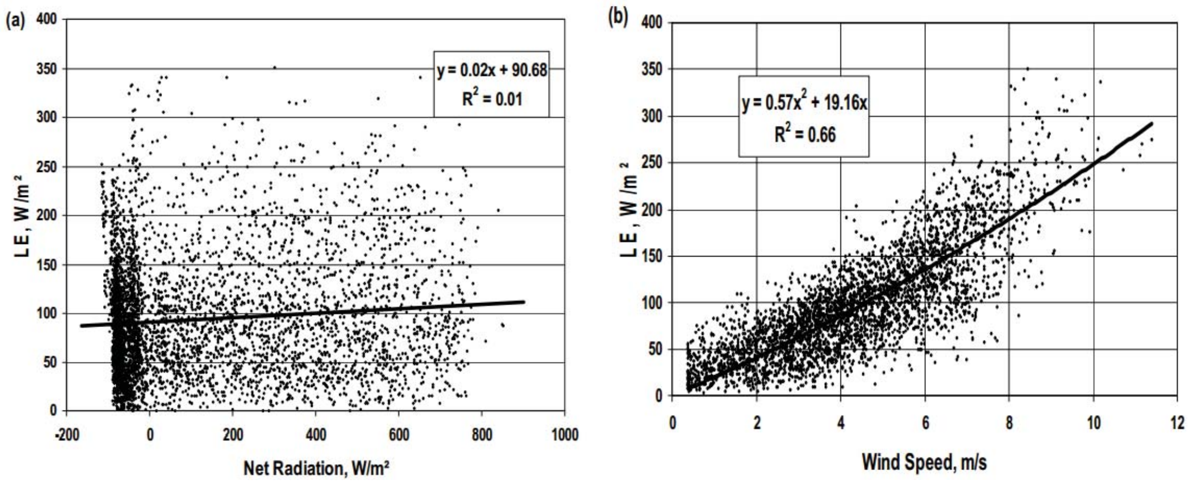

Fig. 2.2 Relationship between the hourly evaporation over Crean Lake, 2006, and (a) net irradiance and (b) wind speed (Granger and Hedstrom, 2011)

2.3.3.2 Humidity

Absolute humidity varies only slightly throughout the day, except with a change of air mass. However, relative humidity is more variable and, as the relative humidity of the air over a water surface increases, so the net transfer of water molecules from the surface is reduced (Finch and Hall, 2001). Relative humidity increases as the temperature of the air decreases resulting in a reduction in evaporation rates.

2.3.4 Water properties

2.3.4.1 Introduction

Many factors may alter the physio-chemical and optical properties of water. These properties may change the storage and transfer of heat in bodies of water and therefore in turn change the evaporation rate. A full review of factors affecting the ability of bodies of water to store and/or transfer heat is given by Finch and Hall (2001) and Finch and Calver (2008).

2.3.4.2 Water depth

Water depth can alter the capacity of water bodies to store heat. Since water depth has a seasonal variation, this capacity can in turn affect evaporation rate. Hence, evaporation rate can be de-coupled in time from the net irradiance.

2.3.4.3 Stored heat

Stored heat flux density F_{stored} (W m^{-2}) may be estimated by determining a vertical profile of water temperature. Thermocouples at different depths may be used for this purpose. These measurements would then allow for ΔT (°C) for a given layer of thickness Δz (m) within the profile to be calculated. The water-stored heat flux density F_{stored} for a particular layer is determined from the change in internal energy of a mass of water M_{water} (kg) with a known density ρ_w =1000 kg m^{-3} and specific heat capacity c_p = 4187 J kg^{-1} K^{-1} per unit time interval Δt per unit horizontal area A_{water} which in turn is determined from a change in water temperature (ΔT_{water}) from one time interval to another (Δt):

$$F_{stored} = M_{water}\, \Delta T_{water}\, c_p \,/(\Delta t \times A_{water}) \tag{2.4}$$

where $$M_{water} \,/\, A_{water} = \rho_w\, V_{water} \,/\, A_{water} = \rho_w\, \Delta z \tag{2.5}$$

Hence $$F_{stored} = \rho_w\, \Delta z\, \Delta T_{water}\, c_p \,/\, \Delta t \tag{2.6}$$

Usually, a 2-min time interval is too short for stored water flux density estimations, so running mean calculations (order 15) may be necessary to obtain half-hourly values of the stored heat flux.

It is generally considered that the effect of water depth can be ignored for water bodies with a depth less than 0.5 m and that the effect reaches a maximum (i.e. the seasonal evaporation ceases to change) once the depth increases beyond 4.5 m (because little of the incoming solar irradiance penetrates below this depth) (Finch and Hall, 2001).

2.3.4.4 Surface reflection coefficient

The surface reflection coefficient (*r*) is affected by a number of factors. Firstly, the proportion of direct to diffuse downward solar radiation is critical because the *r* is a function of the elevation angle of the incoming solar radiation. Once the elevation angle decreases below 37° (elevation angle greater, *r* remains constant), the *r* increases significantly. Secondly, the turbidity of the water changes *r*. A water body with ample suspended particulate matter increases the *r* of the water body. A turbid water body will reflect more solar irradiance reducing the amount of energy absorbed and subsequent evaporation rate. Turbid waters can have *r* values as high as 0.2 compared to 0.08 for clear water. Lastly, the reflection coefficient of the bottom of the water body can also change *r*. However, this only occurs for shallow water bodies where the bottom reflection coefficient has an influence in reflecting solar irradiance (Edinger et al., 1968; Finch and Hall, 2001; Finch and Calver, 2008; Granger and Hedstrom, 2011).

2.3.4.5 Thermal stratification

Thermal stratification or separation due to water density differences as a result of temperature differences occurs in large and deep water bodies. Stratification may increase the time lag between the maximum net irradiance and maximum evaporation rate (Brutsaert, 1967). During seasonal heating from spring to summer, water bodies heat slowly with surface-absorbed heat transported to deeper layers by wind-induced currents and turbulence (Finch and Calver, 2008). With continued heating, heat transfer to shallower layers occurs faster than to deeper layers (Finch and Hall, 2001; Finch and Calver, 2008).

2.3.4.6 Inflow and outflow

The amount of heat stored in a water body may be dependent on the volume of water flowing into a dam compared to that flowing out (Finch and Hall, 2001; Craig, 2006).

2.3.4.7 Vegetation

Vegetation in water may alter the evaporation rate from the water body due to the shade created and the change in the aerodynamic roughness of the surface (Finch and Calver, 2008).

2.3.4.8 Land-lake interactions

Due to vast land surrounding fresh water bodies, the influence of lakes on the equilibrium conditions of the atmospheric turbulence is small when compared with the local water surface. Measurements using EC can test this through back-calculation of the roughness length from the momentum flux and stability measurements. This could show rougher conditions than that from smooth water surfaces (Vesala et al., 2012). As a result, consideration of the dynamics brought about by the land-lake influence on evaporation ensures more precise estimates. In order to reduce the impact of larger scale land-water interactions on EC fluxes, Vesala et al. (2012) and other workers have reduced the averaging period for the flux calculations from 30 min to 5 min.

2.4 Some methods of estimating open water evaporation

Various methods which could potentially be used to estimate open water evaporation are presented in Table 2.1. These include the Class-A pan (Stanhill, 2002) and Symons tank methods, the reference evaporation and crop factor approach, lysimetry, atmometers such as the ETgage and Piche, and a whole range of aerodynamic methods. Excluded from this list are the so-called climate-based estimation methods, largely based on daily maximum and minimum air temperature, which operate at daily, weekly or even monthly time scales. While the use of evaporation pans together with water-body factors is often of historical interest, Stanhill (2002) encourages the continued use of the Class-A pan.

The reference evaporation (ETo) method, based on the Penman-Monteith approach, has recently been updated to allow hourly estimations of ETo, designed mainly for cropped surfaces. Hourly estimations of ETo require measurements of solar irradiance, air temperature, atmospheric humidity and wind speed. Hourly reference evaporation estimation is now possible. The disadvantage of the reference evaporation method is that for estimating *LE*, an open water factor is required.

Methods such as EC involve high frequency measurements of at least two atmospheric variables, vertical wind speed and water vapour pressure, and a theoretical framework and assumptions that allow for the direct calculation of *LE*. Using the same method and instruments, the sensible heat flux density *H* may be determined. Other methods, such as the BREB method, involve up to eight measurements and a theoretical framework and assumptions to estimate *H* and *LE* (Savage et al., 1997; Savage et al., 2004). The temperature-based aerodynamic methods (SR and TV) involve high frequency measurement of a single air temperature from which *H* is calculated and *LE* calculated by measuring the remaining components of the energy balance (Eq. 2.1).

2.4.1 The shortened energy balance

There are many methods for estimating evaporation (Table 2.1). As mentioned by Drexler et al. (2004) in their review, very few methods work well for an hourly time-step, and in some cases, do not work well even for a daily time-step. There is perhaps only one method, the lysimetric method, which allows for the direct measurement of total water loss from a vegetated surface. Virtually all of the methods rely on a theoretical framework for arriving at an expression for *LE* in terms of other measurable quantities, based on certain assumptions or approximations. Many of the methods invoke use of a simplified surface energy balance (Eq. 2.1).

Table 2.1 Possible open water methods for measurement/estimation of sensible heat *H* and/or latent energy flux density (evaporation) *LE* in terms of the surface energy balance where $R_{net} = LE + H + S$

Method	Measurement area, distance or height	Averaging period	Theoretical basis/comment	Closure statement/ Comment
Aerodynamic method (bulk mass transfer)	Measurement height of 8 m	Usually daily	E is related to the product of wind speed (at 8 m) and the difference between the saturated specific humidity (at the water skin temperature) and the measured specific humidity at 8 m	Energy balance not used (Brutsaert, 1982a; Jensen and Allen, n.d.)
BREB	Vertical measurement distance of 1 m (grassland) to 2 m for forests	Usually 20 to 30 min	$LE_{BR} = (R_{net} - S)/(1 + \beta)$, $\beta \neq -1$ where β is the Bowen ratio; $H = \beta\, LE$	By definition, $LE + H = R_{net} - S$ Assumes equality between exchange coefficients: $K_h = K_w$
Class A-pan/Symon's tank	< 5 m^2	Usually daily	$LE_{pan} = L\, \rho_w (\delta W/\delta t)/A_{pan}$ where ρ_w is the density of water, $\delta W/\delta t$ is the rate of change in lysimeter weight and A_{pan} is the pan area	Only pan evaporation measured

Method	Measurement area, distance or height	Averaging period	Theoretical basis/comment	Closure statement/ Comment
Combination method	Various	Daily or hourly	Combination of aerodynamic and energy balance procedures (Penman-Monteith approach)	Ideally, weather data should be obtained above water. Measurements/estimation of stored heat flux required
EC (1 sensor)	Sonic path length of 100 to 150 mm	Usually between 20 and 60 min	$H = \rho\, c_p\, \overline{w'T'}$ $LE = R_{net} - H - S$	By definition, $LE + H = R_{net} - S$
EC (2 sensors)	Sensor path length of 100 to 150 mm	Usually between 20 and 60 min	$LE = \rho\, L\, \overline{w'q'}$, $H = \rho\, c_p\, \overline{w'T'}$ (ρ is the air density and w', q' and T' are fluctuations in vertical wind speed, specific humidity and air temperature respectively)	Generally, $LE + H < R_{net} - S$
Empirical approach: based on Thornthwaite and Holzman (1939) aerodynamic equations		Hourly	Empirical method making use of the relationships between measurements of wind speed, air temperature and water vapour pressure	Method by Granger and Hedstrom (2011)

Method	Measurement area, distance or height	Averaging period	Theoretical basis/comment	Closure statement/ Comment
ETgage atmometer	< 0.01 m^2 Placed about 1 m above the surface	Hourly or daily	A porous surface covered with a material cover of known pore size or known material supplied with water from a reservoir. Differences in the ETgage reservoir depth correspond to the evaporation amount	No examples of use for open water could be found – only short grass or tall crop reference evaporation is estimated
Finite difference model	17 ha, maximum depth of 7.2 m	Daily	Water temperature is estimated by iteration from which R_{net} is calculated, with stored heat flux calculated from the energy balance with H and LE, calculated from standard flux-gradient relations (Brutsaert, 1982)	Closure assumed. Requires weather station data and water depth (Finch and Gash, 2002)
MOST method	Areal measurement (< 25 m^2) of water temperature and wind speed	Hourly	MOST is used to estimate H and LE	Using the MOST iterative method for determining H and LE

Method	Measurement area, distance or height	Averaging period	Theoretical basis/comment	Closure statement/ Comment
Reference evaporation	Point measurements at 2 m above short grass of solar irradiance, air temperature, wind speed, water vapour pressure	Hourly/daily	Penman-Monteith method for estimating reference evaporation (FAO 56), and use of a crop factor (Allen et al., 2006) for short grass (0.1 m tall) and tall crops (0.5 m tall)	Shortened energy balance used and therefore closure is forced. Only reference evaporation and estimated crop evaporation estimated. This method is also applicable to open water
Scintillometer: Large aperture scint-illometer (LAS)	Pathlength: 0.25 m to 3.5 km (up to 10 km for boundary layer scintillometers)	2 min to 60 min	Measures C_n^2, the structure parameter for refractive index fluctuations; MOST is assumed	By definition, $LE + H = R_{net} - S$
Scintillometer: Surface layer scintillometer (SLS)	SLS beam length between 50 and 250 m	2 min and 60 min	MOST used to estimate H and LE estimated using $LE = R_{net} - H - S$	By definition, $LE + H = R_{net} - S$
Surface renewal (SR)	Point measurement at known height	2 min and 60 min	$H \propto$ amplitude of the air temperature ramps/(ramp period)	By definition, $LE + H = R_{net} - S$

Method	Measurement area, distance or height	Averaging period	Theoretical basis/comment	Closure statement/ Comment
Temperature variance (TV)	Point measurement of the friction velocity and the standard deviation in air temperature at known height	30 min	$H \propto \sigma_T$ and u_* where σ_T is the temporal air temperature standard deviation and u_* is the friction velocity (m s^{-1}); MOST is assumed	By definition, $LE + H = R_{net} - S$
Variational method	Large lake		Uses observed hourly meteorological information at 18 m above open water, and MOST	Uses a so-called cost function to minimise errors between the calculated and observed wind speed and air temperature gradient specific humidity gradients (Cao et al., 2006)
Remote sensing methods	Lakes and reservoirs	Daily and longer	Water accounting procedure	Assumed via Penman-Monteith (Karimi et al., 2013; Karimi and Bastiaanssen, 2014)

2.4.1.1 Energy balance closure

If all four components of the shortened energy balance (R_{net}, LE, H and S of Eq. 2.1) are measured independently and correctly, then Eq. 2.1 should be satisfied and closure is said to be satisfied. However, the condition could still be satisfied even if two or more terms have incorrect data values but fortuitously the terms still sum to 0 W m^{-2}. It would be inconceivable, however, that an incorrect set would always sum to 0 W m^{-2} for each time interval. Use of the energy balance equation for independent measurements of the component terms results in:

$$c = R_{net} - LE - H - S \tag{2.7}$$

where c is termed the energy balance closure (W m^{-2}). Closure is said to be satisfied if c = 0 W m^{-2}. A non-zero value for c may be due to measurement errors in one or more of the component energy balance terms, although a near-zero value for c may be due to two or more of the component terms with incorrect values tending to cancel each other. According to Stannard et al. (1994), a near-zero value for c increases confidence in the flux density measurements but does not necessarily verify them. Another measure of the lack of closure is the closure ratio CR, which is given by:

$$CR = (LE + H)/(R_{net} - S) \tag{2.8}$$

for which a closure ratio of 1 yields the shortened energy balance equation (Eq. 2.1).

The spatial scales of measurements of the component energy balance terms are different due to the nature of their measurement. For example, the source area of S measurements using a heat flux plate and soil temperature sensors is less than 1 m^2. A net radiometer at measurement height of 2 m above canopy with a source area radius of 6 m is equivalent to a footprint measurement area of 113 m^2. While the EC measurements of H are point measurements, they may be influenced by downwind source areas of hundreds of square metres, depending on atmospheric stability (Savage et al., 1995, 1996). The differing spatial scales of the energy balance component measurements tend to counter the achievement of closure especially for heterogeneous terrain (Stannard et al., 1994; Foken, 2008).

2.4.1.2 Closure not satisfied?

For their relatively homogeneous terrain, Savage et al. (1997) found that the average closure value c was positive. For their heterogeneous terrain using EC measurements, Stannard et al. (1994) also found that the mean closure value was positive. Stannard et al. (1994) listed a number of possible mechanisms associated with $c > 0$ W m^{-2}:

- the magnitude of one or both of H and LE is underestimated;
- the available energy flux density, R_{net} - S, is overestimated;
- the sensible heat or latent energy content, or both, of the air advected into the source area of the flux density measurements by the mean wind speed is less than that leaving the source area (horizontal flux divergence);
- mismatched source areas for the different measurements of the energy balance component terms.

In addition, $c > 0$ W m^{-2} could be caused by a combination of the above-mentioned possible mechanisms but could also be due to other probabilities such as the lag time between S and other energy balance components R_{net}, LE and H (Stannard et al., 1994). However, if this were to be the main mechanism for lack of closure, there would, for example, be periods for which $c > 0$ W m^{-2} and afternoon periods for which $c < 0$ W m^{-2}. Furthermore, Stannard et al. (1994) reasoned that the influence of horizontal flux divergence on c would be small. They reasoned that divergence of H would tend to be opposite in sign to the divergence of LE since wetter areas tended to be cooler and drier areas tended to be warmer. Therefore, in total, these divergences would tend to nullify. They concluded that a detailed network of air temperature, relative humidity and wind speed sensors would be required to determine the net effect of divergence at any site. They also concluded that underestimation of H and LE was the major cause of the tendency for c to be positive.

Ham and Heilman (2003) found that the energy imbalance persisted in different surfaces with an average of about 20%, but that the energy balance closure was better on average in the afternoon than in the morning, possibly suggesting the underestimation of storage terms, which are usually larger in the morning. Finnigan et al. (2003) found that filtering of the low frequency covariances by the averaging-rotation operations in common use is a large contributory factor to failure to close the energy balance over tall canopies. Cava et al. (2008) maintain that the use of a ‘long-term coordinate system’, together with spectral analysis, with the usual 30-minute averaging time is too short to include the entire contribution of turbulent heat fluxes and that a 2-hour averaging period is more suitable if larger-scale motion effects are to be included. Savage (2009), however, demonstrated, for a mixed grassland site, that even when using a 2-minute averaging period, there was good agreement between H_{EC} and H_{SLS}. This was confirmed by Odhiambo and Savage (2009).

Liu et al. (2006) pointed out that lack of closure of the surface energy budget by 10% or more is not uncommon at eddy (covariance) flux sites. They postulate that site heterogeneities, under conditions that are not perfectly ideal, introduce horizontal and vertical advective flow terms that are not resolvable by single point vertical flux tower measurements. They explain that if these advective terms contribute to vertical fluxes at the site, non-closure of the surface energy balance would be inevitable even though appropriate adjustments are made for high/low frequency losses to the EC data and the canopy storage terms of the energy balance are accounted for. They also postulate that a lack of energy balance closure could be due to the effect of the roughness sub-layer on flux measurements.

Foken (2008) maintains that measuring errors or storage terms are not the reason for the non-closure of the energy balance. He maintains that exchange processes on larger scales of the heterogeneous landscape have a significant influence on the energy balance and that if their fluxes were included, the energy balance would be approximately closed.

In the case of the BREB technique, for which the shortened energy balance is assumed (Eq. 2.3), the closure ratio is necessarily always 1. Other methods for estimating H such as the EC and SLS methods often involve measurements of H and estimation of LE by assuming a closure ratio of 1, *viz.* $LE = R_{net} - H - S$. The EC systems that measure H and LE independently of each other make no assumption of the value of the closure ratio. A number of workers have adjusted their measurements, based on conservation of β before and after adjustment, to force an energy balance closure (Twine et al., 2000). Ham and Heilman (2003), however, point out that such methods have legitimate weaknesses and make assumptions that could result in errors as large as those being amended.

2.4.1.3 Differing footprints as a cause of lack of closure?

Given the previously mentioned limitations of the lysimetric method, the search for an alternative standard for evaporation estimation has been the focus of many studies for several decades. The EC, BREB and aerodynamic temperature-based methods essentially yield point estimates of H and LE although these estimates are influenced by events upwind from the point of measurement. In the case of H, the measurement footprint refers to the relative contribution of upwind surface sources to the H measured at a height above the canopy surface. The extent of the footprint area of influence on the measurement using both EC and BREB methods has received attention. For example, Savage et al. (1995, 1996, 1997) investigated the footprints of EC measurements and Stannard (1997) investigated the footprints of BREB measurements. Agreement between BREB, EC and SLS measurements, for example, may be dependent on the footprint of the measurements which in turn depends on the state of atmospheric stability.

The literature reports on the inadequacy of the EC technique for direct estimation of LE (Wilson et al., 2002; Ham and Heilman, 2003) with the result that $LE + H < R_{net} - S$ (Table 2.1) resulting in a closure ratio CR less than 1 (Eq. 2.8). As an alternative therefore, the EC method could be used to measure *H,* from which *LE* may be estimated from simultaneous measurements of R_{net}, *S* and H_{EC}. The extent of closure in this case then cannot be ascertained.

Each of the methods presented in Table 2.1 result in measurements with different footprints. For example, the footprint of the lysimetric measurements is the area of the lysimeter. In the case of the EC method, the footprint is defined as the relative contribution of upwind surface sources to the measured *H*. As pointed out previously, by theoretical definition and making certain assumptions, BREB measurements always produce exact closure. Problems associated with EC and BREB methods include the following:

- EC measurements of *LE* are often underestimated, as claimed by a number of authors (for example, Twine et al., 2000);
- both EC and BREB estimates of *LE* are based on point measurements;
- due to the theoretical assumptions made using the BREB technique, exact measurement comparisons between BREB and EC measurement techniques have been frustrated by differing assumptions, differing footprint areas, measurement limitations and often-times poor agreement;
- a comparison of two methods does not indicate which method is correct especially if the methods disagree or disagree some of the time.

SLS or LAS measurement methods would remove the limitation of point estimates. The use of SLS or LAS allows for estimation of *H* over distances between 50 and 250 m and 0.25 to 3 km and longer for LAS.

Smooth lake surfaces exhibit lower levels of mechanical turbulence compared to vegetated surfaces and there may be smaller day versus night footprint differences associated with the measurements (Vesala et al., 2012). Also, EC flux measurements may be indicative of current surface conditions but may be difficult to reconcile since they may be more related to turbulent mixing of the water rather than to atmospheric processes.

2.4.2 Reference evaporation estimation

Commonly, *LE* is estimated from grass reference evaporation (Allen et al., 1998, 2006), applied to open water based on point atmospheric measurements at a single level, usually at 2 m, at an automatic weather station, from measurements of solar irradiance, air temperature, water vapour pressure and wind speed. In addition, an open water factor is used for reference evaporation to obtain *LE* which then effectively distinguishes the open water under consideration from the reference. The extension of reference evaporation from daily (Allen et al., 1998) to hourly estimates has been recommended for vegetated surfaces (Allen et al., 2006). Allen et al. (2006) recommend that for application of the FAO-PM ETo method, from FAO 56, applied for hourly or shorter time intervals for short grass, a surface resistance of r_s = 50 s m^{-1} for daytime and r_s = 200 s m^{-1} for nighttime periods, and an aerodynamic resistance of 208/U_2, where U_2 is the horizontal wind speed at a height of 2 m. These adjustments are based on best agreement with computations made on 24-hour time-step basis lysimeter measurements. The daytime surface resistance is also in agreement with that found by Savage et al. (1997) for a grass surface.

Also, for hourly or shorter time intervals for a 0.5-m tall canopy, r_s = 30 s m^{-1} for daytime and r_s = 200 s m^{-1} for nighttime periods and an aerodynamic resistance of 118/U_2 is recommended. Allen et al. (2006) based these adjustments on best agreement with 24-hour time-step lysimeter measurements.

2.4.3 Evaporation from small water bodies

For small water bodies such as shallow lakes, the most widely used evaporation estimation method involves the use of class A-pan monthly totals which are then multiplied by monthly coefficients (Jensen and Allen, n.d.). Jensen and Allen, however, point out that these estimates can be uncertain and biased and suffer from poor pan siting. As a result of this uncertainty, Allen et al. (1998) proposed that (daily) evaporation from shallow water bodies can be approximated by multiplying the reference ETo for short grass by 1.05 (Table 2.2). Presumably the ETo calculation should be based on the reflection coefficient (0.08) for relatively clear water.

2.4.4 Evaporation from larger water bodies

For larger and deeper water bodies – more than 2 to 3 m in depth - the slow increase in water-stored energy flux in summer and when the energy flux reduces later in summer would need to be accounted for. This would entail monthly stored energy flux measurements using temperature profile measurements for the entire water depth in early and late summer, with less frequent measurements in winter. However, as mentioned previously (Section 2.3.1, para 5), water-stored heat flux measurements fluctuate from positive to negative for each measurement period, mainly due to water turbulence in and around the temperature sensors.

2.4.5 Eddy covariance

EC measurements (Swinbank, 1951) allow for absolute point measurements of *H* and *LE* at a defined height above canopy. The EC method is popular since it is a direct method that also allows height-independent estimates of *H* in real-time. The calculation of *H*, for example, using the EC method is based on the covariance between vertical wind speed w and air temperature T which is expressed as $\sum(w - \bar{w})(T - \bar{T})/n$ where the means indicated by the bars are for short time periods, typically 30 minutes. If the covariance is very small, then H_{EC} is small. Positive covariance corresponds to a flux from surface to atmosphere and a negative covariance to a flux toward the surface. The EC method may also be used to directly measure LE_{EC} from the covariance between w and specific humidity q (kg kg^{-1}). Alternatively, LE may be estimated as a residual from the simplified energy balance – measured H_{EC} and measurements of R_{net} and S using the energy balance equation (Eq. 2.3).

Table 2.2 Special case crop factor K values for sub-humid climates (Allen et al., 1998)

"Crop"	Mid-season	End-season
Open water, < 2 m depth or in sub-humid climates or tropics	1.05	1.05
Open water, > 5 m depth, clear of turbidity, temperate climate	0.6525	1.2525

Many of the other methods for estimating H depend on the height-dependent MOST method or depend on height through their theoretical formulation. EC measurements of H, however, are height independent, making the method valuable for above and in-canopy situations. Sensible heat may be estimated using a three-dimensional sonic anemometer. This instrument gives measurements of the three components of wind velocity (u, v and w) as well as an estimate of air temperature using sonic temperature (T_{sonic}) corrected for the influence of water vapour pressure on the speed of sound (Schotanus et al., 1983). Sensible heat is estimated from

$$H_{EC} = \rho\, c_p \sum(w - \bar{w})(T_{sonic} - \bar{T}_{sonic})/n \tag{2.9}$$

where ρ is the density of air (1.12 kg m^{-3}) and c_p the specific heat capacity of air at constant pressure (1040 J kg^{-1} K^{-1}).

The EC method has been used in South Africa by Savage et al. (1997, 2004), Savage (2009) and Odhiambo and Savage (2009). The disadvantage of the EC method is that a plethora of corrections are required for different purposes. For estimations of H_{EC}, the corrections include: coordinate rotation to convert the (u, v, w) wind velocity triplet to (U, 0, 0) as required for the EC theory where $U = (u^2 + v^2 + w^2)^{0.5}$. These corrections are applied to the high frequency data either in real-time using a microprocessor-based EC system or post-data collection if a datalogger is used to collect the high frequency data. In either case, it is advisable to store the original high frequency data; correction of sonic-derived, H_{EC}, for the influence of water vapour pressure through the BR where $H_{EC\,corrected} = H_{EC\,measured}/(1 + 0.07\,\beta)$ (Schotanus et al., 1983). The scintillometer-measured sensible heat estimate, H_{SLS} also requires a correction for β – this correction is smaller than that for H_{EC}. Corrections for EC-measured *LE*, LE_{EC}, include density corrections (Webb et al., 1980); corrections for the spatial separation of the EC sensors, typically 250 mm for the sonic beam and the infrared analyser beam used for water vapour and carbon dioxide concentration (Laubach and McNaughton, 1999). This spatial separation was found to cause LE_{EC} to underestimate actual *LE* by 10%. The H_{EC} measurements are excluded from this since the sonic temperature and the vertical wind speed are measured by the same sensor for the same air sample volume; sensor frequency response (Webb et al., 1980).

Vesala et al. (2012) caution that EC measurements above open water require sturdy construction or a damping system for the measurement platform to prevent the oscillation frequency of the instruments being close to the frequencies of the flux measurements.

2.4.6 Scintillometer method

A scintillometer is used to measure path-weighted *H*. It measures the intensity fluctuations of visible or infrared radiation after propagation above the plant canopy of interest. It optically measures the structure parameter of the refractive index of air, C_n^2 (Thiermann, 1992), reflecting the atmospheric turbulence structure. Using MOST, *H* may be estimated. MOST is empirically based and therefore scintillometer estimates are height dependent. Surface-layer scintillometers (SLS) operate over horizontal distances between 50 and 250 m (Odhiambo and Savage, 2009). Large aperture scintillometers (LAS) operate over typical distances between 0.25 and up to 3 km. In the case of an SLS, a laser beam (low power class 3a as used in laser pointers, 670 nm wave length) is split into two parallel, displaced (2.7 mm separation) beams with orthogonal polarisations. The receiver unit measures the radiation intensity fluctuations from the transmitter at a very high frequency, typically 1 kHz, caused by refractive scattering of small air parcels in the scintillometer path, emitted by the transmitter. A term referred to as the inner scale of refractive index fluctuations (l_o) and C_n^2, is calculated from the variances of the logarithm of the amplitude of the two beams, and the covariance of the logarithm of the amplitude fluctuations between the two beams. Using an iterative technique, and applying MOST, *H* may be calculated.

Essentially, a scintillometer consists of a source of light of known wavelength usually directed over some horizontal distance to a receiver. For an SLS, a laser beam is used so that there is little beam divergence. Changes in the intensity and the phase of the light beam are detected at the receiver position some known horizontal distance from the transmitter (Thiermann, 1992; Thiermann and Grassl, 1992). These changes result from atmospheric perturbations – like a mirage – caused by variations in air temperature that bend (refract) the light beam. Key to implementation of the scintillometer method is the interaction between eddy size, beam distance, beam wavelength and aperture diameter and, for some of the estimates, effective beam height, air temperature and atmospheric pressure. The SLS system is specifically targeted for short path lengths compared to other scintillometer types. A computer or laptop is also required if the unit does not have data storage capability.

Besides cost, a serious disadvantage of all scintillometers, by their very nature, is that they cannot distinguish between upward or downward direction of *H*. Most often, a pair of fine-wire thermocouples are used to measure air temperature at two vertical positions to determine the direction of *H*. This necessitates the use of a second logging system near the midpoint of the light. However, frequently, an automatic weather station system is located near the centre of the beam and this can then be used for the temperature differential measurement. This is problematic for open water research since these measurements would need to be near the midpoint of the optical beam. Alternatively, simultaneous EC measurements of *H* could be used to ascertain the direction of *H* or assuming that unstable conditions corresponding to positive *H* occurs between sunrise and sunset. A second major disadvantage of the scintillometer method is that the method is based on the theory of weak scattering which may not always apply. Strongly turbulent conditions would invalidate the assumption of weak scattering. A third disadvantage of many scintillometer systems is that the friction velocity needs to be known at the time *H* is measured. This is not a problem with an SLS since the friction velocity is estimated from measurements from both beams.

The SLS method has been used in South Africa by Savage et al. (2004), Odhiambo (2008) and Savage (2008) to estimate *H* and *LE* over extended periods for a mixed grassland community. The LAS method has also been used above wattle by Clulow (2007), savanna by Dye et al. (2008), above Renosterveld and wheat by Jovanovic et al. (2011) and by Jarmain et al. (2008). There is no published record of the use of SLS or LAS for extended periods for open water evaporation, in South Africa.

There is an added problem with the use of the scintillometer method. Where SLS or LAS instruments are used, there is an unknown lack of correlation that exists between humidity and temperature fluctuations. Odhiambo and Savage (2009), for the SLS showed the influence of the Bowen ratio on the EC and SLS comparisons. Generally, as the Bowen ratio increased, corresponding to drier conditions, the agreement between EC and SLS determinations of *H* improved. Therefore, it is likely that above open water with high humidity conditions, there may be difficulties with the use of scintillometers. McJannet et al. (2011) proposed a new methodology for obtaining *H* and *LE* fluxes using scintillometers placed over open water. They tested their methodology by comparison with EC measurements. Their methodology used a linearised Bowen ratio approach also implied in Penman-type models.

In summary: an SLS for measurement of *H* consists of a number of components but chiefly a transmitter and a receiver unit separated by between 50 and 250 m with a laser beam emitted by the transmitter and directed at the receiver. For the LAS method, the beam distance is between 0.25 and about 3 km. The SLS method allows *H* to be calculated directly – for the LAS method, additional measurements of wind speed are required.

2.4.7 Bowen ratio method

The calculation of sensible heat flux density ($H = H_{BR}$) and latent energy flux density ($LE = LE_{BR}$) using the Bowen ratio energy balance (BREB) method (Bowen 1926; Sverdrup 1943) is based on the shortened energy balance and the definition of Bowen ratio:

$$LE_{BR} = (R_{net} - S)/(1 + \beta) \tag{2.10}$$

and

$$H_{BR} = \beta \; LE_{BR} \tag{2.11}$$

where β, with condition $\beta \neq -1$, is calculated using:

$$\beta = \gamma \; (\bar{T}_2 - \bar{T}_2)/(\bar{e}_2 - \bar{e}_1) \tag{2.12}$$

where γ (0.066 kPa K^{-1}) is the psychrometric constant, $\bar{T}_2$, $\bar{e}_2$ and $\bar{T}_1$, $\bar{e}_1$ are the time averaged air temperature (˚C) and water vapour pressure (kPa) at profile heights and above the canopy surface, respectively. Assuming that the air temperature and water vapour pressure gradients and *H* and *LE* fluxes are in local equilibrium, with the assumption that the exchange coefficients K_h for *H* and K_w for *LE* are equal, stability dependence of the BREB method is removed (Savage et al., 2009). Two different types of BREB systems have commonly been used. The single-sensor method uses one hygrometer but two sensors for air temperature, with air being pumped alternately from the one level and then from the other (Tanner et al., 1987; Cellier and Olioso, 1993). One type involves an oscillating system in which two sensors, one at each measurement level, are used for air temperature and water vapour pressure determinations (Gay and Greenberg, 1985; Fritschen and Fritschen, 1993). The BREB method has been used in South Africa by Savage et al. (1997, 2004, 2009) and Everson (2001). Data exclusion procedures need to be applied to Bowen ratio data when the Bowen ratio approaches -1 since the theoretical framework causes a mathematical idiosyncrasy when the available energy $H + LE \rightarrow -1$ with the result that Eq. 2.10 is undefined. Usually, this occurs in the early morning and evening periods when evaporation is generally low (except under berg or foehn (or föhn) advective hot and dry conditions). The result is physically inconsistent, and therefore extremely inaccurate and impossibly large positive and negative fluxes are calculated.

2.4.8 Surface renewal

The surface renewal (SR) method (for example, Paw U et al., 1992; Zhang et al., 1992; Paw U et al., 1995; Qiu et al., 1995; Snyder et al., 1996; Anandakumar, 1999; Spano et al., 2000; Castellví, 2004; Castellví et al. 2006) for estimating H is relatively new. The SR method allows $H = H_{SR}$ to be estimated from high frequency measurements of air temperature at a single level using a fine-wire thermocouple. Frequency of measurement for the SR method is typically 8 Hz and post-measurement calculations are used to estimate H. Measurement of R_{net} and S allows LE to be estimated using the shortened energy balance equation. The SR method is attractive because of its simplicity and because it is relatively inexpensive. The method requires knowledge of the measurement height, the rate of change in air temperature, and a weighting factor. The weighting factor needs to be determined, *a priori*, for the vegetation type, thermocouple size and measurement height (Paw U et al., 2005), by comparison of the estimated H with other H measurements from other methods such as EC or SLS. The weighting factor is 0.5 for coniferous forests, orchards and maize when the sensor is at canopy level, and 1 for short grass for a sensor height of about 1 m (Paw U et al., 1995).

Paw U and Brunet (1991) proposed this model by assuming that under unstable atmospheric conditions when the canopy is warmer than the air, any air temperature increase represents air being heated by the canopy. Under stable conditions, when the canopy is cooler than the air, any air temperature decrease represents air being cooled by the canopy. For a given measurement period, H_{SR} can be expressed as the change of heat energy content of air with time per unit area.

$$H_{SR} = M_a \; c_p \; dT_a/(dt \; A) \tag{2.13}$$

where M_a is the mass of air heated (or cooled) by the rate of change in the air temperature difference dT_a in time dt, c_p the specific heat capacity of air at constant pressure (typically 1040 J kg^{-1} K^{-1}) and A the horizontal area of the heated or cooled volume of air. Expressing the mass of air in terms of air density ρ_a and the volume of V_a,

$$H_{SR} = \rho\, c_p\, (V/A)\, dT_a/dt \qquad (2.14)$$

For estimating *H*, Snyder et al. (1996) simplified and modified the SR analysis by substituting V_a/A by the measurement height z and $dT_a/dt\ A$ in Eq. 2.13 by a/τ (˚C s^{-1}) where a is the air temperature amplitude (˚C) and τ the total ramping period for the average rate of change in air temperature for the total ramping period:

$$H_{SR} = \alpha\, z\, \rho\, c_p\, a/\tau \qquad (2.15)$$

So, the SR analysis involves high frequency air temperature measurements and considering air temperature ramps (positive or negative) consisting of quiescent periods (for which there is no change in air temperature with time) andthen ramping periods for which there is an air temperature ramp for unstable conditions (that is, an air temperature increase) or for stable conditions for which there is an air temperature decrease.

The amplitude of the air temperature ramp and the ramp period is estimated using an air temperature structure parameter approach, based on measuring air temperature at a typical frequency of about 8 Hz or greater, using the van Atta (1977) approach which involves estimating the air temperature amplitude. For the calculation of *H*, the average of the second-, third- and fifth-order air temperature deviations from the mean is calculated by the datalogger following which the van Atta approach is applied on a PC. The SR method has been used in South Africa by Savage et al. (2004), Mengistu and Savage (2010a, b) and Mengistu (2008). Other temperature-based methods for estimating *H* have also proved satisfactory (Savage, 2007).

2.4.9 Temperature variance method

For the temperature variance (TV) method, based on MOST, $H = H_{TV}$ is estimated using the method of Tillman (1972) for unstable conditions:

$$H_{TV} = \rho\, c_p\, (\sigma_T^3\, k\, g\, z/\bar{T})^{0.5} \qquad (2.16)$$

where σ_T is the temporal standard deviation of air temperature (K) over a time period (typically 30 min) and where σ_T^2 is the variance in air temperature, *k* the von Kármán constant (0.40), *g* the acceleration of gravity (typically 9.7968 m s^{-2}), for height *z* above flat and short homogeneous vegetated surfaces and where $\bar{T}$ (K) is the mean air temperature. Tillman (1972) extended the method, for the free convection range, to encompass the free and forced convective turbulent ranges through the use of air temperature skewness. Skewness involves the sum over a time interval of the cube of the air temperature deviation from the mean (Savage, 2010, 2014; Abraha and Savage, 2012). It would appear that the TV method has not been applied for determining *H* for open water but can be used to estimate the direction of *H* determined from third-order temperature structure function (Savage, 2010).

2.4.10 Model for daily evaporation using the Penman-Monteith method and water-body equilibrium temperature

2.4.10.1 Model algorithm

Daily evaporation (mm day^{-1}) for a water surface may be estimated using the Penman-Monteith (Monteith, 1965) method:

$$E = \frac{1}{L}\frac{\Delta\,(R_{net} - S) + 86400\;\rho\;c_p(e_s(T_a) - e_a)/r_a}{\Delta + \gamma} \tag{2.17}$$

where e_a is the measured 09h00 water vapour pressure (kPa) and $e_s(T_a)$ (kPa) the saturation water vapour pressure at T_a. The more explicit following form, which includes the modelling of the surface water temperature T_{water} based on the approaches by Edinger et al. (1968), Keijman and Koopmans (1973), de Bruin (1982) and Finch (2001), is used:

$$E = \frac{1}{L}\frac{\Delta_w(R_{net\,wet} - S) + 86400\;\rho\;c_p\;(e_s(T_{water}) - e_a)/r_a}{\Delta_{Twater} + \gamma} \tag{2.18}$$

The specific latent heat of vaporisation L (MJ kg^{-1}) is calculated from the daily-averaged air temperature T_a (˚C).

The slope of the saturation water vapour pressure *vs* temperature relationship at the daily average (modelled) water temperature T_{water} (°C), Δ_{Twater} (kPa K^{-1}), is determined using:

$$\Delta_{Twater} = 4098.02862 \cdot e_s(T_{water})/(237.3 + T_{water})^2 \tag{2.19}$$

where $e_s(T_{water})$ is the saturation water vapour pressure (kPa) at water temperature T_{water}, a modelled parameter.

The term R_{net} in Eq. 2.17 is the net irradiance (MJ m^{-2}) and in Eq. 2.18 is the net irradiance for a wet surface, S the stored heat flux (MJ m^{-2}), 86 400 the 1 day = 86 400 s conversion, ρ_a the air density (typically 1.12 kg m^{-3}), with the specific heat capacity of air at constant pressure, c_p (MJ kg^{-1} K^{-1}) (typically 1020 J kg^{-1} K^{-1}).

The aerodynamic resistance r_a (s m^{-1}) is calculated using wind speed measurements and reservoir water surface area using:

$$r_a = \frac{86400\ \rho\ c_p}{\gamma\ f(U)} \tag{2.20}$$

(Calder and Neal, 1984) from the Sweers (1976) wind function

$$f(U) = \left(\frac{5}{A}\right)^{0.05} (3.80 + 1.57\ U_{10}) \tag{2.21}$$

where A (km^2) is the water surface area and U is the wind speed (m s^{-1}) usually measured at z_2 = 2 m, U_2, scaled to z_{10} = 10 m:

$$U_{10} = (z_{10}/z_2)^{0.31} U_2 \tag{2.21}$$

(Yao, 2000). The psychrometric constant γ (kPa K^{-1}) is calculated using:

$$\gamma = \frac{c_p\ P}{1000\ \varepsilon\ L} \tag{2.22}$$

where ε = 0.62198 is the ratio of the molecular mass of water vapour to that of dry air.

For the model, net irradiance is calculated from measured solar irradiance (MJ m^{-2}), water surface reflection coefficient r (approximately 0.08), the net infrared irradiance which is in turn calculated from air temperature T_a at 09h00, the water surface temperature and a cloudiness factor C_f. The daily average water surface temperature for day i, $T_{w,i}$, is estimated. The land-surface radiation balance is given by:

$$R_{net} = I_s - rI_s + L_d - L_u \tag{2.23}$$

where

$$L_d = \sigma(T_a + 273.15)^4 \left(C_f + \left(1 - C_f\right)\left(1 - 0.261 \exp(-7.77{\times}10^{-4}\ T_a^2)\right)\right) \tag{2.24}$$

is the downward infrared irradiance (MJ m^{-2}) (Idso and Jackson, 1969; Oke, 1987) where σ = 4.9 × 10^{-9} MJ m^{-2} K^{-4} is the Stefan-Boltzmann constant, modified for the daily time scale.

The procedure for determining the cloudiness factor C_f is that of Jegede et al. (2006): for $I_s/I_{s\,clear} \leq 0.9$, where

$$I_{s\,clear} = I_{s\,extra}\,(0.75 + 2\times10^{-5}h) \tag{2.25}$$

is the clear-sky solar irradiance (MJ m^{-2}), and where $I_{s\,extra}$ is the extraterrestrial solar irradiance (MJ m^{-2}), h the site altitude (m) where $I_{s\,extra}$ is calculated using a standard astronomical equation involving day of year, latitude, declination and sunset hour angle, then

$$C_f = 1.1 - I_s/I_{s\,clear} \tag{2.26}$$

Otherwise, if $I_s/I_{s\,clear} > 0.9$ then

$$C_f = 2\,(1 - I_s/I_{s\,clear}) \tag{2.27}$$

The outward infrared irradiance (W m^{-2}) for a surface at temperature T_{water} (°C) is calculated using:

$$L_u = 0.97\,\sigma\,(T_{water} + 273.15)^4 \tag{2.28}$$

and approximated using a Taylor series expansion at T_a by:

$$L_u = 0.97\,(\sigma\,(T_a + 273.15)^4 + 4\sigma\,(T_a + 273.15)^3\,(T_{water\,i-1} - T_a)) \tag{2.29}$$

where the factor 0.97 corresponds to the emissivity for water.

The daily average water temperature on day i, $T_{water\,i}$ (°C), is calculated from the average water temperature of the previous day ($T_{water\,i-1}$), a water-body time constant τ (day) and an equilibrium temperature T_e (°C) where:

$$T_{water\,i} = T_e + (T_{water\,i-1} - T_e)\,\exp(-t/\tau) \tag{2.30}$$

where $t = 1$ day with the change in heat energy flux storage in the water (MJ m^{-2}) between day i and $i - 1$ is given by

$$S = \rho_w\, c_w\, d(T_{water\,i} - T_{water\,i-1}) \tag{2.31}$$

where ρ_w is the density of water (kg m^{-3}), c_w the specific heat capacity of water (0.004185 MJ kg^{-1} K^{-1}), and d the water depth (m). The water-body time constant τ is a function of ρ_w, c_w, d, the wet bulb temperature T_{wet}, the psychrometric constant γ and Δ_{Twet} the slope of the saturation water vapour pressure *vs* temperature relationship evaluated at T_{wet}:

$$\tau = \frac{\rho_w\, c_w\, d}{4\sigma\,(T_{wet}+273.15)^3 + f(U)(\Delta_{Twet}+\gamma)} \tag{2.32}$$

(de Bruin, 1982). The equilibrium temperature T_e (°C) is given by:

$$T_e = T_{wet} + \frac{R_{net\,wet}}{4\sigma(T_{wet}+273.15)^3 + f(U)(\Delta_{Twet}+\gamma)} \tag{2.33}$$

where $R_{net\,wet}$ is the net irradiance for a wet surface that is therefore necessarily at the wet bulb temperature:

$$R_{net\,wet} = I_s - rI_s + L_d - L_{u\,wet} \tag{2.34}$$

where, using Eq. 2.29 as a basis,

$$L_{u\,wet} = 0.97\,(\sigma\,(T_a + 273.15)^4 + 4\sigma\,(T_a + 273.15)^3\,(T_{wet} - T_a)) \tag{2.35}$$

2.4.10.2 Iterative methodology

For the algorithm described, the wet bulb temperature needs to be obtained by iteration, from air temperature and water vapour pressure for greatest accuracy, although other methods have been used such as that by Jensen et al. (1990). A spreadsheet implementation of the iteration procedure that would allow a wet bulb accuracy of 0.01°C is proposed.

The application of Eq. 2.18 would allow daily estimation of *E* from relatively simple daily micrometeorological measurements, water depth and surface area and the calculated equilibrium temperature based on the iterative solution for the wet bulb temperature.

2.4.11 Radiometric Bowen ratio method applied sub-hourly

The Bowen ratio (β) is defined as the ratio of sensible heat flux H to latent energy flux LE ($LE \neq 0$ W m^{-2}):

$$\beta = H/LE \tag{2.36}$$

Assuming equality between the exchange coefficients for *H* and *LE*,

$$\beta = \gamma \, dT/de \tag{2.37}$$

where dT (°C) and de (kPa) are the respective air temperature and water vapour pressure profile differences between two levels above the water surface. The radiometric Bowen ratio (β_o) may be defined as

$$\beta_o = \gamma \, (T_o - T_a)/(e_s(T_o) - e_a) \tag{2.38}$$

where T_o (°C) is the water surface temperature determined radiometrically using an infrared thermometer and $e_s(T_o)$ (kPa) is the saturation water vapour pressure at the water surface temperature T_o. The advantage of the use of β_o compared to β is that β_o only requires surface temperature measurement, air temperature and water vapour pressure measurement at a single level whereas the use of β requires accurate measurement of air temperature and water vapour pressure at two levels above the water surface.

Sub-hourly evaporation may be estimated using β_o and measurements of sensible heat flux *H* by rearrangement of Eq. 2.36 and substitution of β_o for β:

$$LE = H/\beta_o \qquad (\beta_o \neq 0) \tag{2.39}$$

There are two main advantages of the use of β_o and measurements of *H* for determining *LE*:

- 1. Measurements of R_{net} but in particular *S* are not required for calculating *LE* (Eq. 2.39). Stored heat flux measurements are difficult in shallow water bodies due to variable temperatures caused by moving water around the measurement position. The sensible heat flux may be obtained using EC or SR (Mengistu and Savage, 2010a) and β_o calculated using Eq. 2.38; since evaporation is determined using Eq. 2.39.
- 2. From independent measurements of *H*, data rejection procedures similar to that used with the conventional BR method, associated with $\beta \rightarrow -1$ (Savage et al. 2009), need to be established.

The disadvantage of application of Eq. 2.39 is that the measurement *H* is fraught with difficulties – not the least of which is that for water surfaces, *H* is often small, and usually the smallest component of the shortened energy balance. Furthermore, when β is close to 0, corresponding to very small magnitude H values, very large-magnitude and unreliable LE values result. Modifying the data exclusion procedures of Savage et al. (2009), for $\beta \rightarrow$ -1, to that for $\beta_o \rightarrow 0$, it can be shown that for $\beta_o \rightarrow 0$ the measured temperature difference $\delta T = T_o - T_a$ in Eq. 2.38 has exclusion limits defined by:

$$-2E(\theta) - \frac{\delta e}{\gamma} + \frac{de}{\gamma} < \delta T < 2\,E(\theta) - \frac{\delta e}{\gamma} + \frac{de}{\gamma} \qquad (2.40)$$

where $E(\theta)$ is the error in the equivalent temperature $\theta = T + e/\gamma$ where $E(\theta) = E(T) + E(e)/\gamma$, $\delta e = e_s(T_o) - e_a$ is the measured water vapour pressure difference (denominator of Eq. 2.38), de is the true water vapour pressure difference, and dT the true temperature difference between the water surface and the air above.

2.4.12 Monin-Obukhov similarity theory (MOST)

MOST, a semi-empirical micrometeorological theory, applicable only to the surface layer above the roughness sub-layer, relates surface momentum, sensible heat and latent energy fluxes to vertical profiles of horizontal wind speed, air temperature, and specific humidity in a stationary, horizontally homogeneous atmospheric surface layer for which there is negligible vertical wind speed. Foken (2006) discusses the history of MOST for which Monin and Obukhov (1954) made use of dimensionless functions to account for unstable and stable conditions that deviate from neutral stability. Full theoretical details of MOST are discussed in Chapter 3.

2.5 Summary

Determination of reliable and representative evaporation data is an important issue in atmospheric research, with applications in agriculture, catchment hydrology and the environmental sciences, in South Africa and elsewhere. However, long-term measurements of evaporation at different time scales and from different climate regions are not yet readily available (Savage et al., 2004; Savage, 2008). Field measurement of total evaporation (mainly soil evaporation and transpiration) is of paramount importance in determining the water use of vegetation. In general, studies on total evaporation measurement are limited due to the high cost of instrumentation and sensors, instrumentation battery power requirements and the difficulty in obtaining real-time measurements in, for example, remote areas.

Due to the nature of the complexities involved in measuring near real-time sub-daily open water evaporation, very little work (especially in Africa) has been done. Measurements of small time-step evaporation rates, such as hourly evaporation rates, are important yet relatively difficult to obtain. Measuring devices with a high resolution are needed. Also, most hydrological and meteorological models operate with time-steps of the order of an hour and thus a reliable approach to the estimation of hourly open water evaporation is vital.

The aims of this study were to improve the procedures and protocols for open water evaporation estimation, and, at the same time, make a significant contribution to science and society. The hydro-meteorological modelling approach would allow an investigation of climate change impacts on open water evaporation, given the availability of a long-term dataset. To date, there have been no attempts to obtain near real-time estimates of evaporation using SR. The proposed research would therefore make an impact in terms of knowledge contribution, extending the initial SR efforts of Savage et al. (2004), Mengistu and Savage (2010a, b) and Savage (2010) and the web-based agro-environmental data and information system used by Savage et al. (2014). It is anticipated that there could be unexpected knowledge contributions, relevant to this research endeavour, during the course of the research.

The aim of the research was to assist with sustainable development solutions in relation to further knowledge of open water evaporation. This would in turn inform policy and decision making in respect of the assessment of evaporation from open water bodies through a modelling approach. The research experience would also supply South African skills and capacity in a neglected area of research and improved open water evaporation estimates would provide water managers with a very useful tool. Furthermore, this research should further enhance the standing of South African science within the international community. Improved evaporation estimates will mean improved predictions of future water use and impacts, and improved mitigation measures, which might lessen the impact on the economy of South Africa. Furthermore, it was anticipated that this research would have immediate application that would assist scientists, water resource planners and managers and other stakeholders to make timely and informed decisions related to the management of water resources.

2.6 References

Abraha MG and Savage MJ. 2012. Energy and mass exchange over incomplete vegetation cover. *Critical Reviews in the Plant Sciences* 31: 321–341.

Abraha MG and Savage MJ. 2008. Comparison of estimates of daily solar radiation from air temperature range for application in crop simulations. *Agricultural and Forest Meteorology* 1483: 401–416.

Akhurst EGJ. 1983. Seasonality in the rate of primary production. In: CM Green (ed). *Limnology of Lake Modmar.* South African National Scientific Programmes Scientific (CSIR) Report No. 78. pp. 77–88.

Allen RG, Pereira LS, Raes D, Smith M. 1998. Crop evapotranspiration – Guidelines for computing crop water requirements. FAO Irrigation and Drainage paper 56. FAO, Rome, Italy. pp 300.

Allen RG, Pruitt WO, Wright JL, Howell TA, Ventura F, Snyder R, Itenfisu D, Steduto P, Berengena J, Yrisarry JB, Smith M, Pereira LS, Raes D, Perrier A, Alves I, Walter I, Elliott R. 2006. A recommendation on standardized surface resistance for hourly calculation of reference ETo by the FAO56 Penman Monteith method. *Agricultural Water Management* 811: 1–22.

Anandakumar K. 1999. Sensible heat flux over a wheat canopy: optical scintillometer measurements and surface renewal analysis estimations. *Agricultural and Forest Meteorology* 961: 145–156.

Assouline S and Mahrer Y. 1993. Evaporation from Lake Kinneret: 1. Eddy correlation system measurements and energy budget estimates. *Water Resources Research* 294: 901–910.

Assouline S, Tyler SW, Tanny J, Cohen S, Bou-Zeid E, Parlange MB, Katul GG. 2008. Evaporation from three water bodies of different sizes and climates: Measurements and scaling analysis. A*dvances in Water Resources* 31: 160–172.

Bellhouse DR. 2011. A new look at Halley's life table. *Journal of the Royal Statistical Society: Series A (Statistics in Society)* 1743: 823–832.

Biswas AK. 1969. Experiments on atmospheric evaporation until the end of the eighteenth century. *Technology and Culture*: 49–58.

Bowen IS. 1926. The ratio of heat losses by conduction and by evaporation from any water surface. *Physical Review* 27: 779–787.

Breen CM. 1983. Introduction. In: CM Green (ed), *Limnology of Lake Modmar.* South African National Scientific Programmes Scientific CSIR Report No. 78. pp. 16–21.

Brutsaert W. 1967. Evaporation from a very small water surface at ground level: Three-dimensional turbulent diffusion without convection. *Journal of Geophysical Research* 7222: 5631–5639.

Brutsaert W. 1982. *Evaporation into the atmosphere: theory, history, and applications.* Dordrecht, Holland: Reidel. 299 pp.

Brutsaert W. 1982b. *History of the theories of evaporation: A chronological sketch, evaporation into the atmosphere.* Berlin, Germany: Springer-Verlag.

Brutsaert W. 2013. Use of pan evaporation to estimate terrestrial evaporation trends: The case of the Tibetan Plateau. *Water Resources Research* 495: 3054–3058.

Businger JA, Yaglom AM. 1971. Introduction to Obukhov's paper on 'Turbulence in an atmosphere with a non-uniform temperature'. *Boundary-Layer Meteorology* 2: 3–6.

Calder IR, Neal C. 1984. Evaporation from saline lakes: a combination equation approach. *Hydrological Sciences Journal* 29: 89–97.

Cao Z, Ma J, Rouse WR. 2006. Improving computation of sensible heat flux over a water surface using the variational method. *Journal of Hydrometeorology* 7: 678–686.

Castellví F. 2004. Combining surface renewal analysis and similarity theory: a new approach for estimating sensible heat flux. *Water Resources Research* W05201, 1–20.

Castellví F, Martínez-Cob A, Pérez-Coveta O. 2006. Estimating sensible and latent heat fluxes over rice using surface renewal. *Agricultural and Forest Meteorology* 1391: 164–169.

Castellví F, Perez PJ, Ibañez M. 2002. A method based on high frequency temperature measurements to estimate sensible heat flux avoiding the height dependence. *Water Resources Research* 38 (6) WR000486-20, 1-10.

Castellví F, Snyder RL, Baldocchi DD. 2008. Surface energy-balance closure over rangeland grass using the eddy covariance method and surface renewal analysis. *Agricultural and Forest Meteorology* 148: 1147-1160.

Cava D, Contini D, Donateo A, Martano P. 2008. Analysis of short-term closure of the surface energy balance above short vegetation. *Agricultural and Forest Meteorology* 1481: 82–93.

Cellier P, Olioso A. 1993. A simple system for automated long-term Bowen ratio measurement. *Agricultural and Forest Meteorology* 661: 81–92.

Clulow AD. 2007. The long-term measurement of total evaporation over Acacia mearnsii using large aperture scintillometry. MSc dissertation, University of KwaZulu-Natal, South Africa.

Coutant V, Eichenlaub V. 1974. The DeVentis of Theophrastus: Its contributions to the theory of winds. *Bulletin of the American Meteorological Society* 5512: 1454–1462.

Craig I. 2006. Comparison of precise water depth measurements on agricultural storages with open water evaporation estimates. *Agricultural Water Management* 851: 193–200.

Craig IP, Hancock N. 2004. Methods for assessing dam evaporation - an introductory paper. In: IAA Conference, Adelaide, Australia, May 11–13. 16 pp.

de Bruin HAR. 1982. Temperature and energy balance of a water reservoir determined from standard weather data of a land station. *Journal of Hydrology* 593: 261–274.

Desaguliers JT. 1745. A course of experimental philosophy. Printed for: W. Innys, T. Longman and T. Shewell, and C. Hitch. Fleetfreet, Chicago.

Drexler JZ, Snyder RL, Spano D, Paw U, Tha K. 2004. A review of models and micrometeorological methods used to estimate wetland evapotranspiration. *Hydrological Processes* 1811: 2071–2101.

Dye PJ, Gush MB, Everson CS, Jarmain C, Clulow AD, Mengistu MG, Geldenhuys CJ, Wise R, Scholes R, Archibald A, Savage MJ. 2008. *Water use in relation to biomass of indigenous tree species in woodland, forest and/or plantation conditions.* Water Research Commission, Pretoria, South Africa. Report No. TT 361/08, p156, ISBN 978-1-77005-744-9.

Edinger JE, Duttweiler DW, Geyer JC. 1968. The response of water temperatures to meteorological conditions. *Water Resources Research* 45: 1137–1143.

Everson CS. 2001. The water balance of a first order catchment in the montane grasslands of South Africa. *Journal of Hydrology* 241: 110–123.

Ferron G, Soderholm S. 1990. Estimation of the times for evaporation of pure water droplets and for stabilization of salt solution particles. *Journal of Aerosol Science* 213: 415–429.

Finch JW. 2001. A comparison between measured and modelled open water evaporation from a reservoir in south-east England. *Hydrological Processes* 1514: 2771–2778.

Finch JW, Calver A. 2008. Methods for the quantification of evaporation from lakes. World Meteorological Organization Commission for Hydrology. Geneva, Switzerland.

Finch JW, Gash JHC. 2002. Application of a simple finite temperature difference model for estimating evaporation from open water. *Journal of Hydrology* 255: 252–259.

Finch JW, Hall R. 2001. Estimation of open water evaporation. A review of methods. Environment Agency. Bristol, UK.

Finnigan J, Clement R, Malhi Y, Leuning R, Cleugh H. 2003. A re-evaluation of long-term flux measurement techniques part I: averaging and coordinate rotation. *Boundary-Layer Meteorology* 1071: 1–48.

Foken T. 2008. The energy balance closure problem: An overview. *Ecological Applications* 186: 1351–1367.

Fritschen LJ, Fritschen C. 1993. Surface energy balance system. 4th Symposium Global Change Studies, 73rd AMS Annual Meeting, Anaheim, CA, USA.

Gay LW, Greenberg RJ. 1985. The AZET battery powered Bowen ratio system. Proceedings of 17th Conference Agricultural and Forest Meteorolology 7: 329–334.

Granger RJ, Hedstrom N. 2010. Controls on open water evaporation. *Hydrology & Earth System Sciences Discussions* 73.

Granger RJ, Hedstrom N. 2011. Modelling hourly rates of evaporation from small lakes. *Hydrology & Earth System Sciences Discussions* 15, 267–277.

Ham JM, Heilman JL. 2003. Experimental test of density and energy-balance corrections on carbon dioxide flux as measured using open-path eddy covariance. *Agronomy Journal* 956: 1393–1403.

Heeg J. 1983. Physical and chemical limnology. In: CM Green (ed) *Limnology of Lake Modmar*. South African National Scientific Programmes Scientific CSIR Report No. 78. pp. 22–30.

Hemens J, Simpson DE, Warwick RJ. 1977. Nitrogen and phosphorus input to the Midmar Dam, Natal. *Water SA* 3: 193–201.

Idso SB, Jackson RD. 1969. Thermal radiation from the atmosphere. *Journal of Geophysical Research* 7423: 5397–5403.

Iqbal M. 1983. *An introduction to solar radiation*. Academic Press, Canada.

IPCC. 2013. Climate change 2013. The physical science basis. Contribution of Working Group I to the Fifth Assessment Report of the Intergovernmental Panel on Climate Change. In: Stocker TF, Qin D, Plattner G-K, Tignor M, Allen SK, Boschung J, Nauels A, Xia Y, Bex V and Midgley PM (eds). Cambridge : Cambridge University Press. 1535 pp.

Jarmain CD, Le Maitre D, Everson CS, Gush M, Clulow A. 2008. Modelling vegetation water use for general application in different categories of vegetation. Water Research Commission, Pretoria, South Africa.

Jegede O, Ogolo E, Aregbesola T. 2006. Estimating net radiation using routine meteorological data at a tropical location in Nigeria. *International Journal of Sustainable Energy* 252: 107–115.

Jensen ME, Allen RG. Unpublished. Evaporation from water surfaces. In: Jensen ME and Allen RG (eds). Evaporation, Evapotranspiration and Irrigation Water Requirements, 2nd ed. American Society of Civil Engineers, Reston, VA, USA.

Jensen ME, Burman RD, Allen RG. 1990. Evapotranspiration and irrigation water requirements. American Society of Civil Engineers Manuals and Reports in Engineering Practice, no. 70. New York. 360 pp.

Jovanovic NZ, Jarmain CD, De Clercq WP, Vermeulen T, Fey MV. 2011. Total evaporation estimates from a Renosterveld and dryland wheat/fallow surface at the Voelvlei Nature Reserve (South Africa). *Water SA* 34 (4): 471–482.

Kalma JD, McVicar TR, McCabe MF. 2008. Estimating land surface evaporation: A review of methods using remotely sensed surface temperature data. *Surveys in Geophysics* 29: 421–469.

Karimi P, Bastiaanssen WGM, Molden D. 2013. Water Accounting Plus (WA plus) - a water accounting procedure for complex river basins based on satellite measurements. *Hydrology and Earth System Sciences* 17: 2459-2472.

Karimi P, Bastiaanssen WGM. 2014. Spatial evapotranspiration, rainfall and land use data in water accounting – Part 1: Review of the accuracy of the remote sensing data. *Hydrology and Earth Systems Sciences Discussions* 11: 1073-1123

Keijman J, Koopmans R. 1973. A comparison of several methods of estimating the evaporation of Lake Flevo, Proc. IAHS (Helsinki) Symposium on Hydrology of Lakes, pp. 225–232.

Laubach J, McNaughton KG. 1999. A spectrum-independent procedure for correcting eddy fluxes measured with separated sensors. *Boundary-Layer Meteorology* 89: 445-467.

Liou YA, Kar SK. 2014. Evapotranspiration estimation with remote sensing and various surface energy balance algorithms—A review. *Energies* 75: 2821–2849.

Liu BY, Jordan RC. 1960. The interrelationship and characteristic distribution of direct, diffuse and total solar radiation. *Solar Energy* 43: 1–19.

Liu H, Randerson JT, Lindfors J, Massman WJ, Foken T. 2006. Consequences of incomplete surface energy balance closure for CO_2 fluxes from open-path CO2/H2O infrared gas analysers. *Boundary-Layer Meteorology* 1201: 65–85.

Marsh P., Bigras SC. 1988. Evaporation from Mackenzie delta lakes, N.W.T., Canada. *Arctic and Alpine Research* 20: 220–229.

Mason DR. 1966. Eighteenth Century Theories of Evaporation and Rain, Proceedings of the Oklahoma Academy of Science. Oklahoma Academy of Science, USA. pp. 159.

McJannet DL, Cook FJ, McGloin RP, McGowan HA, Burn S. 2011. Estimation of evaporation and sensible heat flux from open water using a large-aperture scintillometer. *Water Resources Research* 47, W05545, doi:10.1029/2010WR010155

McJannet DL, Webster I, Stenson M, Sherman B. 2008. Estimating open water evaporation for the Murray-Darling Basin: A report to the Australian Government from the CSIRO Murray-Darling Basin Sustainable Yields Project. CSIRO, Australia.

Mengistu MG. 2008. Heat and energy exchange above different surfaces using surface renewal. PhD thesis, University of KwaZulu-Natal, South Africa.

Mengistu MG, Savage MJ. 2010a. Open water evaporation estimation for a small shallow reservoir in winter using surface renewal. *Journal of Hydrology* 3801: 27–35.

Mengistu MG, Savage MJ. 2010b. Surface renewal method for estimating sensible heat flux. *Water SA* 361: 9–18.

Monin AS, Obukhov AM. 1954. 'Osnovnye zakonomernosti turbulentnogo peremeshivanija v prizemnom sloe atmosfery (Basic laws of turbulent mixing in the atmosphere near the ground)'. *Trudy geofiz. inst. AN SSSR* 24(151), 163–187.

Monteith JL. 1965. Evaporation and the environment. In: Fogg GE (ed). *The state and movement of water in living organisms.* Cambridge University Press: London.

Odhiambo GO. 2008. Long-term measurements of spatially averaged sensible heat flux for a mixed grassland community using surface layer scintillometer. Ph.D. Thesis, University of KwaZulu-Natal, South Africa

Odhiambo GO, Savage MJ. 2009. Sensible heat flux by surface layer scintillometry and eddy covariance over a mixed grassland community as affected by Bowen ratio and MOST formulations for unstable conditions. *Journal of Hydrometeorology* 10: 479–492.

Oke TR. 1987. *Boundary-layer climates*. Taylor and Francis e-Library. Psychology Press. UK.

Paw U KT, Brunet Y. 1991. A surface renewal measure of sensible heat flux density. Proceedings of the 20th Conference of Agricultura and Forest Meteorolology. 10-13 September, Salt Lake City, UT. American Meteorological Society, Boston, MA. 52-53.

Paw U KT, Brunnet Y, Collineau S, Shaw RH, Maitani T, Qui J, Hipps L. 1992. On coherent structures in turbulence above and within agricultural plant canopies. *Agricultural and Forest Meteorology* 611: 55–68.

Paw U KT, Qiu J, Su H, Watanabe T, Brunet Y. 1995. Surface renewal analysis: a new method to obtain scalar fluxes without velocity data. *Agricultural and Forest Meteorology* 74: 119–137.

Paw U KT, Snyder RL, Spano D, Su HB. 2005. Surface renewal estimates of scalar exchange. In: Hatfield JL, Baker JM (eds). *Micrometeorology in agricultural systems*. Madison, Wisconsin: American Society of Agronomy. Agronomy Monograph No. 47. pp. 455–483.

Penman HL. 1948. Natural evaporation from open water, bare soil and grass. *Proceedings of the Royal Society of London. Series A. Mathematical and Physical Sciences* 1931032: 120–145.

Prueger JH, Kustas WP. 2005. Aerodynamic methods for estimating turbulent fluxes. In Hatfield JL, Baker JM (eds). *Micrometeorology in Agricultural Systems*. ASA Monogr. 47. Pp 387–416 ASA, CSSA and SSSA, Madison, Wisconsin, USA

Qiu J, Su HB, Watanabe T, Brunet Y. 1995. Surface renewal analysis: a new method to obtain scalar fluxes. *Agricultural and Forest Meteorology* 741: 119–137.

Rodda JC. 1963. Eighteenth century evaporation experiments. *Weather* 189: 264–269.

Rosenberry DO, Winter TC, Buso DC, Likens GE. 2007. Comparison of 15 evaporation methods applied to a small mountain lake in the northeastern USA. *Journal of Hydrology* 3403: 149–166.

Savage, M. J. 2007. Sensible heat estimation using a high frequency temperature based method above various canopies. Proc. 13th South African National Commmittee of the International Association of Hydrological Sciences (SANCIAHS) Symposium. Sept. 6–7, Cape Town, South Africa.

Savage MJ. 2009. Estimation of evaporation using a dual-beam surface layer scintillometer and component energy balance measurements. *Agricultural and Forest Meteorology* 1493: 501–517.

Savage MJ. 2010a. Sensible heat flux for estimating evaporation. D.Sc.Agric. thesis, University of KwaZulu Natal, Pietermaritzburg, South Africa. 343 pp.

Savage MJ. 2010b. Sensible heat flux and evaporation using iteration. Paper presentation to the Combined Congress 2010, South African Society for Horticultural Sciences, Weed Science Society, Crop Production Society and Soil Science Society of South Africa, 18 to 21 Jan, 2010, Bloemfontein, South Africa.

Savage MJ 2014. Web-based teaching, learning and research using real-time data from field-based agrometeorological measurement systems. MScAgric thesis, University of KwaZulu-Natal, South Africa.

Savage MJ, Abraha MG, Moyo NC, Babikir ESN. 2014. Web-based teaching, learning and research using accessible real-time data obtained from field-based agrometeorological measurement systems. *South African Journal of Plant and Soil* 31: 13–23.

Savage MJ, Everson CS, Metelerkamp BR. 1997. Evaporation measurement above vegetated surfaces using micrometeorological techniques. Water Research Commission, Pretoria, South Africa.

Savage MJ, Everson CS, Metelerkamp BR. 2009. Bowen ratio evaporation measurement in a remote montane grassland: Data integrity and fluxes. *Journal of Hydrology* 3761: 249–260.

Savage MJ, Everson CS, Odhiambo GO, Mengistu MG, Jarmain C. 2004. Theory and practice of evapotranspiration measurement, with special focus on surface layer scintillometer (SLS) as an operational tool for the estimation of spatially-averaged evaporation. Water Research Commission Report No.1335/1/04, Pretoria, South Africa.

Savage MJ, McInnes KJ, Heilman JL. 1995. Placement height of eddy correlation sensors above a short grassland surface. *Agricultural and Forest Meteorology* 74: 195–204.

Savage MJ, McInnes KJ, Heilman JL. 1996. The "footprints" of eddy correlation sensible heat flux density, and other micrometeorological measurements. *South African Journal of Science* 92: 137–142.

Savage MJ, Odhiambo GO, Mengistu MG, Everson CS, Jarmain C. 2010. Measurement of grassland evaporation using a surface-layer scintillometer. *Water SA* 36: 1–8.

Schotanus P, Nieuwstadt FT, de Bruin HAR. 1983. Temperature measurement with a sonic anemometer and its application to heat and moisture fluxes. *Boundary-Layer Meteorology* 261: 81–93.

Sene KJ, Gash JH, McNeil DD. 1991. Evaporation from a tropical lake: Comparison of theory with direct measurements. *Journal of Hydrology* 127: 193–217.

Snyder RL, Anderson FE, Spano D, Duce P, Paw U KT, Russo AE. 2007. An Excel application program to compute surface renewal estimates of sensible heat flux from the 2nd, 3rd and 5th moments of a structure function using high frequency temperature data and to compute ET and crop coefficients using energy balance. University of California, Davis, California.

Snyder RL, Spano D, Paw U KT 1996. Surface renewal analysis for sensible and latent heat flux density. *Boundary-Layer Meteorology* 773 (4): 249–266.

South African Department of Water Affairs and Forestry, 2007. Information on South African dams. Hydrological Services, Department of Water Affairs and Forestry. http://www.dwaf.gov.za/hydrology/dwafapp2_wma/ (accessed 1 June 2014).

Spano D, Snyder RL, Duce P, Paw U KT. 1997. Surface renewal analysis for sensible heat flux density using structure functions. *Agricultural and Forest Meteorology* 863: 259–271.

Spano D, Snyder RL, Duce P, Paw U KT. 2000. Estimating sensible and latent heat flux densities from grapevine canopies using surface renewal. *Agricultural and Forest Meteorology* 1043: 171–183.

Stanhill G. 2002. Is the Class A evaporation pan still the most practical and accurate meteorological method for determining irrigation water requirements? *Agricultural and Forest Meteorology* 1123: 233–236.

Stannard DI, Blanford JH, Kustas WP, Nichols WD, Amer SA, Schmugge TJ, Weltz MA. 1994. Interpretation of surface flux measurements in heterogeneous terrain during the Monsoon '90 experiment. *Water Resources Research* 305: 1227–1239.

Stannard DI. 1997. A theoretically based determination of Bowen-ratio fetch requirements. *Boundary-Layer Meteorology* 833: 375–406.

Stannard DI, Rosenberry DO. 1991. A comparison of short-term measurements of lake evaporation using eddy correlation and energy budget methods. *Journal of Hydrology* 1221: 15–22.

Sverdrup HU. 1943. On the ratio between heat conduction from the sea surface and heat used for evaporation. *Annals of the New York Academy of Sciences* 441: 81–88.

Sweers HE. 1976. A nomograph to estimate the heat-exchange coefficient at the air-water interface as a function of wind speed and temperature; a critical survey of some literature. *Journal of Hydrology* 30: 375–401.

Swinbank WC. 1951. The measurement of vertical transfer of heat and water vapor by eddies in the lower atmosphere. *Journal of Meteorology* 83: 135–145.

Tanner BD, Greene JP, Bingham GE. 1987. A Bowen ratio design for long term measurements. *American Society of Agricultural Engineers (Microfiche collection)(USA)*.

Tanny J, Cohen S, Assouline S, Lange F, Grava A, Berger D, Teltch B, Parlange MB. 2008. Evaporation from a small water reservoir: Direct measurements and estimates. *Journal of Hydrology* 351: 218–229.

Thiermann V. 1992. A displaced-beam scintillometer for line-averaged measurements of surface layer turbulence, 10th symposium on turbulence and diffusion. Portland, Oregon, USA.

Thiermann V, Grassl H. 1992. The measurement of turbulent surface-layer fluxes by use of bichromatic scintillation. *Boundary-Layer Meteorology* 584: 367–389.

Tillman JE. 1972. The indirect determination of stability, heat and momentum fluxes in the atmospheric boundary layer from simple scalar variables during dry unstable conditions. *Journal of Applied Meteorolology* 11: 783–792.

Twine TE, Kustas WP, Norman JM, Cook DR, Houser PR, Meyers TP, Prueger JH, Starks PJ, Wesely ML. 2000. Correcting eddy-covariance flux underestimates over a grassland. *Agricultural and Forest Meteorology* 1033: 279–300.

van Atta CW. 1977. Effect of coherent structures on structure functions of temperature in the atmospheric boundary layer. *Archiwum Mechaniki Stosowanej* 291: 161–171.

Vesala T, Eugster W, Ojala A. 2012. Eddy covariance measurements over lakes. *In* Aubinet M, Vesala T, Papale D. (eds). *Eddy covariance: A practical guide to measurement of data analysis.* Springer: Dordrecht Heidelberg, London.

Webb EK, Pearman GI, Leuning R. 1980. Correction of flux measurements for density effects due to heat and water vapour transfer. *Quarterly Journal of the Royal Meteorological Society* 106: 85–100.

Wild M, Folini D, Schar C, Loeb N, Dutton EG, Konig-Langlo G. 2013. The global energy balance from a surface perspective. *Climate Dynamics* 4011–12: 3107–3134.

Wilson K, Goldstien A Falge E, Aubinet M, Baldocchi D, Berbigier P, Bernhofer C, Ceulemans R, Dolman, H Field C, Grelle A, Ibrom A, Law BE, Kowalski A, Meyers T, Moncrieff J, Monson R, Oechel W, Tenhunen J, Valentini R, Verma S. 2002. Energy balance closure at FLUXNET sites. *Agricultural and Forest Meteorology* 1131: 223–243.

Wilson M. 2013. Structure and Method in Aristotle's Meteorologica: A More Disorderly Nature. *Cambridge University Press*, UK.

Yao A. 2000. Wind speed measurement over shore and water surface. http://homepages.cae.wisc.edu/−chinwu/CEE618_Environmental_Fluid_Mechanics/Final_Project/2000_final_Project/Accessed 22nd May 2014. Pp 9.

Zapata N, Martınez-Cob A. 2001. Estimation of sensible and latent heat flux from natural sparse vegetation surfaces using surface renewal. *Journal of Hydrology* 2541: 215–228.

Zhang C, Shaw R, Paw U KT. 1992. Spatial characteristics of turbulent coherent structures within and above an orchard canopy. In: Schwartz SE, Slinn (eds). *Precipitation scavenging and atmosphere-surface exchange: atmosphere-surface exchange processes,* Volume 2. Washington: WGN Hemisphere Publishing Co., USA. pp 41–75.

CHAPTER 3: PROTOCOLS FOR THE ESTIMATION OF OPEN WATER EVAPORATION

3.1 Modelling evaporation

3.1.1 Summary

An important aspect of the reported research involves the modelling and measurement protocols that were used for the estimation of open water evaporation. There have been many challenges to theoretical and protocol development for application in models. The detail of the protocols of the various aerodynamic methods, including the Penman-Monteith method, using a daily time-step model developed for determining open water evaporation is presented. Routine measurements for estimating open water evaporation remain a challenge due to the high cost of the various estimation methods.

3.1.2 Theoretical development, protocols and application for modelling open water evaporation based on the Penman-Monteith method

The micrometeorological background and protocols for open water evaporation (spreadsheet-implemented iterative Penman-Monteith model) at a daily time scale are presented in detail. Simplifying assumptions are required to avoid the need for iterative procedures when calculating Penman-Monteith daily grass reference evaporation (ETo) or open water evaporation. Some initial model results for a 44-year weather dataset are presented. Due to the absence of solar irradiance measurements for the period 1970 to 2008, the Hargreaves and Samani solar radiation model, which is based on the daily air temperature range, was used to estimate daily open water evaporation. Evaporation was also estimated based on sunshine duration data (Angström model applied for 1970 to 2008 inclusive, excluding June 1998 to January 1999, due to missing data). These estimates were more problematic due to the missing data and tended to overestimate annual evaporation compared to estimates obtained using the Hargreaves and Samani solar radiation model in most hydrological years, with considerable underestimation in some years. The average annual (hydrological – 1st October of a particular year to 30th September the following year) Midmar Dam model estimates of open water evaporation exceeds 1300 mm per annum, corresponding to a daily average of 3.62 mm. The annual rainfall is 859 mm. In some years, (1982-8 and 2013-4), the ratio of evaporation (expressed in MJ m^{-2}) to the available energy density was almost 1 – indicative of almost no or negative annual sensible heat flux. In spite of the high ratio, and therefore high annual open water evaporation total, this is indicative of significant local drought conditions. Significantly, gradual increases in this ratio occurred for the period 1973 to 1987 (0.96 to 1.00 respectively) and 2000 to 2013 (0.95 to 0.99 respectively) with more fluctuation in the ratio for the 2000 to

2013 period. Between 1987 and 1992 the model results also indicate a gradual but consistent increase of 43% in annual evaporation due mainly to a concomitant increase in available energy density. The increase corresponds to an increase in annual evaporation from 1150 mm to 1534 mm corresponding to a large increase in the available energy density over the same time period from 2793 to 3991 MJ m^{-2} respectively.

3.1.3 Theoretical development and protocols with limited application for modelling open water evaporation based on surface renewal and temperature variance and MOST methods

Besides the Penman-Monteith approach, the investigation used the MOST method. The MOST method requires calibration against EC measurements, but uses normal weather station sensors except for the addition of an infrared thermometer. The physical relations for arriving at the MOST method are presented. For the calibration procedure, a three-dimensional anemometer and an open-path infrared analyser are required for EC determinations of sensible heat, latent energy and momentum fluxes. For the MOST method, measurements of air temperature, specific humidity, wind speed and the surface water temperature at a height of 2 to 2.5 m above the water surface and application of MOST through a spreadsheet-implemented iterative procedure could allow for flux estimation every two minutes for which 30-min averages can be obtained. A number of iterations may be required for solution of the fluxes, with possibly cases for which no solution for the MOST-method equations is possible. The method is dependent on the unknown parameter z_o, the roughness length. The choice of z_o could be determined by a statistical analysis of the friction of the MOST-estimated velocity in comparison to that obtained using EC measurements over a calibration period. There are also analytic expressions for the various z_o values: $z_o = z_{om}$, z_{oh}, and z_{ov}. These have now also been successfully included in a spreadsheet implementation of MOST using an iterative procedure.

A novel iterative method was applied for estimating open water evaporation for sensible heat flux using SR. For the SR method, the air temperature ramp and period and sensible heat flux (H) for the averaging period was calculated in a single cell for stable and unstable conditions. The roots of a third-order polynomial in ramp amplitude, dependent on the second-, third- and fifth-order air temperature structure functions obtained for each half-hourly averaging period, were efficiently determined by the iterative procedure with the result of the polynomial varying between -0.015 and 0.01. The weakness of SR is that a value for H is obtained for half the number of time periods compared to stable events. A single-cell spreadsheet iterative method is described, with separate calculations of H for stable and unstable cases. The method will be demonstrated using open water SR measurements and compared with the traditional method.

The theory and protocols were investigated for determining H using the TV method. Measurements (10-Hz) of air temperature from an unshielded fine-wire thermocouple placed at various heights above an open water surface are used to obtain TV estimates of sensible heat flux. From these measurements, the following air temperature statistics are determined every 30 min: mean, variance and skewness. For the TV method, the direction of H is determined from the sign of the third-order air temperature structure function and the magnitude of H determined from the mean, variance and skewness of air temperature with adjustments for skewness applied for positive skewness and unstable events. As is the case for the Penman-Monteith and SR methods, the shortened surface energy balance is used to determine the latent energy flux and hence evaporation from the measured net irradiance and stored heat flux.

3.2 Introduction

Micrometeorological methods used to estimate evaporation from vegetated or land surfaces present significant challenges and cost (Savage, 2010; Abraha and Savage, 2012) when used to estimate open water evaporation. Climate change issues are creating a great urgency for accurate, reliable and timely estimates of open water evaporation, using robust methods with a sound scientific basis.

EC is generally regarded as the standard method for the determination of fluxes above surface. The method is, however, expensive and requires many corrections and high skill. In addition, the method has a high power requirement that is problematic for measurements above water. Platforms or other methods for supporting the EC equipment are subject to vibration with potential measurement error.

Very few investigations of open water evaporation have applied MOST. This semi-empirical theory has stood the test of time and has been used for the estimation of entity fluxes in many different systems under a variety of atmospheric conditions and climates (Savage et al., 2004; Savage, 2009, 2010).

Evaporation estimation using the surface energy balance and methods such as surface renewal, temperature variance or Penman-Monteith requires measurements or algorithms to obtain the available flux from the surface net irradiance and the water-stored heat flux. Both measurements/estimations are much more difficult for water bodies. In particular, sub-hourly stored heat fluxes are variable to the extent that smoothing is required when using the energy balance equation (Mengistu and Savage, 2010).

The aim of this work was to estimate sub-hourly evaporation in near real-time from a small and shallow reservoir using normal micrometeorological measurements but with the addition of water-surface temperature. For this purpose, the MOST theory was proposed, requiring the relevant flux equations to be solved iteratively by varying the roughness parameter to minimise the differences between MOST-modelled and measured momentum, sensible heat and/or latent energy fluxes.

The research took place in four phases:

1. A review of literature for the estimation of open water evaporation (Chapter 2 of this re).
2. Discussion of Symon's pan data and theoretical development for the modelling of daily open water evaporation. Theoretical development for the estimation of sensible and latent heat fluxes using MOST.
3. Protocols for determining open water evaporation using the following methods: MOST, EC, the BR radiometric method in conjunction with surface renewal. Determination of the impact of error in air temperature and water vapour pressure measurement on the MOST sensible and latent energy estimates. The methods were tested using data collected above open water for an extended period.
4. Comparison between the open water evaporation models and field estimates of open water evaporation. Determination of energy balance components for open water.

3.3 Modelling of, protocols for and results for open water evaporation at a daily time scale

3.3.1 Introduction

Evaporation from a surface can be calculated using the Penman-Monteith (PM) equation, or "combination" method:

$$LE = \frac{\Delta\,(R_n - S) + \rho\, c_p\, (e_s(T_z) - e_z)/r_a}{\Delta + \gamma \cdot (1 + r_s/r_a)} \tag{3.1}$$

where R_n and S are the net irradiance and soil heat flux respectively, ρ the density of air (kg m^{-3}), c_p the specific heat capacity of dry air at constant pressure (J kg^{-1} K^{-1}), T_z the air temperature (°C) and e_z the water vapour pressure (kPa) at a standard height in a Stevenson screen or Gill shield, r_a the aerodynamic resistance (s m^{-1}) to turbulent heat energy and/or water vapour transfer *from the surface to a height z above the surface* (Allen et al., 2006), Δ and γ the psychrometric constant (both with unit kPa K^{-1}) and the slope of the saturation water vapour pressure relationship (kPa K^{-1}) respectively and both demonstrated on the psychrometric chart, and, r_s the bulk surface resistance (s m^{-1}) that describes the resistance to flow of water vapour from inside the leaf, vegetation canopy or soil to outside the surface. For an open water surface, r_s = 0 s m^{-1} and the refection coefficient r (a unitless ratio) used to determine R_n is assumed to be 0.08. Details relating to Δ (kPa K^{-1}) are discussed later. The PM equation is also often used to calculate, by back-calculation, the surface conductance to water vapour (Wohlfahrt et al., 2009).

As pointed out by Wohlfahrt et al. (2009), it is assumed in Eq. 3.1 that the energy balance is closed – *viz*. the balance of energy is assumed *a priori*.

3.3.2 Theory

An examination of the literature shows that the details for determining Δ (Eq. 3.1) are often absent and sometimes incorrect. Grass reference LE using the PM approach (ETo) is frequently calculated using values for Δ and L evaluated at air temperature T_z at height z. More correctly, however, $\Delta = \Delta(T_o, T_z)$ and $L = L(T_o)$ where T_o is the surface temperature since the surface is usually the source of the evaporation and *not the height z*. To avoid the use of what is usually an unknown temperature, *viz*. T_o, most derivations make the assumption that

$$\Delta = \left(\frac{de_s}{dT}\right)_{T = T_z} \tag{3.2}$$

McArthur (1990) refers to this assumption as the first step in an iterative method for arriving at Δ.

Some derivations instead make the assumption that $T_o \cong T_w$, where T_w is the wet bulb temperature at height z, since an evaporating surface is often wet. An examination of surface temperature data for grassed surfaces, obtained using an infrared thermometer, demonstrates that this cannot be the case, with $T_o > T_w$ for most of the daytime.

The procedure for obtaining T_w involves use of the psychrometric equation. Currently, there is no exact analytical method known for determining T_w from measurements of T_z and e_z or T_z and relative humidity. Jensen et al. (1990) used an approximate method for estimating T_w. They assumed that:

$$T_w \cong (\gamma\, T_z + \Delta\, T_{dp})/(\gamma + \Delta) \tag{3.3}$$

where T_{dp}, obtained from T_z and e_z or T_z and RH_z (relative humidity) measurements, is the dewpoint at the standard height z. An iterative method is required for determining T_w from T_z and e_z and the psychrometric equation.

The assumption that $T_o \cong T_w$ allows Δ to be calculated using

$$\Delta = \frac{e_s(T_z) - e_s(T_w)}{T_z - T_w} \tag{3.4}$$

where $e_s(T_z)$ is the saturation water vapour pressure at T_z and $e_s(T_w)$ is that at T_w. However, McArthur (1990) correctly indicates that

$$\Delta = \frac{e_s(T_z) - e_s(T_o)}{T_z - T_o}, \tag{3.5}$$

the theoretical formulation used by Penman (1948). Practically, Penman (1948) assumed that Δ was approximately the slope of the saturation water vapour pressure versus temperature relationship, evaluated at temperature T_z (Eq. 3.2).

Bristow (1987) used an algorithm which employs Newton's iterative method for solving the non-linearised surface energy balance equation to obtain surface temperature to any desired degree of accuracy. Paw U and Gao (1988) found that use of the PM equation can introduce errors as large as 20% when T_o exceeds T_z and suggested that this was due to the linearisation used in the PM equation. McArthur (1990) found that errors in LE can arise if it is assumed that $\Delta = \Delta(T_z)$ – that is, if Eq. 3.4 is used instead of Eq. 3.5 – but the impact of the assumption has not been explored or applied to ETo calculations.

Using the shortened energy balance equation and resistance expressions for LE and H, an expression for T_o may be derived where $\delta e = e_s(T_z) - e_z$ is the water vapour pressure deficit:

$$R_n - \mathrm{S} = LE + H \tag{3.6}$$

$$LE = \frac{\rho\, c_p}{\gamma} \cdot \frac{\delta e}{r_s + r_v} \tag{3.7}$$

$$H = \rho\, c_p \cdot \frac{T_o - T_z}{r_h} \tag{3.8}$$

where r_s is the bulk surface resistance (s m^{-1}), referred to as r_c by McArthur (1990), r_v the boundary-layer resistance (s m^{-1}) to water vapour flux and r_h the boundary-layer resistance (s m^{-1}) to sensible heat flux. As mentioned previously, r_s = 0 s m^{-1} for open water and r (included in the R_n term of Eq. 3.6) is 0.08. In the FAO56 PM formulation, r_h is equated to r_v – that is, similarity between sensible heat and latent energy flux is assumed. Assuming similarity, making $r_h = r_v = r_a$, and substituting Eqs 3.7 and 3.8 into 3.6 and rearranging to obtain T_o:

$$T_o = T_z + \frac{r_a\, \gamma_*\, (R_n - S)}{\rho\, c_p\, (\gamma + \Delta)} \cdot \frac{\delta e}{r_s + r_v} \tag{3.9}$$

where a modified psychrometric constant, γ_* (kPa K^{-1}), is defined as:

$$\gamma_* = \gamma \cdot \left(1 + \frac{r_s}{r_a}\right) \tag{3.10}$$

MacArthur (1990) also found that the error in LE introduced by the assumption that $\Delta = \Delta(T_z)$ depended on $T_o - T_z$ and on the absolute value of T_z and therefore recommended elimination of the error by using an iterative procedure. However, the error in LE will in turn also depend on δe as Eq. 3.9 shows that $T_o - T_z$ is also a function of δe. It is anticipated, therefore, that the error in LE, due to using Δ of Eq. 3.4 instead of Eq. 3.5, will be greatest for locations that experience dry atmospheric conditions or dry periods.

If $T_o \le T_z$, then

$$R_n - S \le \frac{\rho\, c_p\, \delta e}{r_a\, \gamma_*} \tag{3.11}$$

or using Eq. 3.1, for which for evaporative conditions, $LE > \frac{\rho\, c_p\, \delta e}{r_a\, \gamma_*}$, and hence

$$R_n - S \le (LE)_{r_s=0, r_h= r_v=r_a} \tag{3.12}$$

where $(LE)_{r_s=0, r_h= r_v=r_a}$ is the evaporation with a canopy resistance r_s of 0 s m^{-1}, as would be the case for open water, under similarity conditions.

The calculation of T_o using Eq. 3.9, for which Δ depends on T_o and T_z (Eq. 3.5), represents the iterative method from which ETo = ETo(T_o, T_z) is calculated using Eq. 3.1 using r_s and r_a values for short grass, or for open water for which r_s = 0 s m^{-1}. Without using iteration, it is assumed that ETo = ETo(T_z) for which Δ depends on Eq. 3.2.

Iteration would then be required only once, for short-grass surfaces, for determining T_o iteratively and hence ETo for all agro-environmental circumstances excluding open water. For open water, two iterative procedures are required:

- one for determining the surface water temperature T_o;
- another for determining the wet bulb temperature T_w, assuming that this measure is not included as part of the input data.

The application of Eq. 3.1 for calculating ETo for short time periods (hourly or less) may require the inclusion of adjustments for stability (Allen et al., 1998). However, when calculating ETo for a well-watered (grass) reference surface and open water, the heat energy flux exchanged is small, and the stability correction is therefore not normally applied.

The review of literature related to estimation of open water evaporation (Aim 1) at a daily time scale was presented previously and will therefore not be repeated here. This work has resulted in the successful development and implementation of a model for daily evaporation using the Penman-Monteith method (Monteith, 1965), water-body equilibrium temperature and the modelling approach of Monteith (1965) which includes the modelling of the surface water temperature T_{water} based on the approaches by Edinger et al. (1968), Keijman and Koopmans (1973), de Bruin (1982) and Finch (2001).

For the algorithm described, the wet bulb temperature needs to be obtained by iteration, from air temperature and water vapour pressure for greatest accuracy, although other methods have been used such as that by Jensen et al. (1990). A spreadsheet implementation of the iteration procedure that would allow a wet bulb accuracy of 0.01ºC is developed.

The application of the model would allow daily estimation of *E* from relatively simple daily micrometeorological measurements, geo-inputs such as latitude and altitude, water reflection coefficient, water depth and water surface area. It is assumed that the wind function *fU* used does not need correction for atmospheric stability. Usually, for a daily time-step model, no correction is required (Allen et al., 1998, Brutsaert, 2005, p 128). Stability corrections would require use of MOST functions.

3.3.3 Protocols for open water evaporation: spreadsheet-implemented iterative Penman-Monteith model at a daily time scale

The protocols included the development and implementation in Microsoft Excel of a model for daily evaporation using the Penman-Monteith method (Monteith, 1965), water-body equilibrium temperature and the modelling of the Monteith (1965) method which includes the modelling of the surface water temperature T_{water} based on approaches by Edinger et al. (1968), Keijman and Koopmans (1973), de Bruin (1982) and Finch (2001).

Weather data for the period 1970 to April 2015 from Cedara, the nearest weather station, provided by the Agricultural Research Council, were used for the model exercise. The data included daily values of solar irradiance I_s (MJ m^{-2}) but not for the entire period, and for a standard height z, minimum (T_{zmin}, °C) and maximum air temperature (T_{zmax}, °C), minimum (RH_{zmin}, %) and maximum relative humidity (RH_{zmax}, %), as well as wind speed (U_z, m s^{-1}) and rainfall (mm). Also included in the dataset, from a Campbell-Stokes sunshine recorder, were daily values of sunshine duration for the period 1st January 1970 to 31st December 2008 but excluding June 1998 to January 1999 and other periods. Solar irradiance measurements were available from 1st January 2009.

Although air temperature measurements were likely at Stevenson screen height (1970 to 2008 inclusive) and subsequently likely at 2 m in a Gill shield, the World Meteorological Organisation recommends heights between 1.25 and 2 m. Without knowledge of atmospheric stability, it is not easily possible to correct air temperature measurements to a standard height. There is, however, a correction possible for wind speed measurements for neutral conditions. No height corrections were applied to the wind speed measurements, apart from the model-required correction to a height of 10 m, since it was assumed that all measurements were for a height of 2 m.

Since the dataset also included sunshine duration for the period year 1970 to 2008 inclusive, there were two possibilities for estimating daily solar irradiance:

- application of Angström's equation using sunshine duration data and the calculated extraterrestrial solar irradiance;
- application of a modified version of (air temperature only) Hargreaves and Samani (1982, 1985) empirical radiation model test using the daily range in air temperature and the calculated extraterrestrial solar irradiance. The model has shown reasonable ETo results "with a global validity" (FAO 56 – Allen et al., 1998).

The latter approach was preferred since the air temperature thermohygrograph record for the period 1970 to 2008 was deemed more reliable. A comparison of the estimated solar irradiance, and also the model-estimated evaporation, for the radiation estimation methods will be presented so that a decision may be made with regard to the preferred method.

So as to coincide with the hydrological year, data for the period 1st October of a particular year to 30th September the following year were used to constitute a year. Therefore, the data period used for model estimation was 1st October 1970 to 30th September 2014. For 99.26% of all days of the full dataset, model estimates of E (mm) were possible. Model estimates were not

possible for missing solar irradiance and air temperature data. Many data traps were used to filter the data to ensure that only reliable inputs were used. For example, extensive use has been made of the IFERROR statement in Excel not only to check for missing data (recorded as -999, blank, ---, etc.) but also to exclude out-of-range data (such as impossible divide by zero calculations). The IFERROR statement also allows an error calculation to be replaced by another using the nearest best value or nearest best equation. The syntax is as follows:
=IFERROR(A;B)
The result displayed in the cell is the A computed if there is no error and B if there is a result. Extensive use was also made of nest IFERROR statement, IF and nested IF statements.

Crucial to the Excel implementation was the use of names for various cells instead of the normal relative or fixed cells. This enabled much easier checking of the many model equations used. For the future, it would also allow other users much easier understanding of model workings. For example, the cell f1, which would normally be referenced as f$1, was used for the latitude of Midmar. This cell was, however, named latitude using the Defined Names feature available under Formulas. In all subsequent cells that required the latitude, the name latitude was used instead of f$1. The Defined Names feature was also used to name cell contents in a particular column. For example, clicking on column F containing maximum air temperature and then specifying Formulae, Defined Names, Define Name, and then typing in a name such as Tzmax assigns the column F values to the name Tzmax.

The number of iterations used depended on the maximum wet bulb temperature for the entire data set. Since the maximum change value in Excel was 0.001ºC, 100 iterations were required for each 1ºC from the reset wet bulb of 0.05ºC. Typically, 520 iterations were sufficient. Computation time for an Intel i7 computer (CPU 1.80 GHz, 2.40 GHz; 8.00 Gbyte) for the 45-year daily dataset was typically 2 min 15 s. With many software applications running simultaneously, typical computation time increased to 3 min 45 s.

Daily maximum and minimum air temperatures, T_{zmax} and T_{zmin} respectively, were the most important data inputs for the model. Missing solar irradiance data, mainly for the period 1st January 1970 to 31st December 2008, were replaced based on the estimation of solar irradiance I_s (MJ m^{-2}) from air temperature range, altitude and the extraterrestrial solar irradiance I_{sextra} (MJ m^{-2}) (Abraha and Savage, 2010):

$$I_s = 0.17\times(P/P_o)\times(T_{zmax} - T_{zmin})^{0.5}\times I_{sextra} \qquad (3.13)$$

where P and P_o (kPa) are the site and sea level atmospheric pressures.

The daily average water vapour pressure $e_{air\ land}$ (kPa) was computed from daylength ($daylength$) and nightlength ($24 - daylength$) weighted $(RH_{zmin}/100)\times e_s(T_{zmax})$ and $(RH_{zmax}/100)\times \boldsymbol{e_s}(T_{zmin})$ values, where RH_{zmin} and RH_{zmax} are the daily minimum (day) and maximum (night) relative humidity measurements, using:

$$e_{air\ land} = (daylength\times(RH_{zmin}/100)\times e_s(T_{zmax}) + (24 - daylength) \times(RH_{zmax}/100)\times e_s(T_{zmin}))/24) \tag{3.14}$$

For missing relative humidity data, $e_{air\ land}$ was computed using the daily minimum air temperature T_{zmin}:

$$e_{air\ land} = e_{\boldsymbol{s}}(T_{zmin}) \tag{3.15}$$

The wet bulb iterative procedure, implemented in Microsoft Excel, using the psychrometric equation, involved the wet bulb temperature T_{wet_land} (°C), psychrometric constant γ (kPa K^{-1}) and atmospheric pressure P. Theoretically, based on the psychrometric equation, the value of:

$$e_s(T_{wet\_land}) - \gamma\times(P/100)\times(T_{air\_land} - T_{wet\_land})\times(1 + 0.00115\times T_{wet\_land}) \tag{3.16}$$

should equal the water vapour pressure e_{air_land} (kPa). If not, the value of T_{wet_land} is incremented by 0.05°C. The process was initiated for T_{wet_land} = 0.05°C and continued until the correct value was found.

For negative T_{zmin}, the Jensen et al. (1990) method for estimating T_{wet_land} using air and dew point temperatures T_{air_land} and T_{dp_land}, weighted by γ and Δ respectively.

The protocols for the spreadsheet implementation of the model are presented in Table 3.1.

Table 3.1 The various model inputs, water/reservoir characteristics, solar/atmospheric calculations, temperature calculations, temperature/humidity/wind calculations and energy/water/evaporation calculations for the daily incrementing iterative Penman-Monteith equilibrium and water temperature model for open water evaporation

Component	**Mathematical and Excel descriptions**
Raw data inputs: daily values of I_s (MJ m^{-2}), T_{zmax} (ºC), T_{zmin} (ºC), RH_{zmax} (%), RH_{zmin} (%) and U_z (m s^{-1}); $r = 0.08$; $\boldsymbol{d_{water}}$; $\boldsymbol{A_{water}}$	
Model inputs	
Solar irradiance: $\boldsymbol{I_{s\_land}}$ (MJ m^{-2})	Mathematical description $I_{s\_land} = IFERROR(IF(AND(I_s = ""; OR(T_{zmax} = ""; T_{zmin} = ""; T_{zmax} = 0; T_{zmin} = 0)); ""; IF(I_s = IF(I_s > 0; I_s; IF(OR(I_s < 0; I_s = ""); 0.17 \times (P/P_o) \times (T_{zmax} - T_{zmin})^{0.5} \times I_{sextra}))); "")$ Excel $= \boldsymbol{IFERROR}(\boldsymbol{IF}(\boldsymbol{AND}(\boldsymbol{Is} = ""; \boldsymbol{OR}(\boldsymbol{Tzmax} = ""; \boldsymbol{Tzmin} = ""; \boldsymbol{Tzmax} = \boldsymbol{0}; \boldsymbol{Tzmin} = \boldsymbol{0})); ""; \boldsymbol{IF}(\boldsymbol{Is} > \boldsymbol{0}; \boldsymbol{Is}; \boldsymbol{IF}(\boldsymbol{OR}(\boldsymbol{Is} < \boldsymbol{0}; \boldsymbol{Is} = ""); \boldsymbol{0.17} * (\boldsymbol{P}/\boldsymbol{101.325}) * ((\boldsymbol{Tzmax} - \boldsymbol{Tzmin})^\wedge\boldsymbol{0.5}) * \boldsymbol{Isextra}))); "")$
Solar irradiance: $\boldsymbol{I_{s\_Angstrom}}$ (MJ m^{-2})	Mathematical description $= IF(sunshine\_duration = ""; ""; IFERROR(IF(IF(ABS(sunshine\_duration) < daylength; IF(sunshine\_duration/daylength \geq 0.5; ((0.29 + 0.47 \times sunshine\_duration/daylength) \times I_{sextra}); ((0.22 + 0.65 \times sunshine\_duration/daylength) \times I_{sextra})); "") > Isextra; ""; IF(ABS(sunshine\_duration) <$

Component	Mathematical and Excel descriptions
	$daylength; IF(sunshine\_duration/daylength \geq 0.5; ((0.29+0.47\times sunshine\_duration/daylength)\times I_{sextra}); ((0.22+0.65\times sunshine\_duration/daylength)\times I_{sextra})); "")); ""))$ Excel $= IF(sunshine\_duration = ""; ""; IFERROR(IF(IF(ABS(sunshine\_duration) < daylength; IF(sunshine\_duration/daylength >= 0.5; ((0.29+0.47*sunshine\_duration/daylength)*Isextra); ((0.22+0.65*sunshine\_duration/daylength)*Isextra)); "") > Isextra; ""; IF(ABS(sunshine\_duration) < daylength; IF(sunshine\_duration/daylength >= 0.5; ((0.29+0.47*sunshine\_duration/daylength)*Isextra); ((0.22+0.65*sunshine\_duration/daylength)*Isextra)); "")); ""))$
Air temperature: $\boldsymbol{T_{z\_land}}$ (ºC)	Mathematical description $IF(OR(T_{zmax} = ""; T_{zmin} = ""; T_{zmax} = 0; T_{zmin} = 0); ""; T_{z_{land}} = (daylength\times T_{zmax} + (24 - daylength)\times T_{zmin})/24)$ Excel $= \boldsymbol{IF(OR(Tzmax = ""; Tzmin = ""; Tzmax = 0; Tzmin = 0); ""; (daylength * Tzmax + (24 - daylength) * Tzmin)/24)}$
Saturation water vapour pressures: $\boldsymbol{e_s(T_{zmin}), e_s(T_{zmax})}$ (kPa)	Mathematical description $e_s(T_{zmax}) = 0.6108\times EXP((17.2694\times T_{zmax})/(237.3+T_{zmax})),$ $e_s(T_{zmin}) = 0.6108\times EXP((17.2694\times T_{zmin})/(237.3+T_{zmin}))$ Excel

Component	Mathematical and Excel descriptions
	$= \mathbf{0.6108 * EXP((17.2694 * Tzmax)/(237.3 + Tzmax))}$ $= \mathbf{0.6108 * EXP((17.2694 * Tzmin)/(237.3 + Tzmin))}$
Water vapour pressure: $e_{air\ land}$ (kPa)	Mathematical description $e_{air\ land} = IF(OR(RH_{zmin} = ""; RH_{zmax} = ""; RH_{zmin} = 0; RH_{zmax} = 0; ABS(RH_{zmin}) > 100; ABS(RH_{zmax}) > 100); e_s(T_{zmin}); (daylength \times (RH_{zmin}/100) \times e_s(T_{zmax}) + (24 - daylength) \times (RH_{zmax}/100) \times e_s(T_{zmin}))/24)$ Excel $= IF(OR(RHzmin = ""; RHzmax = ""; RHzmin = 0; RHzmax = 0; ABS(RHzmin) > 100; ABS(RHzmax) > 100); esTzmin; ((RHzmin/100) * esTzmax + (RHzmax/100) * esTzmin)/2)$
Wind speed at 10 m: $\boldsymbol{U_{land\ 10\ m\ extrapolated}}$ (m s^{-1})	Mathematical description $U_{land\ 10\ m\ extrapolated} = IF(OR(U_{land\ 2\ m} < 0; U_{land\ 2\ m} = ""; ABS(U_{land\ 2\ m}) > 50); 2; U_{land\ 2\ m} \times (10/2)^{0.31}$ Excel $= \mathbf{IF(OR(U\_land\_2m < 0; U\_land\_2m = ""; ABS(U\_land\_2m) > 50); 2; U\_land\_2m * (10/2)\hat{}0.31)}$
Sunshine duration: $\boldsymbol{sunshine\_duration}$ (h)	Mathematical description $sunshine\_duration = IF(OR(sunshineduration < 0; sunshineduration > daylength; sunshineduration = ""); ""; sunshineduration)$ Excel

Component	Mathematical and Excel descriptions
	$= IF(OR(K11 < 0; K11 > daylength; K11 = ""); ""; K11)$
Solar/atmospheric calculations	
Declination: $\boldsymbol{\delta}$ (radians)	Mathematical description $\delta = IF(latitude < 0; -0.409 \times SIN((2\times\pi/365)\times DoY - 1.39); -0.409\times SIN((2\times\pi/365)\times DoY - 1.39))$ Excel $\boldsymbol{= IF(latitude < 0; -0.409 * SIN((2 * PI()/365) * DoY - 1.39); -0.409 * SIN((2 * PI()/365) * DoY - 1.39))}$
Sunset hour angle: $\boldsymbol{\omega}$ (radians)	Mathematical description $\omega = IF(latitude > 0; ACOS(-TAN((2\times\pi/360)\times -1\times latitude)\times TAN(declination)); ACOS(TAN((2\times\pi/360)\times latitude)\times TAN(declination)))$ Excel $= IF(latitude > 0; ACOS(-TAN((2 * PI()/360) * -1 * latitude) * TAN(declination)); ACOS(TAN((2 * PI()/360) * latitude) * TAN(declination)))$
Extraterrestrial solar irradiance: $\boldsymbol{I_{extra}}$	Mathematical description $I_{extra} = 118.08\times((1 + 0.033\times COS(2\times\pi\times DoY/365))/\pi\times(hour\_angle\_sunset\times SIN((2\times\pi/360)\times -1\times latitude)\times SIN(declination) + SIN(hour\_angle\_sunset)\times COS((2\times\pi/360)\times -1\times latitude)\times COS(declination))$

Component	Mathematical and Excel descriptions
(MJ m^{-2})	Excel $= 118.08 * ((1 + 0.033 * COS(2 * PI() * DoY/365))/PI()) * (hour\_angle\_sunset * SIN((2 * PI()/360) * -1 * latitude) * SIN(declination) + SIN(hour\_angle\_sunset) * COS((2 * PI()/360) * -1 * latitude) * COS(declination))$
Clear-day solar irradiance: $\boldsymbol{I_{sclear}}$ (MJ m^{-2})	Mathematical description $I_{sclear} = I_{extra} \times (0.75 + 2 \times 10^{-5} \times altitude)$ Excel $= Isextra * (0.75 + 2 * 10\text{^} - 5 * altitude)$
Cloudiness factor: $\boldsymbol{f}$	Mathematical description $f = IFERROR((IF(I_{s_{land}}/I_{sclear} \leq 0.9; 1.1 - I_{s_{land}}/I_{sclear}; 2 \times (1 - I_{s_{land}}/I_{sclear})); "")$ Excel $= IFERROR(IF(Is\_land/Isclear <= 0.9; 1.1 - Is\_land/Isclear; 2 * (1 - Is\_land/Isclear)); "")$
Temperature calculations	
Specific latent energy: $\boldsymbol{L_v}$ (MJ kg^{-1})	Mathematical description $L_v = IFERROR(IFERROR(2.501 - T_{water_pred} \times 2.361 \times 10^{-3}; 2.501 - T_{wet} \times 2.361 \times 10^{-3}); "")$Excel $= 2.501 - Twater_pred * 2.361 * 10\text{^} - 3$

Component	Mathematical and Excel descriptions
Atmospheric pressure: **P** (kPa) [P_o = 101.325 kPa]	Mathematical description $P = P_o - ((-0.01094866 \times e_{air\_land} \times 1000 + 2934.7773)/(8.31451 \times (T_{air\_land} + 273.15) + 0.28362157 \times altitude)) \times 9.79267 \times altitude/1000$ Excel $= IFERROR(Po - ((-0.01094866 * eair\_land * 1000 + 2934.7773)/(8.31451 * (Tair\_land + 273.15) + 0.28362157 * altitude)) * 9.79267 * altitude/1000; "")$
Specific heat capacity of air at constant pressure: **c_p** (MPa kg^{-1} K^{-1})	Mathematical description $= IFERROR(10^{-6} \times (1004.722587 + 1148.254385 \times e_{air_land}/(P - e_{air_land}) + 1.256 \times (1 + T_{air_land}/40) \times (1 + (e_{air_land}/(0.6108 \times EXP((17.2694 \times T_{air_land})/(237.3 + T_{air_land})))))); "")$ Excel $= 10\text{^} - 6 * (1004.722587 + 1148.254385 * eair_land/(P - eair_land) + 1.256 * (1 + Tair_land/40) * (1 + (eair_land/(0.6108 * EXP((17.2694 * Tair_land)/(237.3 + Tair_land))))))$
Psychrometric constant: **γ** (kPa K^{-1})	Mathematical description $\gamma = IFERROR(c_p \times P/(0.62198 * L_v); "")$ Excel $= IFERROR(cp * P/(0.62198 * Lv); "")$

Component	Mathematical and Excel descriptions
Temperature/humidity/wind calculations	
Dew point: $\boldsymbol{T_{dp}}$ (°C)	<u>Mathematical description</u> $T_{dp} = (116.9 + 237.3 \times LN(e_{air\_land}))/(16.78 - LN(e_{air\_land}))$ <u>Excel</u> $= (116.9 + 237.3 * LN(eair\_land))/(16.78 - LN(eair\_land))$
Wet bulb: $\boldsymbol{T_{wet}}$ (°C)	<u>Mathematical description</u> $T_{wet} = IF(ABS(0.6108 \times EXP((17.2694 \times T_{wet\_land})/(237.3 + T_{wet\_land})) - \gamma \times (P/100) \times (T_{air\_land} - T_{wet\_land}) \times (1 + 0.00115 \times T_{wet\_land}) - e_{air\_land}) > 0.05; T_{wet\_land} + 0.05; T_{wet\_land})$ <u>Excel</u> $= IF(ABS(0.6108 * EXP((17.2694 * Twet\_land)/(237.3 + Twet\_land)) - gamma * (P/100) * (Tair\_land - Twet\_land) * (1 + 0.00115 * Twet\_land) - eair\_land) > 0.05; Twet\_land + 0.05; Twet\_land)$
Wet bulb (approximation for cross-check): $\boldsymbol{T_{wet\ approx}}$ (°C)	<u>Mathematical description</u> $T_{wet\ approx} = (\gamma \times T_{air\_land} + ((4098 \times e_{air\_land}/(T_{dp\_land} + 237.3)^2) \times T_{dp\_land}))/(\gamma + (4098 \times e_{air\_land}/(T_{dp\_land} + 237.3)^2))$ <u>Excel</u> $= (gamma * Tair\_land + ((4098 * eair\_land/(Tdp\_land + 237.3)^\wedge 2) * Tdp\_land))/(gamma + (4098 * eair\_land/(Tdp\_land + 237.3)^\wedge 2))$

Component	Mathematical and Excel descriptions
Density of air: $\boldsymbol{\rho_{air}}$ (kg m^{-3})	Mathematical description $\rho_{air_land} = 1000\times(101.325\times0.028964 - (0.028964 - 0.01801534)\times e_{air_land})/(8.31451\times(273.15 + T_{air_land}) + 0.028964\times9.79221\times altitude)$ Excel $= 1000 * (101.325 * 0.028964 - (0.028964 - 0.01801534) * eair_land)/(8.31451 * (273.15 + Tair_land) + 0.028964 * 9.79221 * altitude)$
Saturation water vapour pressure at the land temperature: $\boldsymbol{e_{sTland}}$ (kPa)	Mathematical description $e_{sTland} = IFERROR(0.6108\times EXP(17.27\times T_{land}/(T_{land} + 237.3)); "")$ Excel $= IFERROR(0.6108 * EXP(17.27 * Tair\_land/(Tair\_land + 237.3)); "")$
Saturation water vapour pressure at the wet bulb: $\boldsymbol{e_{sTwet}}$ (kPa)	Mathematical description $e_{sTwet} = IFERROR(IFERROR(0.6108\times EXP(17.27\times T_{wet\_land}/(T_{wet\_land} + 237.3)); 0.6108\times EXP(17.27\times T_{wet\_land\_approx}/(T_{wet\_land\_approx} + 237.3))); "")$ Excel $= IFERROR(IFERROR(0.6108 * EXP(17.27 * Twet\_land/(Twet\_land + 237.3)); 0.6108 * EXP(17.27 * Twet\_land\_approx/(Twet\_land\_approx + 237.3))); "")$
Saturation water vapour pressure at the predicted	Mathematical description $e_{sTwater} = IFERROR(IFERROR(0.6108\times EXP(17.27\times T_{water\_pred}/(T_{water\_pred} + 237.3)); 0.6108\times EXP(17.27\times T_{wet\_land}/(T_{wet\_land} + 237.3))); "")$

Component	Mathematical and Excel descriptions
water temperature: $e_{sTwater}$ (kPa)	Excel $= IFERROR(IFERROR(0.6108 * EXP(17.27 * Twater\_pred/(Twater\_pred + 237.3)); 0.6108 * EXP(17.27 * Twet\_land/(Twet\_land + 237.3))); "")$
Slope of e_s *vs* T at the air temperature: $\boldsymbol{\Delta_{Tair}}$ (kPa K^{-1})	Mathematical description $\Delta_{Tair} = IFERROR(4098 \times 0.6108 \times e_{s_{Tland}}/\left(T_{air_{land}} + 237.3\right)^2; "")$ Excel $= IFERROR(4098 * es_Tland/(Tair_land + 237.3)\text{^}2; "")$
Slope of e_s *vs* T at the wet bulb: $\boldsymbol{\Delta_{Twet}}$ (kPa K^{-1})	Mathematical description $\Delta_{Twet} = IFERROR(4098 \times 0.6108 \times e_{s_{Twet}}/\left(T_{wet_land} + 237.3\right)^2; "")$ Excel $= IFERROR(4098 * es_Twet/(Twet_land + 237.3)\text{^}2; "")$
Slope of e_s *vs* T at the dew point: $\boldsymbol{\Delta_{Tdp}}$ (kPa K^{-1})	Mathematical description $\Delta_{Tdp} = IFERROR(4098 \times 0.6108 \times e_{air_land}/\left(T_{dp_land} + 237.3\right)^2; "")$ Excel $= IFERROR(4098 * eair_land/(Tdp_land + 237.3)\text{^}2; "")$

Component	Mathematical and Excel descriptions
Slope of e_s *vs* T at the predicted water temperature: $\boldsymbol{\Delta_{Twater}}$ (kPa K^{-1})	Mathematical description $\Delta_{Twater} = IFERROR(IFERROR(4098 \times e_{s_{Twater}} / \left(T_{water_{pred}} + 237.3\right)^2 ; 4098 \times e_{s_{Twater}} / \left(T_{water_{pred}} + 237.3\right)^2$ Excel $= IFERROR(IFERROR(4098 * es\_Twater/(Twater\_pred + 237.3)\text{^}2; 4098 * es\_Twater/(Twet\_land + 237.3)\text{^}2); "")$
Wind speed function: $\boldsymbol{fU}$ (MPa m^{-2} day^{-1} kPa^{-1})	Mathematical description $fU = (5/A_{water})^{0.05} \times (3.8 + 1.57 \times U_{land\ 10\ m\ extrapolated})$ Excel $= (5/A\_water)\text{^}0.05 * (3.8 + 1.57 * U\_land\_10m)$
Aerodynamic resistance: $\boldsymbol{r_a}$ (s m^{-1})	Mathematical description $r_a = IFERROR(\rho_{air\_land} \times c_p / (\gamma \times fU/86400);"")$ Excel $= IFERROR(rho\_air\_land * cp/(gamma * fU/86400); "")$
Energy/water/evaporation calculations	

Component	Mathematical and Excel descriptions
Incoming infrared irradiance: $\boldsymbol{L_{d\_land}}$ (MJ m^{-2})	Mathematical description $L_{d\_land} = IFERROR((f + (1-f)\times(1-(0.261\times EXP(-7.77\times10^{-4}\times T_{air\_land}{}^{2}))))\times4.9\times10^{-9}\times(T_{air\_land} + 273.15)^{4}; "")$ Excel $= IFERROR((Cloud\_factor + (1 - Cloud\_factor) * (1 - (0.261 * EXP(-7.77 * 10\hat{} - 4 * Tair\_land\hat{}2)))) * 4.9 * 10\hat{} - 9 * (Tair\_land + 273.15)\hat{}4; "")$
Outward infrared irradiance at $\boldsymbol{T_{wet}}$: $\boldsymbol{L_{u\ at\ Twet}}$ (MJ m^{-2})	Mathematical description $L_{u\ at\ Twet} = IFERROR(4.9\times10^{-9}\times\left(T_{air\_land} + 273.15\right)^{4} + 4\times4.9\times10^{-9}\times\left(T_{air\_land} + 273.15\right)^{3}\times\left(T_{wet\_land} - T_{air\_land}\right); "")$ Excel $= IFERROR(4.9 * 10\hat{} - 9 * (Tair\_land + 273.15)\hat{}4 + 4 * 4.9 * 10\hat{} - 9 * (Tair\_land + 273.15)\hat{}3 * (Twet\_land - Tair\_land; "")$
Outward infrared irradiance at $\boldsymbol{T_{water\_pred}}$: $\boldsymbol{L_{u\ at\ Twater\_pred}}$ (MJ m^{-2})	Mathematical description $L_{u\ at\ Twater\_pred} = IFERROR(0.97\times(4.9\times10^{-9}\times(T_{water\_pred} + 273.15)^{4}); L_{u\ at\ Twet})$ Excel $= IFERROR(0.97 * (4.9 * 10\hat{} - 9 * (Twater\_pred + 273.15)\hat{}4); Lu\_Twet)$
Net irradiance at $\boldsymbol{T_{wet}}$: $\boldsymbol{R_{n\ at\ Twet}}$	Mathematical description $R_{n\ at\ Twet} = IFERROR(I_{S_{land}}\times(1-r) + L_{d\ land} - L_{u\ Twet}; "")$ Excel

Component	Mathematical and Excel descriptions
(MJ m^{-2})	$= IFERROR(Is_{land} * (1 - reflection) + Ld_{land} - Lu_{Twet}; "")$
Net irradiance at the water surface: **$R_{n\,water}$** (MJ m^{-2})	Mathematical description $R_{n\,water} = IFERROR(I_{s\_land} \times (1 - r) + L_{d\,land} - L_{u\,T\,water\,pred}; "")$ Excel $= IFERROR(Is\_land * (1 - reflection) + Ld\_land - Lu\_T\_water\_pred; "")$
Equilibrium temperature: **$T_{equilibrium}$** (°C)	Mathematical description $T_{equilibrium} = IFERROR(T_{wet\_land} + R_{n\,Twet}/(4 \times 4.9 \times 10^{-9} \times (T_{wet\_land} + 273.15)^3 + fU \times (\Delta_{T\,wet} + \gamma)); "")$ Excel $= IFERROR(Twet\_land + Rn\_Twet/(4 * 4.9 * 10\hat{}-9 * (Twet\_land + 273.15)\hat{}3 + fU * (delta_{Twet} + gamma)); "")$
Time constant: **τ** (day)	Mathematical description $\tau = IFERROR(1000 \times 0.004185 \times d_{water}/(4 \times 4.9 \times 10^{-9} \times (T_{wet\_land} + 273.15)^3 + fU \times (\Delta_{T\,wet} + \gamma)); "")$ Excel $= IFERROR(1000 * 0.004185 * d\_water/(4 * 4.9 * 10\hat{}-9 * (Twet\_land + 273.15)\hat{}3 + fU * (delta\_Twet + gamma)); "")$
Water temperature predicted: **T_{water_pred}**	Mathematical description $T_{water\_pred} = IFERROR(T_{equilibrium} + (T_{water\_pred-1} - T_{equilibrium}) \times EXP(-1/\tau); T_{wet\_land})$ Excel

Component	Mathematical and Excel descriptions
(day)	$= IFERROR(Tequilibrium + (Twater\_1 - Tequilibrium) * EXP(-1/tau); Twet\_land)$
Change in water-stored heat flux: $\boldsymbol{\Delta S}$ (MJ m^{-2})	Mathematical description $\Delta S = IFERROR(IF(ABS(1000\times 0.004185\times d_{water}\times(T_{water\_pred} - T_{water\_pred-1})) > R_{n\,water}; R_{n\,water}; 1000\times 0.004185\times d_{water}\times(T_{water\_pred} - T_{water\_pred-1})); "")$ Excel $= IFERROR(IF(ABS(1000 * 0.004185 * d\_water * (Twater - Twater\_1)) > Rn\_water; Rn\_water; 1000 * 0.004185 * d\_water * (Twater - Twater\_1)); "")$
Daily evaporation: E (mm)	Mathematical description $E = IFERROR((1/L_v)\times(\Delta_{T\,water}\times(R_{n\,water} - dS) + 86400\times\rho_{air_{land}}\times c_p\times(e_{s\,Twater} - e_{air_{land}})/r_a)/(\Delta_{T\,water} + \gamma); "")$ Excel $= IFERROR((1/Lv) * (delta\_Twater * (Rn\_water - dS) + 86400 * rho\_air\_land * cp * (es\_Twater - eair\_land)/ra)/(delta\_Twater + gamma); "")$

3.4 Protocols and procedures for determining open water evaporation using MOST3.4.1 Introduction

Three exchanges between open water and the atmosphere are of interest in this investigation: momentum flux, sensible heat flux and latent energy flux. Micrometeorological processes may be used to determine the exchange of such fluxes between a surface and the overlying atmosphere. In the surface layer, many parameters are used, required or determined for such determinations (Table 3.2).

In the case of open water, a simple representation of the fluxes for a water surface and the above-surface measurements is shown in Fig. 3.1. The surface layer consists of a roughness sub-layer as well as a layer referred to as the constant-flux layer. The roughness sub-layer has also been referred to as the interfacial sub-layer, the viscous sub-layer and the canopy sub-layer. For the remainder of this investigation, it is assumed that measurements are in the constant flux layer. For vegetated surfaces, the roughness sub-layer may extend to two to three times that of the canopy height. For open water, this is much less a limitation due to the much smoother water surface compared to the much rougher (undulating) bare soil and canopy surfaces.

Equations for the determination of various properties of air, such as atmospheric pressure P, air density ρ, specific heat capacity c_p and humidity parameters such as the saturation water vapour pressure e_s, specific humidity q and others including specific latent energy of vaporisation (L) and gravity g are listed in Appendix 1.

Table 3.2 Summary of meteorological parameters estimated or required by the various measurement methods and MOST

Parameter	Symbol (unit)	Description
Zero-plane displacement height	d (m)	The height, which includes the roughness length, for neutral conditions at which the horizontal wind speed is zero
Roughness length (or momentum roughness parameter)	z_o (m)	A height scale in turbulent flow over roughness elements for which zero wind speed is achieved because of the flow obstacles. The roughness height represents the mean height where momentum is absorbed by the water surface
Reynolds number	$Re = v\, l/\nu$ (unitless)	Ratio of inertial (v is the flow speed) to viscous forces (ν is the fluid kinematic viscosity), $\nu = 1.46 \times 10^{-5}$ m^2 s^{-1}, where l (m) is a characteristic length

Parameter	Symbol (unit)	Description
Reynolds number*	$Re_* = u_*\, z_o/\nu$ (unitless)	Special case Reynolds number used for determining the roughness length z_o
Gravity	g (m s-2)	Gravity is latitude and altitude dependent (Appendix 1)
Richardson number	$Ri = \frac{g}{T}(\partial T/\partial z)/(\partial u/\partial z)^2$ (unitless)	Ratio of free (buoyant) and forced (inertial) convection in a turbulent boundary layer
Obukhov length	$\mathcal{L}$ (m)	The height above the zero-plane displacement height d at which free convection dominates over forced convection
Stability parameter	$\zeta = (z-d)/\mathcal{L}$ (canopy) $\zeta = (z-z_o)/\mathcal{L}$ (open water) (unitless)	Argument of the MOST semi-empirical and dimensionless functions
Momentum flux	τ (Pa)	The turbulent horizontal wind stress in the surface boundary layer
Sensible heat flux	H (W m-2)	The constant flux in the surface layer – a component of the energy balance and one of the terms of the available flux density: $A = H + LE$
Latent energy flux	LE (W m-2)	The constant flux in the surface layer – another component of the energy balance and the second term of the available flux
BR	β (no unit)	The ratio of sensible heat flux to that of latent energy flux
Radiometric BR	$\beta = \gamma \cdot (e_o - e_z)/(T_o - T_z)$	Water surface and atmosphere determined BR where γ is the psychrometric constant (Appendix 1)
Friction velocity	u_* (m s-1)	A basic wind speed scaling parameter for momentum flux τ equal to the square root of τ/ρ where ρ is the air density
Temperature scale of turbulence	T_* (K)	A term for the temperature that an air parcel at a height would potentially have if brought adiabatically (i.e. without thermal contact with the surrounding air) to a given height, i.e. the effective temperature of an air parcel after removing the heat of the parcel associated solely with compression
Humidity scale of turbulence	q_* (kg kg-1)	Specific humidity scaling parameter
Carbon dioxide scale of turbulence	c_* (μmol mol-1)	Carbon dioxide scaling parameter

Parameter	Symbol (unit)	Description
φ_m, φ_h, φ_w	Dimensionless	Universal functions used by MOST
Φ_m, Φ_h, Φ_w	Dimensionless	Integrated versions of the universal functions used by MOST

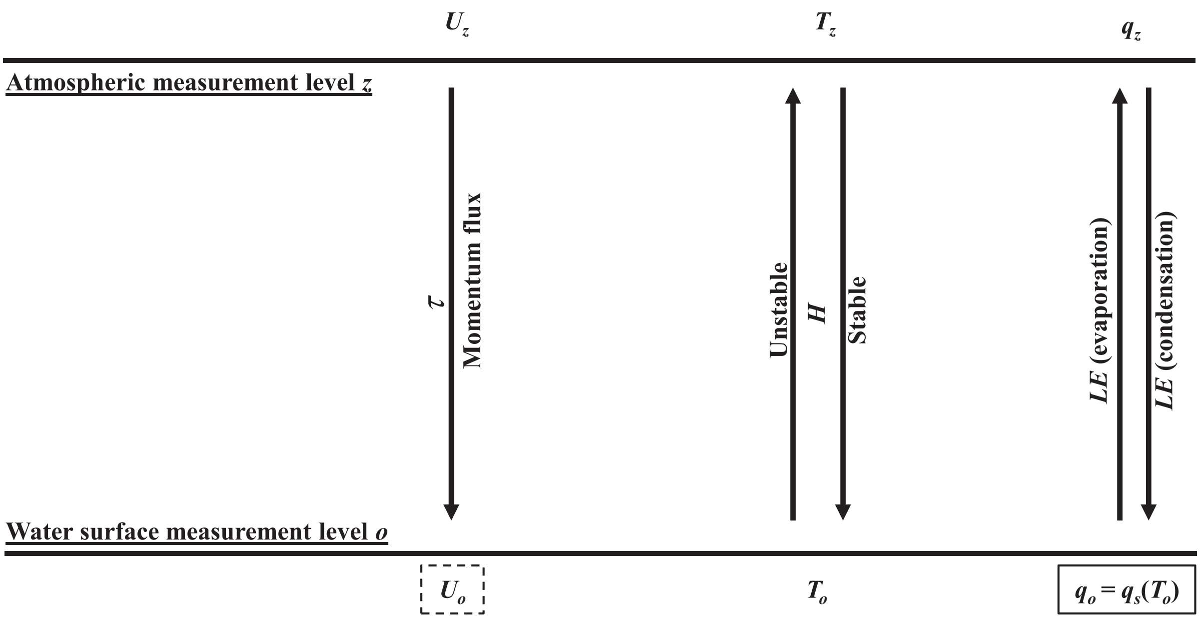

Fig. 3.1 Diagrammatic representation of the two-level water surface and above surface measurements of interest.

The following assumptions are made in respect of the surface boundary conditions of a water surface and above-surface atmosphere (Fig. 3.1):

1. Due to the friction imparted by any surface to the overlying air, it is assumed that U_o = 0 m s^{-1} indicated by a dotted box in Fig. 3.1 The wind energy, it is assumed, is imparted into the water with the result that U_o = 0 m s^{-1}.
2. The surface temperature T_o is estimated using an infrared thermometer suspended above the water surface. Infrared radiation absorption by the water surface, within even a few millimetres, would invalidate thermocouple surface temperature measurements.
3. For an open water body, it is assumed that the specific humidity above the water surface is the saturated value at the temperature T_o – *viz.* $q_o = q_s(T_o)$ indicated by a solid box in Fig. 3.1. This assumption would be invalid in the case of seawater or other highly saline waters.

3.4.2 Richardson number

Parcels of air in the atmosphere experience buoyancy forces, due to vertical temperature differences, that are proportional to $\partial T/\partial z$, the temperature gradient between two neighbouring layers. Inertial turbulent kinetic energy per unit volume of air arise due to the square of the vertical gradient in the horizontal wind speed u, *viz*. $(\partial u/\partial z)^2$. The ratio of these two forces is a measure of the relative importance of free (buoyant) and forced (inertial) convection in a turbulent boundary layer. In order to arrive at a measure for atmospheric stability, the Richardson number (*Ri*), is used:

$$Ri = \frac{g}{T}(\partial T/\partial z)/(\partial u/\partial z)^2 \tag{3.17}$$

In finite difference form, for atmospheric levels 1 and 2 for which the air temperature and wind speed is T_1, u_1 and T_2, u_2 respectively,

$$Ri = \frac{g}{T}(T_2 - T_1) \cdot (z_2 - z_1)/(u_2 - u_1)^2 \tag{3.18}$$

The Richardson number is therefore a dimensionless measure of the intensity of mixing (turbulence), and provides a simple criterion for the existence or non-existence thereof in a stable and stratified environment. Vertical air temperature and wind speed differences therefore play a major role in determining the stability condition of the atmosphere. However, the disadvantage of the use of the Richardson number, as a stability measure, is that it is height dependent. The ideal measure of atmospheric stability would be a height-independent measure that is not reliant on measurement at two levels.

3.4.3 Obukhov stability length

In arriving at a height-independent stability parameter, Obukhov (1946) arrived at a stability length parameter, $\mathcal{L}$ (m), that depended on the Richardson number:

$$Ri = (z - d)/\mathcal{L} \tag{3.16}$$

where z (m) is the measurement height, d (m) is referred to as the zero displacement height (Table 3.2) and $\mathcal{L}$ is the Obukhov length L (m) defined by:

$$\mathcal{L} = \frac{T}{k\,g}\,\frac{\rho\,c_p u_*^3}{(H + 0.61\,c_p\,T\,E)} \tag{3.17}$$

where T is the air temperature (K), k is the von Kármán constant (0.40) and g the acceleration due to gravity (approximately 9.81 m s^{-2}), ρ the air density (kg m^{-3}), c_p the specific heat capacity of air at constant pressure (J kg^{-1} K^{-1}), H the sensible heat flux density (W m^{-2}) and E the latent mass flux density (W m^{-2}). The friction velocity u_* (m s^{-1}) is a basic wind speed scaling parameter (Table 3.2). Early published versions of Obukhov length $\mathcal{L}$ were for dry air which were then modified to account for the effect of water vapour, as shown in Eq. 3.17. The Obukhov $\mathcal{L}$ represents the height above the zero-plane displacement height d at which free convection dominates over forced convection.

A dimensionless stability parameter ζ, which varies with height, was also used to express atmospheric stability. For plant canopies:

$$\zeta = (z - d)/\mathcal{L} \tag{3.18}$$

and for a water surface:

$$\zeta = (z - z_o)/\mathcal{L} \tag{3.19}$$

where z_o (m) is referred to as the roughness length (Table 3.2).

The various stability classes, ranging from strongly stable to convective, are summarised in Table 3.3 together with their corresponding range in ζ.

Table 3.3 Summary of the stability classes using the dimensionless stability parameter ζ (after Panofsky and Dutton (1984) and Deardorff (1978))

Class	Range in ζ	Description
Strongly stable	$\zeta \geq 0.2$	Mechanical turbulence severely reduced by temperature stratification
Slightly-stable	$0.02 \leq \zeta < 0.2$	Mechanical turbulence slightly damped by temperature stratification
Neutral	$-0.02 \leq \zeta < 0.02$	Purely mechanical turbulence
Unstable	$-0.05 \leq \zeta < -0.02$	Mechanical turbulence dominant
Convective	$\zeta < -0.05$	Heat convection dominant

3.4.4 Eddy covariance

There are few direct methods for the measure of momentum, sensible heat and latent energy fluxes (Table 3.4). In 1951, what has become known as the eddy covariance method was developed (Obukhov, 1951; Swinbank, 1951). The method assumes steady-state flow above stationary and horizontally homogeneous surfaces. It can be shown that if there is negligible vertical wind speed, the total turbulent flux is dependent on the covariance between a scalar and the vertical wind speed w (m s^{-1}) (Table 3.4).

In terms of notation, the covariance between the vertical wind speed w, and air temperature T, denoted $\overline{w'T}$, is given by:

$$\text{covariance}\ (w,\ T) = (\sum(w - \bar{w})(T - \bar{T}))/n = \overline{w'T'} \tag{3.20}$$

where n is the sample size. Typically, the averaging period for obtaining $\bar{w}$ and $\bar{T}$ and the covariance (w, T) is 30 min with measurements w and T obtained at a typical frequency of 10 Hz (every 0.1 s). Expressions for the other fluxes (momentum, latent energy and carbon dioxide) are also shown in Table 3.4.

Table 3.4 The various fluxes occurring above open water, their determination in terms of so-called scaling parameters (u_*, T_*, q_*, c_*) and fluctuations (u', T', q', c') and terms and units

Flux density	**Determination**	**Terms and units**
Momentum	$\tau/\rho = u_*^2 = -\overline{u'w'}$	U is the horizontal wind speed (m s^{-1})
Sensible heat	$H/(\rho\ c_p\ ) = u_* T_* = \overline{w'T'}$	T is the air temperature (°C or K)
Latent energy	$LE/(\rho\ L) = u_* q_* = \overline{w'q'}$	q is the specific humidity (kg kg^{-1})
Carbon dioxide	$F_c/\rho = u_* c_* = \overline{w'c'}$	c is the carbon dioxide concentration (μmol mol^{-1})

For a three-dimensional coordinate wind system for which the three components of wind speed are given by u, v and w for which the horizontal wind speed,

$$U = (u^2 + v^2)^{1/2} \tag{3.21}$$

and
$$u_* = \left(\overline{U'w'}\right)^{1/2} = \left(\left(\overline{u'w'}\right)^2 + \left(\overline{v'w'}\right)^2\right)^{1/4} \tag{3.22}$$

The equations in Table 3.3 and the expressions for horizontal wind speed U and friction velocity u_* form the basis for the eddy covariance approach.

3.4.5 Flux-gradient

The flux-gradient-MOST approach involves the use of above-surface scalar measurements at a height z – such as measurements at vertical height z of horizontal wind speed U_z, air temperature T_z and specific humidity q_z (kg kg^{-1}), the latter corresponding to the mass of water vapour per unit mass of air, where air implies dry air and water vapour. These three measurements can be obtained from sensors used in standard automatic weather station systems. In addition, the MOST approach applied to an open water surface requires measurements or estimations of the wind speed, temperature and the specific humidity at the surface – *viz.* U_o, T_o and q_o where the subscript $_o$ indicates surface measurements. The water surface is assumed to have some roughness using the roughness length z_o. The above-surface (z) and surface values (o) for U, T and q are shown in Fig. 3.1 with the fluxes indicated.

Diffusion theory, for neutral conditions (neutral stratification), shows that the flux densities of momentum τ (Pa), sensible heat H (W m^{-2}) and water vapour mass E (kg s^{-1} m^{-2}) may be determined from scalar gradients $\partial\bar{u}/\partial z$ (s^{-1}), $\partial\bar{T}/\partial z$ (K m^{-1}) and $\partial\bar{q}/\partial z$ (kg kg^{-1} m^{-1}) respectively with proportionality (exchange) "constants" ρK_m (kg m^{-1} s^{-1}), $\rho c_p K_h$ (kg m s^{-3} K^{-1}) and ρK_w (kg m^{-1} s^{-1}) where ρ (kg m^{-3}) is the density of air and K (m^2 s^{-1}) is also referred to as the exchange coefficient where its subscript $_m$, $_h$ or $_w$ is for the exchange of momentum, heat and water vapour:

$$\tau = \rho K_m \,{}^{\partial\bar{u}}\!/_{\partial z} \tag{3.23}$$

$$H = \rho\, c_p\, K_h \,{}^{\partial\bar{T}}\!/_{\partial z} \tag{3.24}$$

$$E = -\rho\, K_w \,{}^{\partial\bar{q}}\!/_{\partial z} \tag{3.25}$$

or equivalently $$LE = -L\,\rho\,K_w\,{}^{\partial\bar{q}}/_{\partial z} \tag{3.26}$$

For neutral conditions, the differential form of the wind profile relationship can be written as:

$$\frac{\partial\bar{u}}{\partial z} = \frac{u_*}{k\,(z-d)} \tag{3.27}$$

or $$\frac{\partial\bar{u}}{\partial \ln(z-d)} = \frac{u_*}{k} \tag{3.28}$$

where d (m) is the zero-plane displacement height, u_* the friction velocity (m s^{-1}) and k is known as the von Kármán constant. For open water, d = 0 m. For neutral conditions, a plot of $\bar{u}$ *vs* $\ln(z-d)$ would yield a slope of u_*/k. Experiments over decades have obtained different values of k. The commonly-used value of k today is 0.40 (Högström, 1988). Note then that for a water surface:

$$\frac{\partial\bar{u}}{\partial z}\frac{k}{u_*} = \varphi_m \tag{3.29}$$

where for neutral conditions, the so-called universal function for momentum flux, $\varphi_m = 1$ or for stable conditions $\varphi_m < 1$ and for unstable conditions $\varphi_m > 1$.

Integrating Eq. 3.27 between heights z_o and z,

$$u = \frac{u_*}{k}\ln\frac{z-d}{z_o} \tag{3.30}$$

where u = 0 m s^{-1} for $z = d + z_o$ where z_o (m) is referred to as the roughness length. Equation 3.30 is referred to as the neutral wind profile equation. For open water, for neutral conditions:

$$u = \frac{u_*}{k}\ln\frac{z}{z_o} \tag{3.31}$$

First-order closure, analogous to molecular diffusion approaches (Foken, 2008), may be applied to atmospheric turbulence. The approach is referred to as K-theory (and also Reynolds averaging criterion). With the scalar gradient determined at the location of the flux and using a prime ($'$) to indicate a deviation of a measured scalar for the mean over an averaging period:

$$\tau = \rho\,\overline{u'w'} = \rho K_m\,{}^{\partial\bar{u}}/_{\partial z} \tag{3.32}$$

$$H = -\rho\, \overline{w'T'} = -\rho\, c_p\, K_h\, {}^{\partial \bar{T}}/_{\partial z} \tag{3.33}$$

$$E = -\rho\, \overline{w'q} = -\rho\, K_w\, {}^{\partial \bar{q}}/_{\partial z} \tag{3.34}$$

or equivalently
$$LE = -L\, \rho\, \overline{w'q'} = -L\, \rho\, K_w\, {}^{\partial \bar{q}}/_{\partial z} \tag{3.35}$$

Equations 3.32 to 3.35, through the use of the scalar gradient $\partial/\partial z$ and the shortened energy balance, form the basis of the Bowen ratio energy balance approach (Everson, 2001; Savage et al., 2009).

3.4.6 MOST

Monin and Obukhov (1954) proposed following the definition of the Obukhov length for exchange processes in the so-called surface layer, by Obukhov (1947), the theory of surface layer similarity. MOST relates surface fluxes of momentum, sensible heat, and latent energy to vertical profiles of wind speed, air temperature, and specific humidity in a stationary, horizontally homogeneous atmospheric surface layer for which there is negligible vertical wind speed. Foken (2006) discusses the history of MOST for which Monin and Obukhov (1954) made use of dimensionless functions to account for deviation from neutral stability.

Monin and Obukhov (1954) considered a dimensionless group for which the product of a scalar gradient (e.g. $\partial\bar{u}/\partial z$, $\partial\bar{T}/\partial z$, $\partial\bar{q}/\partial z$, $\partial\bar{c}/\partial z$) and the ratio of z and a scaling parameter for the scalar (e.g. z/u_*, z/T_*, z/q_*, z/c_*) were respectively equated to a dimensionless universal stability function:

- the product of $\partial\bar{u}/\partial z$ (s^{-1}) and $k\, z/u_*$ (s) equal to φ_m
- the product of $\partial\bar{T}/\partial z$ (K m^{-1}) and $k\, z/T_*$ (m K^{-1}) equal to φ_h
- and by extension the product of $\partial\bar{q}/\partial z$ (m^{-1}) and $k\, z/q_*$ (m) equal to φ_v for latent energy
- and also the product of $\partial\bar{c}/\partial z$ (m^{-1}) and $k\, z/c_*$ (m) equal to φ_c for carbon dioxide.

They considered the dimensionless functions φ to be dependent on $\zeta = z/\mathcal{L}$ and this is expressed through the functional notation such as $\varphi_m(\zeta)$. These functions, today referred to as universal functions, are height and stability dependent.

Essentially, the differential form of the MOST fundamental expressions is:

$$\partial\bar{u}/\partial z\ \cdot k\, z/u_* = \varphi_m(\zeta) \tag{3.36}$$

$$\partial\bar{T}/\partial z \cdot k\, z/T_* = \varphi_h(\zeta) \tag{3.37}$$

$$\partial\bar{q}/\partial z \cdot k\, z/q_* = \varphi_w(\zeta) \tag{3.38}$$

$$\partial\bar{c}/\partial z \cdot k\, z/c_* = \varphi_c(\zeta) \tag{3.39}$$

It is usually assumed that $\varphi_h(\zeta) = \varphi_w(\zeta)$. Alternatively, in terms of fluxes, the product of the ratio of the scalar gradient and the flux and the product of the scalar scaling parameter and z and flux is equal to a universal function of stability:

$$\left(\frac{\partial\bar{u}}{\partial z}/\tau\right) \cdot \rho\, k\, u_*\, z = \varphi_m(\zeta) \tag{3.40}$$

$$\left(\frac{\partial\bar{T}}{\partial z}/H\right) \cdot \rho\, c_p k\, T_*\, z = \varphi_h(\zeta) \tag{3.41}$$

$$\left(\frac{\partial\bar{q}}{\partial z}/E\right) \cdot \rho\, k\, q_*\, z = \varphi_w(\zeta) \tag{3.42}$$

$$\left(\frac{\partial\bar{c}}{\partial z}/F_c\right) \cdot \rho\, k\, c_*\, z = \varphi_c(\zeta) \tag{3.43}$$

A limitation on the application of MOST, using Eqs 3.36 to 3.39 or, equivalently, Eqs 3.40 to 3.43, is the requirement of profile measurements, or at least two measurement levels. Furthermore, an iterative procedure for the solution of the fluxes is required since both the left-hand side of either equation set (through the so-called scaling parameters u_*, T_*, q_*, c_*, Table 3.3) and the right-hand side (through use of ζ) are stability dependent.

3.4.7 Universal stability functions for MOST

Many decades of research have been devoted to the choice of stability function for stable and unstable conditions for momentum, sensible heat, latent energy and carbon dioxide. In these decades, different values for the von Kármán were used with values ranging between 0.32 and 0.65 (Högström, 1996; Prueger and Kustas, 2005). Furthemore, different ratios of K_h/K_m were used. This resulted in different universal equations for determining momentum and sensible heat fluxes, conflicting somewhat. Högström (1996) reviewed the literature and found that, for the surface atmospheric layer, k varied in a narrow range between 0.39 and 0.41. He then used $k = 0.40$, the same value that had been found for flow experiments in the laboratory. For a range of surfaces that included forests and oceans, he obtained expressions for the universal functions φ_m and φ_h assuming that $K_h/K_m = 1.05$ (Foken, 2006) for a wide range of stable and unstable conditions (Table 3.5).

For latent energy flux, apart from the work by Dyer and Hicks (1970) for unstable conditions above ploughed soil, Webb (1970) for stable conditions above short grass, and a few others, universal functions for φ_q are more conspicuous by their absence (Table 3.5). Probably, this is due to the difficulties in obtaining accurate profile measurements of specific humidity. Högström (1996) gives formulations for φ_m and φ_h for stable conditions but does not mention φ_w explicitly. Assuming that $K_h/K_m = K_q/K_m = 1$, Foken (2008) in his

Table 3.5 The various fluxes and corresponding universal semi-empirical MOST functions applicable for a wide range of surfaces from forests to water for unstable and stable conditions

Flux	Stability	Universal function	Stability	Universal function
Momentum	Unstable	$\varphi_m = (1 - 19\,\zeta)^{-1/4}$ $-2 < \zeta < 0$ Högström (1996)	Stable	$\varphi_m = 1 + 5.3\,\zeta$ $0 < \zeta < 0.5$ Högström (1996)
Sensible heat	Unstable	$\varphi_h = 0.95\,(1 - 11.6\,\zeta)^{-1/2}$ $-2 < \zeta < 0$ Högström (1996)	Stable	$\varphi_h = 1 + 8.0\,\zeta$ $0 < \zeta < 0.5$ Högström (1996)
Latent energy	Unstable	$\varphi_w = (1 - 16\,\zeta)^{-1/2}$ $-1 < \zeta < -0.1$ Dyer and Hicks (1970)	Stable	$\varphi_w = 1 + 5.2\,\zeta$ $-0.03 \le \zeta \le 1$ Webb (1970) $\varphi_w = 1 + 8.0\,\zeta$ $0 \le \zeta \le 0.5$ Högström (1996) (based on comment in Table 2.8 of Foken (2008))
Momentum, sensible heat, latent energy			Stable	$\varphi_m = \varphi_h = \varphi_w$ $\varphi_m = 1 + 6.1\,\dfrac{\zeta + \zeta^{2.5}(1+\zeta^{2.5})^{-1+1/2.5}}{\zeta + (1+\zeta^{2.5})^{1/2.5}}$ $\Phi_m = -6.1\ln\,(\zeta + (1+\zeta^{2.5})^{1/2.5})$ $\zeta \ge 0$ Cheng and Brutsaert (2005)

Table 2.8 indicates that $\varphi_h \sim \varphi_w$ and that $\varphi = 0.95 + 7.8\,\zeta$ based on Högström (1988). This formulation for φ was updated by Högström (1996) to $\varphi = 1 + 8.0\,\zeta$.

Brutsaert (1982, 2005) also indicate that for stable conditions less attention has been devoted to φ_w, compared to universal functions φ_m and φ_h. Through the work of Cheng and Brutsaert (2005), a formulation for $\varphi_m = \varphi_h = \varphi_w$ for $\zeta \geq 0$ was proposed (Table 3.6).

3.4.8 Integrated universal stability functions for MOST

Profile measurements of wind speed, air temperature, and specific humidity involve measuring scalar differences – essentially finite differences, for example, $\overline{U_z} - \overline{U_o}$, $\overline{T_o} - \overline{T_z}$ and $\overline{q_o} - \overline{q_z}$. These, when divided by the vertical height difference between the water surface level $_o$ and atmospheric level $_z$, only approximate the partial derivatives $\partial\bar{u}/\partial z$, $\partial\bar{T}/\partial z$ and $\partial\bar{q}/\partial z$, respectively. Hence, when using MOST and the universal functions, an integration from, in the case of open water (Fig. 3.1), the roughness distance z_o to height z is required (Prueger and Kustas, 2005; Foken 2008).

As pointed out by Foken (2008), such integrations are not trivial; the integration of the profile equations, Eqs 3.40 to 3.43, using a generic form for the universal functions for the unstable case, was first published by Paulson (1970). The integrated stability correction functions summarized in Table 3.6, column 3 correspond to.

$$\Phi_m = 2\ln\left((1+\varphi_m)/2\right) + \ln\left((1+\varphi_m^2)/2\right) - 2\,\mathrm{atan}\,(\varphi_m) + \pi/2 \quad (3.44)$$

$$\Phi_h = 2\ln\left((1+\varphi_h^2)/2\right) \quad (3.45)$$

$$\Phi_q = 2\ln\left((1+\varphi_q^2)/2\right) \quad (3.46)$$

3.4.9 Roughness length

The roughness length z_o (m) for a water surface varies with the friction velocity u_* (Charnock 1955):

$$z_o = a\,u_*^2/g \quad (3.47)$$

where $a \cong 0.0016$ is an empirically-determined constant. Brutsaert (1982) found differences between z_o and z_{oT} and z_{ow}:

$$z_{oT} = 7.4 \times z_o \exp\left(-2.46\, Re_*^{1/4}\right) \tag{3.48}$$

and
$$z_{ow} = 7.4 \times z_o \exp\left(-2.25\, Re_*^{1/4}\right) \tag{3.49}$$

where
$$Re_* = u_* z_o / \nu \tag{3.50}$$

Garratt (1994), however, proposed:

$$z_{oT} = z_o \exp\left(-2.48\, Re_*^{1/4} + 2\right) \tag{3.51}$$

and
$$z_{ow} = z_o \exp\left(-2.28\, Re_*^{1/4} + 2\right) \tag{3.52}$$

Table 3.6 The various fluxes and associated integrated, universal, semi-empirical MOST functions (Φ) applicable for a wide range of surfaces from forests to water, for unstable and stable conditions (from Högström, 1996)

Exchange	Flux	Integrated universal function
Unstable		
Momentum	$\tau = 0.40\, U_z/(\ln {}^{z}/_{z_o} - \Phi_m)$	$\Phi_m = 2\ln\ ((1 + (1 - 19\,\zeta)^{1/4})/2) + \ln\ ((1 + (1 - 19\,\zeta)^{1/2})/2)$ $- 2\,\mathrm{atan}\ ((1 - 19\,\zeta)^{1/4}) + \pi/2$ $-2 < \zeta < 0$ Högström (1996)
Sensible heat	$H = \rho\, c_p(T_o - T_z)\ 0.40\, u_{*_{\mathrm{MOST}}}/(\ln {}^{z}/_{z_o} - \Phi_h)$	$\Phi_h = 2\ln((1 + 0.95\,(1 - 11.6\,\zeta)^{1/2})/2)$ $-2 < \zeta < 0$ Högström (1996)
Latent energy	$LE = \rho\left(q_{s\_T_o} - q_z\right) 0.40\, u_{*_{\mathrm{MOST}}} L/(\ln {}^{z}/_{z_o} - \Phi_w)$	$\Phi_w = 2\ln((1 + 0.95\,(1 - 11.6\,\zeta)^{1/2})/2)$ $-2 < \zeta < 0$ Högström (1996) $\Phi_w = 2\ln((1 + (1 - 16\,\zeta)^{1/2})/2)$ $-1 < \zeta < -0.1$ Dyer and Hicks (1970)
Stable		
Momentum	$\tau = 0.40\, U_z/(\ln {}^{z}/_{z_o} - \Phi_m)$	$\Phi_m = -5.3\,\zeta + 5.3\, z_o/\mathcal{L}$ $0 < \zeta < 0.5$ Högström (1996)

Exchange	Flux	Integrated universal function
Sensible heat	$H = \rho\, c_p(T_o - T_z)\; 0.40\; u_{*_{\mathrm{MOST}}}/(\ln {}^{z}/_{z_o} - \Phi_h)$	$\Phi_h = -8.0\,\zeta + 8.0\; z_o/\mathcal{L}$ $0 < \zeta < 0.5$ Högström (1996)
Latent energy	$LE = \rho\,\left(q_{s\_T_o} - q_z\right)\; 0.40\; u_{*_{\mathrm{MOST}}}L/(\ln {}^{z}/_{z_o} - \Phi_w)$	$\Phi_w = -8.0\,\zeta + 8.0\; z_o/\mathcal{L}$

3.4.10 Protocols for determining H and LE for open water using MOST

Four measurements are required for application of MOST for open water: air temperature, water vapour pressure and wind speed at a standard height, and the surface temperature of the water, measured using an infrared thermometer. The standard height is typically 2 m above the water surface.

From these inputs, the specific humidity at height z, q_z (kg kg^{-1}), is determined (Table 3.7). The various MOST functions, applied to open water, are shown in Table 3.8.

Table 3.7 The various terms required for application of MOST above open water. The equations have been adapted from Savage et al. (1997)

Terms	Determination	Comment
Gravity g (m s^{-2})	$g = 9.77989 + 0.00014155 \times ABS(Latitude) + 1.00545 \times 10^{-5} \times Latitude^2 - 0.3086 \times Altitude/10^6$	$Latitude$ = -29.5419°, $Altitude$ = 985 m
Atmospheric pressure P (kPa)	$P = 101.325 - ((-0.01094866 \times e_z \times 1000 + 2934.7773)/(8.31451 \times (T_z + 273.15) + 0.28362157 \times Altitude)) \times g \times Altitude/1000$	e_z (kPa) is the water vapour pressure, T_z the air temperature (°C)
Density of air ρ (kg m^{-3})	$\rho = 1000 \times (101.325 \times 0.028964 - (0.028964 - 0.01801534) \times e_z)/(8.31451 \times (273.15 + T_z) + 0.028964 \times g \times Altitude)$	
Specific latent energy L_v (MJ kg^{-1})	$L_v = 2.501 - T_o \times 2.361 \times 10^{-3}$	

Terms	Determination	Comment
Specific heat capacity c_p (J kg^{-1} K^{-1})	$c_p = (1004.722587 + 1148.254385 \times e_z/(P - e_z) + 1.256 \times (1 + T_z/40) \times (1 + ((2.501 - T_o \times 2.361 \times 10^{-3})/(0.6108 \times exp\,((17.2694 \times T_z)/(237.3 + T_z))))))$	
M_w, M_d: molecular mass for water vapour and dry air respectively where $M_w/M_d = 0.62198$; e_z and P (kPa): water vapour and atmospheric pressure respectively		
Psychrometric constant γ (kPa K^{-1})	$\gamma = c_p \times P/(M_w/M_d \times L_v \times 10^6)$	
Specific humidity q_z (kg kg^{-1})	$q_z = M_w/M_d \times e_z/(P - e_z \times (1 - M_w/M_d))$	
Specific humidity q_o (kg kg^{-1})	$q_o = q_s(T_o) = M_w/M_d \times 0.6108 \times EXP((17.2694 \times T_o)/(237.3 + T_o))/((P + (M_w/M_d - 1) \times 0.6108 \times EXP((17.2694 \times T_o)/(237.3 + T_o))))$	$q_s(T_o) = M_w/M_d \times e_s(T_o)/(P - (1 - M_w/M_d) \times e_s(T_o))$

Table 3.8 The various roughness lengths (z_o, z_{oT} and z_{ow}), integrated universal functions, Obukhov length L and fluxes associated with MOST applied to open water evaporation

Component	Mathematical and Excel descriptions
Integrated universal MOST functions	
Momentum: $\boldsymbol{\Phi_m}$ Unstable: $\boldsymbol{z/L > 0}$	Mathematical description $\Phi_m = IFERROR(IF(z/L > 0; -5.3\times(z/L) + 5.3\times z_o/L; 2\times LN(0.5\times(1-19\times z/L)^{0.25})) + LN(0.5\times(1-19\times z/L)^{0.5})) - 2\times ATAN((1-19\times z/L)^{0.25}) + \pi/2); "")$ Excel $\boldsymbol{= IFERROR(IF(z/L > 0; -5.3 * (z/L) + 5.3 * zo/L; 2 * LN(0.5 * (1 + (1-19 * z/L)\text{^}0.25)) + LN(0.5 * (1 + (1-19 * z/L)\text{^}0.5)) - 2 * ATAN((1-19 * z/L)\text{^}0.25) + PI()/2); "")}$
Sensible heat $\boldsymbol{\Phi_h}$	Mathematical description $\Phi_h = IFERROR(IF(z/L > 0; -8\times z/L + 8\times z_{oT}/L; 2\times LN(0.5\times(1+(0.95-0.95\times 11.6\times z/L)^{0.5}))); "")$ Excel $\boldsymbol{= IFERROR(IF(z/L > 0; -8 * z/L + 8 * zoT/L; 2 * LN(0.5 * (1 + (0.95 - 0.95 * 11.6 * z/L)\text{^}0.5))); "")}$

Component	Mathematical and Excel descriptions
Latent energy $\boldsymbol{\Phi_w}$	Mathematical description $\Phi_w = IFERROR(IF(IF(z/L > 0; -8\times z/L + 8\times z_{ow}/L; 2\times LN(0.5\times(1 + (1 - 16\times z/L)^{0.5}))) > 6; ""; IF(z/L > 0; -8\times z/L + 8\times z_{ow}/L; 2\times LN(0.5\times(1 - 16\times z/L)^{0.5})))); "")$ Excel $\boldsymbol{= IFERROR(IF(IF(z/L > 0; -8 * z/L + 8 * zow/L; 2 * LN(0.5 * (1 + (1 - 16 * z/L)\text{^}0.5))) > 6; ""; IF(z/L > 0; -8 * z/L + 8 * zow/L; 2 * LN(0.5 * (1 + (1 - 16 * z/L)\text{^}0.5)))); "")}$
Scaling parameters	
Obukhov length L	Mathematical description $L = IFERROR(-\rho\times {u_{*MOST}}^3/(0.4\times g\times(H_{MOST}/((T_z + 273.15)\times c_p) + 0.61\times LE_{MOST}/(L_v\times 10^6))); "")$ Excel $= IFERROR(-rho * ustar\_MOST\text{^}3/(0.4 * g * (H\_MOST/((Tz + 273.15) * cp) + 0.61 * LE\_MOST/(Lv * 10\text{^}6))); "")$
z/L	$\boldsymbol{= IFERROR(z/L; "")}$
Friction velocity $\boldsymbol{u_{*MOST}}$	Mathematical description $u_{*MOST} = IFERROR(0.4\times U_z/(LN(z/z_o) - \Phi_m); "")$ Excel $\boldsymbol{= IFERROR(0.4 * Uz/(LN(z/zo) - PSIm); "")}$

Component	Mathematical and Excel descriptions
Roughness lengths	
Roughness length $\boldsymbol{z_o}$, $\boldsymbol{z_{oT}}$ and $\boldsymbol{z_{ow}}$ (m)	$z_o = a\, u_*^2/g$ where a = 0.0016 $z_{oT} = 7.4\times z_o\, EXP\left(-2.46\, (u_* \times z_o/\nu)^{1/4}\right)$ where viscosity of air $\nu = 1.46\times10^{-5}$ m^2 s^{-1} $\boldsymbol{z_{ow} = 7.4\times z_o\, EXP\left(-2.25\, (u_* \times z_o/\nu)^{1/4}\right)}$
Sensible heat flux $\boldsymbol{F_h}$	Mathematical description $F_h = IFERROR((T_o - T_z)\times\rho\times c_p\times0.4\times u_{*MOST}/(LN(z/z_{oT}) - \Phi_h);"")$ Excel $\boldsymbol{= IFERROR((To - Tz) * rho * cp * 0.4 * ustar\_MOST/(LN(z/zoT) - PSIh);"")}$
Latent energy flux LE	Mathematical description $= IFERROR((q_o - q_z)\times\rho\times0.4\times u_{*MOST}\times(L_v\times10^6)/(LN(z/z_{ow}) - \Phi_w);"")$ Excel $= IFERROR((qo - qz) * rho * 0.4 * ustar\_MOST * (Lv * 10\text{^}6)/(LN(z/zow) - PSIw);"")$

3.4.11 Determination of the impact of error in air temperature and water vapour pressure measurement on MOST estimates of sensible and latent energy

Four measurements are required for application of MOST to open water for determining momentum, sensible heat and latent energy fluxes: T_z, T_o, q_z, and U_z. Note that q_o is determined assuming $q_o = q_s(T_o)$.

3.4.11.1 Iteration procedures in Excel and iteration efficiency

Iterative methods consume computer resources and therefore it is essential that the number of iterations required for convergence is kept to a minimum. For a spreadsheet implementation of MOST for open water, the number of iterations for adequate convergence was investigated.

To specify iteration and the iteration choices in Excel, click on File, Options, Formulas. Ensure that there is a tick to enable iterative calculations. Specify the maximum number of iterations required for iteration and the maximum change for the iteration. To ensure that Excel does not automatically iterate whenever there is change to the worksheet, specify manual calculations. Click OK to end the setup for iterative calculations in Excel. Excel indicates that calculations need to be updated by displaying “Calculate” at the bottom left of the display. The shortcut for manual forcing all iteration calculations is by pressing the F6 function key, or for the current worksheet, SHIFT+F9 (i.e. hold down the shift key while pressing F9).

For these iteration efficiency exercises, the maximum number of iterations was set to 1 so as to manually record the MOST fluxes on completion of the iteration. The maximum change for the iteration was specified as 0.001.

3.4.12 Protocols and methods for a simple iterative method for surface renewal

Snyder et al. (1996) used air temperature structure functions and the procedure of van Atta (1977) to calculate the amplitude a (ºC) and the ramp period τ (s) of high frequency air temperature measurements, above a canopy, over an averaging period.

Various (air) temperature methods, involving high frequency measurements and statistics, have been used to estimate sensible heat flux *H*. These methods include SR and TV for which statistics for *n* temperature measurements for a typical averaging period of 30 min, such as the mean ($\bar{T}$, ºC), variance (σ_T^2, ºC^2) and skewness (S_T, no units), are required:

$$\bar{T} = \sum_{i=1}^{n} T_i / n \tag{3.53}$$

$$\sigma_T^2 = \sum_{i=1}^{n} (T_i - \bar{T})^2 / (n-1) \tag{3.54}$$

$$S_T = (1/\sigma_T^3) \sum_{i=1}^{n} (T_i - \bar{T})^3 / (n-1) \tag{3.55}$$

and, in addition, the air temperature structure functions S_r^k of order $k = 2$, 3 or 5 (°C^2, °C^3 and °C^5 respectively) with sample time lag r (s) where:

$$S_r^k = \frac{1}{n-j} \sum_{i=1+j}^{n} (T_i - \bar{T}_{i-j})^k \tag{3.56}$$

for which the number of temperature measurements is $n - j$ with the measurement frequency f (Hz) is given by

$$j = f \times r. \tag{3.57}$$

In the case of the SR method, array-based dataloggers such as the older CR10X, 21X and 23X dataloggers (Campbell Scientific, Logan, Utah, USA) allow scan rates of 0.125 s with typical temperature lags of 0.25 and 0.5 s used – corresponding to 2 and 4 lags respectively. The newer and faster table-based dataloggers (CR1000, CR3000 and CR5000) allow scan rates of 10 Hz and greater. Typical lags of 0.2 and 0.4 s or 0.4 and 0.8 s are employed. The newer loggers also allow storage of high frequency air temperature data. Any desired time lag can then be used post-data collection for calculating S_r^2, S_r^3 and S_r^5.

The ramp period τ is also referred to as the inverse ramp frequency corresponding to the sum of the quiescent and ramping periods. The SR sensible heat flux $H = H_{SR}$ is then calculated using:

$$H_{SR} = \alpha\, z\, \rho\, c_p a / \tau. \tag{3.58}$$

The term α is a correction or weighting factor, z the measurement height above the soil surface, ρ the density of air (kg m^{-3}) and c_p the specific heat capacity of air at constant pressure (J kg^{-1} K^{-1}). The variable $a\, z$ represents the volume of air per unit ground area exchanged on average for each ramp in the sample period for height z (Paw U et al., 1995). Castellví et al. (2002) interpreted $a\, z$ as the mean eddy size responsible for the renewal process. The weighting factor α is usually determined empirically from the slope of the linear regression of EC estimates of $H = H_{EC}$ (y) against $H = H_{SR}$ (x) using $\alpha = 1$.

For the SR method, the second, third and fifth air temperature structure functions are calculated in near real-time from high frequency air temperature measurements. Typically, lag times r of 0.4 and 0.8 s are applied to the high frequency air temperature measurements used. The air temperature amplitude a (ºC) and inverse ramp frequency τ (s) for the SR method can be determined from S_r^2, S_r^3 and S_r^5 for air temperature (van Atta, 1977). An estimate of the ramp amplitude a for the averaging time interval is determined by solving for the real roots of

$$a^3 + pa + q = 0 \quad (3.59)$$

where

$$p = 10\, S_r^2 - S_r^5 / S_r^3 \quad (3.60)$$

$$q = 10\, S_r^3 \quad (3.61)$$

(van Atta, 1977). The ramping period τ is then calculated using

$$\tau = -a^3\, r / S_r^3. \quad (3.62)$$

By definition, τ is always positive. By definition, for unstable conditions, $a > 0$ºC and therefore $a^3\, r > 0$ºC^3 s with the result that $S_r^3 < 0$ºC^3 from Equation 3.62 since $\tau > 0$ s (Savage, 2010). Similarly, for stable conditions, $a < 0$ºC forces $S_r^3 > 0$. The key to the SR approach is the solution of the real roots of the cubic equation and that the direction of H_{SR} is indicated by the sign of a.

For the SR theory to be valid, τ should be much greater than the time lag r, typically

$$\tau > 10\, r. \quad (3.63)$$

Since $\tau \propto a^3$ (Eq. 3.62), this condition usually effects stable conditions for which a is usually small in magnitude compared to unstable conditions often experienced during the daytime. Snyder et al. (2007) also imposed an upper condition that

$$\tau < 600 \text{ s}. \quad (3.64)$$

To date, there has been no simple methodology nor near real-time methodology proposed for the solution of the real roots of the van Atta (1977) cubic equation.

The objective of this section is to describe a simple iterative method to obtain the real roots to the van Atta (1997) depressed cubic polynomial in a single cell in a spreadsheet and hence calculate $H = H_{SR}$ for both stable and unstable conditions.

Following an adaptation of the method credited to del Ferro and Tartaglia, published by Cardano in 1545 (http://en.wikipedia.org/wiki/Cubic_function), the real roots of Eq. 3.59 are given as

$$a = (-q/2 + \sqrt{F})^{1/3} + (-q/2 - \sqrt{F})^{1/3}. \tag{3.65}$$

where $F = p^3/27 + q^2/4$. Applying real arithmetic, this method, while finding the real roots for usually more than half of the number of unstable cases, does not allow determination of real roots when $F < 0$.

However, iteration may be applied using a rearrangement of Eq. 3.59:

$$a = (-pa - q)^{1/3}. \tag{3.66}$$

Accounting for unstable conditions, for which $a > 0$ºC, is possible using the multiplicative term $-S_r^3/|S_r^3|$ which equates to 1 for unstable conditions and -1 for stable conditions. Hence, combining Eqs 3.66, 3.60 and 3.61, in terms of the air temperature structure functions:

$$a = \frac{-S_r^3}{|S_r^3|}(|(10\, S_r^2 - S_r^5/S_r^3)\, a - 10\, S_r^3|)^{1/3},\ S_r^3 \neq 0. \tag{3.67}$$

Note that if $S_r^3 < 0$ºC^3, then $a > 0$ºC which corresponds to unstable conditions for which $H_{SR} > 0$ W m^{-2}.

Eq. 3.67 therefore forms the basis for the iterative procedure for both stable and unstable conditions. The ramping period τ is then calculated using Eq. 3.62 with the limiting conditions imposed by Eqs 3.63 and 3.64. The sensible heat flux H_{SR} is then calculated using Eq. 3.58 with $\alpha = 1$. The various inputs for the SR method are shown in Table 3.9.

3.4.13 Temperature variance

The sensible heat flux using temperature variance $H = H_{TV}$ (Tillman, 1972) is determined for unstable conditions using

$$H_{TV} = \rho\, c_p\, (\sigma_T^3\; k\; g\; z/\bar{T})^{0.5} \tag{3.68}$$

where k is the von Kármán constant, g the acceleration of gravity (m s^{-2}), σ_T^2 is the air temperature variance and $\bar{T}$ the average air temperature for the output time interval. The TV method, also often referred to as flux variance, has received much attention (Savage, 2010; Abraha and Savage, 2012), particularly for strongly unstable conditions. The method, however, applies no correction for stability. For stability correction, the Tillman (1972) method involves the use of air temperature skewness S_T through use of a skewness factor $f(S_T)$, applied in this study only for $S_T > 0$ for which $f(S_T) < 2.238$ (Fig. 3.2):

$$H_{TVST} = \rho\, c_p\, (\sigma_T^3\; k\; g\; z/\bar{T})^{0.5} \times f(S_T) \tag{3.69}$$

where

$$f(S_T) = \frac{\left(0.0549 + 0.0137\; exp\; (4.39\; S_T)\right)^{0.5}}{(0.0137\;\; exp\;\; (4.39\; S_T))^{0.5}} \tag{3.70}$$

where the flux direction is given by S_r^3:

$$H_{TVST} = \frac{-S_r^3}{|S_r^3|} \rho\; c_p\; (\sigma_T^3\; k\; g\; z/\bar{T})^{0.5} \times f(S_T) \tag{3.71}$$

Table 3.9 The various fixed data input requirements, measurement data and mathematical descriptions for the parameters associated with surface renewal sensible heat flux determination applied to open water evaporation

Data/component/exclusions	Mathematical and Excel descriptions
Fixed input data	
Required inputs for z (m), lag time r (s) and averaging period dt (s)	Measurement height z = 2 m Lag time r = 1 s Averaging period dt = 1800 s
Datalogger data	S_r^2, S_r^3 and S_r^5, every 2 and 30 min.
Surface renewal ramp amplitude a (ºC) Exclusions Error in determining S_r^5/S_r^3, or missing data	Mathematical description $a = IFERROR((-S_r^3/ABS(S_r^3))\times ABS(-10\times S_r^2\times a + (S_r^5/S_r^3)\times a - 10\times S_r^3)^{1/3};"")$ Excel $= IFERROR((-S3/ABS(S3)) * ABS(-10 * S2 * a + (S5/S3) * a - 10 * S3)\text{^}(1/3);"")$
Surface renewal ramp period τ (s) Exclusions $-a^3\times r/S_r^3 \geq 5\times r$ $-a^3\times r/S_r^3 \leq dt/3$ Error in determining $-a^3\times r/S_r^3$ Missing data	Mathematical description $= IFERROR(IF(AND(-a^3\times r/S_r^3 \geq 5\times r; -a^3\times r/S_r^3 \leq dt/3); -a^3\times r/S_r^3;""); "")$ Excel $= IFFERROR(IF(AND(-a\text{^}3 * r/S3 >= 5 * r; -a\text{^}3 * r/S3 <= dt/3); -a\text{^}3 * r/S3;""); "")$
Surface renewal sensible heat flux (W m^{-2}) Exclusions $10\times S_r^2 - S_r^5/S_r^3)\times a + 10\times S_r^3) < 0.001$	Mathematical description $H_{SR} = IFERROR(IF(AND(ABS(a^3 + (10\times S_r^2 - S_r^5/S_r^3)\times a + 10\times S_r^3) < 0.001; \tau \leq 5\times r); ""; 1216\times z\times a/\tau); "")$

Data/component/exclusions	Mathematical and Excel descriptions
$\tau \leq 5\times r$ Error in determining $1216\times z\times a/\tau$ Missing data	Excel $= IFERROR(IF(AND(ABS(a\string^3 + (10 * S2 - S5/S3) * a + 10 * S3) < 0.001; tau <= 5 * r); ""; 1216 * z * a/tau); "")$

(Savage, 2010). For skewness values $S_T > 0.83$, the correction for stability is less than 5%, i.e. $f(S_T) < 1.05$ (Fig. 3.2). As far as is known, much of the research using flux variance has either not involved stability correction, or is applied offline using MOST stability corrections that require friction velocity or wind speed measurements (Hsieh et al., 1996). The intention of this study was not to require wind speed measurements and that the stability correction is performed online, thereby allowing near real-time stability-corrected flux variance estimates of sensible heat flux.

For the SR method, lag times of 0.4 and 0.8 s were used and the second- (S_r^2), third- (S_r^3) and fifth-order (S_r^5) air temperature structure functions determined in real-time and stored in datalogger memory together with other temperature statistics. An iterative procedure, applied in the logger program, was used to calculate the air temperature ramp amplitude and the (sum of) quiescent and ramping periods (τ) for each time lag from which H_{SR} was calculated. For the TV method, the mean, variance and statistical moment of order 3 and hence the skewness of air temperature were calculated from the high frequency air temperature measurements from which H_{TV} and H_{TVST} were calculated in near real-time.

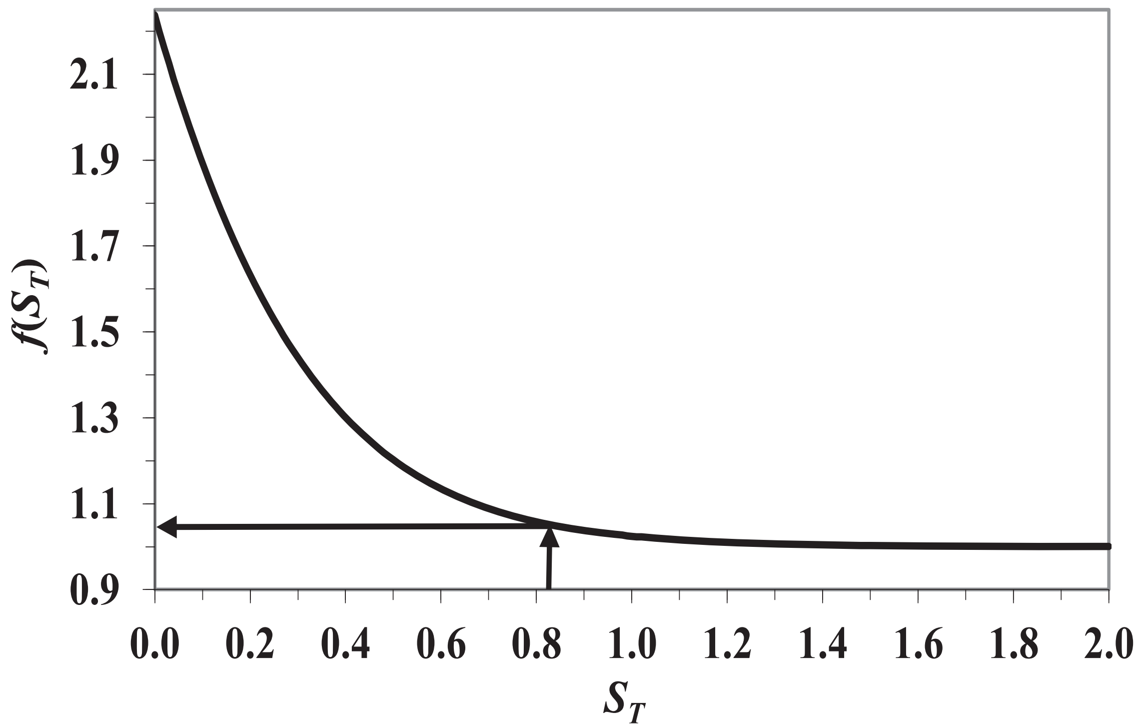

Fig. 3.2 The functional dependence of $f(S_T)$ on air temperature skewness S_T (Eq. 3.70) showing that for skewness values $S_T > 0.83$, $f(S_T) < 1.05$.

3.5 Materials and methods

The materials and methods for application of the MOST method to open water are relatively simple. The instrumentation is summarised in Fig. 3.1 and Table 3.10 with the methodology summarised in the datalogger programme (Appendix 2) and instrumentation details listed in Table 3.10. The instrument specifications and the sensor accuracy are also listed in Table 3.10. The instruments used for MOST and automatic weather station (AWS) measurements are displayed below Table 3.10 and Fig. 3.3.

The infrared thermometers were laboratory-calibrated using the methods of Savage and Heilman (2009).

3.5.1 Symon's pan data

Daily Symon's pan evaporation data for Midmar (30.1234° S, 30.1234° W, altitude of 892 m), for the period 1952 to 2006 inclusive were supplied by the Department of Water and Sanitation. Data for the hydrological years 1953 and 1954, 1960 to 1966 and year 1975 were unreliable or insufficient.

3.5.2 Instrumentation

Table 3.10 Instrumentation details, including sensor accuracy (adapted from manufacturer specifications). Shaded rows are for land measurements, unshaded for open water.

Measurement	Model	Supplier	Comments
Solar irradiance (W m^{-2})	CMP3	Kipp and Zonen (Delft, The Netherlands)	No active heating/ventilation possible Solar irradiance daily totals error within 5% Infrared daily totals within 10% Tilt response (±80° at 1000 W m^{-2}): < ±2%.
Four-component irradiances (W m^{-2}) (R_{net} as well as the two solar and two infrared components of the energy balance)	CNR4	Kipp and Zonen (Delft, The Netherlands)	Active heating/ventilation possible Solar irradiance daily totals error within 5% Infrared daily totals within 10% Solar irradiance tilt error < 1% at any angle at 1000 W m^{-2} Infrared tilt error: < 20 W m^{-2} at angle up to 80° with 1000 W m^{-2} If the instrument is z (m) above the surface, 99% of the irradiance measured by the lower sensors is from an area (m^2) of $100\,\pi\,z^2$

Table 3.10 Instrumentation details, including sensor accuracy (adapted from manufacturer specifications). Shaded rows are for land measurements, unshaded for open water.

Measurement	Model	Supplier	Comments
Air temperature (T_z) (ºC)	HC2S3	Rotronic AG (Bassersdorf, Switzerland)	Accuracy at 23°C: ±0.1°C with standard configuration settings Due to the optical properties of water in relation to efficiently reflecting solar irradiance at low solar angles, a 10-plate Gill radiation shield (RM Young) was required for air temperature and relative humidity measurements – six-plate for land measurement and 10-plate for water
Relative humidity (%) for determining q_z (kg kg^{-1})	HC2S3	Rotronic AG (Bassersdorf, Switzerland)	Accuracy between 10 and 30°C: ±0.8% RH with standard configuration settings
Sonic anemometer (U_z), wind direction and air temperature	DS-2	Decagon Devices (Pullman, WA, USA)	Wind speed: accuracy ±0.30 m s^{-1} or ±3% (whichever is greater); resolution 0.01 m s^{-1}; range 0 to 30 m s^{-1} Wind direction: accuracy ±3º; resolution 1º; range 0 to 359º Air temperature: no specifications
Wind direction (º)	03002	RM Young, (Traverse City, MI, USA)	Threshold: 0.8 m s^{-1} at 10° displacement; 1.8 m s^{-1} at 10° displacement Accuracy: ±5°

Table 3.10 Instrumentation details, including sensor accuracy (adapted from manufacturer specifications). Shaded rows are for land measurements, unshaded for open water.

Measurement	Model	Supplier	Comments
Water-surface temperature (T_o) (°C) and for determining $q_o = q_s(T_o)$ (kg kg^{-1})	Various	Apogee Instruments (Logan, USA)	Model SI-111 Field of view (FOV) = 22.0°; model SI-121 FOV = 18.0° For target temp within 20°C of sensor body temperature: accuracy ±0.2°C (SI-111, SI-121); uniformity ±0.1°C; repeatability ±0.05°C While it is desirable to position the sensor vertically, this may not be possible. Due to the critical importance of this measurement and also to ensure a larger spatial measurement representation of the surface water temperature, two sensors will be employed.
Rain gauge	TE525	Texas Electronics (Dallas, USA)	Resolution: 0.254 mm Accuracy ±1% (rainfall intensity < 25.4 mm h^{-1}), 0 to -3% (rainfall intensity 25.4 to 50.8 mm h^{-1}), 0 to -5% (rainfall intensity 50.8 to 76.2 mm h^{-1})
Water temperature profile	Type E thermocouples (model EXTT-E-24)	Omega Inc. (Stamford, Connecticut, USA)	Water temperatures at depths of 20, 40, 80, 160, 320 and 640 mm below the surface will be measured

CMP3

CNR4

DS-2

Ten-plate Gill radiation shield for housing a HC2S3

HC2S3

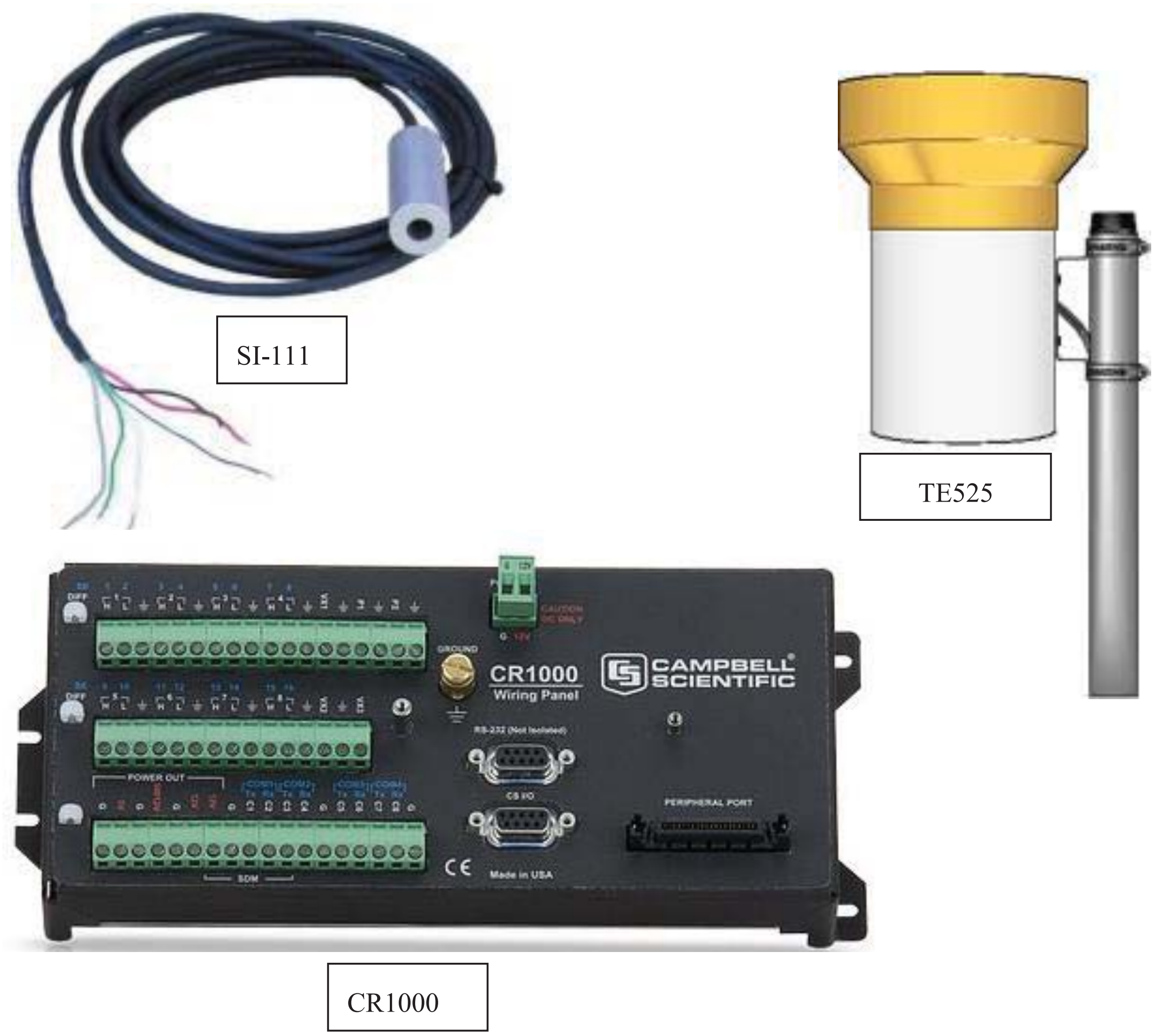

Fig. 3.3 Details of the equipment used at the land and water stations for the measurement of open water evaporation

CHAPTER 4: OPEN WATER EVAPORATION USING SYMON'S PAN AND DPMETHS MODEL METHODS AT A DAILY TIME SCALE

4.1 Summary

From an energy and water balance perspective, evaporation is regarded as the largest energy and water loss term for most open water bodies such as that considered in this study. This study focuses on the estimation of daily evaporation from an open water surface. Evaporation was estimated using two datasets. Symon's pan evaporation (hydrological years 1956/7 to 2005/6 inclusive) together with monthly pan to dam factors were used to estimate evaporation. In addition, open water evaporation was modelled using a 52-year weather dataset (hydrological years 1962/3 to 2014/5 inclusive) and a spreadsheet-implemented Penman-Monteith type model based on the concept of equilibrium water-body temperature to estimate water-stored heat that assumes that the water body is uniformly mixed with no thermal stratification. An iterative procedure was applied for determining the wet bulb temperature and an additional iterative approach to determining the slope (first derivative) of the saturation water vapour pressure versus temperature relationship evaluated between the water body temperature (T_o) and the air temperature (T_z). The evaporation estimates were not corrected for atmospheric stability but it may be possible to do so using an iterative procedure. Other features of the model include automatic patching of missing data. For example, missing relative humidity data were patched based on determining an average daily water vapour pressure from the daily minimum air temperature. Due to the absence of solar irradiance measurements for the period 1962 to 2008, the Hargreaves and Samani daily solar radiation model, based on the daily air temperature range only, was used to estimate daily open water evaporation. The Angström model for estimating daily solar radiant density was also applied, based on sunshine duration data only. Evaporation estimates were obtained using both radiation models for hydrological years 1962/3 to 2007/8 inclusive (excluding June 1998 to January 1999, as the sunshine duration data were missing). The daily evaporation estimates based on the Angström radiation model were more problematic due to the missing data and tended to overestimate annual evaporation compared to estimates obtained using the Hargreaves and Samani solar radiation model. The average daily Midmar Dam model (hydrological-year) estimate of open water evaporation was 1202 mm per annum, corresponding to a daily average of 3.29 mm. The annual rainfall was 855 mm. The evaporative fraction (the ratio of evaporation (expressed in MJ m^{-2}) to the available energy density) exceeded 1 – indicative of almost no, or negative, annual average sensible heat flux. This is indicative of significantly dry conditions in the local and surrounding areas for these years – resulting in mesoscale advection. Between 1971/2 and 1982/3 there was a gradual increase in annual evaporation from 3.05 to 3.80 mm and between 1986/7 and 1992/3 there was a consistent increase from 3.16 to 3.93 mm day^{-1}. During the latter period, there were small

changes in the annual solar radiant density (16.15 to 17.27 MJ m^{-2}, a 6.9% increase) but only between 1989/90 and 1991/92. The annual evaporation trends were generally in phase with wind speed, indicating the important role of wind speed as a determining factor. Rainfall for the full period was usually in anti-phase with annual evaporation in years with high rainfall corresponding to years with low evaporation and vice versa. The increase in evaporation for the 1971/2 to 1982/3 and 1986/7 to 1992/3 periods is explained by the increased wind speed affecting both the radiative and aerodynamic components of evaporation. Specifically, the former is increased by increased wind speed reducing the water-body temperature and hence the outgoing infrared radiant density and therefore increasing the net radiant density of the open water. Between 2006/7 and 2010/11, there was a 28% reduction in annual daily solar radiant density followed by a gradual increase after 2010/11 with a gradual reduction in wind speed post 2008/9. This decreased the evaporation of open water by 26% (2011/12) following which it increased slightly. A limitation of the model is that it assumes that the water body is uniformly mixed and thus thermal stratification is not accounted for. Annual estimates of evaporation using pan data were compared with the modelled estimates, showing correspondence in peaks and troughs for 1957 to 2006 even though their exact correspondence was poor.

4.2 Introduction

The energy balance method, used by Penman (1948), is regarded as an accurate method for estimating evaporation from open water for periods of a week or longer (Winter, 1981; Rosenberry et al., 2007). However, for a daily time scale, problems with data availability, particularly in South Africa, and an adequate description of the water-stored heat remain significant challenges. Many modelling studies, even today, ignore the water-stored heat (Duan, 2014). Monteith (1965) added a surface resistance term to the Penman equation, assumed to be 0 s m^{-1} in this study, and modified the Penman aerodynamic term.

This study focuses on estimation of daily evaporation from an open water surface. Evaporation was estimated using two datasets. Symon's pan evaporation (hydrological years 1956/7 to 2005/6 inclusive) together with monthly pan to dam factors were used to estimate evaporation. In addition, evaporation was estimated using a 52-year weather dataset (1962/3 to 2014/5 hydrological years inclusive). Relative humidity was available from 1970. A spreadsheet-implemented Penman-Monteith type model was used, based on the concept of equilibrium water-body temperature to estimate water-stored heat, an iterative procedure for determining the wet bulb temperature and an additional iterative approach to determining the slope (first derivative) of the saturation water vapour pressure versus temperature relationship evaluated between the water body temperature (T_o) and the air temperature (T_z). The evaporation model estimates were not corrected for atmospheric stability but it may be possible to do so using an iterative procedure.

The Department of Water and Sanitation supplied daily Symon's pan evaporation data, together with pan to dam factors (Table 4.1), for the period 1962/3 to 2005/6 inclusive. Monthly pan data and monthly pan factors were used to estimate open water evaporation.

Table 4.1 Monthly pan to dam factors (Department of Water and Sanitation)

Month	Pan to dam factor
January	0.88
February	0.87
March	0.85
April	0.83
May	0.81
June	0.81
July	0.81
August	0.82
September	0.83
October	0.84
November	0.88
December	0.88

Two model methods for estimating daily open water evaporation were used, implemented in Excel, using two iterative procedures. Both methods rely on the Penman-Monteith approach and assume energy balance closure. Arguably, it is not the Penman (1948) approach used here but the Penman-Monteith approach (Monteith, 1965) and not just since the bulk stomatal resistance of the big leaf is set to 0 s m^{-1}. In the case of the model used, the aerodynamic term differs from the Penman approach and follows that of Monteith (1965). Both models in the present study are based on the concept of water-body equilibrium temperature (Edinger et al., 1968; Keijman and Koopmans, 1973; de Bruin, 1982; Finch, 2001) (Section 2.4.10). One evaporation model incorporates the Hargreaves and Samani (1982, 1983) daily solar radiation estimation model using only the range in daily air temperature and is referred to as the DPMETHS daily model (Daily Penman, Monteith, Equilibrium Temperature Hargreaves-Samani). The second model implemented is identical to the first but uses the Angström equation for estimating daily solar radiant density from sunshine duration and is referred to as DPMETA.

Missing relative humidity data were patched based on determining an average daily water vapour pressure from the daily minimum air temperature. The daily average water vapour pressure was determined from day-length:night-length weighted minimum and maximum relative humidity where the two relative humidities were converted to water vapour pressure using the saturation water vapour pressure evaluated at the maximum and minimum air temperatures.

4.3 Daily solar radiant density estimation (1914 to 2008)

For the years for which there was no solar radiation data, daily maximum and minimum air temperature and sunshine duration data were available. Model procedures (Table 3.1) were applied and the two estimates compared. Comparison of estimated daily solar radiant density (MJ m^{-2}) estimated using the Hargreaves and Samani (1982, 1983) and Angström methods for 1970/1 (Fig. 4.1 upper, 16 months) and for 1971/3 are shown (Fig. 4.1 lower, 20 months). There is quite tight correspondence between the two estimates. A broken stick model was used for the Angström method (Table 4.1). It may be possible to improve on the empirical Angström constants used in this study but this aspect was not pursued.

For the period for which solar radiant density measurements were available (1st January 2009 to 16th March 2015), comparisons were made against the Hargreaves and Samani (HS) radiation model estimates (Fig. 4.4 top) resulting in R^2 = 0.6321 and a slope of 0.6491 and intercept of 8.1051 MJ m^{-2}. In order to improve the HS radiation estimates for the 1970 to 2008 period, a statistical prediction procedure was used. This prediction was based on the measured radiation and the HS estimates for the 2009 to 2015 period. A statistical prediction of X (measured solar daily radiant density I_{s_land}) from a measured Y (I_{HS} radiation) was applied using the regression statistics of Fig. 4.4 (top): the slope a and intercept b as well as the Student t value $t(0.05,\ n-2)$ where n is the number of data points (n = 2248 for the 2009 to 2015 period), the standard error of the slope SE_{slope}, $S_{y.x}$ and $SD_{x\ population}$ where $S_{y.x}$ is standard error for predicted value of x from y in a regression and $SD_{x\ population}$ is the standard deviation of the x population. These procedures were based on Snedecor and Cochran (1980):

$$I_{s\_land} = \left(\frac{I_{HS}-a}{b}\right) / (1 - C^2) \tag{4.1}$$

$$C^2 = \frac{(t(0.05, n-2))^2 \times SE_{slope}^2}{b^2} \tag{4.2}$$

$$SE_{slope} = \left(S_{y.x}/SD_{x\ population}\right)/n^{0.5} \tag{4.3}$$

The statistical output is shown in Table 4.2.

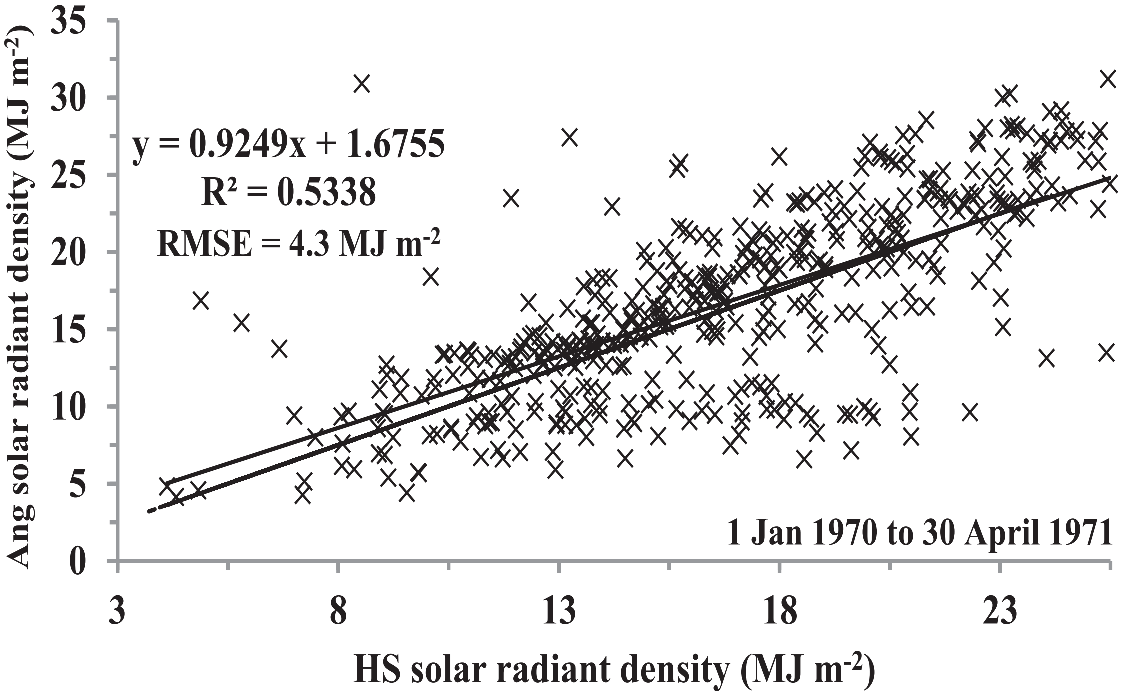

y = 0.9249x + 1.6755
R² = 0.5338
RMSE = 4.3 MJ m-2
1 Jan 1970 to 30 April 1971
Ang solar radiant density (MJ m-2)
HS solar radiant density (MJ m-2)

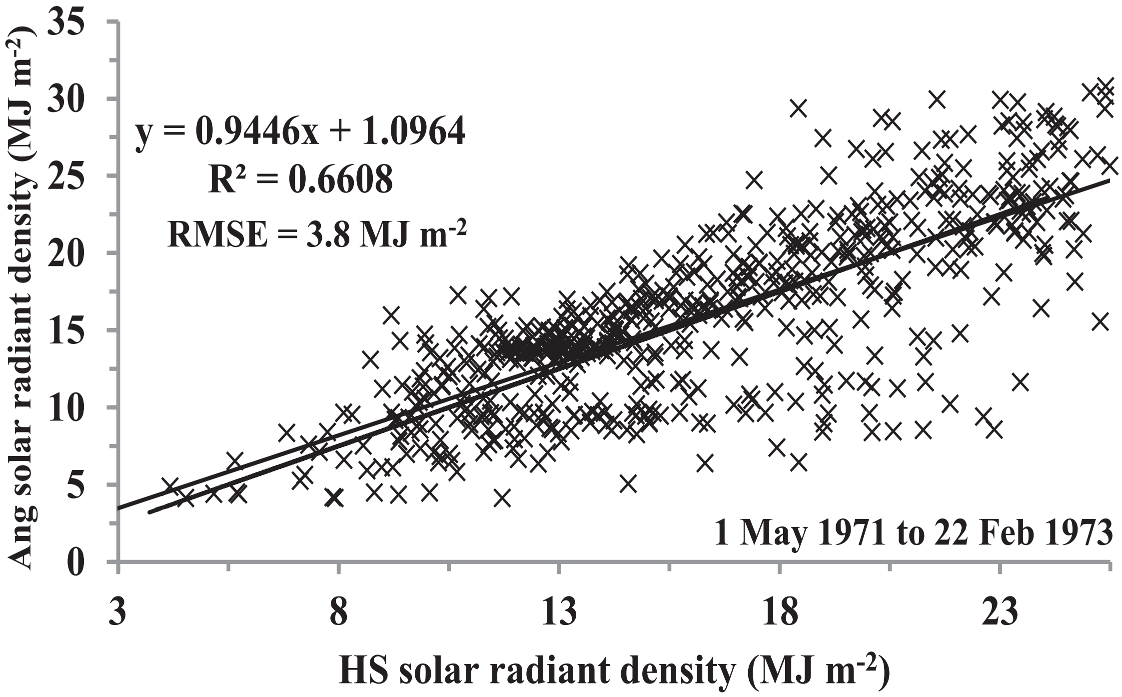

y = 0.9446x + 1.0964
R² = 0.6608
RMSE = 3.8 MJ m-2
1 May 1971 to 22 Feb 1973
Ang solar radiant density (MJ m-2)
HS solar radiant density (MJ m-2)

Fig. 4.1 Comparison of estimated daily solar radiant density (MJ m^{-2}), estimated using the Hargreaves and Samani (1982, 1983) and Angström methods for two different time periods

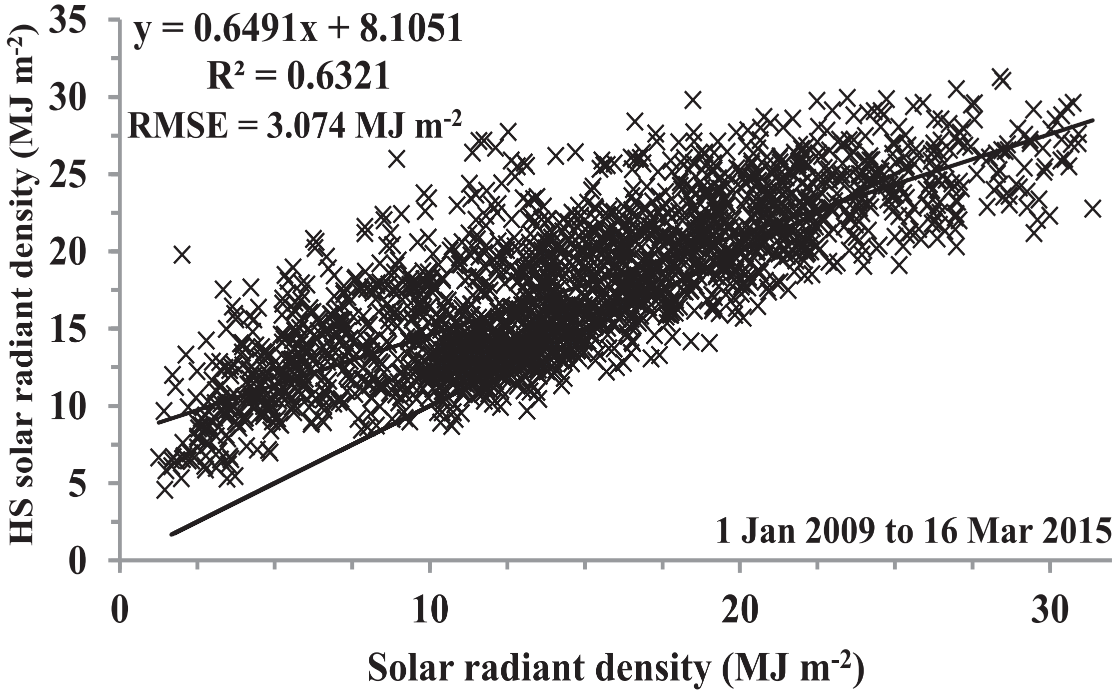

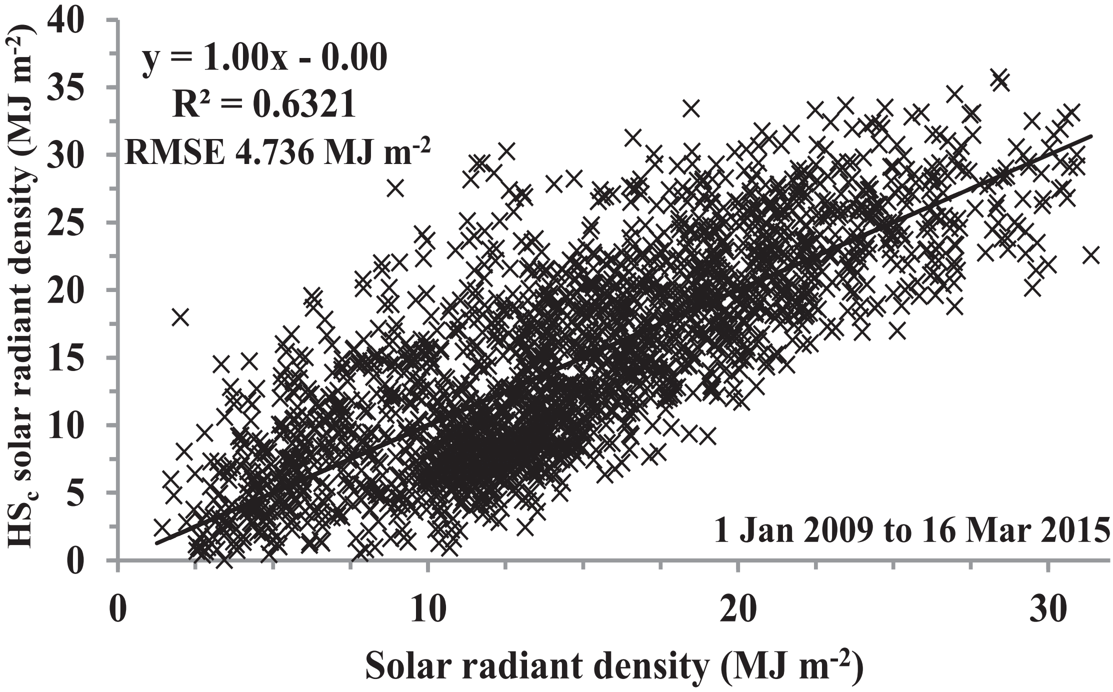

Fig. 4.2 Comparison of measured daily solar radiant density (MJ m^{-2}) (x-axis) against that estimated using (a) the original HS method (y-axis); (b) the corrected HG method ("HS$_c$")

Table 4.2 Statistics for the regression of measured solar radiant density (*x*) *vs* that estimated using the HS radiation model (*y*) for the period 2009 to 2015

Y = a + b X

R^2	0.63206		
T	62.11458		
F	3858.22145		
Slope b	0.64908	TINV(0.05, n-2)	1.9610
Intercept a (MJ m^{-2})	8.10509	TINV(0.01, n-2)	2.5780
N	2248	FINV(0.05,2,n-2)	2.9997
Sy.x (MJ m^{-2})	3.0743	FINV(0.01,2,n-2)	4.6146
Min X (MJ m^{-2})	1.250	CxC_95%	0.00099673
Max X (MJ m^{-2})	31.380	CxC_99%	0.00172260
Min Y (MJ m^{-2})	4.556	sum $d_{y.x}^2$	21227.0952
Max Y (MJ m^{-2})	31.286	$Sy.x^2$	9.4511
SEslope	0.0104		
b+SEb 99%	0.6760		
b-SEb 99%	0.6221		
b+SEb 95%	0.6696		
b-SEb 95%	0.6286		
SEintercept (MJ m^{-2})	0.0648		
a+SEa 99% (MJ m^{-2})	45.3469		
a-SEa 99% (MJ m^{-2})	-29.1367		
a+SEa 95% (MJ m^{-2})	36.4338		
a-SEa 95% (MJ m^{-2})	-20.2236		
MBE (mean bias error) (MJ m^{-2})	3.0357		
MAE (mean absolute error) (MJ m^{-2})	3.7317		
d-index (Wilmott 1981, 1982)	0.7751		
% unsystematic (random)	40.3540		
% systematic (bias)	59.6460		
Bias b	-3.0357		
Comparability b	4.8373		
Precision	14.1840		

(Table 4.2). The corrections for C were in fact minor due to the large sample size (n = 2248) resulting in $SE_{slope} = 0.0104$ W m^{-2} and the magnitude of the slope value (b = 0.6491). The corrected value, using Eq. 4.1, for the 2009 to 2015 HS radiation estimate (HS_c) is shown (Fig. 4.4 bottom).

4.4 Midmar water depth

Water depth is an input to the DPMETHS model that directly effects the time constant used in the model and hence the modelled water temperature, with both affecting the daily change in water-stored heat flux. The Midmar Dam surface area is also an input for the model.

Midmar Dam was constructed in 1960. The daily water depths for the period 31st October 1963 to 31st August 2015 were obtained from the Department of Water and Sanitation (DWS) (Fig. 4.5). Of particular note is the significant decrease in dam water depths for: 1982/3, 1992/3, 2002/3 and 2014/5. In 2002, the raising of the wall from 11.8 to 14.8 m was completed. This accounts for the increase in the water depth after this.

The Midmar Dam surface area is also an input for the model. The surface area of the dam affects the wind speed function of the model through a weak function $(5/A_{WATER})^{0.05}$. Even if A_{water} = 13 km^2 were halved, the function would decrease by only 3.5%. This weak influence also impacts on daily values of the aerodynamic component of evaporation, equilibrium temperature, time constant and therefore the modelled water temperature and the change in water-stored heat flux. The area data were supplied as a lookup table of water depth and surface area (Fig. 4.4). A fifth-order polynomial was fitted to determine the surface area from the measured water depth for each day. This function was used to determine the water surface area from the measured depth for each depth for each day for hydrological years 1963 to 2015 inclusive.

4.5 Daily evaporation for open water (1914 to 2015)

The daily DPMETHS model estimates of E from late April to early July (0.4 to 0.6 of a year) of each year, roughly corresponding to winter, show quite a tight range for all years 1981/2 to 1986/7 (Fig. 4.7). Typically, E is less than 2 mm day^{-1} for this radiation-limiting period. Between 1st October and 31st January of the next year (0.75 to 0.08 of the next year), there is a much greater variation in E mainly due to variable cloud cover during the main rain season but also due to increased wind speed, particularly in September/October of each year. Daily E seldom exceeded 6 mm during this "summer" period.

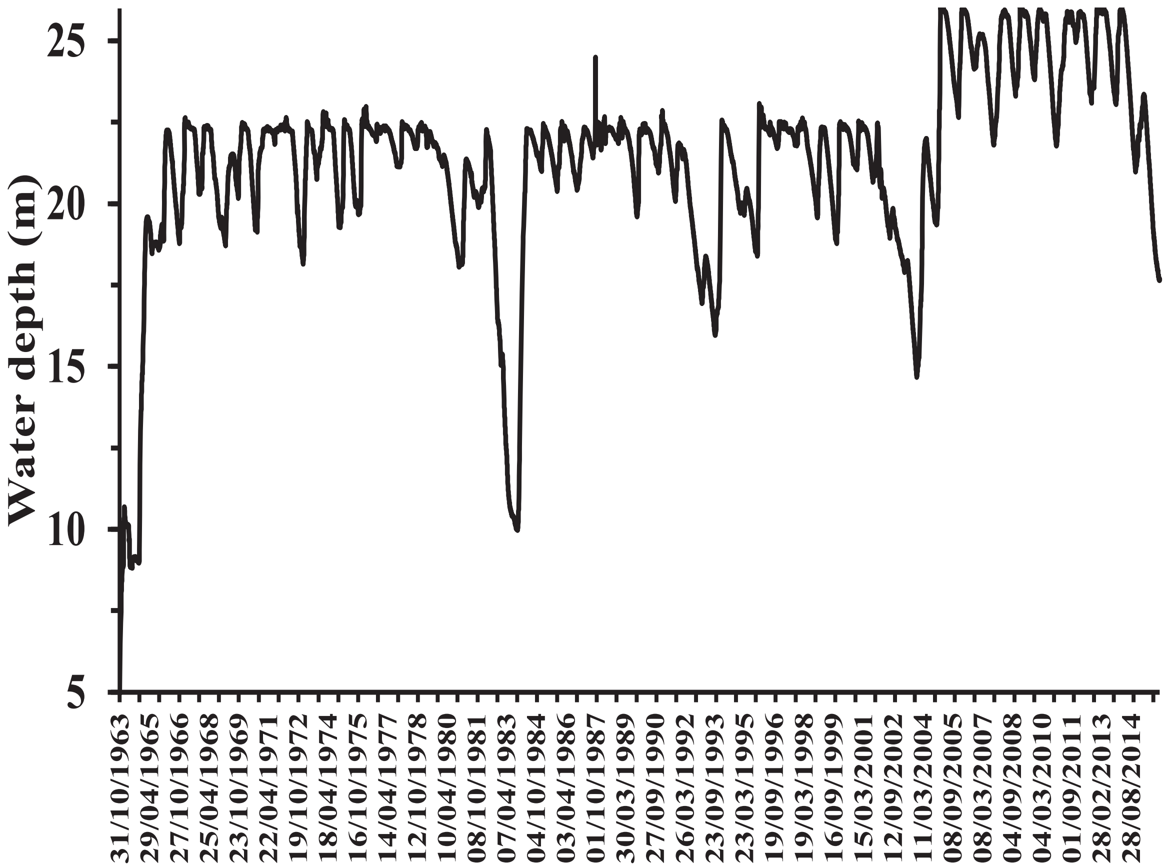

Fig. 4.3 Water depths for Midmar Dam (data source: DWS)

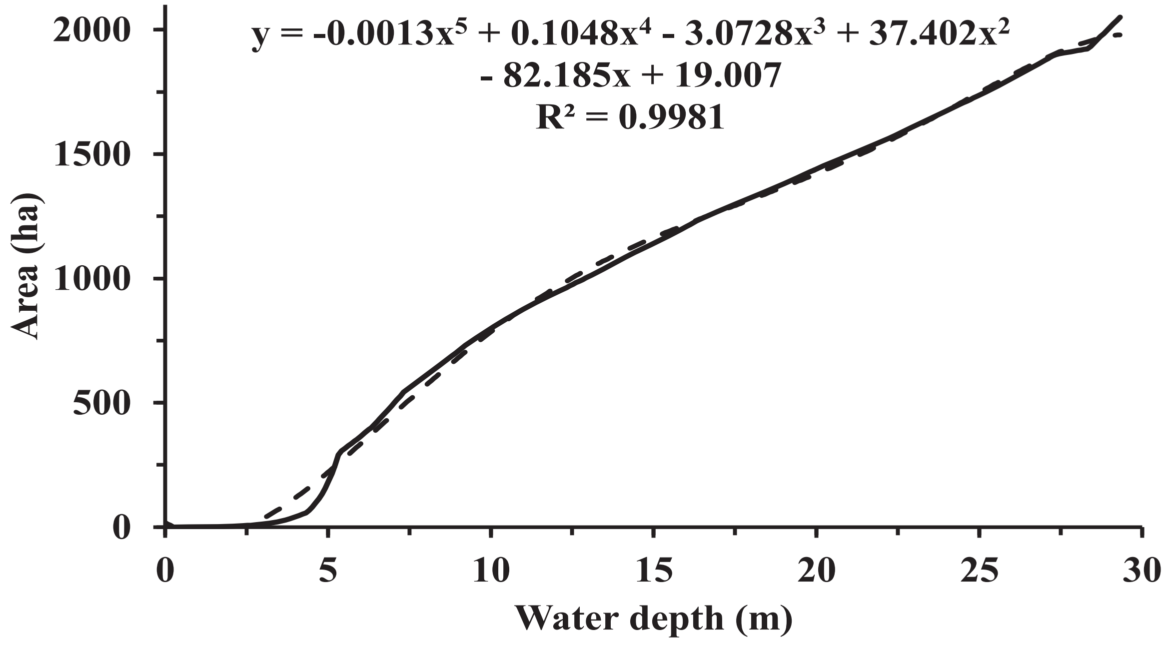

Fig. 4.4 Water depths vs dam area lookup data plotted together with the fifth-order fitted polynomial (dashed curve)

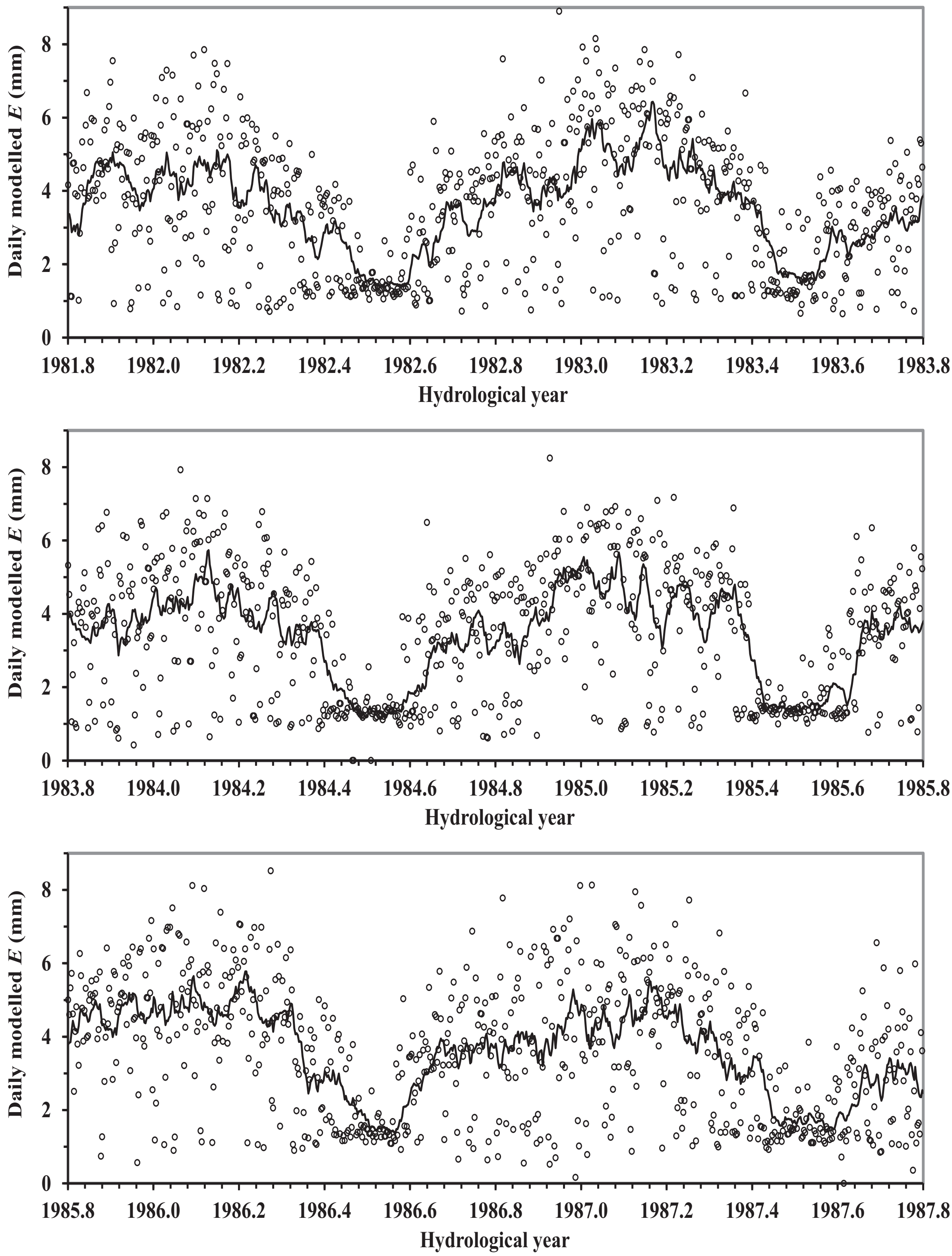

Fig. 4.5 Daily evaporation E (circles) and the running mean E of order 14 days (solid curve) for six hydrological years for the DPMETHS model: top 1981/2, 1982/3; middle: 1983/4, 1984/5; bottom: 1985/6, 1986/7

For the 1962/3 to 2014/5 period, the average annual DPMETHS model-estimated evaporation for Midmar is 1202 mm (3.29 mm day^{-1}) with a standard deviation of 103 mm (Table 3.13). For the period 1962/3 to 2007/8 for which there was no solar radiation data, the average annual evaporation is 1228 mm. The DPMETA model average was slightly lower at 1217 mm (Table 4.3).

The annual DPMETHS model-estimated E is 1202 mm or 3.29 mm day^{-1} (Fig. 4.8 top). Generally, the DPMETA model, using sunshine duration, tended to overestimate E in most years (Fig. 4.8 bottom).

The annual average daily available energy density $R_{n\,water} - dS$ ranged between 6.02 and 9.03 MJ m^{-2} (Fig. 4.9). The average annual DPMETHS evaporation exceeded the available flux. This is indicative of a negative sensible heat flux. The evaporative fraction EF (latent energy divided by available energy density) therefore exceeds 1, as shown in Fig. 4.10 (left y-axis).

4.6 Why the increase in annual average daily evaporation for open water from 1970/1 to 1982/3 and 1987/8 to 1992/3?

There was a relatively large increase in E for the periods 1970/2 to 1982/3 and 1987/8 to 1992/3 (Fig. 4.8 top) and also an increase in the available energy density for the same time period (Fig. 4.9).

What could have caused the increase in E for these periods (Fig. 4.8 top)?

The temporal variation in the annual average daily solar radiant density $I_{s\,land}$ for the entire period only shows significant increases for the period 2011/2 to 2013/4 (Fig. 4.11). The modelled net irradiance for the water surface $R_{n\,water}$ tracks the variation in $I_{s\,land}$ (Fig. 4.11). Changes in $I_{s\,land}$ do not show convincing evidence for the increase in E for the period 1987/8 to 1992/3, showing only a slight increase.

If not $I_{s\,land}$, then what else could be the cause for the increase in E and $R_{n\,water} - dS$ for these periods (Fig. 4.9)?

The variation in annual average air temperature and maximum, average and minimum air temperatures are shown in Figs 4.10 (top: average, bottom: maximum, average, and minimum) and 4.11 (range, minimum and maximum as separate figures). The minimum annual average air temperature trend yielded no clue (Fig. 4.12 top) with the maximum air temperature increasing for part of the period – 1990/1 to 1992/3 (Fig. 4.13 middle). The range of annual air temperature (Fig. 4.13 top), used for determining $I_{s\,land}$ using the HS radiation model (Fig. 4.11), is shown in Fig. 4.13 top. There is a small increase in $T_{z\,max} - T_{z\,min}$ between 1991/2 and 1992/3 – as was the case with $I_{s\,land}$ (Fig. 4.11). For completeness, the annual average $T_{z\,max}$ and $T_{z\,min}$ temperatures are also shown (Fig. 4.13 middle and bottom).

Table 4.3 Summary statistics of annual total and daily average *E* (mm)† for Midmar open water for the DPMETHS and DPMETA models for the 1962/3 to 2007/8 and 1962/3 to 2013/4 hydrological years

Model	Annual total *E* (mm) statistics for various hydrological years		Daily average *E* (mm) statistics for various hydrological years		Comment
	1962/3 to 2007/8	1962/3 to 2014/5	1962/3 to 2007/8	1962/3 to 2014/5	
DPMETHS	Average 1148 SD 118 Maximum 1430 (1993/4) Minimum 973 (1976/7)	Average 1137 SD 117 Maximum 1430 (1993/4) Minimum 973 (1976/7)	Average 3.14 SD 0.32 Maximum 3.91 (1993/4) Minimum 2.66 (1976/7)	Average 3.11 SD 0.32 Maximum 3.91 (1993/4) Minimum 2.66 (1976/7)	Measurements of solar irradiance commenced on 1st January 2009
DPMETA	Average 12021 SD 148 Maximum 1452 (1992/3) Minimum 771 (1973/4)	-	Average 3.29 SD 0.40 Maximum 3.98 (1992/3) Minimum 2.11 (1972/3)	-	Missing sunshine duration data: 12th June 1988 to 31st January 1989; sunshine duration data ends 31st March 2008

Rainfall statistics

† Annual rainfall	856.7 mm	
SD	179.0 mm	
Maximum annual rainfall	1461.8 mm	(1987/8)
Minimum annual rainfall	538.1 mm	(2008/9)

The variation in the annual average water vapour pressure is shown in Fig. 4.14 and in general the increases/decreases are coincident with that of annual rainfall. These variations are generally in anti-phase with *E*. The water vapour pressure is used, together with the saturation water vapour pressure and wind speed in determining the aerodynamic term $E_{aerodynamic}$ (mm) of the DPMETHS model for determining evaporation.

The variation in the annual average wind speed is shown in Fig. 4.15. Of note is the large increase in wind speed from about 1.27 to 1.88 m s^{-1} between 1971/2 and 1976/7 and from 1.63 to 1.88 m s^{-1} between 1987/8 and 1992/3 respectively. Can this be the cause for the increase in *E*? The change from a manual weather station to an AWS system occurred on 1st January 2009 and is therefore not a possible cause for these increases in the wind speed. These large increases in wind speed are consistent with the increases in *E* for the same time periods (Fig. 4.8, top). The variation in $E_{aerodynamic}$ shows a 27 % increase over the 1987/8 to 1992/3 period and a gradual increase between 1970/1 to 1980/1 (Fig. 4.16 top). The radiative term of the model:

$$E_{radiative} = \Delta_{T\,water} \times (R_{n\,water} - dS)/(\Delta_{T\,water} + \gamma) \tag{4.4}$$

does not directly depend on wind speed. And yet, there is also a 33 % increase in $E_{radiative}$ for the 1988/9 to 1994/5 period (Fig. 4.16 middle).

The variation in the outgoing and "returned" infrared irradiance components are shown if Fig. 4.17 (top) with the net infrared irradiance shown in Fig. 4.17 (bottom). There variations are remarkably in phase with those of wind speed (Fig. 4.15).

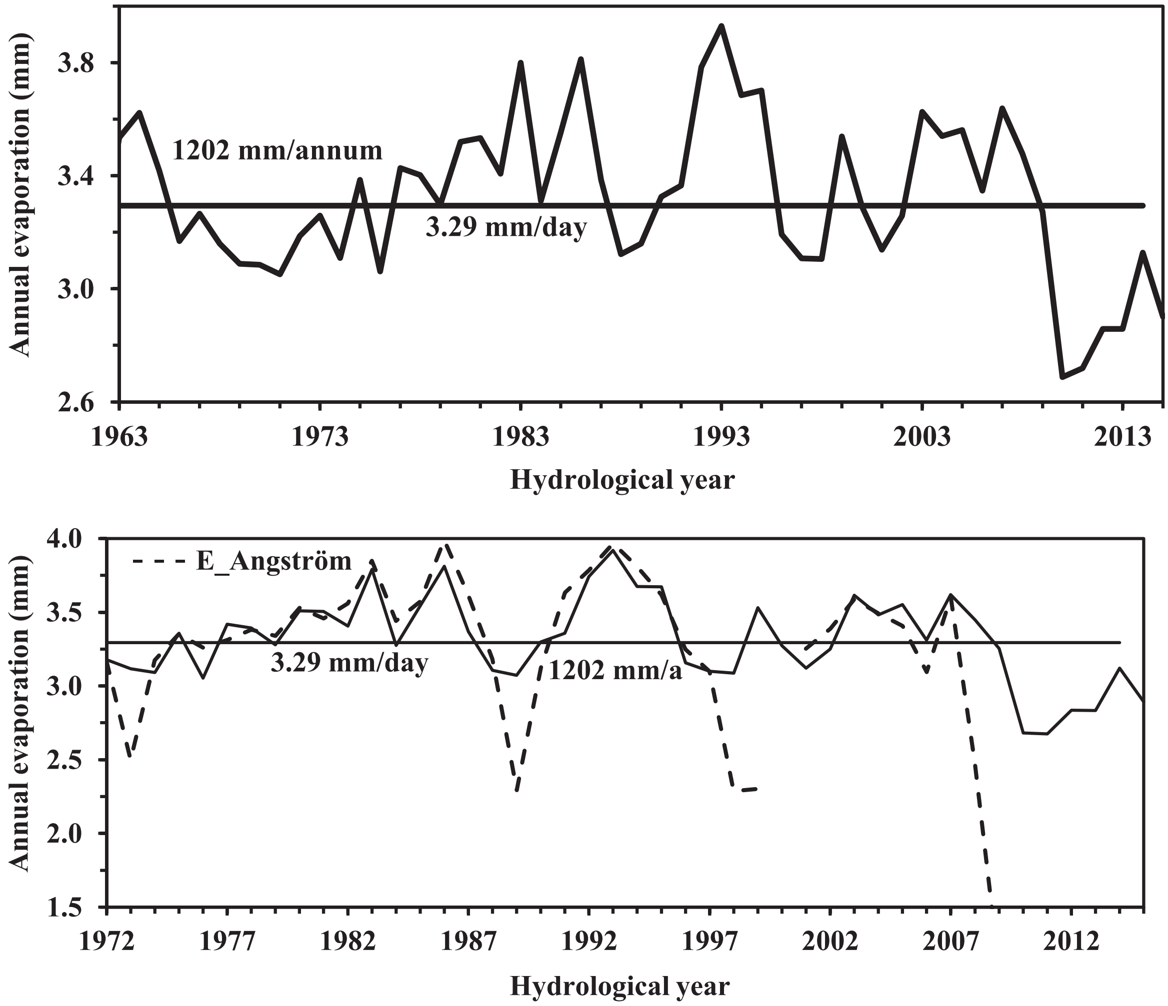

Fig. 4.6 Annual evaporation *E* modelled using the DPMETHS model (top) and *E* modelled using the DPMETHS (solid curve) and DPMETA models (bottom). The horizontal line (top and bottom) indicates the average daily evaporation

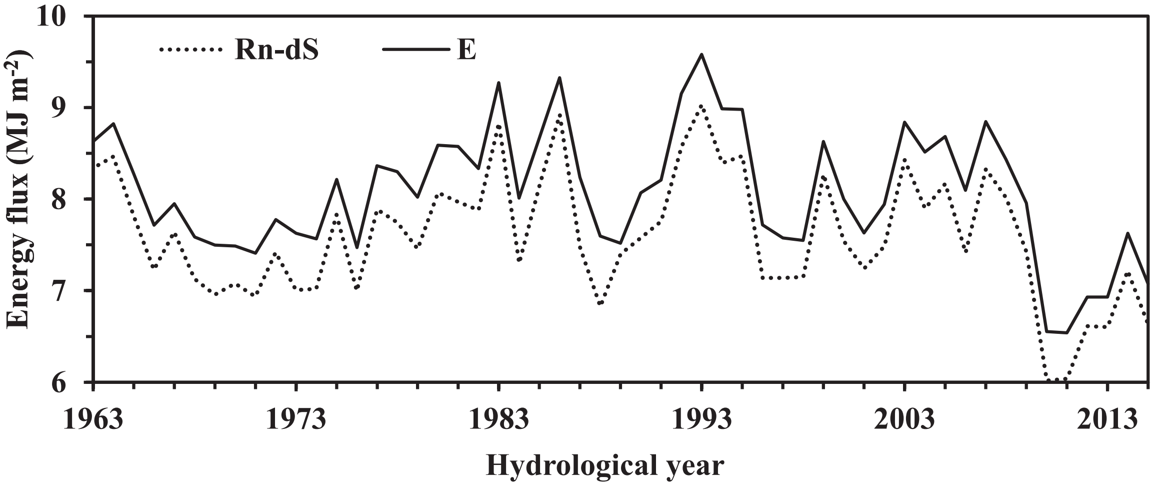

Fig. 4.7 Annual evaporation E (MJ m^{-2}) (solid curve) and the available daily energy density $R_{net} - S$ (dotted curve) modelled using the DPMETHS model for the full data period (hydrological years 1970/1 to 2013/4)

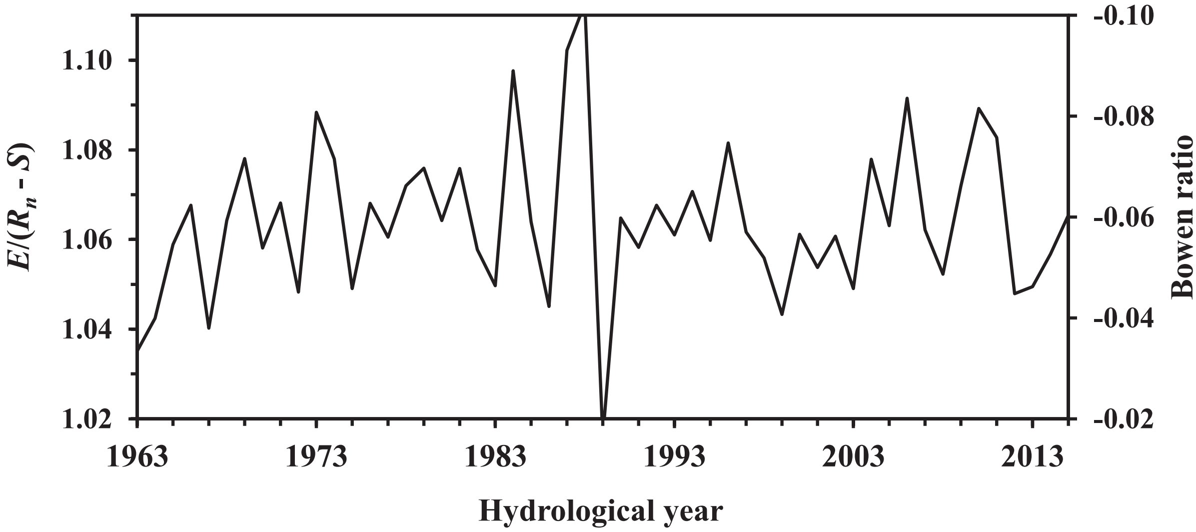

Fig. 4.8 The ratio of latent energy density to the available energy density $LE/(R_{net} - S)$ (left y-axis), the evaporative fraction EF, and the Bowen ratio H/LE (right y-axis) using LE obtained using the DPMETHS model. The curve applies to both axes. The dotted line corresponds to EF = 1 and Bowen ratio = 0

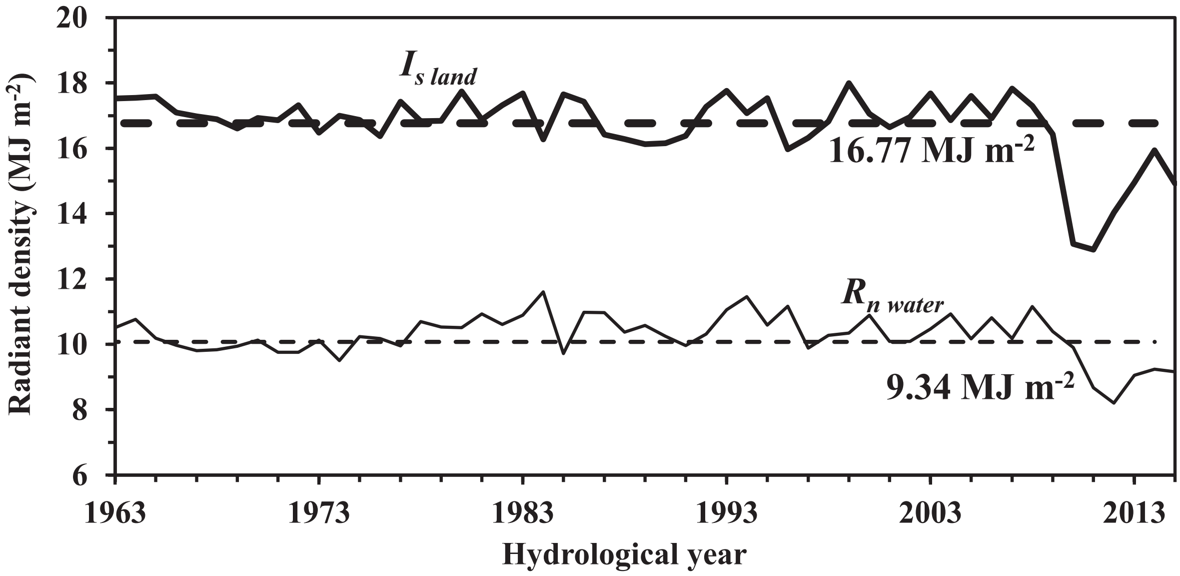

Fig. 4.9 Upper curve: estimated (Hargreaves and Samani) and measured daily solar radiant density (MJ m^{-2}) for hydrological years 1962/3 to 2014/5 and 2008/9 to 2013/4 respectively; lower curve: shows the net radiant density for the water surface for the full data period

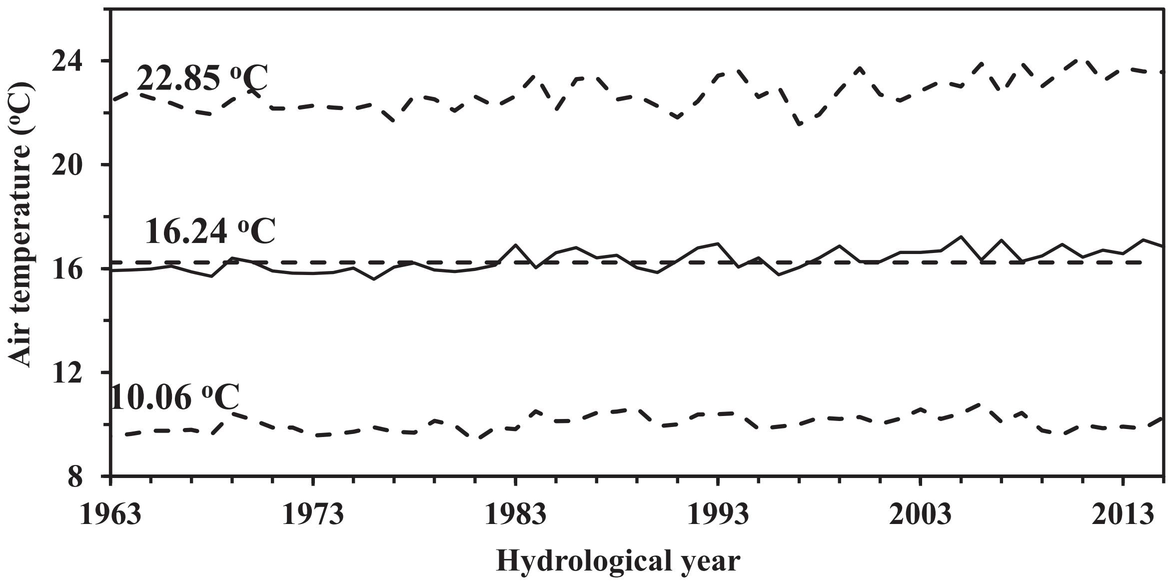

Fig. 4.10 Annual daily average (top) and daily, maximum, average and minimum air temperature (bottom) for the full data period

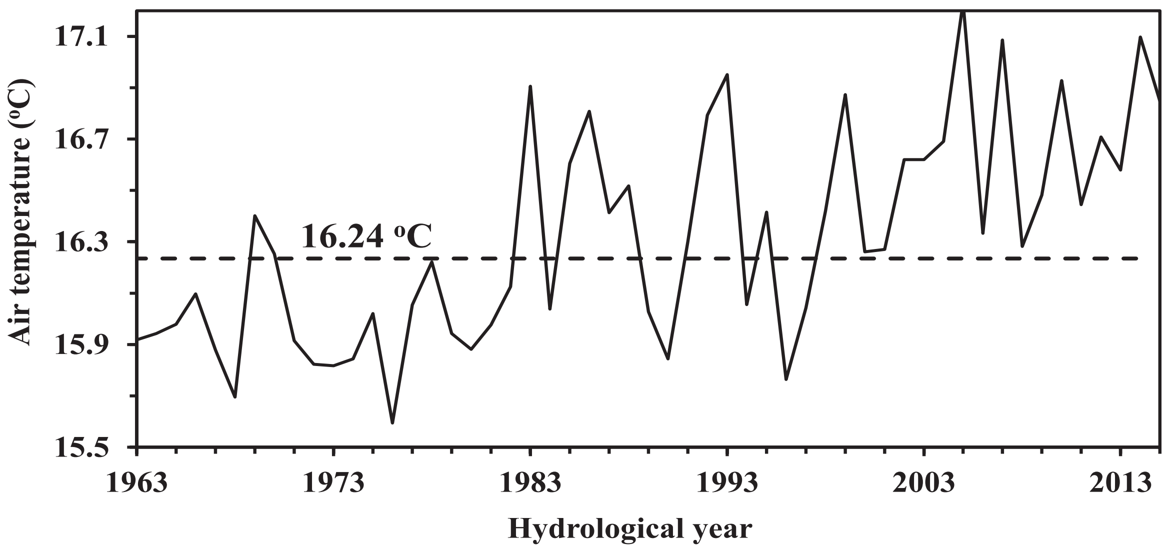

17.1
16.7
16.3
15.9
15.5
Air temperature (oC)
16.24 oC
1963
1973
1983
1993
2003
2013
Hydrological year

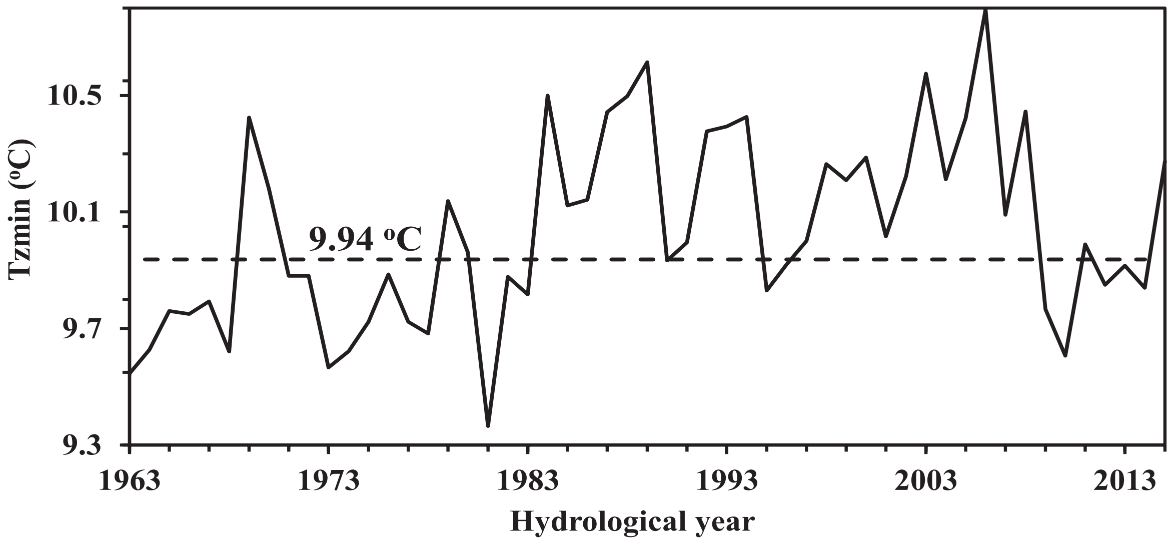

10.5
10.1
9.7
9.3
Tzmin (oC)
9.94 oC
1963
1973
1983
1993
2003
2013
Hydrological year

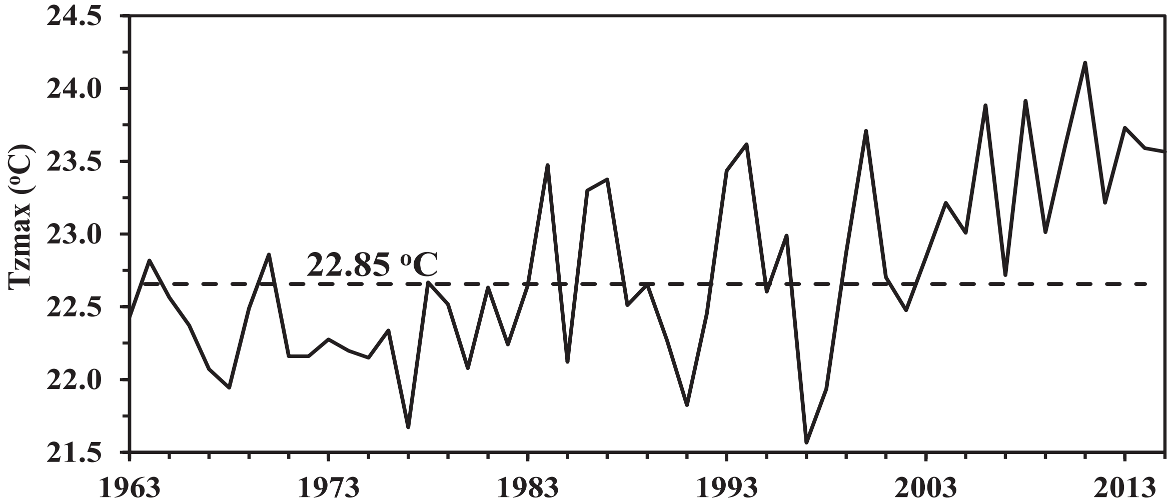

24.5
24.0
23.5
23.0
22.5
22.0
21.5
Tzmax (oC)
22.85 oC
1963
1973
1983
1993
2003
2013

Fig. 4.11 Annual daily average air temperature (top), minimum (middle) and maximum (bottom) for the full data period

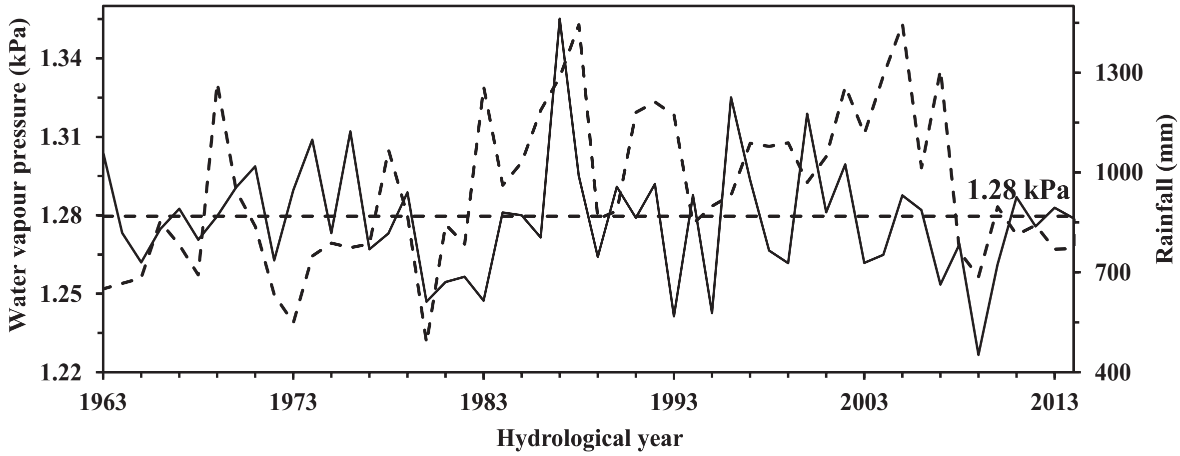

Fig. 4.12 Average daily water vapour pressure, and rainfall (right y-axis) with dashed curve, for the full data period

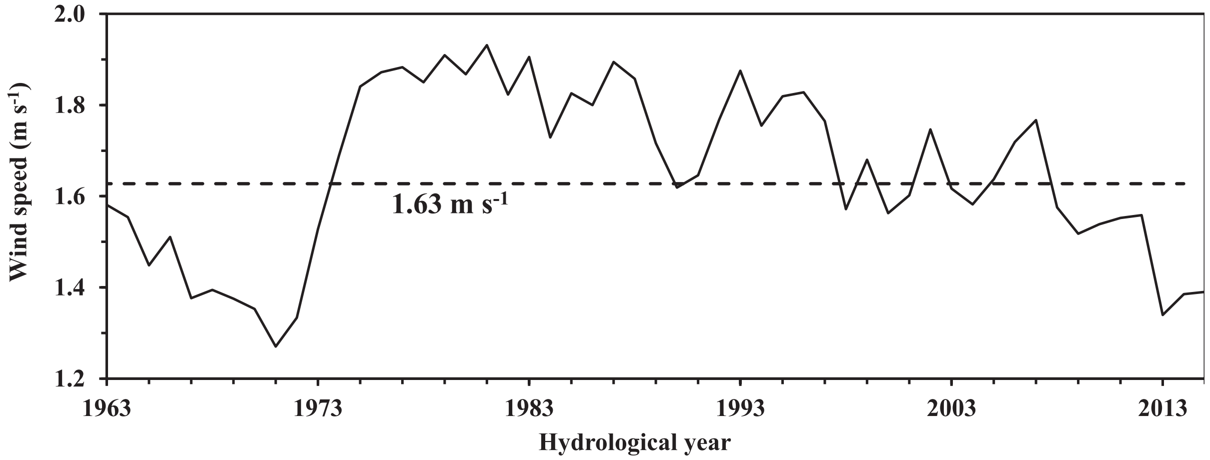

Fig. 4.13 Annual average daily wind speed at 2 m for the full data period

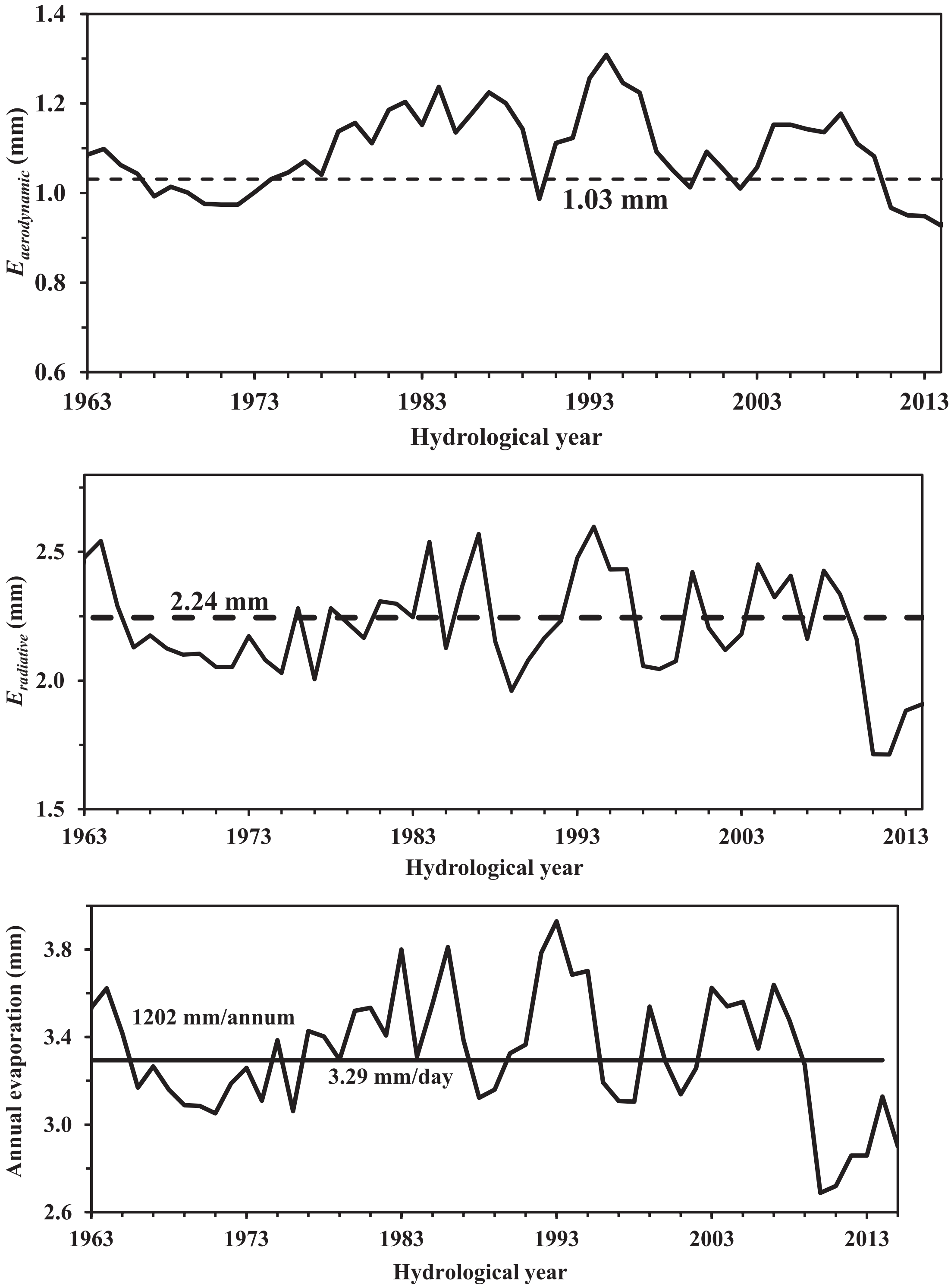

Fig. 4.14 The aerodynamic (top), radiative (middle) and total (bottom) annual daily evaporation for the full data period

The proposed mechanisms for the increase in E for the 1970/1 to 1981/2 and 1987/8 to 1992/3 periods, recorded in Table 4.4 in more detail, are as follows:

1. increased annual average wind speed (Fig. 4.15);
2. the increased wind speed results in surface cooling and decreased water-body temperature T_{water_pred};
3. decrease in T_{water_pred} reduces the infrared irradiance $L_{u\ at\ Twater\_pred}$ from the water surface to the atmosphere;
4. reduced $L_{u\ at\ Twater\_pred}$ in turn results in increased $R_{n\,water} - dS$ where:

$$R_{n\,water} - dS = I_{s\_land} \times (1 - r) + L_{d\ land} - L_{u\ T\ water\ pred} - dS \tag{4.5}$$

5. the increased wind speed also results in an increase in r_a and hence an increase in $E_{aerodynamic} \propto 1/r_a$;
6. an increased wind speed also increases $E_{aerodynamic}$: a decrease in $L_{u\ at\ Twater\_pred}$ results in an increase in $R_{n\,water} - dS$;
7. the increase in $R_{n\,water} - dS$ increased $E_{radiative}$;
8. increases in $E_{aerodynamic}$ and $E_{radiative}$ increase E.

In summary, an increased wind speed results in increases in $E_{aerodynamic}$ and indirectly increases $E_{radiative}$. And the influence is significant since the open water evaporation is the sum of the two terms:

$$E = (\Delta_{T\,water} * (R_{n\,water} - dS) + 86400 \times \rho_{air_{land}} \times c_p \times (e_{s\,Twater} - e_{air_{land}})/r_a)/(\Delta_{T\,water} + \gamma) \tag{4.6}$$

Jung et al. (2010) investigated evapotranspiration variations over the same time period using an ensemble of process-based land-surface models. They used a data-driven estimate of global land evapotranspiration from 1982 to 2008, enabling a compilation using a global monitoring network, meteorological and remote sensing observations, and a machine learning algorithm.

Table 4.4 Record of the various mechanisms for the significantly increased open water evaporation for the period 1970/1 to 1982/3 and 1987/8 to 1992/3

Term	Event/result	Change	Cause	Comment
$U_{land\ 2\ m}$ (r_a)	Increase (and decrease in r_a) between 1987/8 to 1992/3	1.27 to 1.93 m s^{-1} (52%) for 1971/2 to 1980/1 and 1.63 to 1.87 m s^{-1} for 1989/90 to 1992/3	Unknown	
$E_{aerodynamic}$	Increase between 1987/8 to 1992/3	0.86 to 1.29 mm (50%)	Wind speed	Due to increase in $U_{land\ 2\ m}$
I_{s_land}	Relatively constant between 1987/8 and 1990/1 with increase between 1990/1 and 1992/3	Increase from 16.06 to 18.02 MJ m^{-2} (12 %)	3.11 (upper curve)	
$R_{n\ water} - dS$ $R_{n\ water}$	Gradual increase between 1970/1 and 1982/3 and increase between 1987/8 and 1992/3	Gradual increase between 1970/1 and 1982/3 from 7.41 to 9.27 MJ m^{-2}; increase between 1987/8 and 1992/3 from 9.06 to 11.79 MJ m^{-2} (50%)	3.9 (bottom) and 3.11 (lower curve)	
$E_{radiative}$	Increase between 1987/8 and 1992/3	Increase from 2.31 to 3.23 mm (40%)	3.16 middle	Due to increase in $R_{n\ water} - dS$ for 1987/8 to 1992/3
E	Gradual increase between 1970/1 and 1982/3; increase between 1987/8 and 1992/3	Gradual increase between 1970/1 and 1982/3 of 3.05 to 3.8 mm (25 %); increase from 3.12 to 3.93 mm (27%)	3.8 top (mm)	Due to increases in $E_{radiative}$ and $E_{aerodynamic}$ respectively

Jung et al. argued that global annual actual evaporation increased, on average by 7.1 mm annum^{-1} decade^{-1}, between 1982 and 1997 following which the increase ceased. Based on microwave satellite observations, they suggested that the increase was due mainly to reduced soil water in the southern hemisphere, particularly Africa and Australia. They maintained that cessation was coincident with the last major El Niño event in 1998, and that the global evaporation increase appears to have ceased until 2008. The increases shown in Fig. 4.8 (top) are much larger than the increases postulated by Jung et al. (2010).

4.7 Why the sudden decrease and slight increase in annual average daily evaporation for open water between 2008/9 and 2013/4?

Between 2008/9 and 2011/12, there was a 28% reduction in annual daily solar radiant density (Fig. 4.11) followed by a gradual increase after 2010/11, with a gradual reduction in wind speed post 2008/9 (Fig. 4.15). This decreased the evaporation of open water, and its radiative and aerodynamic components, by 25% (2011/12) (Fig. 4.16), following which *E* increased slightly.

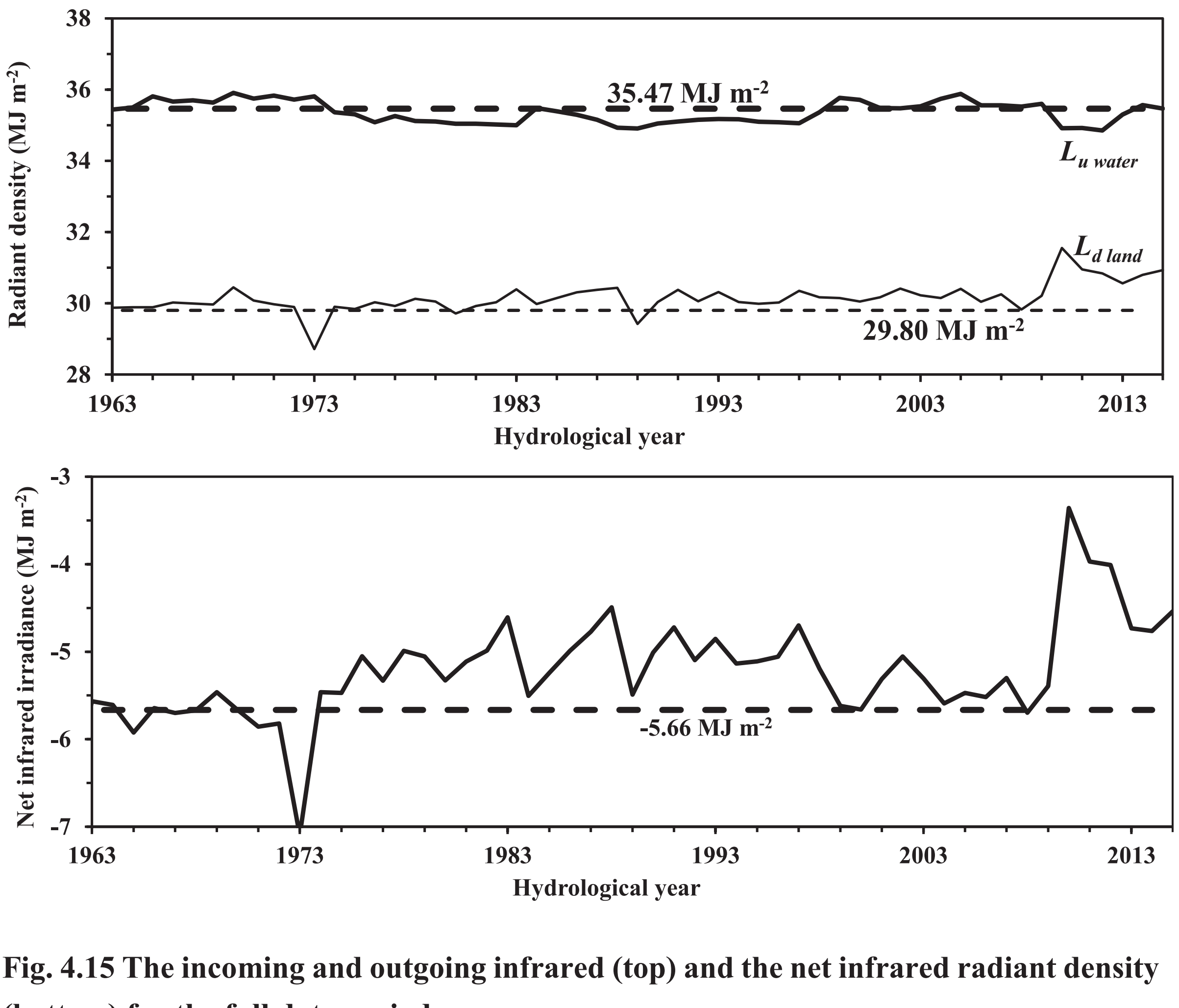

Fig. 4.15 The incoming and outgoing infrared (top) and the net infrared radiant density (bottom) for the full data period

4.8 Global climate considerations

The Southern Oscillation Index (SOI) is a representation of El Niño and La Niña events in the south equatorial Pacific. The SOI is related to standardised pressure anomaly differences between Tahiti (eastern Pacific) and Darwin (western Pacific). Negative SOI values correspond to El Niño conditions with positive values corresponding to La Niña. The procedures for determining SOI values are summarised in Appendix 3. These procedures were applied in a spreadsheet using monthly sea level atmospheric pressure data for Tahiti and Darwin supplied by the United States National Weather Service Climate Prediction Centre (http://www.cpc.ncep.noaa.gov/data/indices/. Monthly SOI was calculated for 1st October 1913 to 31st September 2015. The monthly values were averaged for each hydrological year for the period 1914 to 2015.

The linear correlation between DPMETHS annual evaporation for Midmar Dam and the SOI for the 52-year period was not significant (slope = -0.221 mm per SOI unit; intercept = 3.29 mm, R^2 = 0.223, n = 81) and is not reported here. Repeating the correlation but advancing evaporation by one year, decreased R^2 to 0.179. The relative temporal variation in annual evaporation and the SOI is, however, very revealing (Fig. 3.18). Generally, years with very low annual evaporation, for example 2011, correspond to La Niña conditions (positive SOI) or at least within a year. Similarly, years with very high annual evaporation usually correspond to La Niña conditions (positive SOI), for example 1993.

The year 1992 coincided with a SOI of -1.18 – corresponding to an El Niño – and an annual daily average evaporation of 4.08 mm.

The years 1988 to 2010 coincided with high evaporation – above the long-term average – and generally negative SOI values, corresponding to El Niño conditions.

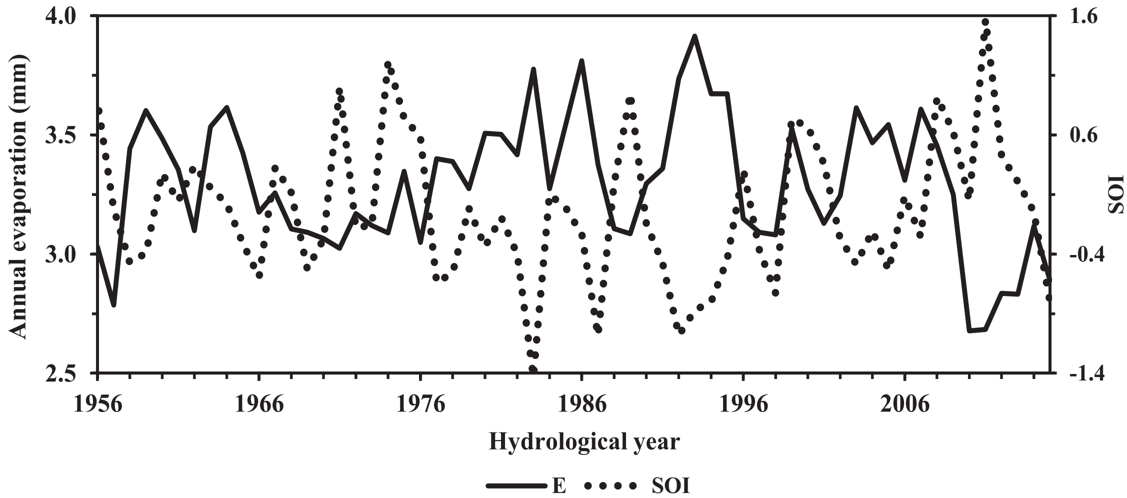

Fig. 4.16 The 60-year annual variation in annual daily average DPMETHS evaporation (solid curve, left hand y-axis, mm day^{-1}) and the Southern Oscillation Index (SOI) (dotted curve, right hand y-axis)

4.9 Symon's pan and DPMETHS evaporation comparisons

A comparison of two independent methods for measuring evaporation (Symon's pan and DPMETHS), for hydrological years 1962/3 to 2006/7 is shown in Fig. 4.17. Both methods show a large increase in evaporation for almost the same period – 1987 to 1993 with a gradual decline for 1993 to 2006. The in-phase correspondence between the two methods is pleasing but the actual correspondence is poor. The wind speed at the surface of the Symon's pan is different from that used in the DPMETHS model and this is a likely cause of the differences.

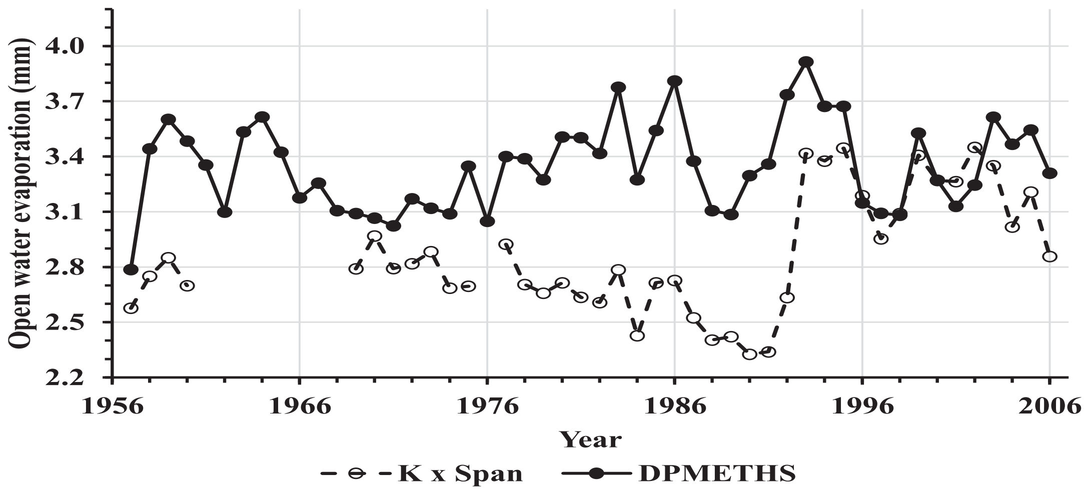

Fig. 4.17 Annual average daily evaporation for 1962/6 to 2006/7 for the Symon's pan and DPMETHS methods

CHAPTER 5: OPEN WATER EVAPORATION AT A SUB-DAILY TIME SCALE

5.1 Summary

Using a sensitivity analysis, an investigation was conducted to determine the sensitivity of the MOST equation, used for determining the latent energy flux LE, to input measurements. The measurements included air temperature T_z at 2 m, water-surface temperature T_o and specific humidity q_z at 2 m. Measurement errors all impacted on LE but in different ways. The measurement error that had the greatest impact was an error in T_o with an error in LE of about 12.9% for each 1°C measurement error. For air temperature, the error in LE was about -3.7% $^{o}C^{-1}$ and for specific humidity, the error in LE was about -0.54% for a 1% error in q_z. Using the manufacturer's stated instrument accuracies, the error in LE was 2.6% due to a 0.2°C error in T_o, -0.4% due to a 0.1°C error in T_z and about -0.5% due to an error of less than 1% in q_z. Measurement error in T_o can be minimised by frequent field checking of measurements using an independent instrument. The error in sensible heat flux H was reduced due to errors in T_o and T_z having the tendency to cancel.

The MOST, EC and SR methods for estimating open water evaporation are compared. The SR method depends on the energy balance, estimates of water-stored heat flux and SR estimates of H_{SR} for calculation of LE_{SR}. These estimates were variable and did not compare well with either MOST or EC estimates. The quality assurance protocols followed for data rejection resulted in an EC rejection rate of about 59% for daytime hours and 69% for nighttime. It was therefore not possible to obtain reliable estimates of daily LE using the EC method. At times, there was very good comparison between the EC and MOST methods for estimating LE (R^2 of 0.64 and a slope of 0.89 for LE_MOST (y) and LE_EC (x) for 30-min quality-assured data for the period 12th February to 24th March 2016). The MOST method yielded the most consistent estimates of H and LE and allowed the half-hourly estimates to be scaled to a daily timescale and compared with the DPMETHS estimates for the period 14th February to 25th May 2016. Daily Penman-Monteith open water estimates were within 9.2% of MOST evaporation measurements with the former lower.

Correction to the water surface temperature T_o for water-surface emissivity and reflected backward infrared irradiance resulted in a consistent bias of 0.037°C. This increase resulted in an increase of all LE_MOST estimates by 1.72 %. Applying this correction allowed MOST to be used without the need for measurement of the background infrared irradiance and resulted in DPMETHS and MOST estimates of daily evaporation agreeing to within 10.7 %. The

DPMETHS daily estimate of evaporation for the period 14th February (day of year 44) to 25th May 2016 (day 145) was 2.88 mm compared to 3.26 mm for the corrected MOST method.

MOST estimates of evaporation using land-based wind speed measurements resulted in poor agreement with previous estimates obtained using the above-water wind speed. The nighttime MOST evaporation represented 43.5 % of the total (24-hour) evaporation over the 101 days of the measurement study with the daytime evaporation therefore representing 56.4 %. The influencing factor or driving force for this significant amount of evaporation during the nighttime appeared to be wind speed – the total cumulated nighttime hours wind run was 41.7 % of the total wind run and 58.3 % for the daytime.

The dominant term of the energy balance, the evaporative flux, using the MOST method, was 86 % of the available energy flux. Sensible heat flux was the smallest component of the energy balance, slightly less than the estimated water-stored heat flux, and about 12 % of net irradiance.

The radiometric BR compared reasonably favourably with that obtained using MOSR estimates of H and LE. The combination BR radiometric and SR method for estimating LE, based on H_{SR}, was in poor agreement with MOST estimates of LE. The H_{SR} were variable and small in magnitude, seldom agreeing with H_{MOST}.

5.2 Introduction

Sub-daily measurements of open water evaporation are rare and difficult. An apparent advantage of some of them – such as MOST and EC – is that they allow estimates of H and LE independent of the energy balance. The advantage of this is that these methodologies are therefore not reliant on the usually unreliable estimates of the water-stored heat flux. By contrast, the SR method allows sub-daily estimates of LE but only by use of the energy balance. These three methods are above-water measurements which results in a whole range of challenges. These methods attempt to more closely represent the evaporative conditions of the water surface. All three methods have very different underpinning theoretical development and assumptions and are to some extent independent methods. They also have very different cost, ranging from relatively inexpensive (SR) to intermediate (MOST) to expensive (EC). All three methods are technically complex. It is hoped that the level of complexity can be reduced to routine through a set of well-defined protocols.

The results of these three above-water methods are presented: MOST, EC and SR. Also, MOST 30-min measurements, scaled to a daily timescale, are compared with those for the

DEPMETHS model. The aim is to arrive at a sub-daily methodology that can be used to obtain open water evaporation using standard instrumentation and protocols that can be fairly simply implemented.

5.3 Impact of error in surface temperature, air temperature and water vapour pressure measurements on MOST estimates of sensible heat and latent energy fluxes

Four measurements are required for application of MOST for open water: air temperature, water vapour pressure and wind speed at a standard height, and the surface temperature of the water which is measured using an infrared thermometer (Section 3.4.11): air temperature T_z, specific humidity q_z (g g^{-1}), wind speed U_z, (m s^{-1}) and T_o (ºC) (from which q_o is calculated assuming $q_o = q_s(T_o)$, a saturated value. The accuracy of the air temperature measurements is ±0.1°C for temperatures between 10 and 30°C. The manufacturer's stated accuracy for the infrared thermometer, for a target temperature within 20°C of the sensor body temperature, is ±0.2°C (Section 3.5.1). The accuracy in relative humidity is ±0.8% *RH*.

Larger errors than those stated by the manufacturer were used (Figs 5.1, 5.2). For the temperatures (Fig. 5.1), it was assumed for graphical purposes that measurement accuracy ranged between -2.0 and 2.0°C.

For the water-surface temperatures, the error in *LE* was about $\pm$12.9% ºC^{-1} (Fig. 5.1). Using the manufacturer's error of ±0.2°C, the error in *LE* is roughly $\pm$2.6%. Using an error of ±0.5ºC, possibly worst-case, the error in *LE* is roughly $\pm$6.5%.

For air temperature, the error in *LE* was $\mp$-3.7% ºC^{-1} (Fig. 5.1). Using the manufacturer's error of ±0.1°C, the error in *LE* is roughly $\mp$0.4%. Using an accuracy of ±0.5ºC, possibly worst-case, the error in *LE* is roughly $\mp$2%.

The error in surface temperature T_o makes a greater impact on *LE* than the error in air temperature. The error in T_o impacts directly on $q_{s\_T_o}$, the saturation specific humidity at surface temperature T_o at the water surface, through an exponential function. However, the error in T_z impacts on the Obukhov length (Table 3.2) and therefore on the integrated universal function Φ_w in the MOST equation for *LE*:

$$LE = \rho \left(q_{s\_T_o} - q_z\right) 0.40\, u_{*\mathrm{MOST}} L/(\ln {}^{z}/_{z_o} - \Phi_w) \qquad (5.1\ 3.78)$$

An over-/underestimate in T_o would increase/decrease $q_{s\_T_o}$ and there is no other influence other than this. The impact of error in T_z is more difficult to track. For example, an over-

/underestimate in T_z would likely increase/decrease the Obukhov length and therefore increase/decrease Φ_w. However, the error would also impact on the friction velocity $u_{*\mathrm{MOST}}$.

The error in atmospheric specific humidity q_z makes a much smaller impact on *LE* than error in T_o and T_z (Fig. 5.2). For error in specific humidity, the error in *LE* was $\mp 0.54\%$ for a 1% error in q_z. This error would not impact on the determination of sensible heat flux *H*.

The temperature measurement errors are likely to have a reduced impact on sensible heat flux *H*. Since *H* is given by:

$$H = \rho\, c_p(T_o - T_z)\, 0.40\, u_{*\mathrm{MOST}}/(\ln {}^{z}/_{z_o} - \Phi_h), \tag{5.2}$$

the errors in T_o and T_z tend to cancel when determining *H* since *H* is directly proportional to the temperature difference between the surface and the overlying air.

Measurement errors in T_z, T_o and q_z all impact on MOST determination of *LE*. However, the errors are not likely to be significant. The error in the surface temperature T_o has the greatest impact in terms of determining *LE*. For this reason, the infrared thermometer used needs to be frequently checked for correct measurement by using a second instrument for comparison.

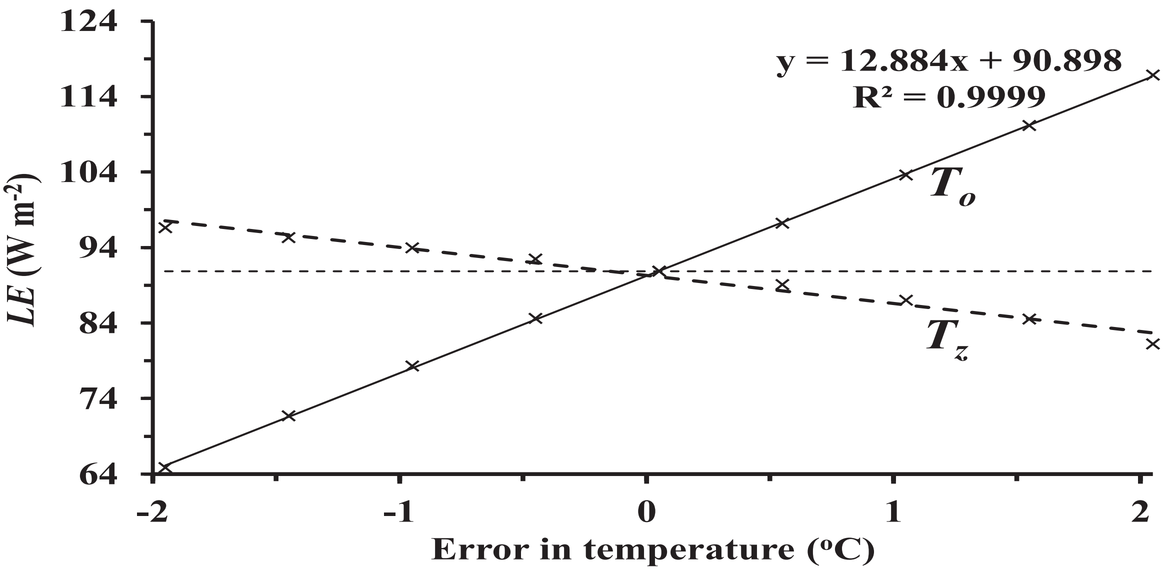

Fig. 5.1 The impact of errors in measured water-surface (T_o) and air (T_z) temperatures on the latent energy flux (*LE*). The horizontal line (dashed) is the MOST-estimated *LE*

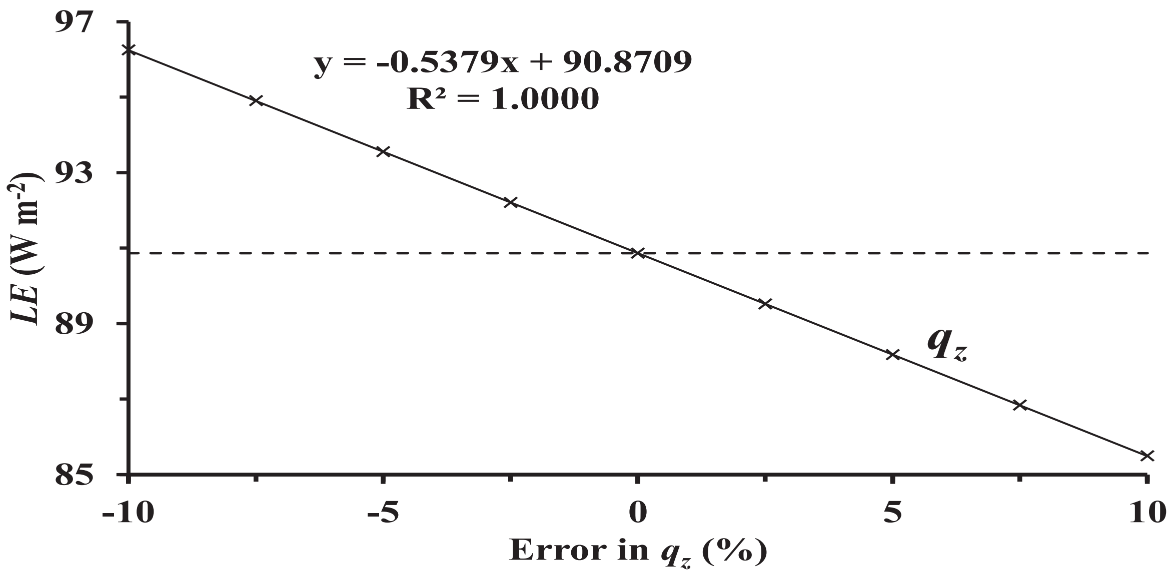

Fig. 5.2 The impact of error in measured specific humidity at 2 m (q_z) on the latent energy flux (*LE*). The horizontal line (dashed) is the MOST-estimated *LE*

5.4 Soil heat flux

The water-stored heat flux for a water depth Δz (m) was estimated using a profile of water temperature measurements using type E thermocouples at depths of 20, 80, 160 and 350 mm. The stored heat flux is determined from the change in internal energy of a mass of water M_{water} (kg) with a density ρ_w (kg m^{-3}), the average temporal change in the water temperature $\overline{\Delta T_{water}}$ (ºC) from one time interval to another, typically 30 min, and the specific heat capacity of water c_w (J kg^{-1} K^{-1}) per unit time interval Δt per unit horizontal area A_{water} which in turn is determined using:

$$S = F_{stored} = M_{water}\ \overline{\Delta T_{water}}\ c_w\ /(\Delta t\ \times A_{water}) \tag{2.4}$$

where $$M_{water}\ /\ A_{water}\ = \rho_w\ V_{water}\ /\ A_{water} =\ \rho_w\ \Delta z. \tag{2.5}$$

Hence $$S = \rho_w\ \Delta z\ \overline{\Delta T_{water}}\ c_p\ /\ \Delta t. \tag{2.6}$$

Using the convention that $R_{net} = LE + H + S$, then:

$$\Delta T_{water\ depth\ x} = T_{water\ time\ t+1} - T_{water\ time\ t}, \tag{5.3}$$

which then ensures that ΔT_{water} for a 30-min period was positive during most of the day and negative during most of the night. Hence:

$$\overline{\Delta T_{water}} = (\Delta T_{water\ depth\ z} + \Delta T_{water\ depth\ \Delta z})/2). \qquad (5.4)$$

Values of *S* were determined for each water layer and then summed for all layers to determine the total water-stored flux for each 30-min interval. Half-hourly measurements of *S* may show a wide variation between two consecutive time intervals. A running mean of order 3, corresponding to 1.5 h, was used to obtain half-hourly values of *S*. Even with using a running mean, the *S* estimates often showed very wide variation and were unreliable due to variable temperatures caused by moving water around the thermocouple measurement position. The implication of this variability in *S* has unfortunate consequences for the surface renewal, temperature variance and BR radiometric methods for estimating open water evaporation, all of which depend directly on *S*, for two main reasons. Firstly, the calculation of *LE* using

$$LE = R_{net} - H - S$$

would also be highly variable. Secondly, since *H* is usually a minor component of the shortened energy balance for open water, *LE* depends strongly on R_{net} and the unreliable *S* estimate. As an illustration of this, the temporal variation in R_{net} and the variability in *S*, two components of the available flux, are shown in Fig. 5.3, for two days in 2016. For day 56 of the year, the measurements of *S* track R_{net}, but in the late afternoon a sudden decrease to -415 W m^{-2} cannot be attributed to R_{net}. In the case of day 114, just before midday, there was a large and unexplained decrease to -1113 W m^{-2}. This magnitude of decrease, in spite of a moving average of order 3, would swamp all components of the energy balance and make nonsense of *LE* calculated as a residual of the energy balance. As a result, this report focuses on EC and MOST methods for determining *LE*.

5.5 MOST

MOST estimates of sensible heat (H_{MOST}) and latent energy fluxes (LE_{MOST}) require four measurements together with MOST iterative calculations, implemented in Excel: horizontal wind speed, U_z, at height *z* above the water surface, air temperature, $T_{z,}$, at height *z* above the water surface, specific humidity q_z (g g^{-1}) at height *z* above the water surface and water surface temperature, T_o. Due to the importance of the temperature of the water surface, two infrared thermometers were used. The extent of the variability of the water-surface temperature, based on LANDSAT 8 TIRS (Thermal Infrared Sensor) band 10: 10600 to 11190 nm, is discussed in Appendix 4. The LANDSAT images showed a 1.5 to 2°C variation in water-surface temperature. The impact of this variation on LE_MOST is shown in Fig. 5.1, *viz.* 12.9 W m^{-2} $^{o}C^{-1}$). It is assumed that the specific humidity just above the water surface is the calculated saturation value $q_s(T_o)$ (g g^{-1}). Other inputs include the measurement height and the roughness lengths z_o, z_{oT} and z_{ow} for momentum, sensible heat and latent energy fluxes respectively. Expressions for three roughness lengths were given in Section 3.4.9. Alternatively, Blanc (1983) recommended $z_o = z_{oT} = z_{ow} = 0.2$ mm.

Presentation of the MOST fluxes, in isolation, serves little purpose. The fluxes will therefore be presented together with EC fluxes.

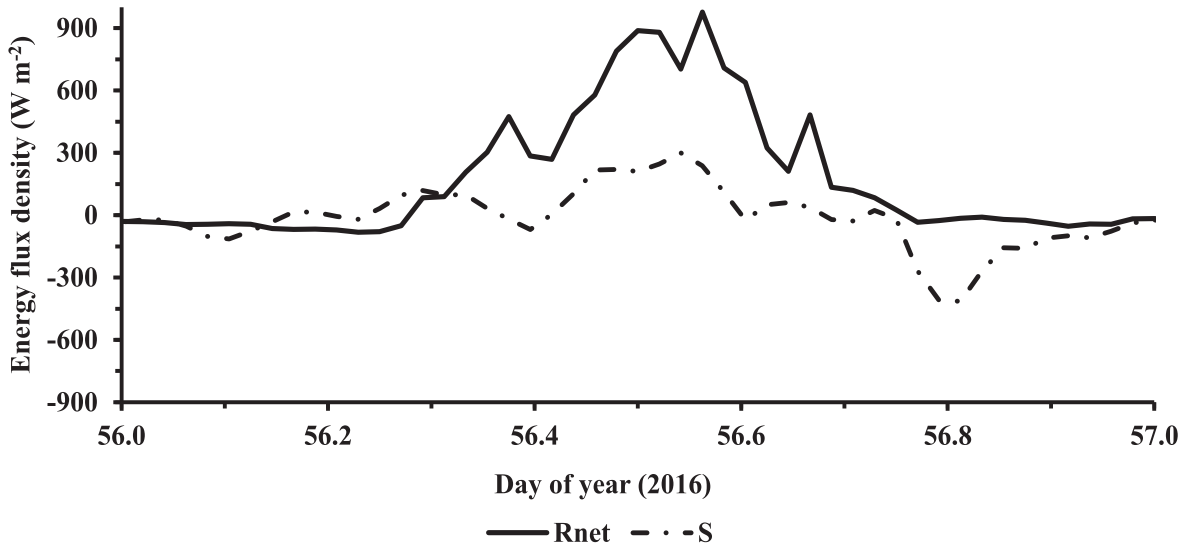

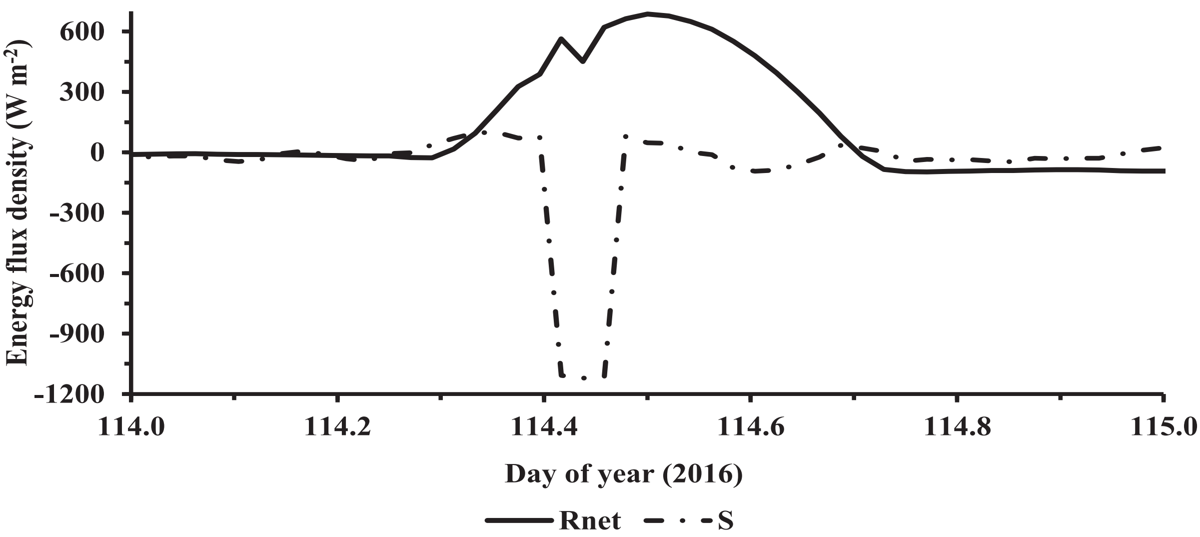

Fig. 5.3 The diurnal variation in the (measured) R_{net} and S components of the available energy flux for the 26th Feb (day 56) and 24th April (day 114) 2016, illustrating the variability in S

5.6 Eddy covariance and comparison with MOST estimates of sensible heat and latent energy fluxes

5.6.1 Eddy covariance quality assurance

Quality assurance protocols were applied to the eddy covariance (EC) fluxes. These protocols, based on Foken et al. (2012), are outlined briefly. The fluxes were checked using three quality assurance tests:

- stationarity (SQA)
- turbulence development (TQA)
- wind flow distortion by the sonic support arms (WQA).

Quality assurance grade 0 was assigned when there were no flux data (datalogger NAN – not a number) for a particular 30-min period. This is usually as a result of mist or rain on the sonic transducer and/or gas analyser windows.

The SQA test for the relative percentage difference involved determining six 5-min fluxes within each 30-min period. If the relative percentage difference between the averaged 5-minute and the 30-minute covariance value was less than 15%, grade 1 is assigned where for *H*, for example,

$$\text{relative percentage difference} = 100 \times \left| \frac{\frac{1}{6}\sum_{i=1}^{6} H_i - H}{H} \right| \quad (5.5)$$

where the H_i and H values are those after coordinate rotation with H_i the 5-min fluxes and H the 30-min flux. If the relative percentage difference was between 15 and 30%, grade 2 was assigned. Grade 9 was assigned if the relative difference was greater than 1000%. Other relative percentage difference ranges result in the assignment of grades 3 to 8 (Table 5.1).

The TQA test compares the behaviour of the measured surface-layer atmospheric turbulence to its expected or modelled behaviour. Turbulence may be characterised in different ways. One way is to use the integral turbulence characteristic (ITC). Normalised standard deviations, such as σ_w/u_* and σ_T/T_* (no units), characterise atmospheric turbulence in the surface layer and are referred to as ITCs where σ_w and σ_T are the standard deviation for the vertical wind speed and sonic temperature respectively and u_* (m s^{-1}) and T_* (K) are the friction velocity and scaling temperature respectively. Since ITC values can be reasonably accurately modelled, the percentage relative difference between the modelled and measured values may be calculated for each 30-min interval. If the relative percentage difference between modelled and measured values was less than 15%, grade 1 was assigned. If the relative percentage difference was between 15 and 30%, grade 2 was assigned. Grade 9 was assigned if the relative difference was greater than 1000%. Other relative percentage difference ranges result in the assignment of grades 3 to 8 (Table 5.1).

The wind flow distortion (WQA) test involves determining the wind directions most favourable for minimising distortion by the 3-D sonic anemometer support arms. For example, if wind directions are 0 to 150° or 210 to 360°, the highest grade, 1, is assigned to the data (Table 5.1). If wind directions are 150 to 170° or 190 to 210°, the second highest grade, 2, is assigned to the data. If wind direction is between 170 and 190°, then the lowest grade is assigned (grade 3). No other grades are assigned.

The overall QA grades for EC fluxes for grades 1 to 5 inclusive, deemed acceptable data, are listed in Table 5.2.

An examination of the EC fluxes, without QA, showed a large amount of spikiness when compared to the corresponding MOST fluxes and EC fluxes for plant canopies. This was unexpected. The major difference between plant canopies and open water is the Bowen ratio. For open water, the BR is close to 0. It may be the influence of the humid environment that causes the spikiness.

5.6.2 Roughness height for MOST fluxes

Two methods were used for calculation of MOST fluxes:

- MOST method 1: fluxes calculated using the expressions for z_o, z_{oT} and z_{ow} given in Section 3.4.9;
- MOST method 2: fluxes calculated assuming that $z_o = z_{oT} = z_{ow} = 0.2$ mm.

To justify the use of $z_o = 0.2$ mm in the MOST iterative calculations, an independent set of data from a previous Water Research Commission project was used (Jarmain et al., 2009;, data from 29th June to 20th July 2007). For this set of data, sensible heat fluxes using the MOST method were estimated, for z_o varying between 5 and 0.00001 mm, and compared with the corresponding EC sensible heat fluxes (Fig. 5.4). The left arrow in Fig. 5.4 corresponds to z_o =

0.2 mm and the right arrow to 0.3 mm. This result therefore justifies the choice of z_o = 0.2 mm used routinely in this study and recommended by Blanc (1983).

Table 5.1 Grades of relative non-stationarity (SQA), relative integral turbulence characteristics (TGA), and wind direction in the sonic instrument coordinate system (WQA)

SQA Non-stationarity [model (2.3) in Foken et al. (2012)]		TQA Integral turbulence characteristics [model (2.5) in Foken et al. (2012)]		WQA Wind direction tests	
Grade	**Range (%)**	**Grade**	**Range (%)**	**Grade**	**Range (º)**
0 (NAN data)					
1 (best)	$\geq 0; < 15$	1 (best)	$\geq 0; < 15$	1 (best)	$\geq 0; \leq 150$ and $\geq 210; \leq 360$
2	$\geq 15; < 30$	2	$\geq 15; < 30$	2	$\geq 150, \leq 170$ and $\geq 190, \leq 210$
3	$\geq 30; < 50$	3	$\geq 30; < 50$	3	$\geq 170, \leq 190$
4	$\geq 50; < 75$	4	$\geq 50; < 75$		
5	$\geq 75; < 100$	5	$\geq 75; < 100$		
6	$\geq 100; < 250$	6	$\geq 100; < 250$		
7	$\geq 250; < 500$	7	$\geq 250; < 500$		
8	$\geq 500; < 1000$	8	$\geq 500; < 1000$		
9 (worst)	≥ 1000	9 (worst)	≥ 1000		

Table 5.2 Overall QA grades 1 to 5 inclusive (deemed acceptable) for EC fluxes for relative non-stationarity, relative integral turbulence characteristic and 3-D sonic wind direction (Table 4.5 of Foken et al. (2012))

Overall quality grade	**SQA Relative non-stationarity**	**TQA Relative ITC (maximum of that for *H* and *LE*)**	**WQA Wind direction test**
1 (best)	1	1-2	1
2	2	1-2	1
3	1-2	3-4	1
4	3-4	1-2	1
5 (worst of the grades deemed acceptable)	1-4	3-5	1

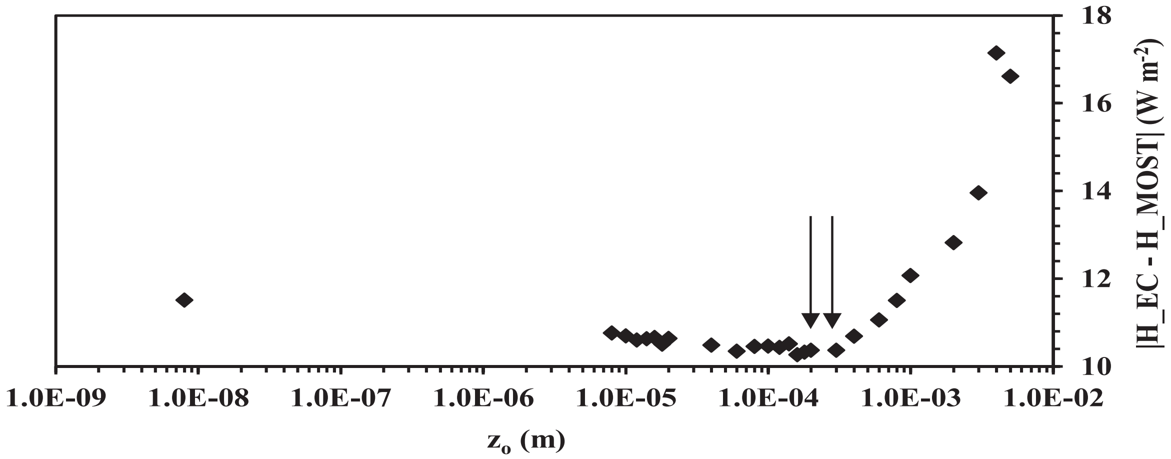

Fig. 5.4 The absolute difference in H_{EC} measurements and H_{MOST} calculations for a varying value of $z_o = z_{oT} = z_{ow}$ (log scale) used in the MOST equations

5.6.3 MOST compared to EC (without QA)

Besides the four measurements U_z, T_z, q_z and T_o previously mentioned, the iterative MOST method also depends on measurement height and the roughness length z_o. In the case of MOST, it was noted that MOST latent energy fluxes (LE_MOST) significantly underestimated compared to the EC (LE_EC) measurements (Fig. 5.5). In the case of MOST method 2, for which z_o = 0.2 mm was assumed, there was reasonable to very good agreement between MOST and EC latent energy fluxes (Fig. 5.6).

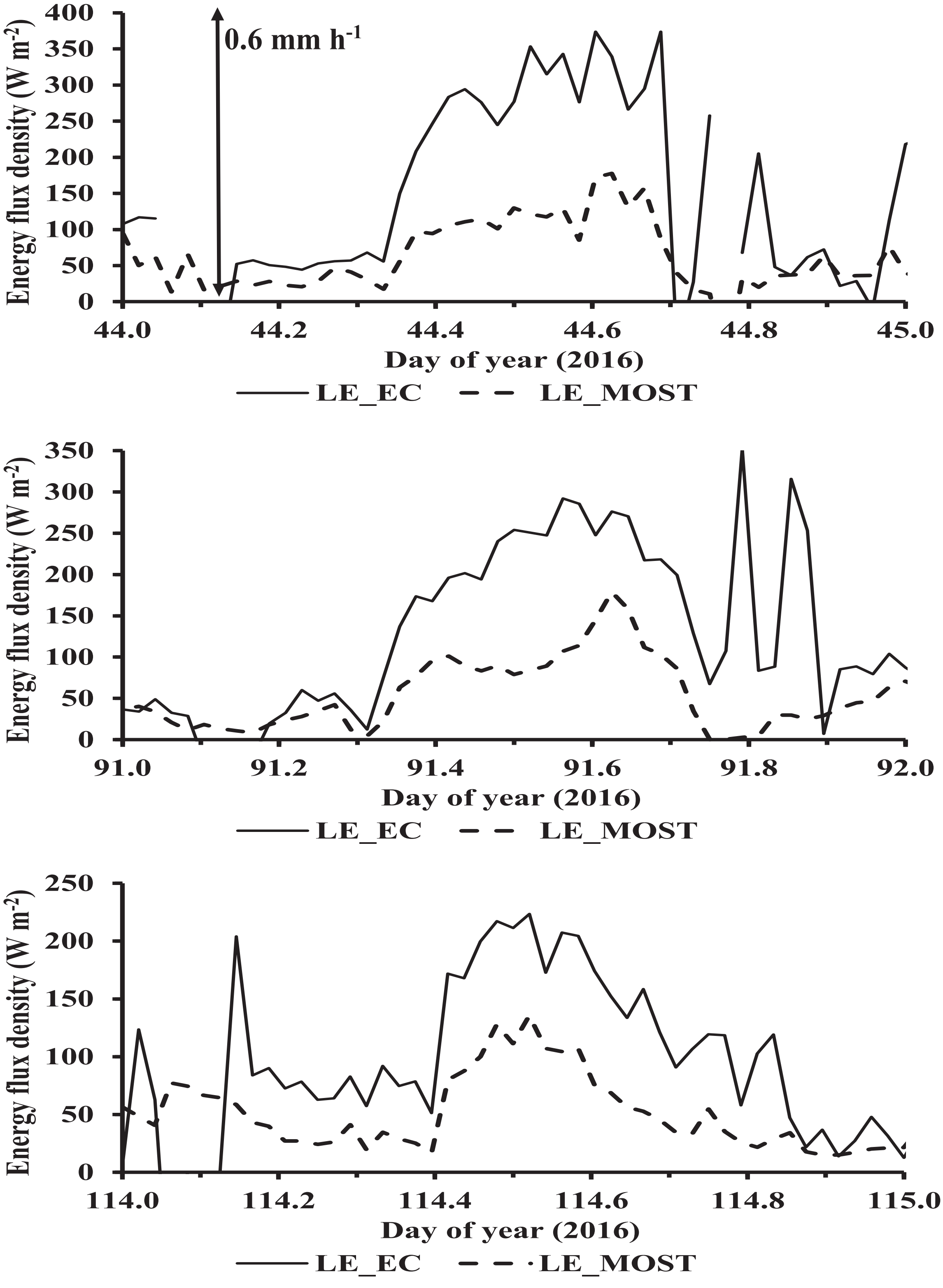

Fig. 5.5 *LE* fluxes for three selected days (day 114, 14th Feb and 1st and 24th April, 2016 – days 91 and 144 respectively) for EC (without QA) and MOST for which expressions for z_o, z_{oT} and z_{ow} are used

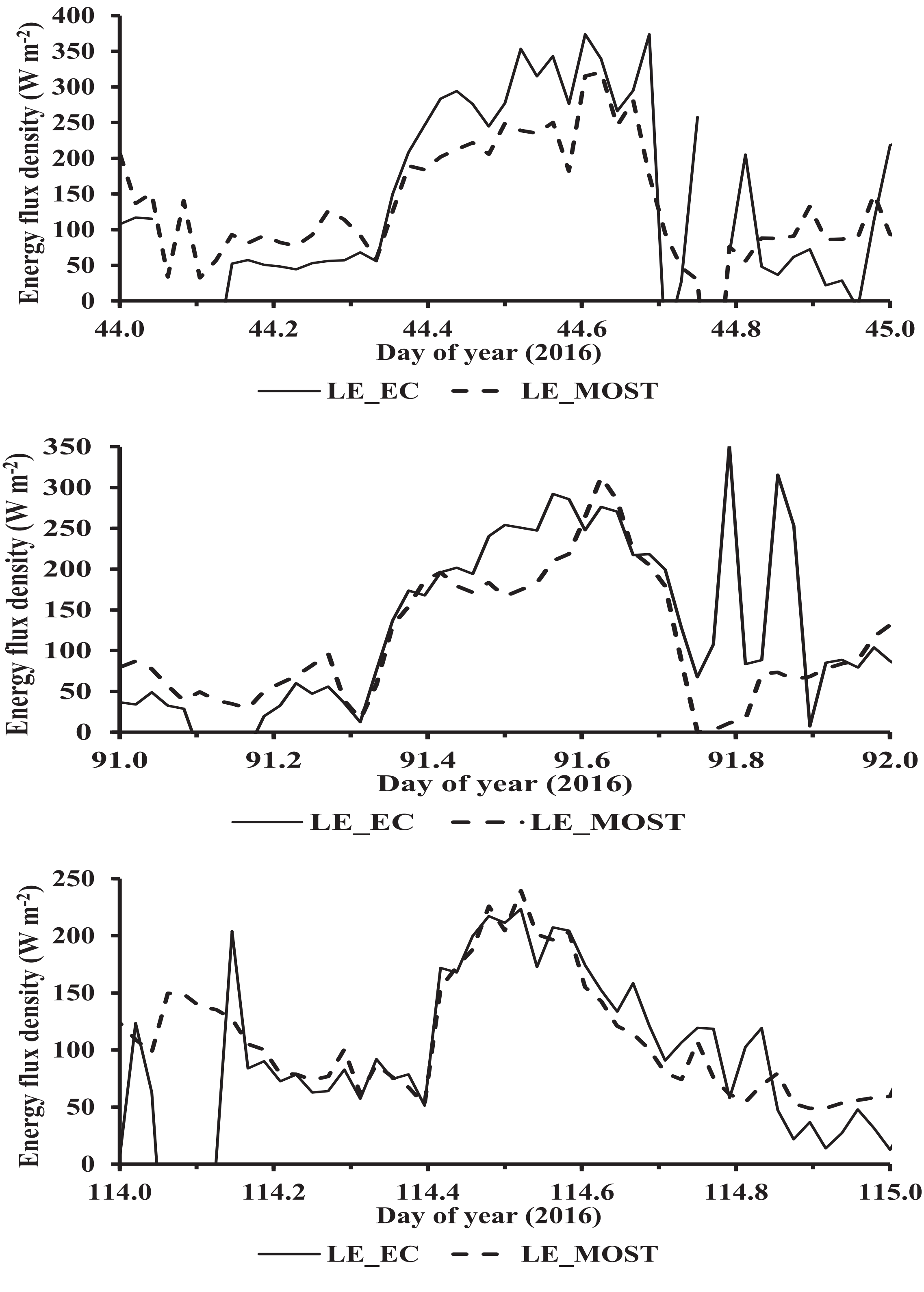

Fig. 5.6 ***LE*** **fluxes for EC (without QA) and MOST (for which z_o = 0.2 mm) for three selected days**

This is a very pleasing result considering the cost, setup complexity and numerous corrections applied to the EC fluxes compared with that for the MOST iterative methodology.

Another feature of the data presented in Fig. 5.6 is that the EC latent energy fluxes, without QA, are much more variable from one 30-min period to another compared to the MOST flux estimates.

These reasonable LE_EC and LE_MOST comparisons (Fig. 5.6), even without applying EC QA, further justifies the use of z_o = 0.2 mm. For the rest of this report, only MOST fluxes for which z_o = 0.2 mm are used.

5.6.4 MOST (z_o = 0.2 mm) and EC flux comparisons

MOST (using z_o = 0.2 mm) and EC fluxes were compared for different ranges in EC QA grades (Fig. 5.7): grades 1 to 3 (19.8% of the total EC dataset), grades 1 to 4 (27.0% of total data), grades 1 to 5 (31.2% of total data). For each category set of grades, slope and R^2 alters.

Based on the regressions of Fig. 5.7, on the diurnal temporal variation of the fluxes, and their comparison with the MOST fluxes, all data that were assigned grades 1 to 5 inclusive (Table 5.3) were accepted and otherwise not used (Fig. 5.8 with no QA and Fig. 5.9 with QA for grades 1 to 5 inclusive). This choice of grades was a compromise between the amount of data loss and data quality (with R^2 = 0.6391, slope = 0.8853).

The temporal comparisons for the EC measurements of LE without QA and LE_MOST were poor due to the spikiness of the LE_EC measurements (Fig. 5.8). Using just the LE_EC_QA data, the comparisons with LE_MOST were reasonable (Fig. 5.9) apart from, for example, days 79 and 80 for which the LE_EC_QA were lower than LE_MOST.

5.6.5 Loss of EC data through QA protocols

The loss of data as a result of the QA procedures was substantial (Table 5.3). Only 40.9% of the daytime EC data was of sufficient quality, as a result of the choice of grades 1 to 5 inclusive, compared to 31.2% for the nighttime. This high loss of LE_EC data meant that daily totals of *ET* for the EC method would not be accurate. This was not the case for the MOST data set which was a lot less spikey. The only QA tests appropriate to the MOST calculations would be for stationarity and wind direction. For most of the 2016 measurement study, this was not possible since an output interval of 30 min was used for all MOST measurements. The SQA test was, however, applied to the 2007 Midmar Dam open water MOST dataset. In that case, 2-min output data were collected.

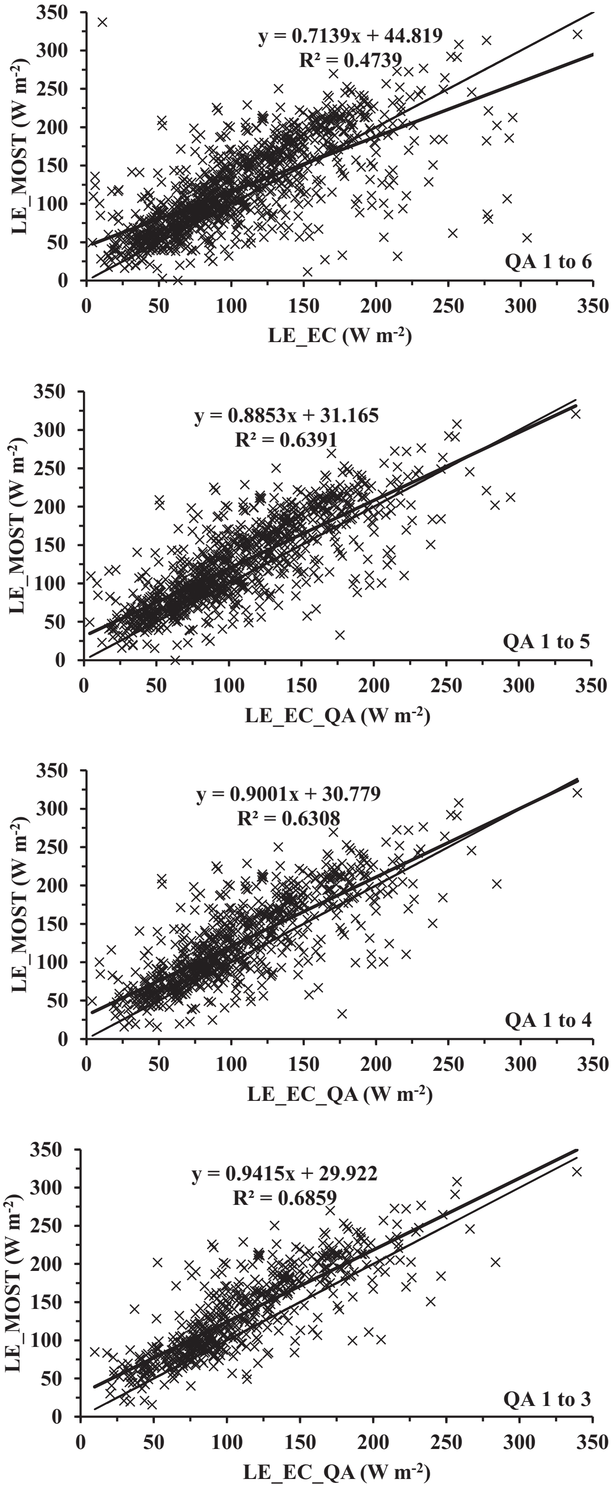

Fig. 5.7 Regression comparisons for the period 12th Feb to 24th April 2016 inclusive, between 30-min *LE* for EC_QA and MOST methods for the various QA grades, for which grades 1 to 5 (second from top) were deemed acceptable EC_QA data

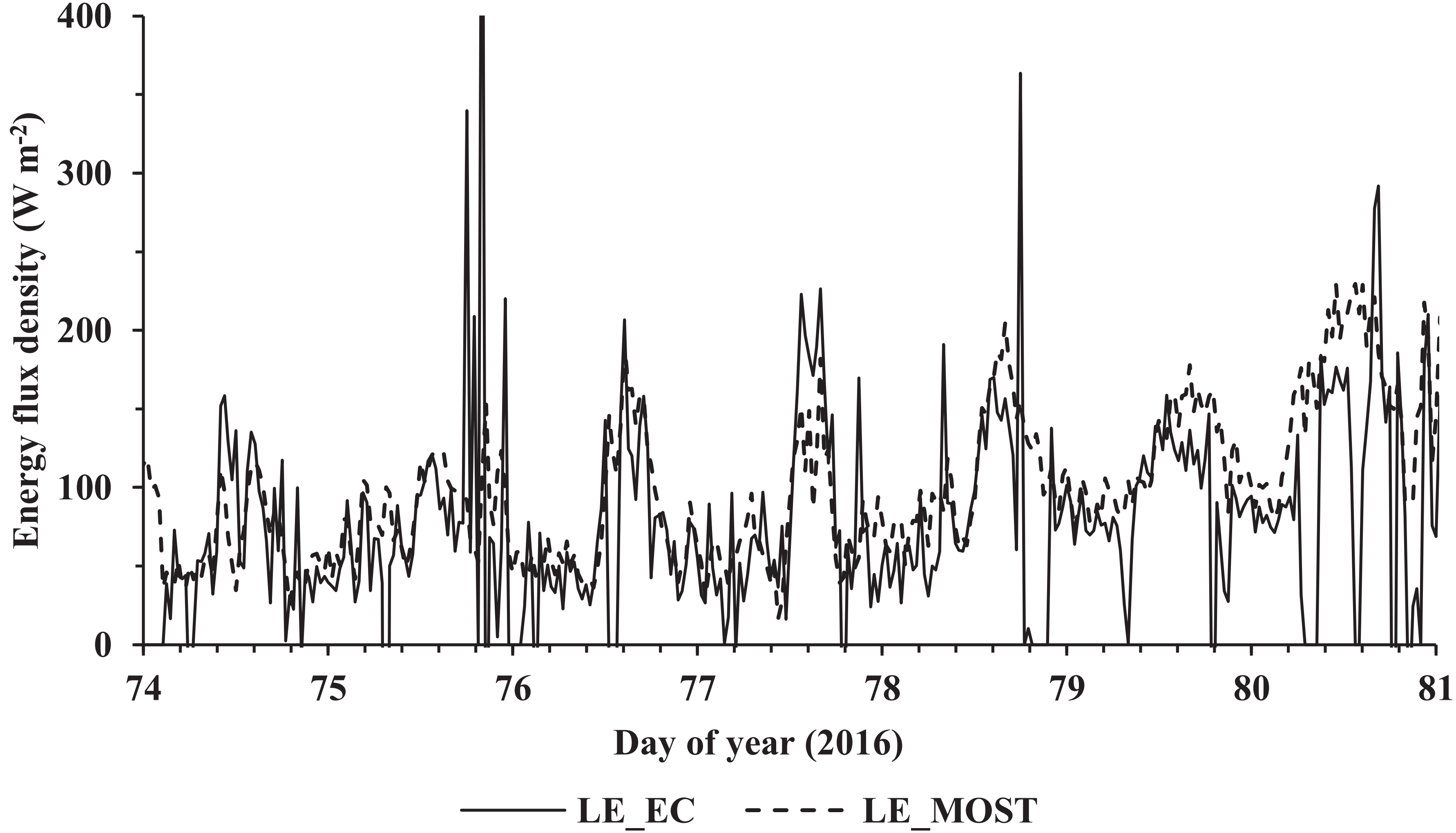

Fig. 5.8 LE_EC (uncorrected) and LE_MOST 30-min measurements for the period 15th March (day of year 74, 2016) to 21st March

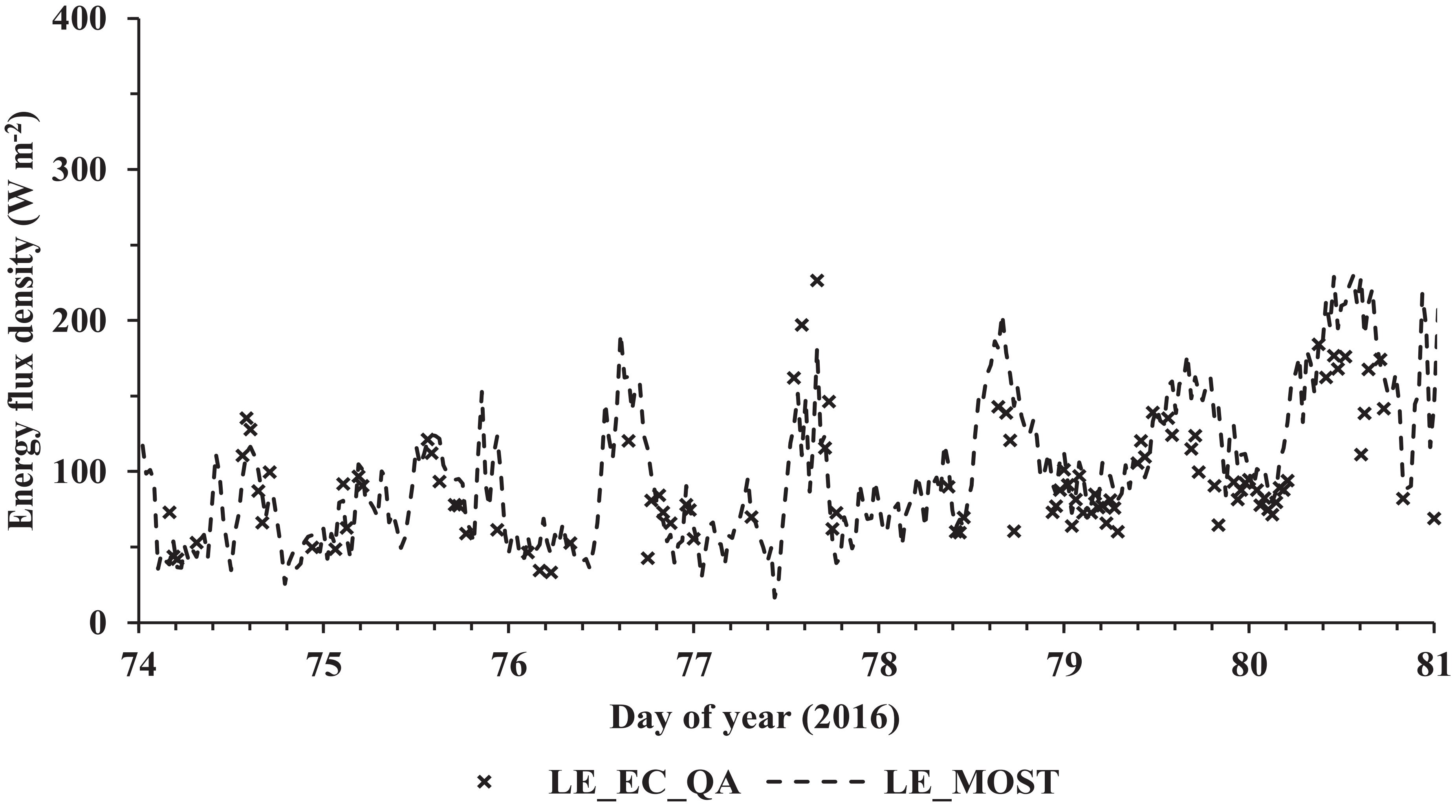

Fig. 5.9 LE_EC (with QA, grades 1 to 5 inclusive) and LE_MOST 30-min measurements for the period 15th March (day of year 74, 2016) to 21st March

The average of 15 LE_MOST 2-min values for a 30-min interval was compared with the *LE* value for the 30-min interval and a grade assigned according to the SQA test of Table 5.1. For the 17-day period, 83% of the 30-min LE_MOST data were assigned grades 1 to 5 inclusive. This bodes well for the future use of MOST applied to open water for routine estimation of LE.

5.6.6 Energy balance closure

Closure of the energy balance was investigated using the EC measurements of *LE* and *H*, with QA, R_{net} and *S*. The shortened energy balance is defined as closed when the closure ratio, given by:

$$CR = (LE + H)/(R_{net} - S) \tag{2.8}$$

equals 1. The closure results were poor (data not shown), probably due to the previously mentioned problems with the *S* estimates and also reported on by Mengistu and Savage (2010).

5.6.7 H and LE comparisons for EC_QA and MOST estimates

The energy balance components for the EC and MOST methods (*H* and *LE*) are shown for two selected days in Fig. 5.10. These comparisons, between EC (with QA) and MOST measurements of *H,* were reasonable whereas comparisons for *LE* were fair (Fig. 5.10). Of note is that for days 57 and 58 for which there is reasonable agreement between H_MOST and H_EC_QA, there is poor agreement between LE_MOST and LE_EC_QA. Also of note are the large *LE* values occurring during nighttime hours for day 57 (27th Feb 2016) – compared to negligible nighttime *LE* values for plant and soil systems. Night periods with high wind speeds, for example, may result in EC (and MOST) *LE* values in excess of 200 W m^{-2} (day of year 57, 2016) – equivalent to more than 0.3 mm h^{-1}.

In the case of plant canopies, changes in net irradiance R_n due to the impact of variable cloud on the solar irradiance, usually result in changes in *LE* and *H*. The diurnal variation in R_n and *LE* (for MOST and EC_QA estimates) for two days, one with high R_n (day of year 78, 2016) and another for a cloudy day (day of year 57) is shown in Fig. 5.11. Of note for both days is that despite fairly large changes in R_n, *LE* (MOST or EC_QA) does not vary significantly during the daytime hours. For day of year 78, the rejection of EC data due to the QA protocols applied is high compared to fairly stable LE_MOST data. For day of year 57, Fig. 5.8, early morning and late afternoon *LE* estimates remained high – for an average wind speed of close to 4 m s^{-1} for both periods. LE_MOST was 17.95 MJ m^{-2} (equivalent to 7.4 mm). Besides a low R_n, this day was also a day with low air temperatures – average of 16.6°C. This demonstrates the impact of wind speed, during the day and the night, on *LE* for open water. The evaporation, estimated using MOST, for this day was the highest of all days in this study.

Table 5.3 Occurrences and percentages of data for the various QA grades for daytime (06h00 to 18h00 inclusive) and nighttime for the period 12th February to 24th April 2016

QA grade	Occurrences	Percentage	Occurrences	Percentage
	Day		Night	
1	13	0.9	4	0.3
2	6	0.4	2	0.2
3	294	21.0	235	19.3
4	130	9.3	87	7.2
5	130	9.3	51	4.2
6	74	5.3	83	6.8
7	441	31.5	399	32.8
8	210	15.0	239	19.7
9	104	7.4	115	9.5
0	93	6.6	165	13.6
Total (excluding flag 0)	1402	100.0	1215	100.0
Flags 1 to 5	573	40.9	379	31.2

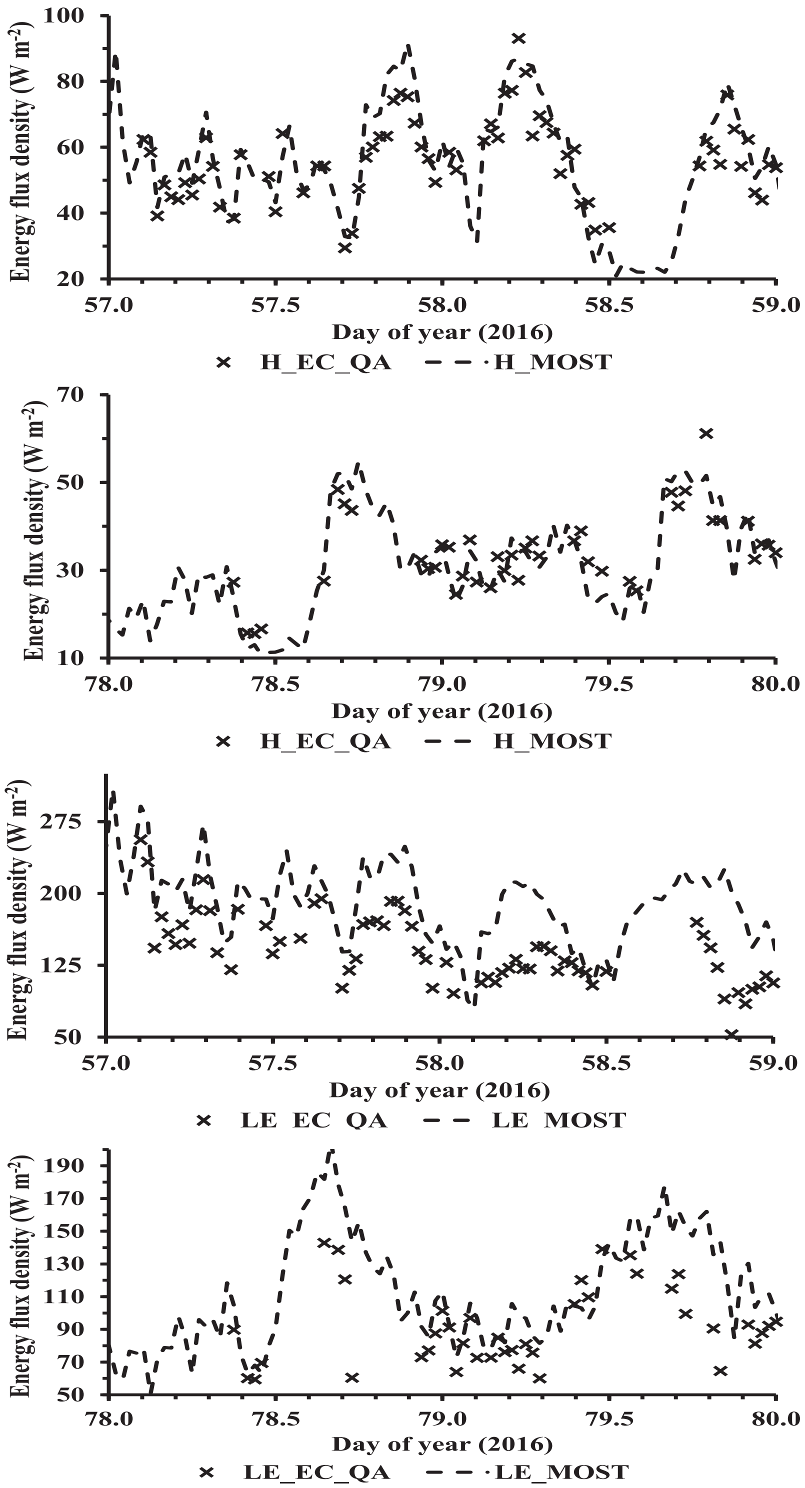

Fig. 5.10 Comparison between 30-min MOST and EC (with QA) fluxes of sensible heat (upper two graphs) and latent energy fluxes (lower two graphs) for two selected two-day periods (27th/28th Feb (days 57 and 58) and 19th/20th March 2016 (days 78 and 79)

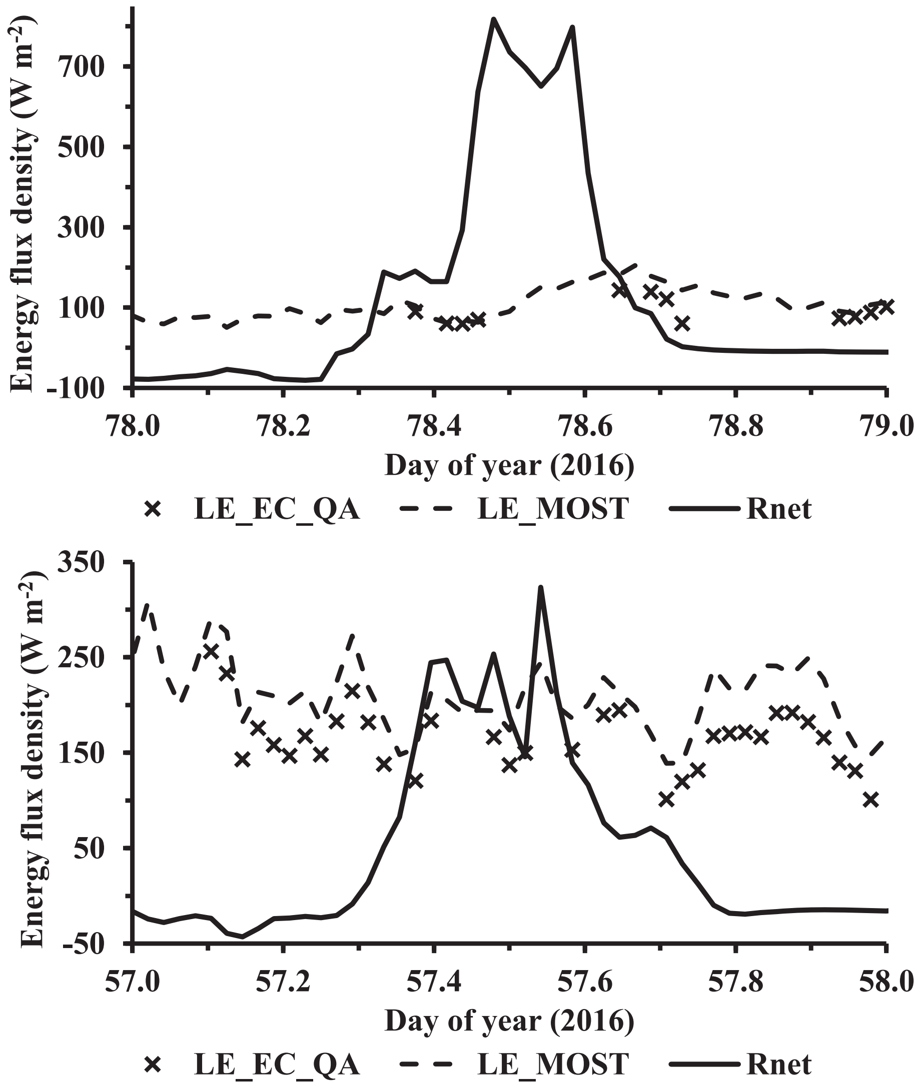

Fig. 5.11 Diurnal variation in 30-min LE for EC_QA and MOST methods for a day (top, 27th Feb, 2016) with low and variable R_n and a day (bottom, 19th March, 2016) with relatively high R_n

5.6.8 Use of land AWS measurements for MOST fluxes

Practically, it would be convenient if the measurement inputs for MOST fluxes were from a land-based AWS instead of a water-based platform. This, however, may not be feasible for the water-surface temperature but could be possible for the measurements of T_z, q_z and U_z. A comparison of H_MOST and LE_MOST determined using water- and land-based 30-min weather data is shown in Fig. 5.12. Without exception, both H_MOST and LE_MOST were greater when the water-based measurements were used. The reasons for these differences were investigated by comparing the various weather elements T_z, e_z and U_z (Fig. 5.13).

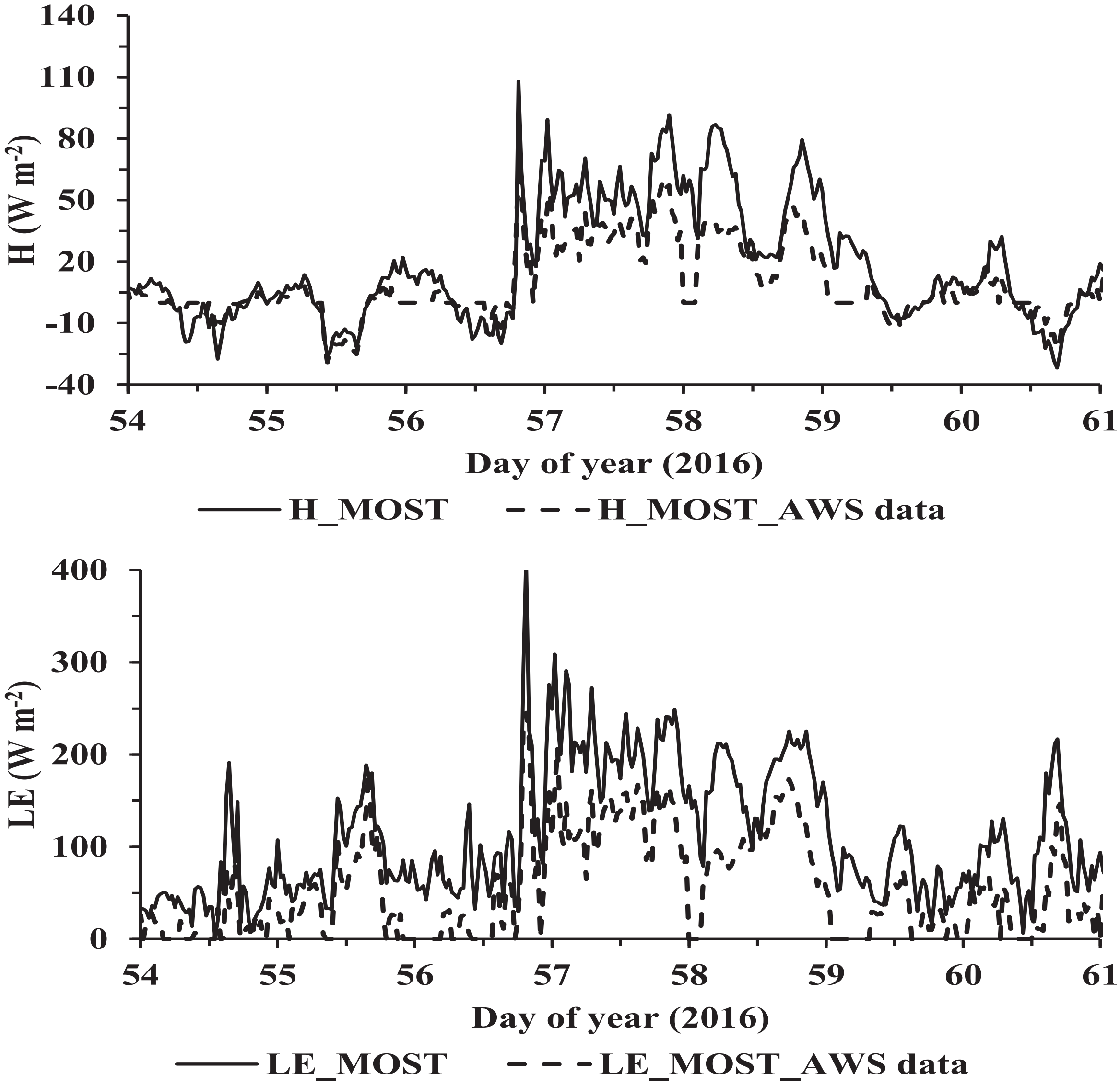

Fig. 5.12 Diurnal variation in 30-min *H* and *LE* for days of year 54 to 61 (24th Feb to 2nd March 2016) for the MOST method using water-based data (H_MOST and LE_MOST) and land-based AWS data (H_MOST_AWS data and LE_MOST_AWS data)

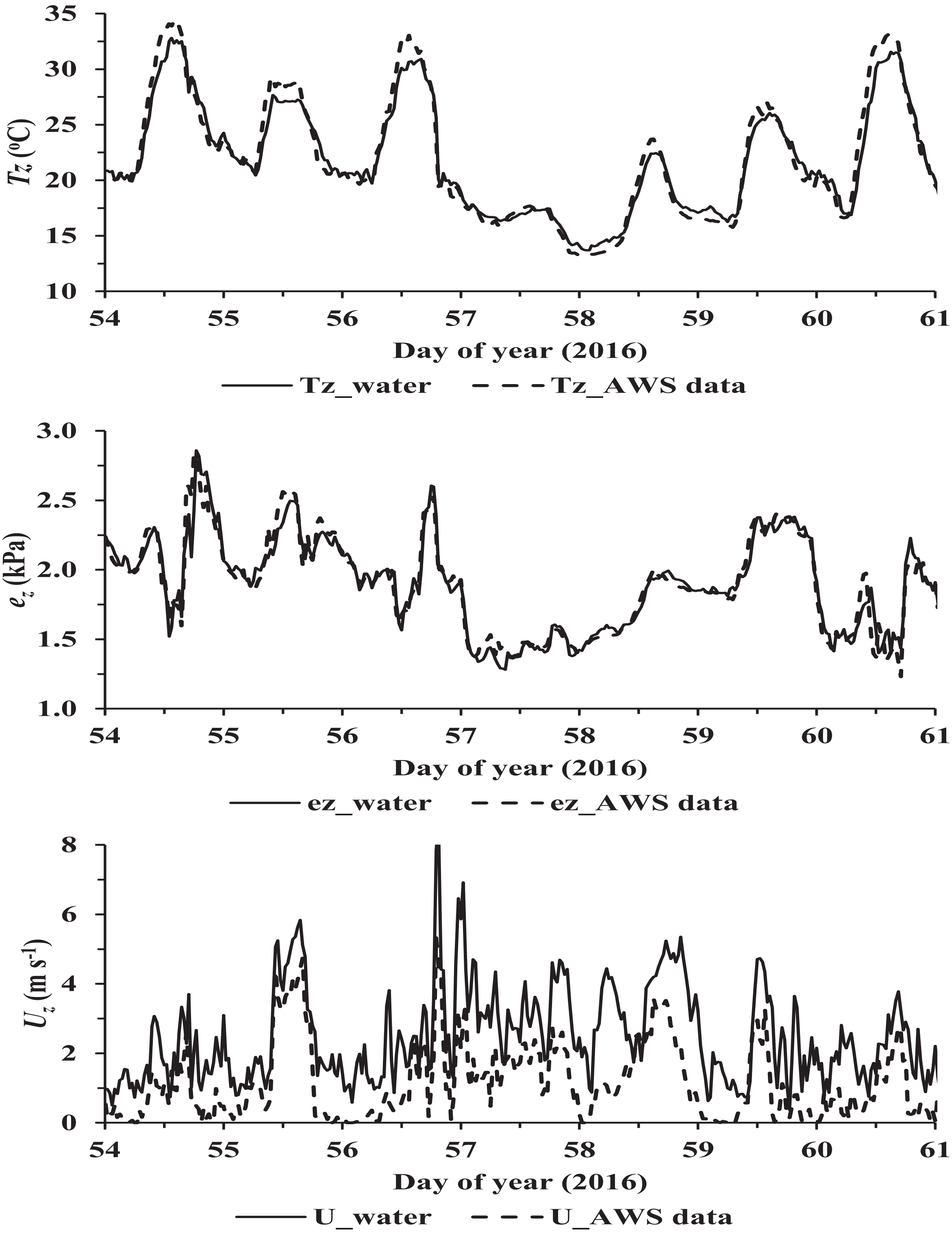

Fig. 5.13 Diurnal variation in (from top to bottom): 30-min T_z, e_z and U_z for days of year 54 to 61 (24th Feb to 2nd March 2016 respectively) for the water-based and AWS land-based data inputs to MOST

5.7 Comparison of MOST, DPMETHS and FAO56 estimates of daily evaporation

For these comparisons, MOST 30-min estimates of evaporation for the period 14th February (day of year 44) to 26th May (day 146), 2016, were totalled to daily values. Although the period covers 104 days, effectively there was only data for 81 days as some data was missing. The above-water solar irradiance, T_z, e_z and U_z measurements were used as inputs to the DPMETHS model – actually in this case the DPMET model since the Hargreaves-Samani model was not applied since solar irradiance was measured. The cumulative comparisons were within 9.2% of each other with the DPMETHS model estimates consistently underestimating compared to the MOST cumulative evaporation for the period (Fig. 5.14). The average daily evaporation for the MOST method was 3.20 mm compared to 2.88 mm for the DPMETHS method. Everson (1999) also found that the Penman method underestimated measured (Bowen ratio) evaporation by 9%. The FAO56 estimates were initially and finally similar to MOST estimates but lower for days of year 64 to 124. The DPMETHS tended to underestimate and the FAO56 model overestimate compared to the MOST measurement method.

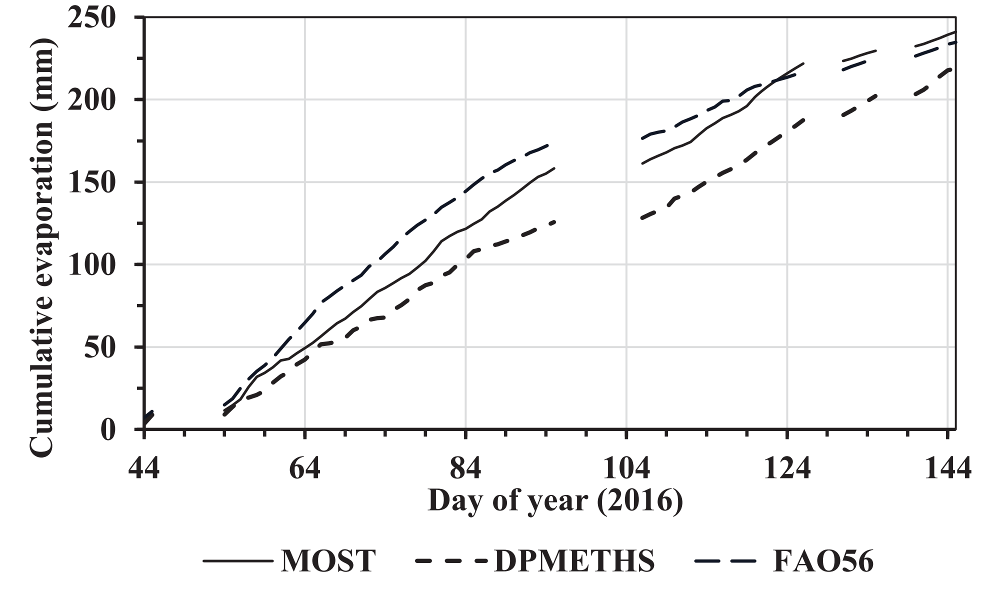

Fig. 5.14 Cumulative evaporation using MOST measurement, the DPMETHS model methods and the FAO56 method for the period 14th February (day 44 of year) to 25th May (day 145), 2016.

Of note is that the MOST method is independent of solar or net irradiance whereas these inputs are important for the DPMETHS and FAO56 model methods. By contrast, the MOST method is reliant on wind speed, and T_z, q_z and T_o. It was previously noted that nighttime high wind speeds result in larger than expected evaporation estimated using MOST and EC_QA methods. The DPMETHS and FAO56 models, both daily models, are dependent on the daily averaged wind speed and therefore do not explicitly account for nighttime evaporation. These events, with high nighttime wind speeds, reduced the DPMETHS and FAO56 cumulative evaporation estimates compared to MOST method estimates, for most of the measurement period.

From a physical process point of view, it would appear that there is reasonable agreement between the three methods. However, the DPMETHS and FAO56 model methods are normally reliant on AWS measurements which do not represent conditions above the water surface, unlike MOST measurements.

Also, from a process point of view, what the DPMETHS and FAO56 models do not reveal is the significance of nighttime evaporation relative to daytime evaporation (defined, for simplicity, as 06h00 to 18h00). This is demonstrated in Fig. 5.15 which gives cumulative totals for daytime and nighttime, using MOST evaporation measurements. It was not possible to use EC data for these cumulative calculations due to the large amount of data excluded. Nighttime MOST evaporation represents 41.9% of the total (24-hour) evaporation over the 81 days of the measurement study with daytime evaporation therefore representing 58.1%. The influencing factor or driving force for this significant amount of evaporation during nighttime must be wind speed, as alluded to previously, in spite of the much lower water vapour pressure deficits at night compared to the day (data not shown). It may be possible to modify the DPMETHS model so as to estimate night- and daytime evaporative processes separately. Wind speed above open water for nighttime and daytime would be modelled, based on previous (historic) above-water wind speed data, which is currently unavailable, by comparing wind run for daytime and nighttime.

The cumulated wind run (km) for each day, for daytime hours and nighttime hours, was calculated based on the 3-D sonic anemometer data for the duration of the 2016 field study (Fig. 5.16). The total cumulated nighttime hours wind run was 41.7% of the total wind run – that for the daytime was therefore 58.3% of the total cumulated wind run. Furthermore, nightime maximum wind speeds exceeded daytime maximum wind speeds (Fig, 5.17). The maximum nighttime wind speeds often exceeded 5 m s^{-1}. This is indeed a surprising result considering the expected relative lack of unstable atmospheric conditions during the nighttime hours and expected unstable conditions during the day. Certainly, the nighttime latent energy flux (evaporation) cannot be regarded as minor, as one might have expected.

In terms of processes, evaporation for an open water system, stored heat flux aside, depends on daytime net radiative and aerodynamic (wind speed) conditions and nighttime

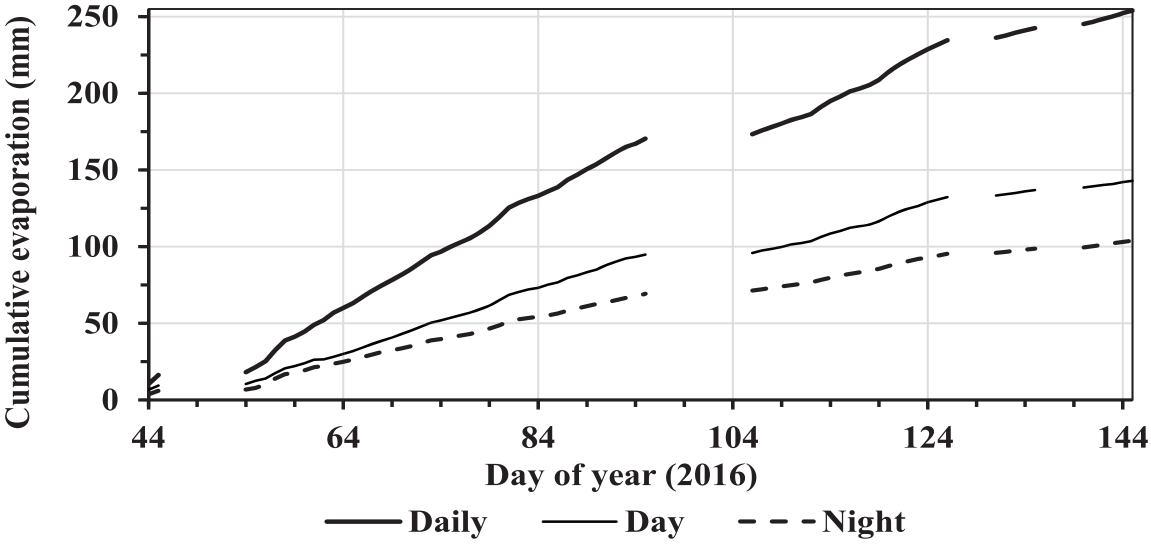

Fig. 5.15 Cumulative evaporation using the MOST measurement method for the day, daytime (06h00 to 18h00) and nighttime for the 101-day period

aerodynamic conditions and, to a lesser extent net, (infrared) radiative conditions. These are somewhat different mechanisms from canopy surfaces for which the surface conductance at night is assumed to be 0 m s^{-1} due to stomatal closure – so that even with significant nighttime wind speed, no total evaporation is assumed to occur. The implication of this is that daily models for open water evaporation may perform poorly unless nighttime processes with nighttime wind speed are also taken into account.

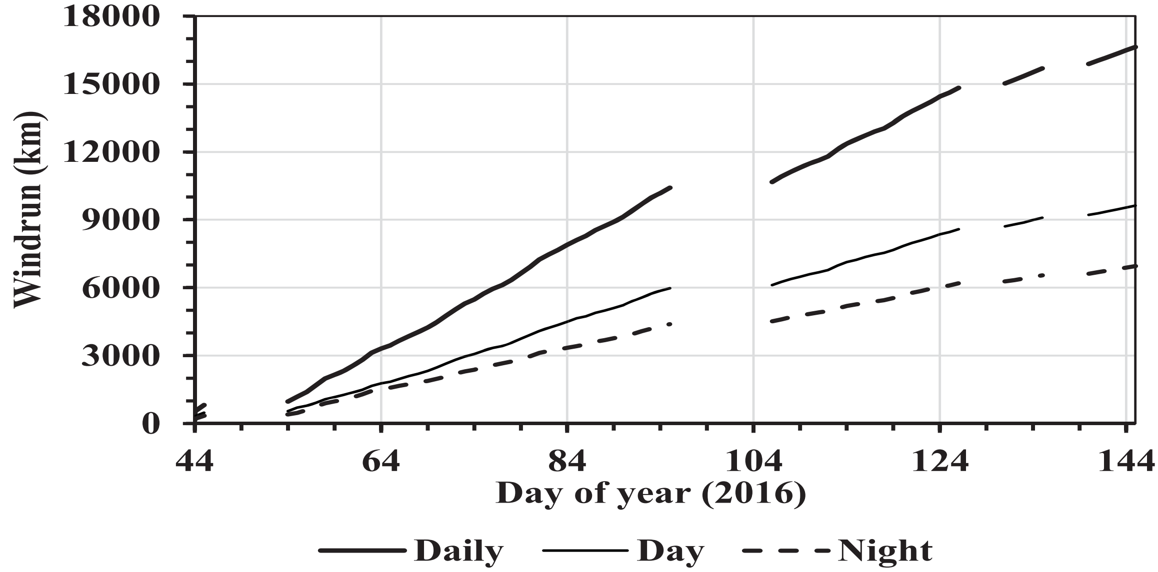

Fig. 5.16 Wind run (km) for the day, daytime and nighttime hours for the period 14th February (day 44 of year) to 25th May (day 145 of year), 2016

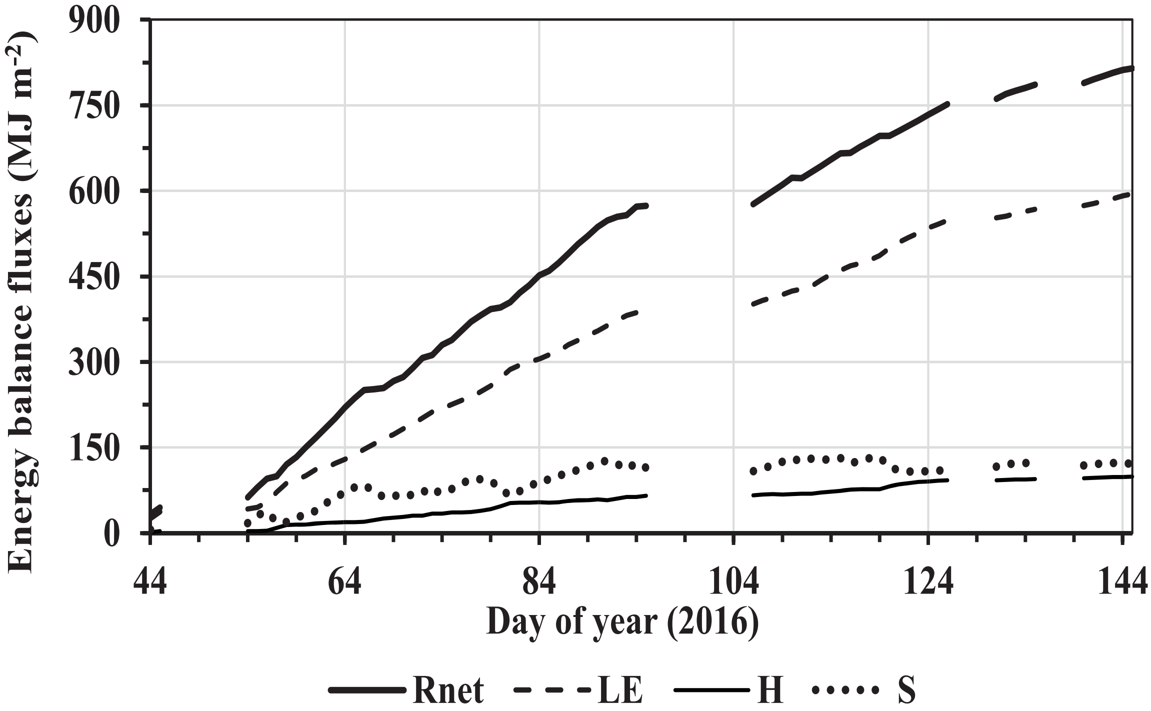

Fig. 5.17 Cumulated energy balance fluxes from MOST *H* and *LE* estimates and measurements of R_{net} with *S* calculated as a residual of the energy balance for the study period

Using MOST estimates of *H* and *LE*, the cumulated energy balance component fluxes, with *S* calculated as a residual, are shown in Fig. 5.17. As expected, the latent energy flux is the dominant term of the energy balance, making up 86% of the available energy flux $R_n - S$. The curve for *S* shows some decreases with day of year since for some days, $LE + H$ exceeded R_{net}. Sensible heat flux, 12.1% of R_n, was the smallest component of the energy balance, slightly less than the estimated water-stored heat flux, which was about 14.8% of net irradiance.

5.8 Correction of the MOST estimates of *H* and *LE* for target emissivity and reflected background infrared irradiance

Corrections for target emissivity, and reflected background infrared irradiance, are required for accurate surface temperature measurements. The infrared irradiance detected by an infrared thermometer includes the infrared irradiance from the surface and the reflected background infrared irradiance:

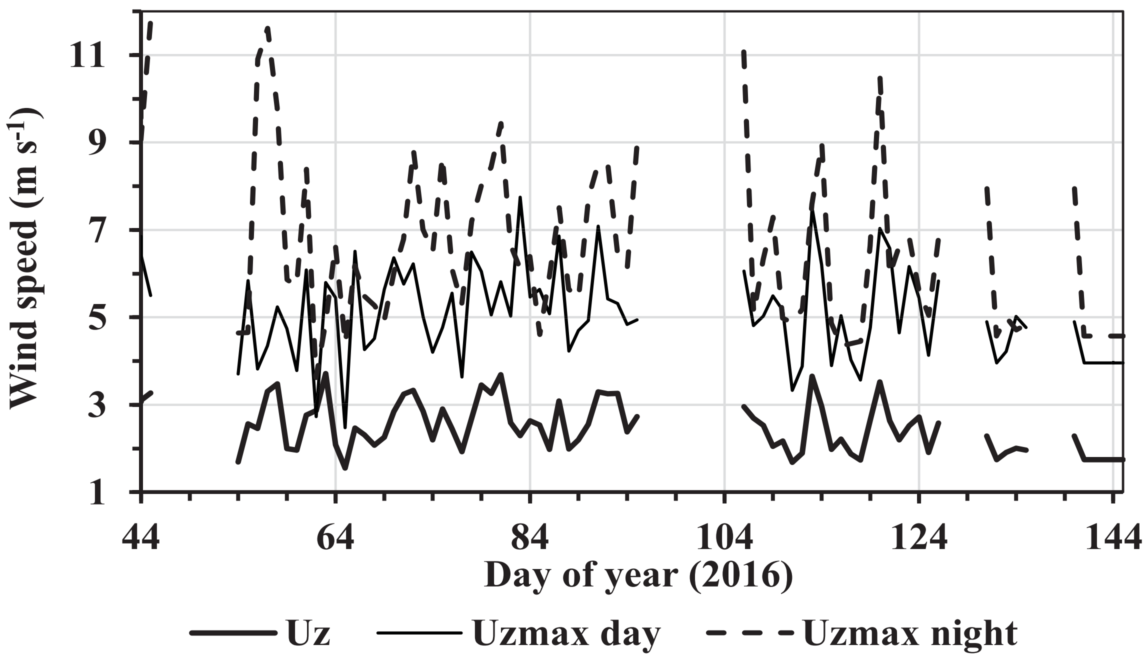

Fig. 5.18 Average daily wind speed (U_z), and 30-min maximum wind speed for day- and nighttime hours for the measurement study period

$$L_{u\,IRT} = L_{u\,target} + \left(1 - \varepsilon_{target}\right) L_{d\,background} \tag{5.6}$$

where $L_{u\,IRT}$ is the infrared irradiance measured by the IRT, $L_{u\,target}$ the infrared irradiance emitted by the target surface, ε_{target} the emissivity of the target surface, and $L_{d\,background}$ the infrared irradiance emitted by the background (sky). If $\varepsilon_{surface} = 1$, $L_{u\,IRT} = L_{u\,target}$ and hence $T_{IRT} = T_{target}$.

If $\varepsilon_{surface} < 1$, in terms of temperature:

$$\sigma T_{IRT}^4 = \varepsilon_{target}\,\sigma T_{target}^4 + \left(1 - \varepsilon_{target}\right) L_{u\,background} \tag{5.7}$$

where T_{IRT} (K) is the IRT-measured temperature of the target surface, σ = 5.67 x 10^{-8} W m^{-2} K^{-4} is the Stefan-Boltzmann constant and T_{target} (K) the target (surface) temperature. The emissivity of the background (sky) is not required since the infrared irradiance of the background (sky) is all that is required.

Hence, from Eq. 5.7:

$$T_{target} = \left(\left(\sigma T_{IRT}^4 - (1 - \varepsilon_{target})\, L_{u\,background}\right) / \left(\varepsilon_{target}\, \sigma\right)\right)^{1/4} \tag{5.8}$$

Most (thermal) infrared thermometers have a measurement waveband of 8 to 14 μm which corresponds to the far infrared waveband. The infrared emissivity for open water varies over this wavelength range (Fig. 5.19; Wan, 2012).

The temperature of the water surface varies between 0 and 35ºC. This temperature range was used to calculate λ_{max}, using Wien's Displacement Law:

$$\lambda_{max} \times T_{surface} = 2.889777 \times 10^6 \tag{5.9}$$

where λ_{max} (μm) is the wavelength corresponding to the peak spectral irradiance of the Planck curve for a particular temperature $T_{surface}$ (K). Each λ_{max} was then used to determine an emissivity ε using the following procedures. A linear relationship was fitted to the curve of Fig. 3.38 for the wavelength range 9 000 to 10 600 nm, corresponding roughly to the λ_{max} values for 0 to 35ºC but extended so as to cover a slightly greater wavelength range (Fig. 5.20). A relationship between emissivity and surface temperature was then generated for each wavelength and a linear relationship fitted (Fig. 5.21). This relationship was then used to correct the measured target temperatures and the H_{MOST} and LE_{MOST} values recalculated by iteration.

F
8

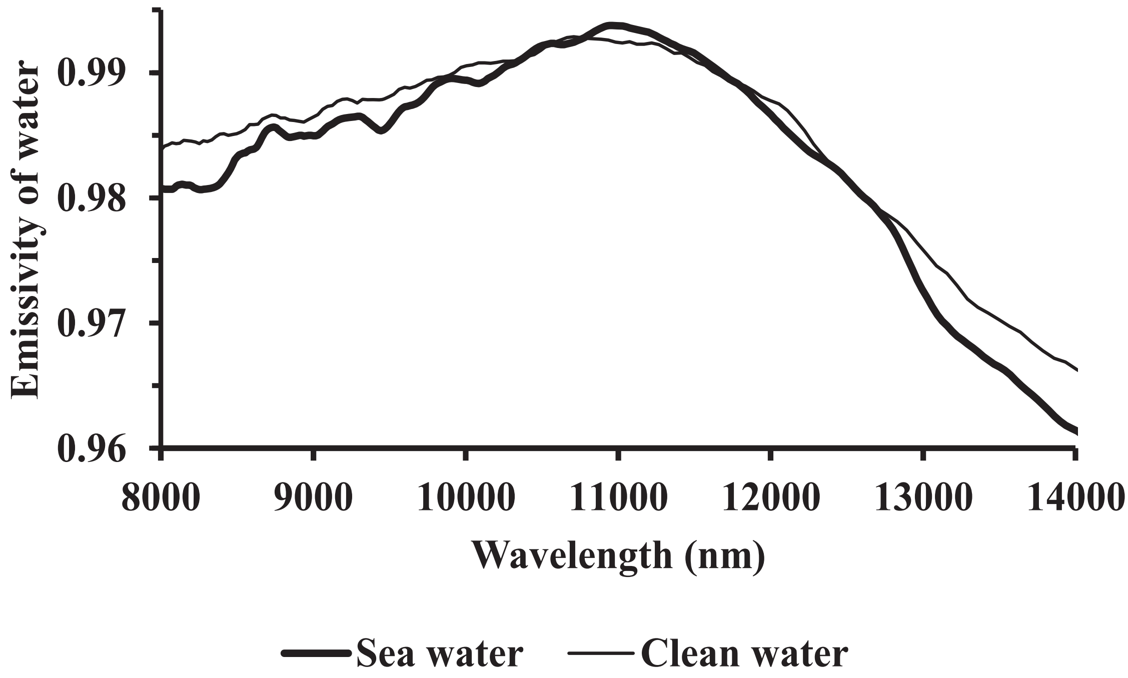

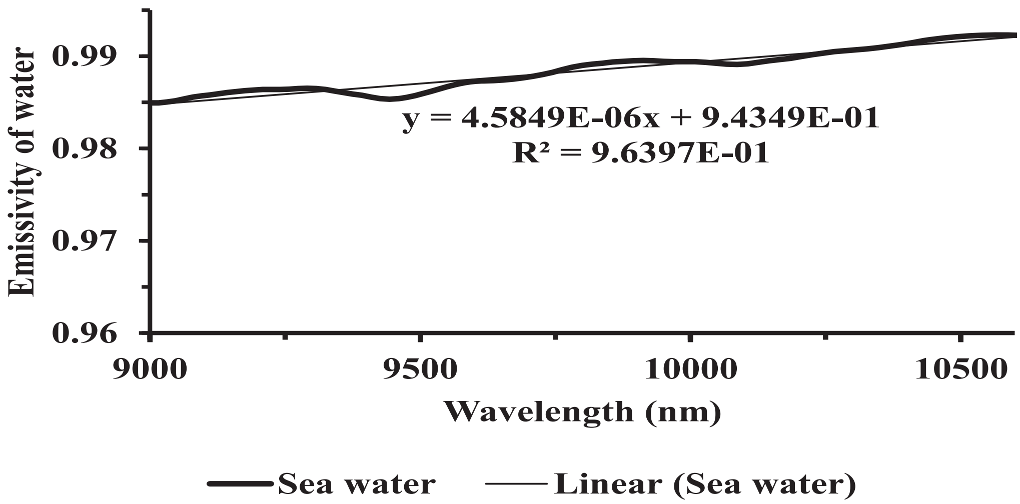

Fig. 5.20 The emissivity of sea water for the wavelength range 9 000 to 11 000 nm with fitted a linear relationship (emissivity data source: Wan, 2012)

The requirement of an additional measurement, *viz.* the downward infrared irradiance (Eq. 5.8), would significantly increase the cost of the MOST method. The uncorrected target temperatures, T_o, were compared to the corrected values, using Eq. 5.8 to determine if a systematic correction was possible. The comparison between T_o and T_o corrected for target emissivity shows excellent agreement but with T_o requiring bias correction by 0.14°C (Fig. 5.20). The impact of this correction on the H and LE MOST estimates was investigated by recalculating the fluxes for the entire measurement period using the corrected T_o (H) and $e_s(T_o)$ (LE) values (Fig. 5.21). The correction to H_{MOST} was more variable (R^2 = 0.9849), requiring a 1.5% decrease to the uncorrected estimates (Fig. 5.22, top). The correction to LE_{MOST} was less variable (R^2 = 0.9998), requiring a 3.1% increase to the uncorrected LE_{MOST} estimates (Fig. 5.23, bottom). These corrections, particularly the correction to T_o for the target temperature, negate the need for measurement of the infrared background irradiance. The only disadvantage is the slightly increased uncertainty in the corrected H_MOST values (Fig. 5.22, top). The focus

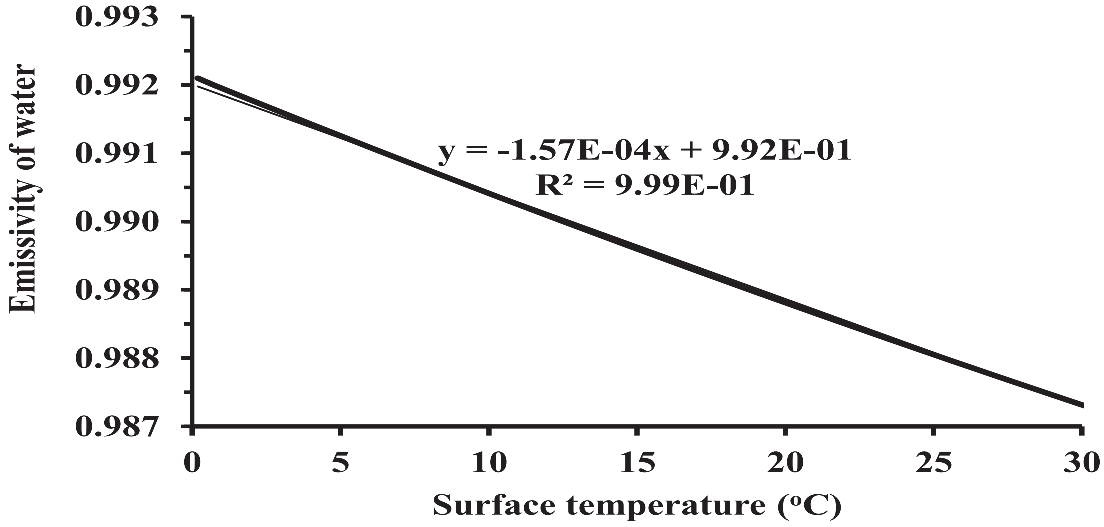

Fig. 5.21 The emissivity of sea water as a function of surface temperature, allowing corrections to be applied to target temperature

of the study, however, is on LE_{MOST} for which the corrections are very reliable and easily corrected by an upwards adjustment of T_o by 0.037°C (Fig. 5.22).

As a result of corrections for target emissivity and reflected background infrared irradiance, the LE_{MOST} estimates were increased very slightly, yielding reduced agreement between the cumulative ET for the MOST and DPMETHS methods from 9.2 to 10.7% (Fig. 5.24).

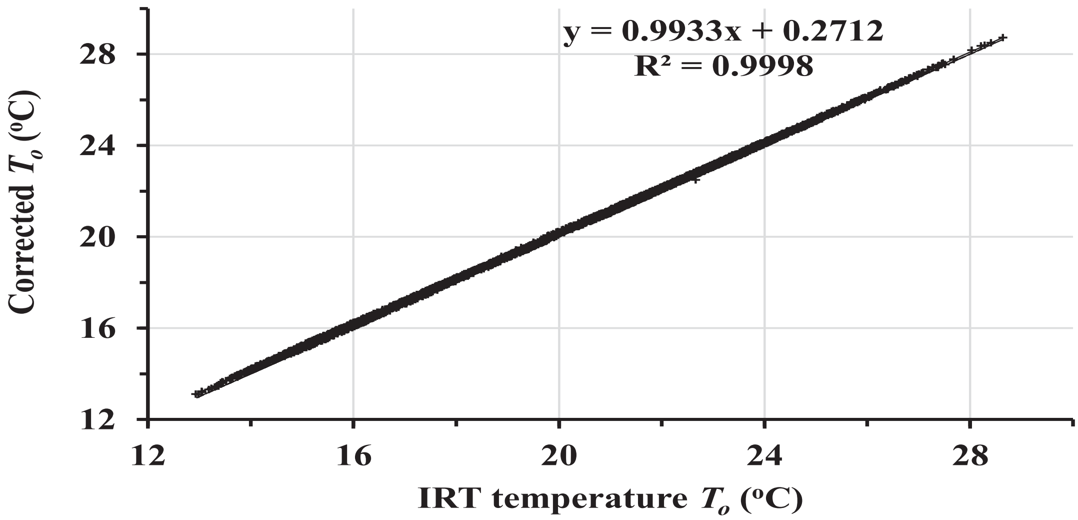

Fig. 5.22 Target temperature T_o corrected for water-surface emissivity and reflected background infrared irradiance (y-axis) vs measured T_o values, for 12th February to 26th May 2016

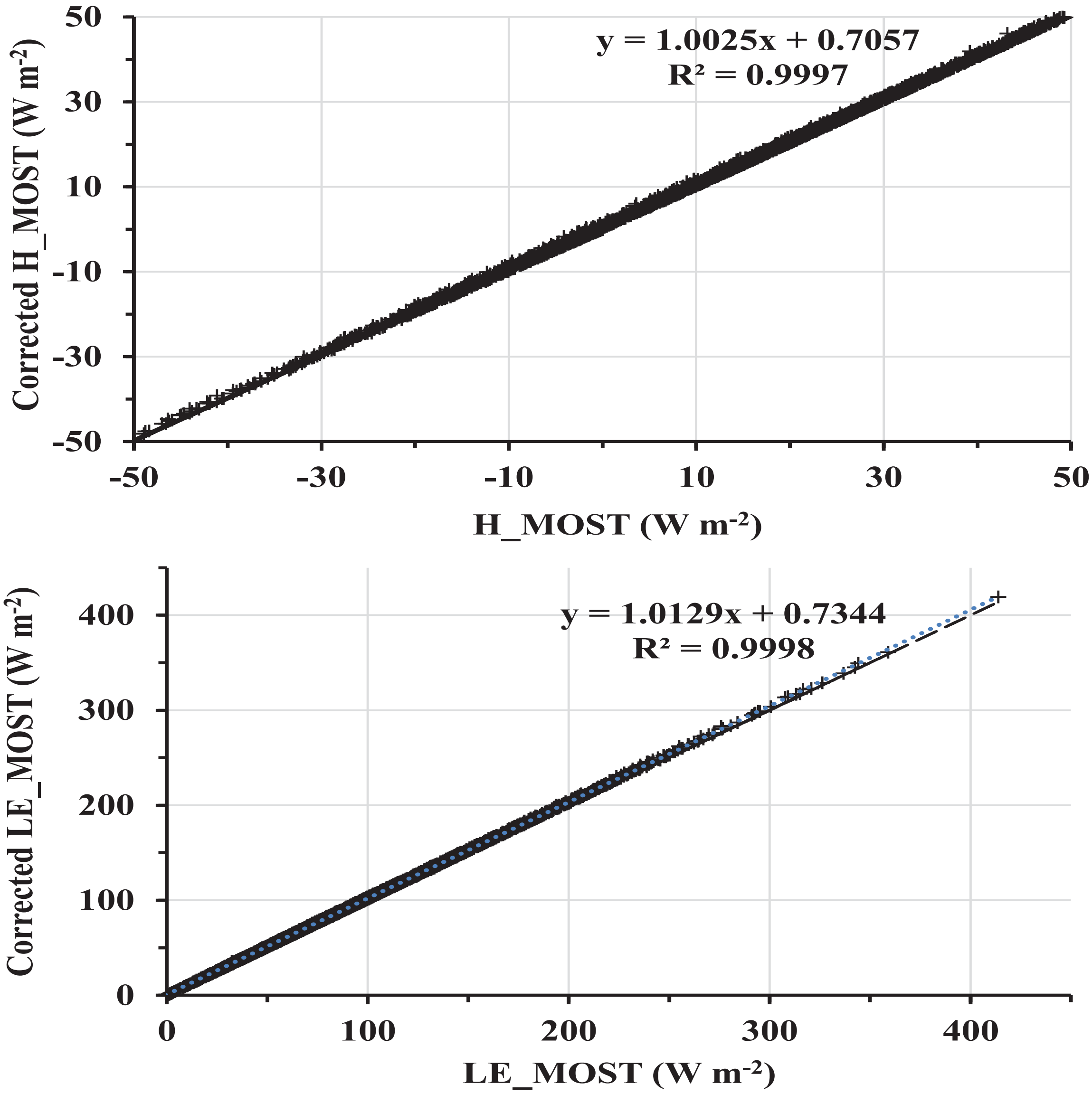

Fig. 5.23 Regression plots, following correction for target emissivitivity of 0.992 and reflected background infrared irradiance, of (top): H_MOST and H_MOST corrected and (bottom): LE_MOST and LE_MOST corrected for the period 12th February to 26th May 2016. The bottom line in each graph is the 1:1 line.

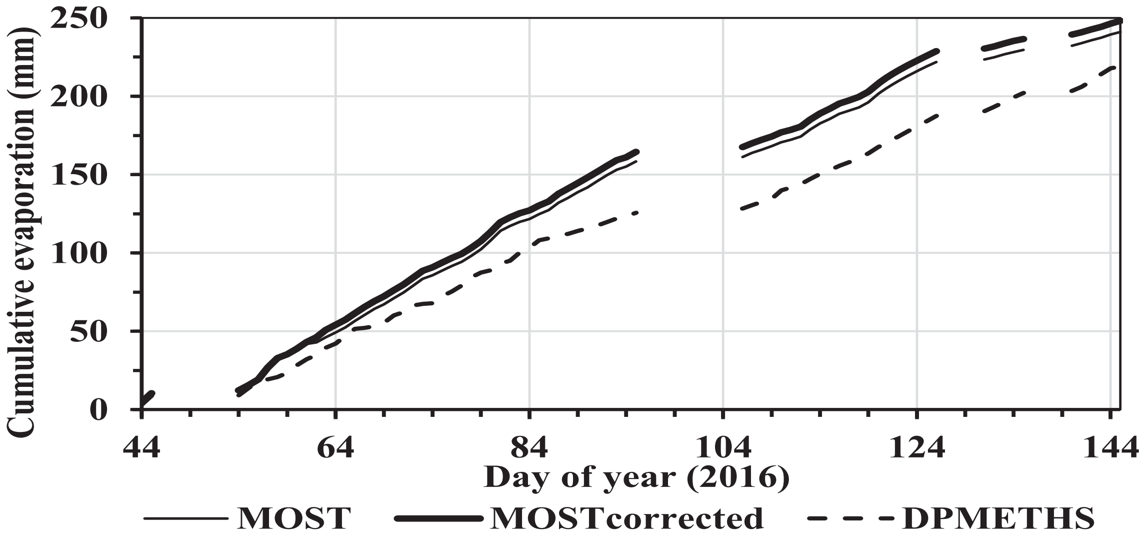

Fig. 5.24 Cumulative evaporation for MOST and MOST corrected, for target emissivity and reflected background infrared irradiance, and DPMETHS model methods, for the period 14th February (day of year 44) to 25th May (day of year 145), 2016

CHAPTER 6: RADIOMETRIC BOWEN RATIO AND SURFACE RENEWAL METHODS FOR ESTIMATING *LE*

6.1 Summary

For the surface renewal (SR) method, the air temperature ramp and period and sensible heat flux (H) for the averaging period was calculated in a single cell for stable and unstable conditions. The roots of a third-order polynomial in ramp amplitude, dependent on the second-order, third-order and fifth-order air temperature structure functions obtained for each half-hourly averaging period, were efficiently determined by the iterative procedure with the result of the polynomial varying between -0.015 and 0.01. For SR measurements, over a four-week period, for stable conditions, a value for H was obtained less than 40% of the time compared to in excess of 95% for unstable conditions. This is a weakness of the SR method. Comparisons, using data for open water, between the van Atta and an independent method using an iterative approach implemented in a spreadsheet were exact. The iterative approach obtained a slightly greater number of sensible heat flux estimates. This work paves the way for the methodology for near real-time determination of SR sensible heat flux. The iterative SR method was implemented in a CR3000 datalogger. A comparison between H_{SR} obtained using the iterative method applied in Excel and implemented in a CR3000 CRBasic programme showed very good agreement.

6.2 Introduction

The radiometric Bowen ratio (BR) method for determining $LE = LE_o$, as previously proposed, depends on the radiometric BR:

$$\beta_o = \frac{T_o - T_z}{e_s(T_o) - e_z}, \tag{6.1}$$

where T_o is the corrected target temperature, and either the available energy flux $R_{net} - S$ or H using either:

$$LE_o = \frac{R_{net} - S}{1 + \beta_o} \tag{6.2}$$

where $\beta \neq -1$ or

$$LE_o = H/\beta_o \tag{6.3}$$

where $\beta_o \neq 0$ where H is measured using, say, surface renewal.

Due to the unreliability of the water-stored heat flux S, application of Eq. 6.2 for determining LE is problematic. The disadvantage of Eq. 6.3, which depends on H and β_o, is that usually, H is the smallest component of the energy balance and, secondly, that when $|\beta_o| \rightarrow 0$, the LE values are unreliable. Excluding data for which $|\beta_o| \rightarrow 0$ could exclude data for conditions when LE is large and H is small.

For the SR method, the air temperature ramp and ramp period are used to obtain the sensible heat flux (H) at sub-hourly intervals. For the method, unshielded high frequency air temperatures measurements, using fine-wire thermocouples, are required, together with application of the van Atta (1978) approach for determining the roots of a cubic equation. To date, these procedures for obtaining the roots have been difficult, and to our knowledge no one has found a method to determine them in real-time. This work should make the real-time solution possible.

6.3 Materials and methods

For the SR method, several unshielded and naturally-ventilated type E thermocouples (75-μm diameter) were used to measure air temperature, placed at heights of 1.0, 1.3, 1.9 and 2.5 m above the water surface. Each sensor consisted of a pair of 75 μm thermocouples in parallel. The thermocouples were connected to a CR3000 datalogger. The metal panel placed above the connecting channels was covered with additional insulation foam to further reduce temperature changes in the vicinity of the connecting thermocouple wires. The thermocouples were pointed into the predominant wind direction which occurred mainly during daylight hours. Measurements were made every 0.1 s, equivalent to a frequency of 10 Hz, and then lagged by 0.4 s and 0.8 s before calculating the second-, third- and fifth-order air temperature structure functions required by the van Atta (1977) approach for SR analysis. Then these were averaged every 2 min and every 30 min. Software calculations, post-data collection, were used to calculate SR sensible heat fluxes using the van Atta (1977) approach. For this purpose, three methods were used to solve the real roots of the cubic equation (Eq. 3.59):

1. A Microsoft QuickBASIC 4.0 programme, provided by Snyder (2003, pers. comm.[1]).
2. The SR Excel spreadsheet of Snyder et al. (2007). The spreadsheet contains 52 columns for performing the same SR calculations as in the QuickBasic programme, for two thermocouples and two time lags.
3. The single-cell iterative spreadsheet method was used for calculating each of a (Eq. 3.67), and τ (Eq. 3.62), with conditions imposed by Eq. 3.63, and H_{SR} (Eq. 3.58 with $\alpha = 1$).

---

[1] Dr. R.L. Snyder, Department of Land, Air and Water Resources, University of California, Davis, California, USA

Methods 2 and 3 were compared using 19 days of open water SR measurements. The output period in this instance was 2 min.

The single-cell iterative spreadsheet methodology was implemented in CRBasic for use in a CR3000 datalogger. The output data interval chosen was 30 min. The second-, third- and fifth-order air temperature structure function values, S_r^2, S_r^3 and S_r^5, for each 30-min period, were also stored and subsequently used in Excel. SR sensible heat fluxes using the single-cell iterative spreadsheet and online datalogger methodologies were compared.

6.4 Results and discussion

The variation in β_o over a one-week period (Fig. 6.1), shows that β_o has a fairly predictable pattern for fair weather conditions – less than 0 for both methods for the week of 19th to 26th April, 2016. The BR, Beta_MOST determined from the ratio of H and LE from the MOST method, is in reasonable agreement with β_o during the daytime hours. This is not surprising given the expressions in Eqs 3.78 and 3.79. In general, the troughs in Fig. 6.1 correspond to times at or after midnight (H and LE opposite in direction with negative β_o), peaks/plateaus at midday and the afternoon (LE large relative to H with large but still negative β_o), with β_o largely negative for the early morning hours and late afternoon (LE and H opposite and of similar magnitude).

Surface renewal data and Bowen ratio radiometric data collected above open water (29th June to 20th July 2007) were used to determine H_{MOST} and β_o from which LE_o was determined as the ratio of the two. Compared to the MOST and EC LE values, LE_o were often much larger in magnitude and opposite in sign. The statistical relationship between LE_{MOST} or LE_{EC} and LE_o was poor (data not shown). The reasons for this are not evident apart from the fact, as expected, that LE_o was large when $|\beta_o| \rightarrow 0$. This poor result does not invalidate the MOST method in spite of the fact that some of the measurement inputs for MOST and β_o are similar: the MOST method does not depend on β_o with H_{MOST} and LE_{MOST} values calculated separately.

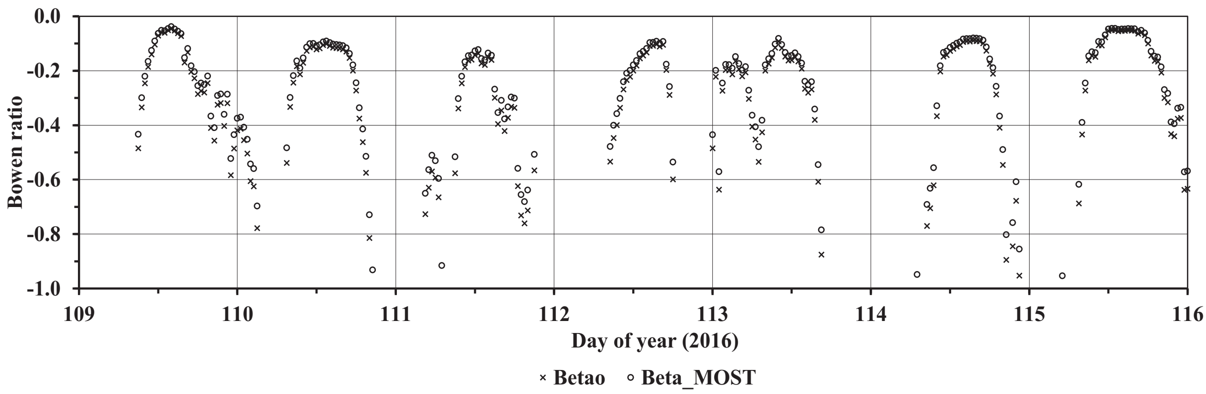

Fig. 6.1 Diurnal variation in 30-min radiometric Bowen ratio (Betao) and the Bowen ratio determined from the ratio MOST fluxes H_{MOST} and LE_{MOST} (Beta_MOST), corrected for target emissivity and reflected background infrared irradiance, for days of year 109 to 116 (19th to 26th April, 2016)

Furthermore, the LE_{MOST} and LE_{EC} estimates are in reasonable agreement following application of the QA protocols applied to the EC data.

For the 2-metre measurement height, the time lag of 1 s corresponded to the maximum of $-(S_r^3/r)^{1/3}$, used by Chen et al. (1997) in their SR analysis using a ramp model with finite microfront period, for unstable conditions (Fig. 6.2). The value of $-(S_r^3/r)^{1/3}$ decreased for lag times greater than 0.1 s, and then tended to plateau at around 1 s. For these time periods, H_{MOST} was negative (decreasing from -9 to -20 W m^{-2} between 14h00 and 15h30). At the same times, L_{EMOST} 73 to 100 W m^{-2}. While the use of a shorter time lag may be too short for the formation of air temperature ramps, the use of a longer time lag such as 1 s may be too long for nighttime stable conditions, resulting in a different H_{SR} estimate. From a practical point of view, it is only possible to use one time lag and hence a 1-s time lag was used for all subsequent calculations for the SR method.

Correspondence of sensible heat flux between SR, using an α factor for open water of 0.245 (Mengistu and Savage, 2010), MOST and EC methods was poor (Fig. 6.3). The H_{SR} estimates which were small in magnitude showed wide variation, often opposite in sign compared to MOST or EC estimates. The LE_SR estimates based on H_SR and β_o were mostly negative, showing even greater variation (Fig. 6.3). Of the three estimates, the MOST estimates of LE were the most stable, and compared reasonably with the EC estimates.

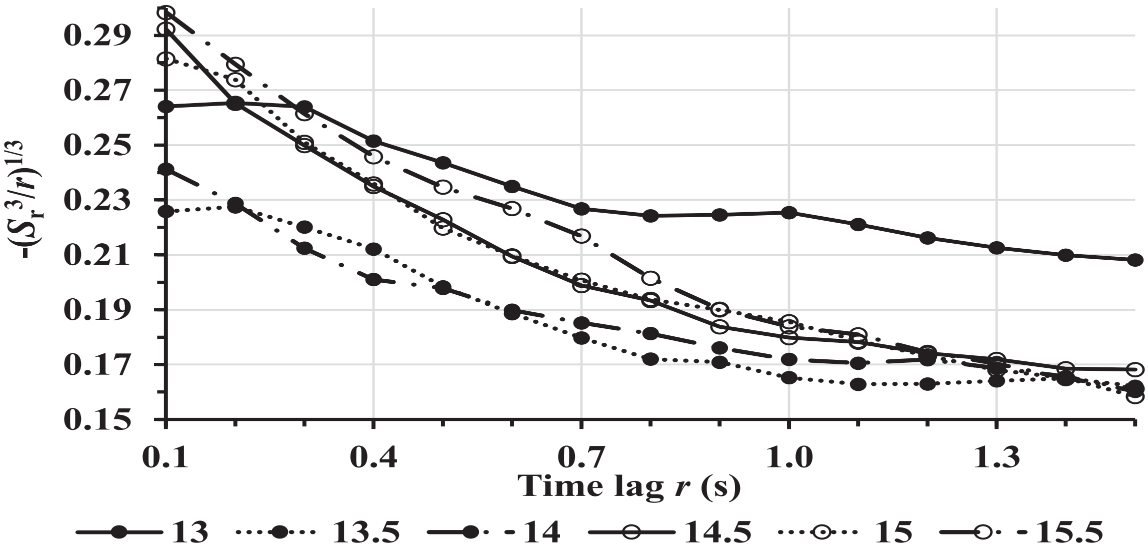

Fig. 6.2 Measured half-hourly averages of $-(S_r^3/r)^{1/3}$ *vs* time lag *r* (s) at 2 m above the open water surface for measurements for 22[th] April 2016 from 13h00 (13) to 15h30 (15.5) showing a minima (negative H_{MOST}) corresponding to around $r = 1$ s for each time period

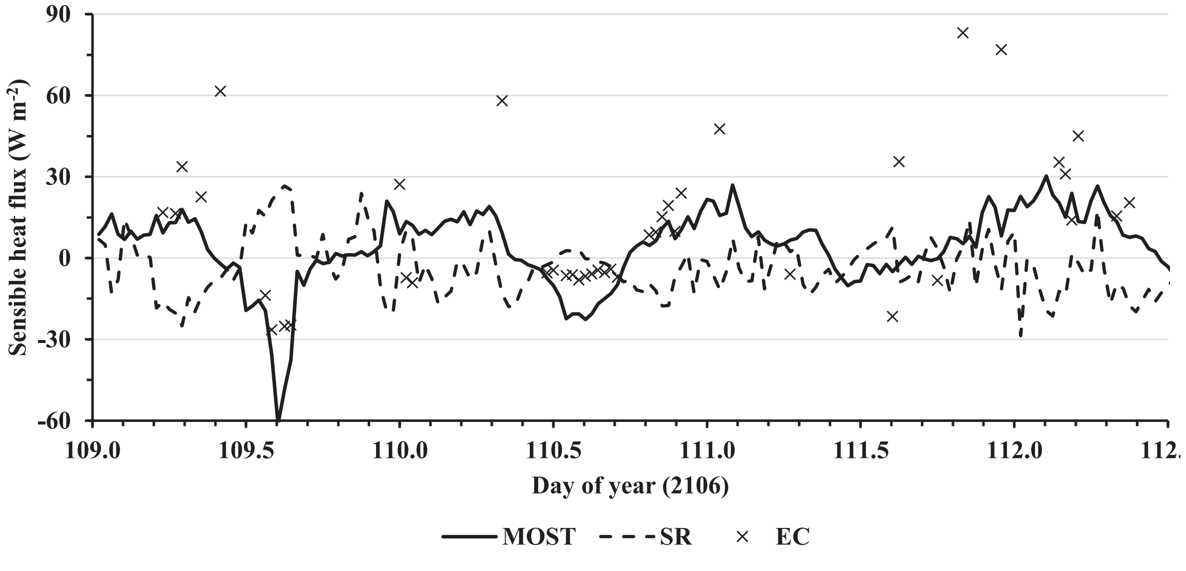

Fig. 6.3 Temporal variation in (top): *H* measured using MOST, SR and EC methods and (bottom) *LE* using the same techniques for the days of the year 109 to 112 (19[th] to 22[th] April, 2016)

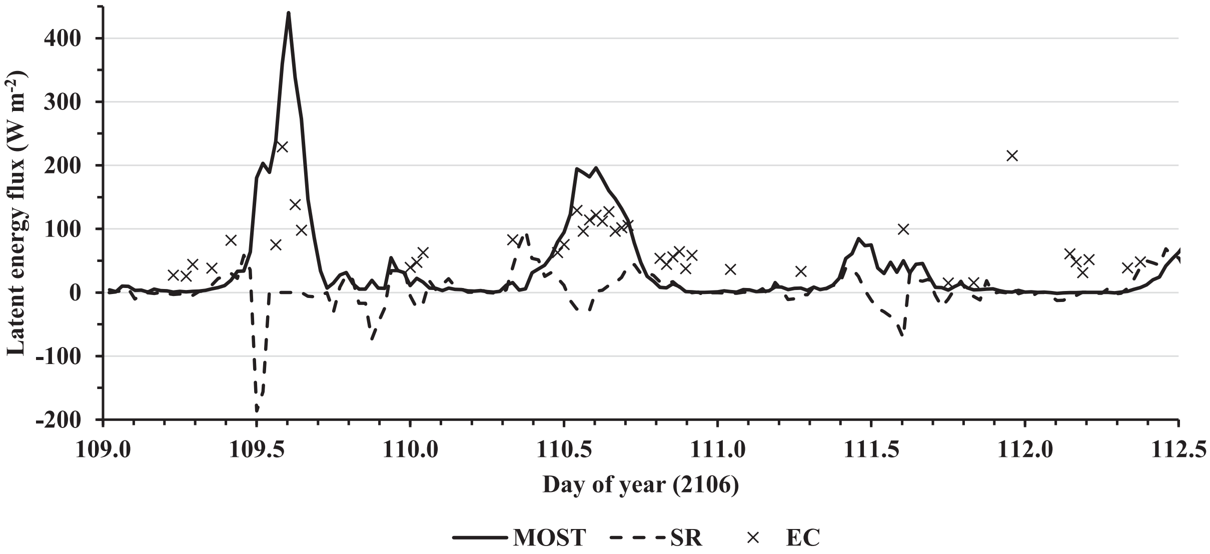

The QuickBASIC approach of determining the ramp amplitude a suffers from a resolution limitation (Figs 6.4 and 6.5). The check of the solution, *viz.* that Eq. 3.59 is satisfied, shows that a varies between about -1.0 and 1.0 for the QuickBASIC method compared to between -0.015 and 0.01 for the single-cell iterative method (Fig. 6.4). The results of the two spreadsheet methods show exact correspondence but unpredictable H values are obtained for the QuickBASIC method – when a is not an exact root of Eq. 3.59 (Fig. 6.6). The single-cell iterative method for both stable and unstable cases is quick, accurate and convenient, easy to repeat following changes to equations or data, allows easy manipulation and allows convenient visual inspection of data and graphics, compared to other methods involving Fortran, Visual Basic, C or other language programming. For half-hourly SR measurements, for stable conditions, a sensible heat flux value was obtained by iteration less than 40% of the time compared to in excess of 95%for unstable conditions. The inability of the SR method to obtain a solution for many of the stable conditions is a significant weakness of the method. In defence of the SR method for such cases, Castellví et al. (2008) point out that the fluxes are small and more affected by (measurement) errors. Furthermore, for such cases, the magnitude of S_r^2, S_r^3 and S_r^5 are considerably smaller and therefore limiting the accurate calculation of the air temperature ramp periods and amplitudes.

The van Atta (1977) approach for determining the roots of the cubic equation (Eq. 3.18) and the SR sensible heat flux (Eq. 3.20) has been implemented in a spreadsheet by Snyder et al. (2007). Independently of the van Atta (1977) approach, but through use of an iterative approach for solving the roots of the cubic equation, a spreadsheet implementation is proposed.

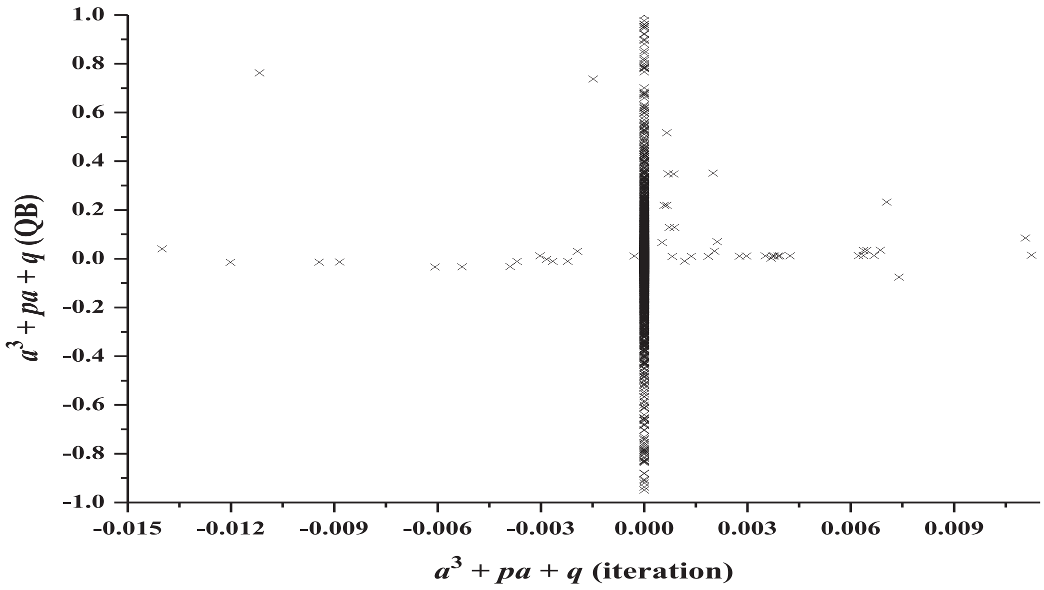

Fig. 6.4 A comparison of the root of the SR polynomial, checked by evaluating $a^3 + pa + q$ for 0, using the QuickBASIC and spreadsheet iterative methods, for a month of 30-min SR data

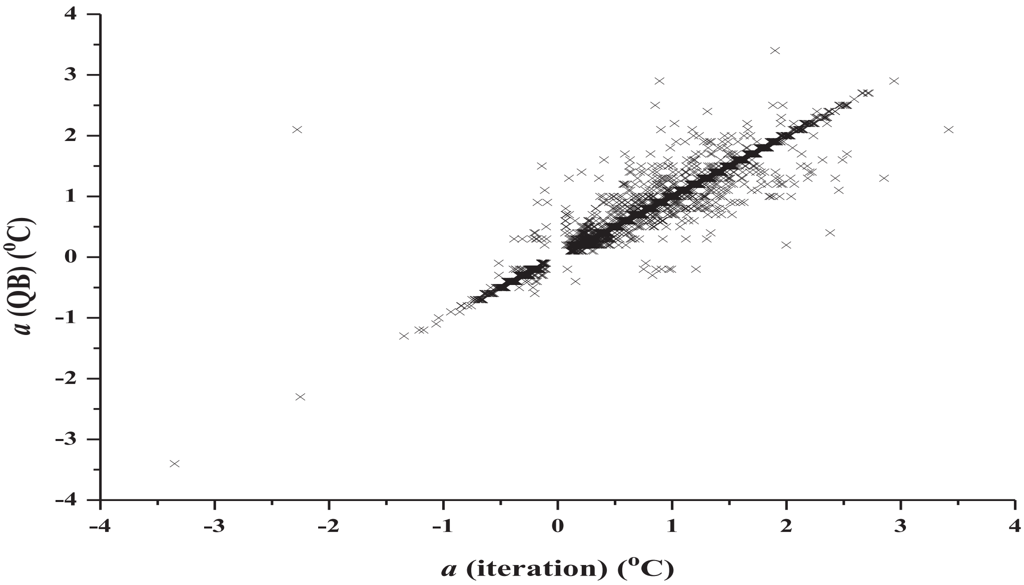

Fig. 6.5 A comparison of 30-min SR air temperature ramp amplitude *a* (°C), using the QuickBASIC and spreadsheet iterative methods

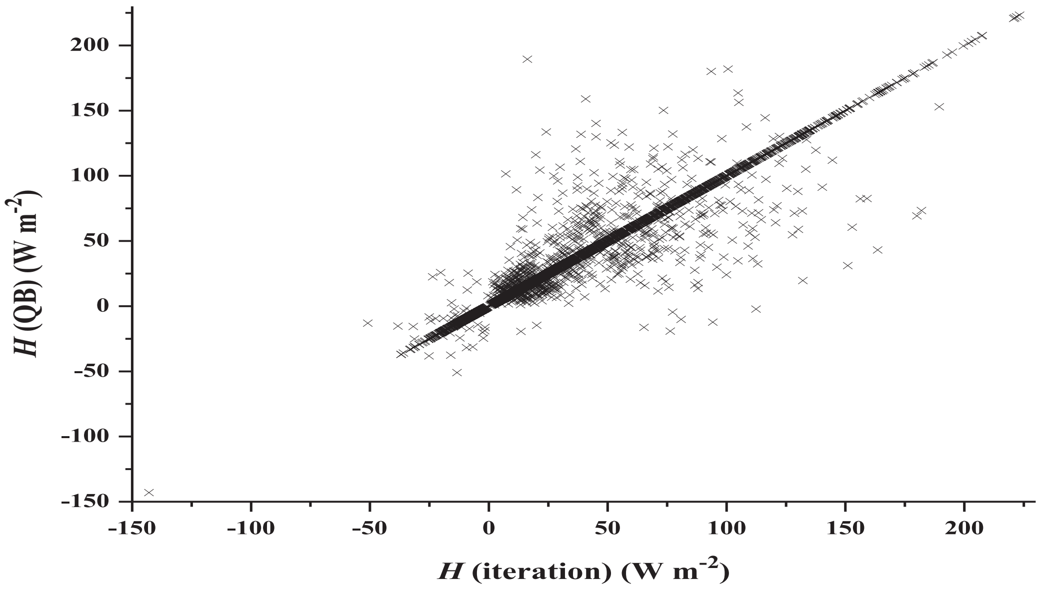

Fig. 6.6 A comparison of 30-min H_{SR} (W m^{-2}) estimates, using the QuickBASIC and spreadsheet iterative methods

The results of the two methods were compared using 19 days of open water measurements (Fig. 6.6). The inputs include measurement height, sample time lag, and the 2-min second-order, third-order and fifth-order air temperature structure function values (using Eq. 3.56 with k = 2, 3 and 5). The two methods are perfectly correlated. Note that while there is a large range in values for H_{SR}, these values require adjustment since $H = \alpha\, H_{SR}$. Mengistu and Savage (2010) obtained values for α of 0.198 for the height and lag value of Fig. 3.50 (1 m and 0.4 s respectively). The range is therefore -63 to 70 W m^{-2}.

The details of the comparison are shown in Table 6.1. There is a high percentage of occurrences for which both methods find no solution (roughly 33%). The iterative method finds slightly more solutions (64.6%) than the van Atta (1977) approach (33.4%). On occasion the iterative method finds a and τ which should allow H to be calculated but it does not do so.

In general, the result is pleasing and paves the way for a near real-time solution of surface renewal sensible heat flux.

The H_{SR} values for the spreadsheet and online datalogger methods, for half-hourly values, were compared (Fig. 6.8). The comparisons are very good apart from six measurement pairs. The routine application of the SR method for estimation of open water evaporation suffers from the problem that the sensible heat flux is usually the smallest component of the energy balance and that the highly variable water-stored heat flux needs to be measured.

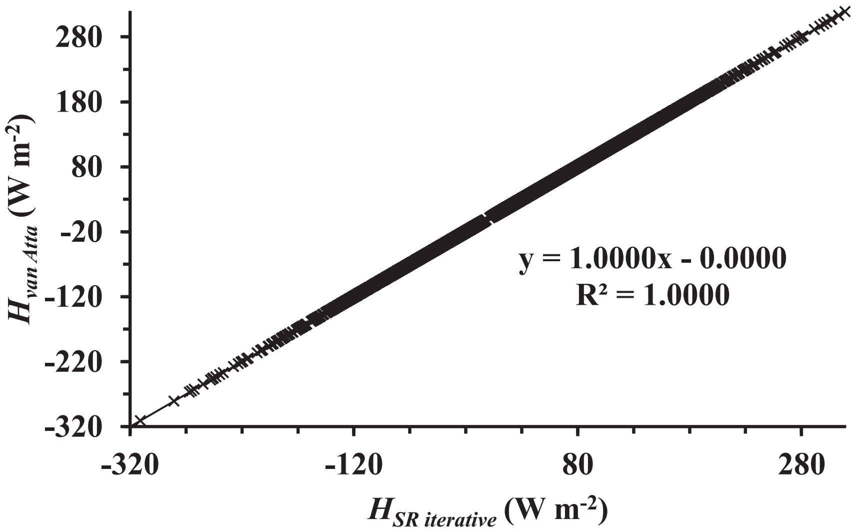

Fig. 6.7 A comparison of 30-min H_{SR} (W m^{-2}) estimates, using on the y-axis the van Atta (1977) approach implemented in a spreadsheet (Snyder et al., 2007) and on the x-axis the spreadsheet iterative methods

Table 6.1 Details of the van Atta (1977) spreadsheet-implemented approach for determining surface renewal sensible heat flux (Snyder et al., 2007) and that implemented in a spreadsheet using a single-cell iteration approach

	Percentage occurrence	Days/number of points
Time period of data (days)		19
Iterative method has solution for *H*	66.6	5 278
Both methods have the same *H*	64.6	9 646
Both methods have no *H*	33.4	4 982
Iterative solution but not for the van Atta approach	0.2	23
Iterative method yields a and τ but not *H*	1.8	273
Total	100.0	14 924

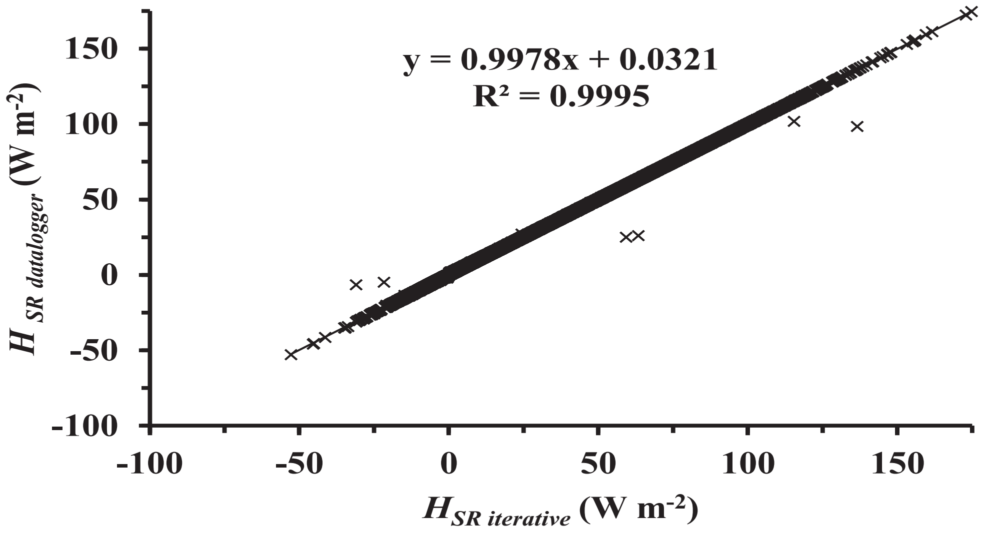

Fig. 6.8 A comparison of 30-min H_{SR} (W m^{-2}) estimates, using on the y-axis the online (CR3000 datalogger) iterative method and on the x-axis the spreadsheet iterative method

CHAPTER 7: CONCLUSIONS AND RECOMMENDATIONS FOR FUTURE RESEARCH AND TECHNOLOGY TRANSFER

7.1 Background

Evaporation is an important component of the water balance. Evaporation from open water surfaces is a neglected research area in water resources management in South Africa, in spite of South Africa's known high evaporative demand. Our previous WRC-funded research into evaporation has focused almost exclusively on evaporation from vegetation (Savage et al., 1997, 2004; Savage, 2009, 2010). Comparatively little research attention has been devoted to the hydrometeorological modelling or measurement of open water evaporation in spite of its general importance and its particular importance in relation to climate change.

Investigating the impacts of global warming on open water evaporation requires measurements and a model for open water evaporation. Many methods have been used to measure evaporation from soil and vegetated systems. However, there is a severe lack of measurements, and methodology for measuring open water evaporation.

At the beginning of the research work, three methods had been used previously for the estimation of open water evaporation in South Africa, namely the Symon's tank method, EC and SR, the latter two based on work over a two-week period by Mengistu and Savage (2010a). Traditionally, daily open water evaporation is estimated using Symon's pan daily measurement and a pan-to-dam multiplicative factor.

It was therefore decided to use a whole range of methods in this study: Symon's pan, EC, SR, the Monin-Obukhov similarity theory (MOST) method, (modified) Bowen ratio (BR), temperature variance (TV) and a daily Penman-Monteith equilibrium temperature Hargreaves-Samani (DPMETHS) model that requires land-based meteorological measurements, that was implemented in a spreadsheet. All of these methods, apart from Symon's pan and DPMETHS methods, allow half-hourly estimations of open water evaporation.

While measurements for Midmar Dam in the KwaZulu-Natal Midlands were taken for the period February 2016 to February 2017, the measurements reported on were for the period 14^{th} February to 25^{th} May 2016.

The objectives of the study were to investigate the use of a variety of measurement methods for the estimation of daily and sub-daily open water evaporation. Furthermore, the DPMETHS daily evaporation model was used to estimate daily evaporation for the history of Midmar Dam for periods when only daily weather data were available (1963 to 2014).

7.2 Conclusions

The DPMETHS model estimates of evaporation, accumulated annually, exceeded 1300 mm during El Niño years. The maximum annual evaporation for the 1963 to 2014 period exceeded 1400 mm with a minimum of 975 mm. Annually, evaporation rates peaked at 8 mm day^{-1} during the summer months, decreasing to less than 1 mm day^{-1} in winter. Average evaporation rates ranged between 1 mm day^{-1}in winter and 5 mm day^{-1} in summer. The average evaporation rate for the 1963 to 2014 period was 3.3 mm day^{-1}. Statistically, there has been no significant change in annual evaporation for the 1963 to 2014 period.

Agreement between Symon's pan (annual) open water evaporation estimates, available for the period 1976 to 2006, and the DPMETHS model estimates was poor for the period 1976 to 1993, with the Symon's pan method significantly underestimating compared to the DPMETHS estimates. For the period 1994 to 2006, the agreement was improved.

The sub-daily evaporation methods are divided into two main categories: methods that rely on the energy balance equation for the open water surface and those that do not. Sub-daily measurements were collected in a field study above Midmar Dam.

The SR, (modified) BR and TV methods, dependent on the energy balance for estimating evaporation, allow for sub-daily measurements of the sensible heat flux term of the energy balance. It was subsequently established that sensible heat flux is the smallest component of the energy balance. If the net irradiance and the water-stored heat flux S are measured, then evaporation can be estimated as a residual of the energy balance. However, taking measurements is challenging as, unlike the measurement of soil heat flux, where the soil is stationary, water is not stationary and water movement around the temperature sensors used for the measurement of S results in considerable variation. Due to the small magnitude of the sensible heat flux for open water and the variable nature of S, the SR, TV and BR methods were not pursued further as methods for estimating open water evaporation.

The EC and MOST methods received close attention as they do not require measurements of S. The EC method is expensive and relies on high frequency measurements of vertical wind speed, air temperature and atmospheric humidity. For the first time in South Africa, the EC fluxes of sensible heat and evaporation were determined in near real-time without the need for post-calculations. The MOST method is relatively inexpensive, relying only on routine measurements of air temperature, surface water temperature (using an infrared thermometer), atmospheric humidity and wind speed. The MOST method requires iterative calculations which were implemented in a spreadsheet.

The MOST method is dependent on the roughness length z_o (mm), and the height above the water surface at which the horizontal wind speed is 0 m s^{-1}. Two approaches were used for determining z_o. A fixed value of 0.2 mm was obtained as a "best" value by comparing MOST and EC measurements of sensible heat flux for z_o varying between 0.00001 and 5 mm. The value of z_o = 0.2 mm agreed with that used by Blanc (1983). Alternatively, various expressions found in the literature were used for estimating z_o. Temporal comparisons between the EC and MOST measurements of evaporation showed much improved agreement when z_o = 0.2 mm was used in the MOST iterative calculations, compared to use of the various expressions for z_o. However, the EC measurements were much more variable than the MOST measurements. Recommended (standard) quality assurance data protocols were applied to the EC measurements. The choice of EC quality assurance grades was a compromise between the amount of data loss and data quality when compared to the MOST measurements. Following data quality control of the EC data, there was reasonable to good comparison between the EC and MOST evaporation estimates. More than 30% of the EC evaporation measurement data were discarded as a result of application of the quality assurance protocols. It was therefore not possible to use the EC method to obtain continuous 30-min measurements of evaporation.

The MOST estimates of evaporation demonstrated that even on near-cloudless days, evaporation can be lower than for cloudy but windier days. Unlike vegetated surfaces, for which there is stomatal control of evaporation during the daytime and virtually no evaporation at night due to stomatal closure, open water surfaces are not constrained. MOST measurements for the 100-day measurement period (14th February to 26th May 2016) demonstrated that 44% of daily total evaporation occurs at night with 56% occurring during the daytime. The MOST measurements demonstrated the wind control influence on the evaporation estimates. Surprisingly, too, maximum wind speeds generally occurred at night with the nighttime wind run comprising 42% of the total wind run over the measurement period. Over land, vegetation would offer more resistance to wind, so wind effects on evaporation would be reduced, compared to open water surfaces.

Evaporation was the greatest component of the energy balance by far, representing about 75% of net irradiance, 12.8% for water-stored heat flux and 12.1% for sensible heat flux. Evaporation was 86% of the available energy flux, with sensible heat flux 14%, representing a long-term average BR of 0.16. Vegetated surfaces would usually have much higher BR values.

Comparison between the DPMETHS and MOST cumulative evaporation totals showed that the DPMETHS estimates were, over the period of 100 days, 9% lower than the MOST estimates. MOST estimates of evaporation have the significant advantage of being independent of the available energy flux compared to the DPMETHS method.

MOST estimates of evaporation increase with increasing surface water temperature and these estimates are also dependent on wind speed, air temperature and atmospheric stability. Other controls for open water evaporation include increased atmospheric water vapour pressure which reduces evaporation. LANDSAT data showed that the greatest water temperatures occur along the shoreline with increases in water depth away from the shoreline resulting in decreased surface water temperatures. It can be hypothesised therefore that shallower dams could have increased evaporation compared to deeper dams. Furthermore, dams in cooler areas could have reduced evaporation compared to those in warmer climates.

7.3 Recommendations for future research and technology transfer

Automatic weather stations are now common in South Africa. At present, however, there is not a single above-water automatic weather station. This study has demonstrated the importance of above-water weather data collection for evaporation estimation. Future research should focus on collecting data above open water over an extended period that includes a full summer season. A more permanent water station would greatly assist in future testing and refining of the MOST method and collection of evaporation data using the EC method. This research would require the support of water boards and government departments in providing infrastructure and facilities.

While the MOST measurement method is robust, the results of the study are for a summer rainfall area on one dam. Ideally, the study needs to be repeated in other areas, using a tethered system well away from the shoreline, for large and small, deep and shallow dams, in different climates, and in both winter and summer rainfall areas.

In terms of technology transfer, workshops on the important techniques used in this project are recommended, which should include the following topics:

- While the SR method was eventually not favoured for open water evaporation, the method forms the basis of a number of vegetation-based WRC research projects, but using methods that are nearly a decade out of date. Researchers need to be updated on the SR methods used in this study;

- The online EC method is also new and researchers need to be made aware of this capability and the capability of offline post-calculations;
- Water managers need to be made aware of the outcomes of this research project through a one-day workshop conducted in Pretoria. In particular, they need to be made aware of the problems associated with the use of the Symon's pan for estimating open water evaporation;
- The suggestion that there should be follow-up studies for large vs small dams, winter rainfall and summer rainfall dams, and dams located in cool compared to warmer climates should be pursued.

REFERENCES

Abraha MG, Savage MJ. 2008. Comparison of estimates of daily solar radiation from air temperature range for application in crop simulations. *Agricultural and Forest Meteorology* 148: 401–416.

Abraha MG, Savage MJ. 2012. Energy and mass exchange over incomplete vegetation cover. *Critical Reviews in Plant Sciences* 31: 321–341.

Allen RG, Pereira LS, Raes D, Smith M. 1998. *Crop evapotranspiration - Guidelines for computing crop water requirements* - FAO Irrigation and drainage paper 56 FAO - Food and Agriculture Organization of the United Nations, Rome, Italy. 315 pp.

Allen RG, Pruitt WO, Wright JL, Howell TA, Ventura F, Snyder R, Itenfisu D, Steduto P, Berengena J, Yrisarry JB, Smith M, Pereira LS, Raes D, Perrier A, Alves I, Walter I, Elliott R. 2006. A recommendation on standardized surface resistance for hourly calculation of reference ETo by the FAO56 Penman method. *Agricultural Water Management* 81: 1–22.

Blanc TV. 1983. An error analysis of profile flux, stability, and roughness length measurements made in the marine atmospheric surface layer. *Boundary-Layer Meteorology* 26: 243–267.

Bristow KL. 1987. On solving the surface energy balance equation for surface temperature. *Agricultural and Forest Meteorology* 39: 49–54.

Brutsaert W. 1982. *Evaporation into the atmosphere: theory, history, and applications*. Dordrecht, Holland: Reidel. 299 pp.

Brutsaert W. 2005. *Hydrology: an introduction*. Cambridge University Press, Cambridge, UK. 605 pp.

Campbell GS, Norman JM. 1998. *An Introduction to Environmental Biophysics*. Springer-Verlag, New York, NY, USA.

Castellví F, Perez PJ, Ibañez M. 2002. A method based on high frequency temperature measurements to estimate sensible heat flux avoiding the height dependence. *Water Resources Research* 38 (6), WR000486–20: 1–10.

Charnock H. 1955. Wind stress on a water surface. *Quarterly Journal of Royal Meteorological Society* 81: 639–640.

Cheng Y, Brutsaert W. 2005. Flux-profile relationships for wind speed and temperature in the stable atmospheric boundary layer. *Boundary-Layer Meteorology* 114: 519–538.

Deardorff JW. 1978. Observed characteristics of the outer layer. In: Short course on the planetary boundary layer. Blackadar AK, (ed.) American Meteorological Society, Boston, MA, USA.

de Bruin HAR. 1982. Temperature and energy balance of a water reservoir determined from standard weather data of a land station. *Journal of Hydrology* 59: 261–274.

Duan Z. 2014. Estimating water balance components of lakes and reservoirs using various open access satellite databases. PhD thesis, Delft University of Technology, The Netherlands.

Dyer AJ, Hicks BB. 1970. Flux-gradient relationships in the constant flux layer. *Quarterly Journal of Royal Meteorological Society* 96: 715–721.

Edinger JE, Duttweiler DW, Geyer JC. 1968. The response of water temperature to meteorological conditions. *Water Resources Research* 4: 1137–1143.

Everson CS. 1999. *Evaporation from the Orange River: Quantifying open water resources*. Water Research Commission Report No. 683/1/99, p80, ISBN 1-86845-520-3.

Everson CS. 2001. The water balance of a first order catchment in the montane grasslands of South Africa. *Journal of Hydrology* 241, 110–123.

Finch JW. 2001. A comparison between measured and modelled open water evaporation from a reservoir in south-east England. *Hydrological Processes* 1514: 2771–2778.

Foken T. 2006. 50 years of the Monin-Obukhov similarity theory. *Boundary-Layer Meteorology* 119: 431–447.

Foken T. 2008. *Micrometeorology*. Springer-Verlag, Berlin, Germany. 328 pp.

Foken, T, Leuning R, Onley SR, Mauder M, Aubinet M. 2012. Corrections and data quality control. In Aubient M, Vesala T, Papale D. (eds). *Eddy Covariance: A Practice Guide to Measurement and Data Analysis.* Springer, New York. p 85-131.

Garratt JR. 1994. *The atmospheric boundary layer*. Cambridge University Press. Cambridge, UK. 336 pp.

Hargreaves GH, Samani ZA. 1982. Estimation of potential evapotranspiration. Journal of Irrigation and Drainage Division, Proceedings of the American Society of Civil Engineers 108, 223–230.

Hargreaves GH, Samani ZA. 1985. Reference crop evapotranspiration from temperature. *Applied Engineering in Agriculture* 1(2): 96–99.

Hargreaves GH, Allen RG. 2003 History and evaluation of Hargreaves evapotranspiration equation. *Journal of Irrigation and Drainage Engineering* 129(1): 53–63.

Högström U. 1988. Non-dimensional wind and temperature profiles in the atmospheric surface for the MOST layer: A re-evaluation. *Boundary-Layer Meteorology* 42: 55–78.

Högström U. 1996. Review of some basic characteristics of the atmospheric surface layer. *Boundary-Layer Meteorology* 78: 215–246.

Hsieh C-I, Katul GG, Schieldge J, Sigmond J, Knoerr KR. 1996. Estimation of momentum and heat fluxes using dissipation and flux-variance methods in the unstable surface layer. *Water Resources Research* 32: 2453–2462.

Jarmain C, Everson CS, Savage MJ, Mengistu MG, Clulow AD, Gush MB. 2009. *Refining tools for evaporation monitoring in support of water resources management.* Water Research Commission Report No. 1567, p137, ISBN 978-1-77005-798-2.

Jensen ME, Burman RD, Allen RG. 1990. *Evapotranspiration and irrigation water requirements.* American Society of Civil Engineers Manuals and Reports in Engineering Practice, No. 70. New York. 360 pp.

Jung M, Reichstein M, Ciais P, Seneviratne SI, Sheffield J, Goulden ML, Bonan G, Cescatti A, Chen J, de Jeu R, Dolman AJ, Eugster W, Gerten D, Gianelle D, Gobron N, Heike J, Kimball J, Law BE, Montagnani L, Mu Q, Mueller B, Oleson K, Papale D, Richardson AD, Roupsard O, Running S, Tomelleri E, Viovy N, Weber U, Williams C, Wood E, Zaekle S, and Zhang K. 2010. Recent decline in the global land evapotranspiration trend due to limited moisture supply. *Nature*, 467, 951–954.

Keijman JQ, Koopmans RWR. 1973. A comparison of several methods of estimating evaporation of Lake Flevo. In *Hydrology of Lakes*. IAHS publication no 109, Helsinki. Pp 225–232.

Masuda K, Takashima T, Takayama, Y. 1988. Emissivity of pure and sea waters for the model sea surface in the infrared window regions. *Remote Sensing and Environment* 24: 313–329.

McArthur AJ. 1990. An accurate solution to the Penman equation. *Agricultural and Forest Meteorology* 51: 87–92.

Mengistu MG, Savage MJ. 2010a. Open water evaporation for a small shallow dam in winter using surface renewal and eddy covariance methods. *Journal of Hydrology* 380: 27–35.

Mengistu MG, Savage MJ. 2010b. Surface renewal method for estimating sensible heat flux. *Water SA* 36, 9–17.

Monin AS and Obukhov AM. 1954. 'Osnovnye zakonomernosti turbulentnogo peremeshivanija v prizemnom sloe atmosfery (Basic laws of turbulent mixing in the atmosphere near the ground)'. *Trudy geofiz. inst. AN SSSR* 24(151), 163–187.

Monteith JL. 1965. Evaporation and the environment. In: Fogg GE (ed). *The state and movement of water in living organisms.* Cambridge University Press: London.

Newman S.M, Smith J.A, Glew MD, Rogers SM, Taylor J.P. 2005. Temperature and salinity dependence of sea surface emissivity in the thermal infrared. *Quarterly Journal of the Royal Meteorological Society* 131, 2539–2557.

Obukhov 1951

Obukhov 1947

Paw U KT, Gao W. 1988. Applications of solutions to non-linear energy budget equations. *Agricultural and Forest Meteorology* 43: 121–145.

Paw U KT, Qui J, Su HB, Watanabe T, Brunet Y. 1995. Surface renewal analysis: a new method to obtain scalar fluxes. *Agricultural and Forest Meteorology* 74: 119–137.

Prueger JH, Kustas WP. 2005. Aerodynamic methods for estimating turbulent fluxes. In J.L. Hatfield and J.M. Baker (eds). *Micrometeorology in Agricultural Systems.* ASA Monogr. 47. Pp 387–416 ASA, CSSA and SSSA, Madison, Wisconsin, USA.

Mengistu MG, Savage MJ. 2010. Open water evaporation estimation for a small shallow reservoir in winter using surface renewal. *Journal of Hydrology* 380: 27–35.

Monin AS, Obukhov AM. 1954. Basic laws of turbulent mixing in the ground layer of the atmosphere. Tr. Geofiz. Inst. Akad. Nauk, SSSR no. 24 (151) p. 163–187. In H. Goering (ed). (German translation, 1958) *Sammelbandzur Statistischen Theorie der Turulenz* Akademie Verlag, Berlin.

Obukhov AM. 1946. Turbulence in an atmosphere with a non-uniform temperature. *Boundary-Layer Meteorology* 2(1): 7–29.

Panofsky HA, Dutton JA. 1984. *Atmospheric turbulence. Models and methods for engineering applications.* Wiley, New York, USA.

Paulson CA. 1970. The mathematical representation of wind speed and temperature profiles in the unstable atmospheric surface layer. *Journal of Applied Meteorology* 9: 857–861.

Penman HL. 1948. Natural evaporation from open water, bare soil and grass. Proceedings of the Royal Society of London. Series A. *Mathematical and Physical Sciences* 193: 1032: 120–145.

Prueger JH, Kustas WP. 2005. Aerodynamic methods for estimating turbulent fluxes. In: Hatfield JL, Baker JM (eds). Micrometeorology in agricultural systems. Madison, Wisconsin: American Society of Agronomy. Agronomy Monograph No. 47. pp. 407–436.

Savage MJ. 2009. Estimation of evaporation using a dual-beam surface layer scintillometer and component energy balance measurements. *Agricultural and Forest Meteorology* 149: 501–517.

Savage MJ. 2010. Sensible heat flux for estimating evaporation. DSc Agric thesis, University of KwaZulu-Natal, South Africa.

Savage MJ. 2014. Web-based teaching, learning and research using real-time data from field-based agrometeorological measurement systems. MSc Agric thesis, University of KwaZulu-Natal, South Africa.

Savage MJ, Everson CS, Metelerkamp BR. 1997. *Evaporation measurement above vegetated surfaces using micrometeorological techniques.* Water Research Commission Report No. 349/1/97, p248, ISBN 1-86845-363-4.

Savage MJ, Everson CS, Metelerkamp BR. 2009. Bowen ratio evaporation measurement in a remote montane grassland: Data integrity and fluxes. *Journal of Hydrology* 376: 249–260.

Savage MJ, Everson CS, Odhiambo GO, Mengistu MG, Jarmain C. 2004. *Theory and practice of evaporation measurement, with special focus on surface layer scintillometry as an operational tool for the estimation of spatially averaged evaporation*. Water Research Commission Report No. 1335/1/04, p204, ISBN 1-77005-247-X.

Savage MJ, Heilman JL. 2009. Infrared calibration of net radiometers and infra red thermometers. *Agricultural and Forest Meteorology* 149: 1279–1293.

Snedecor GW, Cochran WG. 1980. *Statistical Methods* (7th edition). Iowa State University Press, Iowa, USA.

Snyder RL, Anderson FE, Spano D, Duce P, Paw U KT, Russo AE. 2007. An Excel application program to compute surface renewal estimates of sensible heat flux from the 2nd, 3rd and 5th moments of a structure function using high frequency temperature data and to compute ET and crop coefficients using energy balance. University of California, Davis, California, USA.

Snyder, RL, Spano D, Paw U KT. 1996. Surface renewal analysis for sensible heat and latent heat flux density. *Boundary-Layer Meteorolology* 77: 249–266.

Swinbank WC. 1951. The measurement of vertical transfer of heat and water vapor by eddies in the lower atmosphere. *Journal of Meteorology* 83: 135–145.

van Atta CW. 1977. Effect of coherent structures on structure functions of temperature in the atmospheric boundary layer. *Archives Mechanics* 29: 161–171.

Wan Z. 2012. Distilled Water - Emissivity averaged over 6 sets. http://g.icess.ucsb.edu/modis/EMIS/images/diswat06.prn Accessed May 2012.

Webb EK. 1970. Profile relationships: The log-linear range and extension to strong stability. *Quarterly Journal of Royal Meteorological Society* 96: 67–90.

Wikipedia. http://en.wikipedia.org/wiki/Cubic_function. Accessed 24 May 2015.

Willmott CJ. 1981. On the validation of models. *Physical Geography* 2: 184–194.

Willmott CJ. 1982. Some comments on the evaluation of model performance. *Bulletin of the American Meteorological Society* 63: 1310–1313.

Wohlfahrt G, Haslwanter A, Hörtnagl L, Jasoni RL, Fenstermaker LF, Arnone JA, Hammerle A. 2009. On the consequences of the energy imbalance for calculating surface conductance. *Agricultural and Forest Meteorology* 149: 1556–1559.

APPENDICES

Appendix 1 Equations for the determination of various properties of air, such as atmospheric pressure P, air density ρ and specific heat capacity c_p, and humidity parameters such as the saturation water vapour pressure e_s, specific humidity q and others including specific latent energy of vaporisation (L) and gravity g

Term	Equation	Units	Comment
Specific latent energy of vaporisation	$L = 2.50095 - 0.00236679\, T_z$	MJ kg^{-1}	T_z in °C
Saturation water vapour pressure at temperature T_z	$e_s(T_z) = 0.6108 \cdot \exp(17.2694\, T_z/(237.3 + T_z))$	kPa	
Dewpoint temperature	$T_{dp} = -273.16 + (273.16 - 2.0765067 \ln(e_z/0.6108))/(1 - 0.0579059 \ln(e_z/0.6108)))$	°C	e_z in kPa
Slope of saturation water vapour pressure *vs* temperature relationship (Δ at temperature T_z)	$\Delta = 4098.02862 \cdot e_s(T_z)/(237.3 + T_z)^2$	kPa $°C^{-1}$	
Specific heat capacity	$c_p = 1004.723 + 1148.254\, e_z/(P - e_z) + \delta c_p$ $\delta c_p = 1.256 \cdot (1 + T_z) \cdot (1 + e_z/e_s)$	J kg^{-1} K^{-1}	e_z in kPa; atmospheric pressure P in kPa

Term	Equation	Units	Comment
Psychrometric constant γ	$\gamma = c_p\ P/(10^6 \cdot 0.62198\ L)$	kPa $^{o}C^{-1}$ L (MJ kg^{-1})	Slope of the wet bulb line of the psychr-ometric chart
Psychrometric equation	$e = e_s(T_w) - \gamma \cdot\ (RH/100) \cdot (T_z - T_w) \cdot (1 + 0.00115 \cdot T_w)$	kPa	T_w may be determined iteratively using $e = e_s(T_z) \cdot (RH/100)$
Gravity	$g = 9.77989\ +\ 0.00014155 \cdot \mathrm{abs}\,(Latitude)\ +\ 1.00545 \cdot 10^{-5} \cdot Latitude^2\ -\ 0.3086 \cdot altitude/1000000$	m s^{-2}	*Latitude* in decimal degrees, *altitude* in m (Savage et al., 1997)
Atmospheric pressure	$P = 101.325 - ((-10.94866 \cdot e_z + 2934.7773)/(8.31451 \cdot (T_z + 273.15) + 0.28362157 \cdot altitude)) \cdot g \cdot altitude/1000$	kPa	e_z in kPa, T_z in ^{o}C, *altitude* in m (Savage et al., 1997)
Specific humidity	$q = 0.62198\ e_z/(P - 0.37802\ e_z)$	kg kg^{-1}	e_z in kPa; atmospheric pressure P in kPa

Term	Equation	Units	Comment
Density of air	$\rho = (2834.7773 - 10.94866\ e_z)/(8.31451 \cdot (T_z + 273.15) + 0.28362157\ altitude)$	kg m^{-3}	e_z in kPa, T_z in °C, *altitude* in m (Savage et al., 1997)

Appendix 2 Datalogger programme for the measurement of the outputs required for application of the MOST method

Datalogger programme

```
'CR1000

'Created by Short Cut (3.0)

'CM3_993297 used; SI-111 IRT number 3589 (Apogee); NRLite2 number 134770; Globe 5 (thermistor 5)

'Type E thermocouple on 6H, 6L


'Declare Variables and Units

Dim TT_K, SBT_K, m, b, WindCorr, AirTC_2, SPkPa, Twg, Twpg, Vpg, Vp, SVp, Twch, VpgVpd, Top, Bottom, SVpW, N

Dim HITF, WCTF, WCWSMPH, BattV, PTemp_C

Public SlrW, SlrMJ, AirTC, RH, WS_ms, WindDir, TT_C, SBT_C, TTmV, NR_Wm2, CNR_Wm2, TdC, TwC, HI_C, WC_C, Rain_mm
```

```
Units BattV=Volts
Units PTemp_C=Deg C
Units SlrW=W/m^2
Units SlrMJ=MJ/m^2
Units AirTC=Deg C
Units RH=%
Units WS_ms=meters/second
Units WindDir=degrees
Units TT_C=Deg C
Units SBT_C=Deg C
Units NR_Wm2=W/m^2
Units CNR_Wm2=Watts/meter^2
Units TdC=Deg C
Units TwC=Deg C
Units HI_C=Deg C
Units WC_C=Deg C
Units Rain_mm=mm
```

Datalogger programme

```
Public rTime(9)                'declare as public and dimension rTime to 9
Alias rTime(1) = Year          'assign the alias Year to rTime(1)
Alias rTime(2) = Month         'assign the alias Month to rTime(2)
Alias rTime(3) = DOM           'assign the alias DOM to rTime(3)
Alias rTime(4) = Hour          'assign the alias Hour to rTime(4)
Alias rTime(5) = Minute        'assign the alias Minute to rTime(5)
Alias rTime(6) = Second        'assign the alias Second to rTime(6)
Alias rTime(7) = uSecond       'assign the alias uSecond to rTime(7)
Alias rTime(8) = WeekDay       'assign the alias WeekDay to rTime(8)
Alias rTime(9) = Day_of_Year   'assign the alias Day_of_Year to rTime(9)
Dim DoY, ToD


'Define Data Tables
DataTable(MOSTwater_2min,True,-1)
  DataInterval(0,2,Min,10)
  TableFile("USB:"+Status.SerialNumber+"MOSTwater_2min",8,-1,0,0,Hr,0,0)
  Sample(1,DoY,IEEE4)
```

```
  Sample(1,ToD,IEEE4)

  Average(1,SlrW,IEEE4,False)

  Average(1,AirTC,IEEE4,False)

  Sample(1,RH,IEEE4)

  WindVector (1,WS_ms,WindDir,IEEE4,False,0,0,0)

  FieldNames("WS_ms_S_WVT,WindDir_D1_WVT,WindDir_SD1_WVT")

  Maximum(1,WS_ms,IEEE4,False,False)

  Totalize(1,Rain_mm,FP2,False)

  Average(1,TT_C,IEEE4,False)

  Average(1,SBT_C,IEEE4,False)

  Average(1,TdC,IEEE4,False)

  Average(1,TwC,IEEE4,False)

  Average(1,HI_C,IEEE4,False)

  Average(1,WC_C,IEEE4,False)

EndTable


DataTable(MOSTwater_60min,True,-1)

  DataInterval(0,60,Min,10)
```

Datalogger programme

```
TableFile("USB:"+Status.SerialNumber+"MOSTwater_2min",8,-1,0,0,Hr,0,0)

Sample(1,DoY,IEEE4)

Sample(1,ToD,IEEE4)

ETsz(AirTC,RH,WS_ms,SlrMJ,330,-30,725,2,0,FP2,False)

FieldNames("ETos,Rso")

Average(1,SlrW,IEEE4,False)

Average(1,AirTC,IEEE4,False)

Sample(1,RH,IEEE4)

WindVector (1,WS_ms,WindDir,IEEE4,False,0,0,0)

FieldNames("WS_ms_S_WVT,WindDir_D1_WVT,WindDir_SD1_WVT")

Maximum(1,WS_ms,IEEE4,False,False)

Totalize(1,Rain_mm,FP2,False)

Average(1,TT_C,IEEE4,False)

Average(1,SBT_C,IEEE4,False)

Average(1,TdC,IEEE4,False)

Average(1,TwC,IEEE4,False)

Average(1,HI_C,IEEE4,False)

Average(1,WC_C,IEEE4,False)
```

```
EndTable


'Main Program
BeginProg
  'Main Scan
  Scan(5,Sec,1,0)
    'Default Datalogger Battery Voltage measurement 'BattV'
    Battery(BattV)
    'Default Wiring Panel Temperature measurement 'PTemp_C'
    PanelTemp(PTemp_C,_50Hz)

    DoY=Day_of_Year+Hour/24+Minute/(60*24)+Second/(60*60*24)+uSecond/(10^6*60*60*24)-1
    Real-Time(rTime)
    ToD=Hour/24+Minute/(60*24)+Second/(60*60*24)+uSecond/(10^6*60*60*24)

    'CMP3/CMP6/CMP11 Pyranometer measurements 'SlrMJ' and 'SlrW'
    VoltDiff(SlrW,1,mV250,1,True,0,_50Hz,1,0)
    If SlrW<0 Then SlrW=0
```

```
SlrMJ=SlrW*0.0002096436

SlrW=SlrW*41.92872

'HC2S3 (panel switched power) Temperature & Relative Humidity Sensor measurements 'AirTC' and 'RH'

PortSet(9,1)

Delay(0,3,Sec)

VoltSe(AirTC,1,mV2500,3,0,0,_50Hz,0.1,-40)

VoltSe(RH,1,mV2500,4,0,0,_50Hz,0.1,0)

PortSet(9,0)

If RH>100 AND RH<103 Then RH=100

'03002 Wind Speed & Direction Sensor measurements 'WS_ms' and 'WindDir'

PulseCount(WS_ms,1,1,1,1,0.75,0.2)

If WS_ms<0.21 Then WS_ms=0

BrHalf(WindDir,1,mV2500,5,1,1,2500,True,0,_50Hz,352,0)

If WindDir>=360 OR WindDir<0 Then WindDir=0

'SI-111 Precision Infrared Radiometer measurements 'TT_C' and 'SBT_C'

'Measure SI-111 sensor body thermistor temperature

Therm109(SBT_C,1,6,1,0,_50Hz,1,0)

'Measure SI-111 output of thermopile
```

Datalogger programme

```
VoltDiff(TTmV,1,mV2_5,4,True,0,_50Hz,1,0,)

'Calculate slope (m) and offset (b) coefficients for target temperature calculation

'                    m=0+(0*SBT_C)+(0*SBT_C^2)

'                    b=0+(0*SBT_C)+(0*SBT_C^2)

m=1442350000+(7763110*SBT_C)+(75618.1*SBT_C^2)

b=-13723700+(257054*SBT_C)+(8733.4*SBT_C^2)


'Calculate target temperature using calculated slope (m) and offset (b)

SBT_K=SBT_C+273.15

TT_K=SBT_K^4+TTmV*m+b

TT_K=SQR(SQR(TT_K))

'Convert target temperature into desired units

TT_C=TT_K-273.15

'NR-LITE Net Radiometer (dynamic wind speed correction) measurement 'NR_Wm2' and 'CNR_Wm2'

VoltDiff(NR_Wm2,1,mv25,5,True,0,_50Hz,74.07407,0)

If WS_ms>=5 Then

  CNR_Wm2=NR_Wm2*(1+0.021286*(WS_ms-5))

Else
```

```
  CNR_Wm2=NR_Wm2
EndIf
'Dew Point and Wet Bulb calculation prep
AirTC_2=AirTC
SPkPa=92.96901
SatVP(SVp,AirTC_2)
Vp=RH*SVp/100
'Dew Point calculation 'TdC'
DewPoint(TdC,AirTC_2,RH)
If TdC>AirTC_2 OR TdC=NAN Then TdC=AirTC_2
'Find Wet Bulb 'TwC'
Top=AirTC_2
Bottom=TdC
For N = 1 To 25
  Twpg=Twg
  Twg=((Top-Bottom)/2)+Bottom
  WetDryBulb(Vpg,AirTC_2,Twg,SPkPa)
  VpgVpd=Vpg-Vp
```

```
    Twch=ABS(Twpg-Twg)

    If VpgVpd>0 Then

      Top=Twg

    Else

      Bottom=Twg

    EndIf

    If Twch<0.01 OR N=25 Then ExitFor

  Next

  TwC=Twg

  'Heat Index calculation 'HI_C'

  HITF=1.8*AirTC+32

  HI_C=-42.379+2.04901523*HITF+10.14333127*RH-0.22475541*HITF*RH-6.83783*10^-3*HITF^2-5.481717*10^-2*RH^2+1.22874*10^-
3*HITF^2*RH+8.5282*10^-4*HITF*RH^2-1.99*10^-6*HITF^2*RH^2

  If HITF<80 OR RH<40 OR HI_C<HITF OR HI_C=NAN Then HI_C=HITF

  HI_C=(5/9)*(HI_C-32)

  'Wind Chill calculation 'WC_C'

  WCTF=1.8*AirTC+32

  WCWSMPH=WS_ms*2.236936
```

```
    WC_C=35.74+0.6215*WCTF-35.75*WCWSMPH^0.16+0.4275*WCTF*WCWSMPH^0.16

    If WC_C>WCTF OR WC_C=NAN Then WC_C=WCTF

    If WCTF>50 OR WCWSMPH<3 Then WC_C=WCTF

    WC_C=(5/9)*(WC_C-32)

    'TE525/TE525WS Rain Gauge measurement 'Rain_mm'

    PulseCount(Rain_mm,1,2,2,0,0.254,0)

    'Call Data Tables and Store Data

    CallTable(MOSTwater_2min)

    CallTable(MOSTwater_60min)

  NextScan

EndProg
```

Appendix 2 (continued) Datalogger wiring, assuming NR-Lite net radiometer and not four-component net radiometer

5/28/2014
10:17:49
Created by Short Cut (3.0)
Short Cut Program: MOST open water.DEF

-Wiring for CR1000-

CMP3/CMP6/CMP11 Pyranometer
1H: White
1L: Black
1L: Jumper to Ground
Ground: Clear
Ground: Jumper to 1L

HC2S3 (panel switched power)
2H: Brown
2L: White
Ground: Yellow
Ground: Grey
Ground: Clear
SW-12: Green

03002 Wind Speed & Direction Sensor
Ground: Black
3H: Green
Ground: Clear
Ground: White
VX1 or EX1: Blue
P1: Red

SI-111 Precision Infrared Radiometer
3L: Green
Ground: Blue
Ground: Clear
4H: Red
4L: Black
VX1 or EX1: White

NR-LITE Net Radiometer (dynamic wind speed correction)
Ground: Clear
5H: White
5L: Green
5L: Jumper to Ground
Ground: Jumper to 5L

TE525/TE525WS Rain Gauge
Ground: Clear
Ground: White
P2: Black

-Measurement Labels-

Default Measurements
BattV
PTemp_C

CMP3/CMP6/CMP11 Pyranometer
SlrW
SlrMJ

HC2S3 (panel switched power)
AirTC
RH

03002 Wind Speed & Direction Sensor
WS_ms
WindDir

SI-111 Precision Infrared Radiometer
TT_C
SBT_C

NR-LITE Net Radiometer (dynamic wind speed correction)
NR_Wm2
CNR_Wm2

Dew Point and Wet Bulb
TdC
TwC

Heat Index
HI_C

Wind Chill
WC_C

TE525/TE525WS Rain Gauge
Rain_mm

Appendix 3 Determination of the Southern Oscillation Index

The Southern Oscillation Index (SOI) is computed using monthly mean sea level pressure anomalies at Tahiti (T) and Darwin (D). The SOI for Tahiti-Darwin is an index that reduces the Southern Oscillation for the south equatorial Pacific to a single index. There is a five-step process for determining $SOI_{Tahiti\text{-}Darwin}$. The procedures outlined here are those followed by the National Weather Service Climate Prediction Centre (http://www.cpc.ncep.noaa.gov/data/indices/) except for the filtering procedures.

Step 1

For convenience, sea level pressures are adjusted by subtracting 100 kPa from the monthly pressure values. Then the pressure anomalies are determined. The base period for the baseline pressure value is the average of the 1951 to 1980 pressures. Two baseline (average) values are obtained:

$$\overline{P_{\text{Tahiti 51-80}}}$$

for Tahiti and

$$\overline{P_{\text{Darwin 51-80}}}$$

for Darwin. Hence two pressure anomalies are determined for each month:

$$PA_{\text{Tahiti}} = P_{\text{Tahiti}} - \overline{P_{\text{Tahiti 51-80}}}$$

$$PA_{\text{Darwin}} = P_{\text{Darwin}} - \overline{P_{\text{Darwin 51-80}}}$$

Step 2

The 1951-80 pressure standard deviations $\sigma_{P_{\text{Tahiti 51-80}}}$ and $\sigma_{P_{\text{Darwin 51-80}}}$ are required for a normalization procedure – one for the Tahiti dataset and one for Darwin.

Step 3

In statistics, any normal random variable x with a mean $\bar{x}$ and standard deviation σ is can be transformed into a standard normal variate z using

$$z = (x - \bar{x})/\sigma$$

Similarly, monthly standard anomalies SA, one for Darwin and one for Tahiti, are determined using

$$SA_{\mathrm{Tahiti}} = PA_{\mathrm{Tahiti}}/\sigma_{P_{\mathrm{Tahiti\ 51-80}}} = (P_{\mathrm{Tahiti}} - \overline{P_{\mathrm{Tahiti\ 51-80}}})/\sigma_{P_{\mathrm{Tahiti\ 51-80}}}$$

and

$$SA_{\mathrm{Darwin}} = PA_{\mathrm{Darwin}}/\sigma_{P_{\mathrm{Darwin\ 51-80}}} = (P_{\mathrm{Darwin}} - \overline{P_{\mathrm{Darwin\ 51-80}}})/\sigma_{P_{\mathrm{Darwin\ 51-80}}}$$

and their difference computed as:

$$SAD = SA_{\mathrm{Tahiti}} - SA_{\mathrm{Darwin}}$$

Step 4

The monthly standard deviation of this difference (*MSD*) is computed:

$$MSD = \sqrt{SAD^2/n}$$

Step 5

Determine SOI:

$$SOI = SAD/MSD$$

Negative SOI values correspond to $SA_{\mathrm{Tahiti}} < SA_{\mathrm{Darwin}}$, negative SAD values, and corresponding to El Niño.

Appendix 4 Determination of radiance temperature using LANDSAT 8 Band 10

The process takes the DN digital number and converts it to radiance in K. Radiance is then improved by including the sine of the elevation of the satellite. It then converts the corrected radiance to temperature in Kelvin using the K1 and K2 and addition factor specifications of band 10 in the LANDSAT 8 image, supplied by the United States Geological Service in the metadata file for the satellite scene.

The principal calculations behind the method are found at the following site:

http://landsat.usgs.gov/Landsat8_Using_Product.php

The radiance temperatures for 25th February 2016 at 09h50 for Midmar Dam are shown in Figure A4.1. Of note are the slightly elevated temperatures along the shoreline of the dam. The variation in radiance temperature across the dam water surface is 1.5 to 2°C. The sensitivity of LE_MOST to water-surface temperature is demonstrated in Fig. 3.20, *viz.* 12.9 W m^{-2} $°C^{-1}$. The measured water-surface temperature, an average of two infrared thermometers, was 24.67°C and the air temperature 27.68°C. The micrometeorological conditions, together with the MOST calculations, are shown in Table A4.1.

Table A4.1 Micrometeorological conditions, MOST calculations and LANDSAT 8 band 10 radiance temperature for 25th February at 10h00

Surface temperature T_o (°C)	24.67
Air temperature T_z (°C)	27.68
Specific humidity q_z (kg kg^{-1})	0.01450
Saturation specific humidity at the surface temperature q_o (kg kg^{-1})	0.02144
Wind speed U_z (m s^{-1})	3.375
H_MOST (W m^{-2})	-18.26
LE_MOST (W m^{-2})	99.14
LANDSAT radiance temperature (°C)	25.25

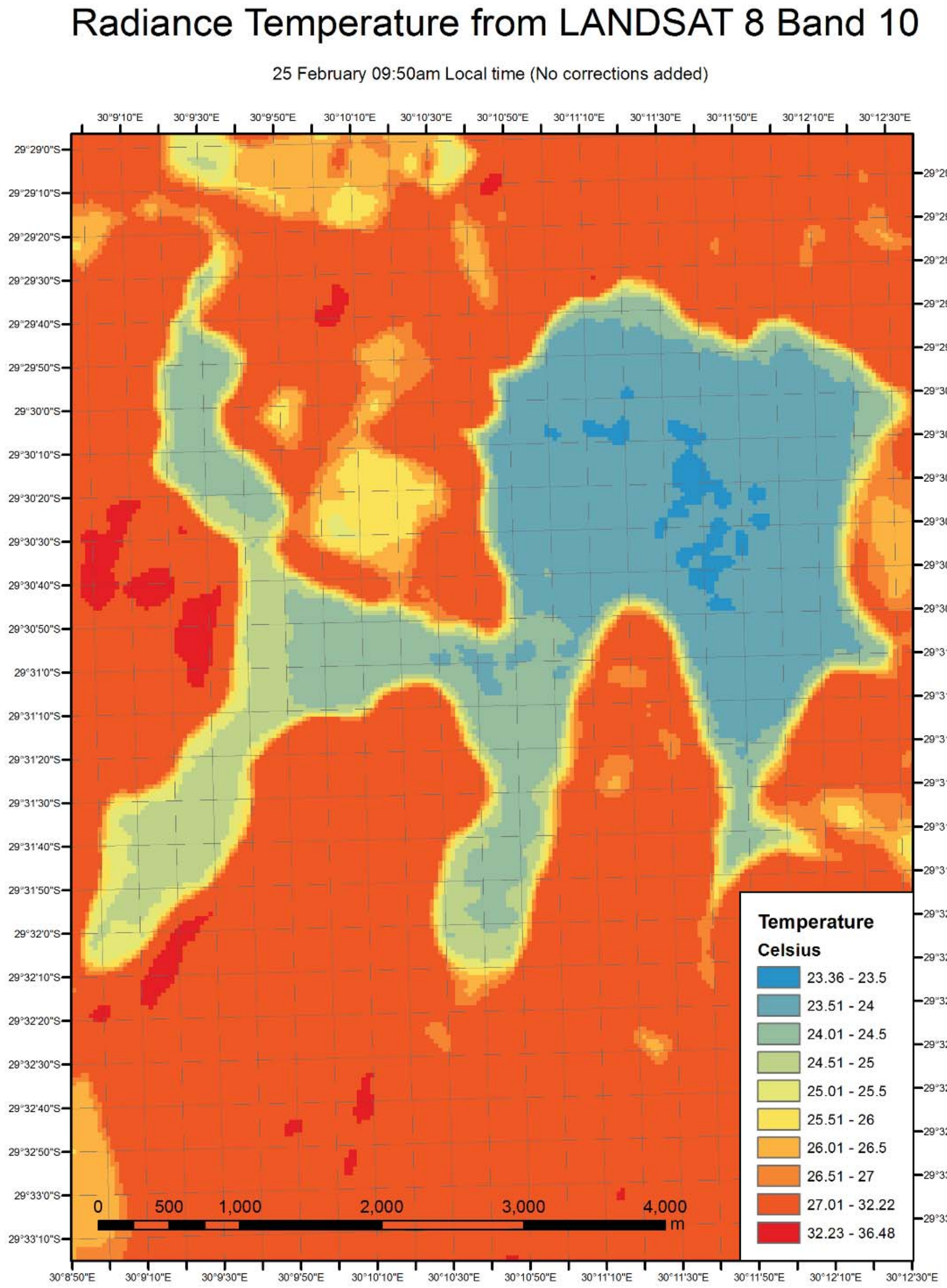

Fig. A4.1 The LANDSAT 8 Band 10 (10600 to 11190 nm) for 25th February 2016 at 09h50

9781431209132